University of South Florida

Scholar Commons

Graduate Theses and Dissertations   Graduate School

3-12-2010

Improving Ground Penetrating Radar Resolution of Features of Active Sinkholes

Bradley Tyler Gooch
University of South Florida

Follow this and additional works at: https://scholarcommons.usf.edu/etd

Part of the American Studies Commons

Improving Ground Penetrating Radar Resolution of Features of Active Sinkholes

by

Bradley Tyler Gooch

A thesis submitted in partial fulfillment
of the requirements for the degree of
Master of Science
Department of Geology
College of Arts and Sciences
University of South Florida

Major Professor: Sarah Kruse, Ph.D.
Mark Stewart, Ph.D.
Mark Rains, Ph.D.

Date of Approval:
March 12, 2010

Dedication

I dedicate this work to one who inspired my love for science:

Stephen Lee Hopkins (1946-2010)

Acknowledgements

I acknowledge all the help my adviser, Dr. Sarah Kruse, has given me throughout the thesis process. I also thank my committee members, Drs. Mark Stewart and Mark Rains, for their guidance and review of my thesis. Final thanks go to all my family, friends, and fellow graduate students at USF for all their help and support during my time as a graduate student. Without you, none of this would have been possible. Thank you all!

Table of Contents

ii

List of Figures

iii

iv

ix

Improving Ground Penetrating Radar Resolution of Features of Active Sinkholes

Bradley Tyler Gooch

ABSTRACT

Ground penetrating radar (GPR) is widely used to identify locations of sinkholes in covered karst terrain in Florida. Some sinkholes serve as hydraulic conduits between the surficial and underlying aquifers. Their role is critical in determining the surficial aquifer response to pumping in deeper aquifers. Improved methods for discriminating between hydraulically active sinkholes and plugged sinkholes could help regional water management. In the covered karst of west-central Florida a clay-rich weathering horizon forms over the limestone. The clay-rich layer is in turn overlain by surficial sands. Ground penetrating radar profiles typically show a strong reflector from the top of clay-rich horizon as well as internal layering within sands. Active sinkholes are expected to have sandy conduits that broach the clay layer, and perhaps layering in the overlying sand indicative of ongoing subsidence. Three dimensional simulations of GPR profiles over sinkhole with and without conduits were run with the finite-difference time-domain (FDTD) program GPRMAX. Results from the synthetic surveys were then processed with standard techniques, including migration. The modeling confirms that conduits appear in GPR records primarily as gaps in the return from the clay layer. The modeling also shows that non-traditional survey geometries (varying antenna spacing and orientation) are unlikely to recover more information than traditional proximal

x

transmitter-receiver separation. Also examined are GPR profiles and 3D grids over a set of active and inactive sinkholes in Tampa, Florida. Results from these surveys showed decent structural recovery of a small sinkhole similar in structure to that of the modeled ones. Indications of active subsidence and possible conduit structure were apparent from this data. Finally, the dense surveys served as a benchmark to compare interpretations taken with the same surveys at lower spatial resolutions and profiles with 2D-only processing methods in order to understand errors in analysis and interpretation that are possible from 2D surveys. Two-dimensional surveys, 2D processed and migrated, showed some similarity to the 3D results previously mentioned but contained more complexities and artifacts, which led to poorer interpretation ability.

Active v. Inactive Sinkholes as a Problem

Sinkholes are naturally occurring geologic features caused by the dissolution of underlying bedrock. The mixing of carbon dioxide (CO_2) and water (H_2O) from the air and soil leads to the creation of carbonic acid, a weak acid. This acid, formed above the bedrock in the overlying sediment, readily dissolves carbonate (limestone and dolostone) bedrock (Figure 1.1). When this process occurs over a widespread area, it can cause exaggerated topographic irregularity known as karst terrain. This terrain may either be exposed or have a sediment cover over it. The latter is referred to as covered-karst terrain. These sediment covers can be excessively thick, sometimes more than 60 meters (m) (Sinclair and Stewart, 1985). The way the sediment cover and the dissolving bedrock interact determines the type of sinkhole that forms. When the overburden sediments (generally thin) that cover the dissolving bedrock fill in the depression at the same rate of dissolution, it is known as a solution sinkhole (Tihanksy, 1999; see Figure 1.2). When dissolution of the bedrock takes place primarily inside the bedrock via subsurface conduits, a process known as "piping", void spaces can form within the limestone. This process can occur with little sediment displacement, and hence little change to the surface above. Eventually, the void space will fill in with weathered bedrock and overlying

1

sediment, by a process called "raveling", causing a surface depression (Figure 1.3). These sinkholes are known as cover-subsidence (Tihanksy, 1999). A third way sinkholes form occurs where the overlying sediments are so cohesive (clay-rich) that they will not move into the void spaces created by the dissolving bedrock below. Instead, the void migrates into the overburden. Eventually, the surface will collapse and form a depression (Figure 1.4). This is known as a cover-collapse sinkhole (Tihanksy, 1999).

All three sinkhole types are common to Florida (Sinclair and Stewart, 1985) and can pose significant hazards to their environment and people living in their vicinity. Florida is prone to abundant sinkhole development because the entire state is underlain by a thick carbonate platform, with
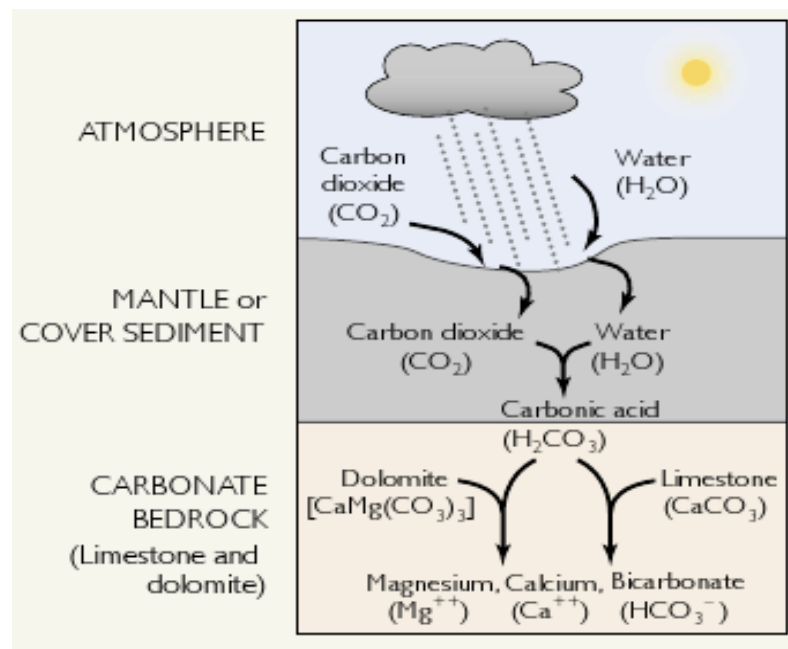
Figure 1.1. Complete process of the dissolution of carbonate rock (from Tihansky, 1999).

2
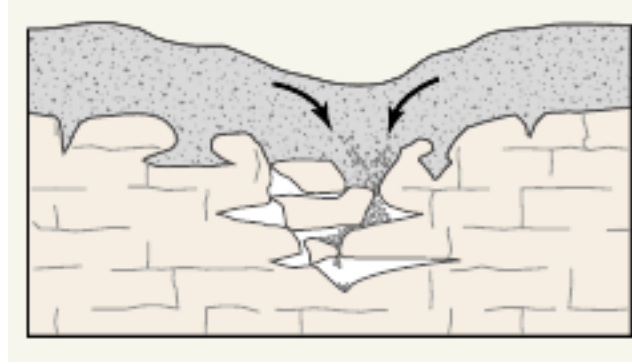
Figure 1.2. Basic process of sinkhole formation, where unconsolidated sediments above dissolved bedrock fill into void spaces created by dissolution process (from Tihansky, 1999).
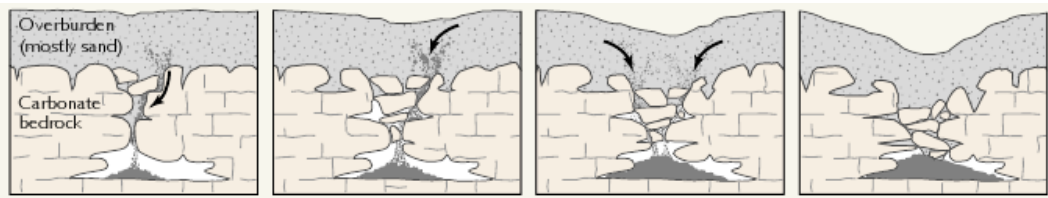
Figure 1.3. Process of cover-subsidence sinkhole formation where unconsolidated sediments gradually funnel down conduits to larger void spaces creating a general lag in the topography (from Tihansky, 1999).

3
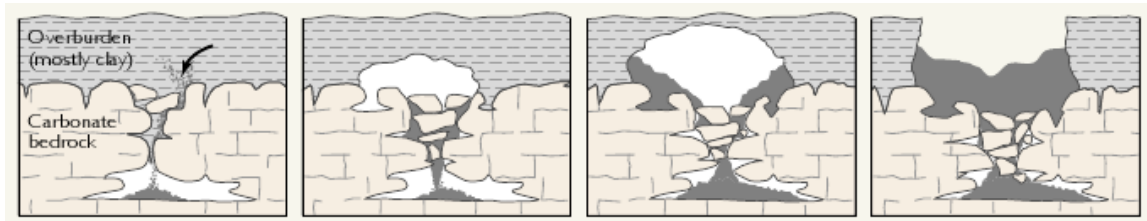
Figure 1.4. Process of cover-collapse sinkhole formation where clay-rich

overburden holds surface topography while sediments move into void spaces.

Eventually, this process will lead to abrupt surface failure and create the sinkhole

(from Tihansky, 1999).

mostly mantled, insoluble siliciclastics over it. Occurrence of sinkholes in Florida is

hastened by the growing population whose equally growing need of water resources

depletes aquifer volumes, which leads to an increase in cavity roof instability due to lack

of ground water to support the suspended material (Ford and William, 1989). Most of the

sinkholes in Florida can be found in the mantled karst of West-central area of the state.

The mantled karst of west-central Florida area contains a higher density of sinkholes than

other areas of the state (Figure 5). This high level of sinkhole occurrence is because the

karst in this area is heavily dissolved and is overlain by approximately $10 - 60$ m of sand

to clayey sand, common to cover-subsidence and cover-collapse sinkhole development.

4

Reported sinkholes
from 1960 to 1991
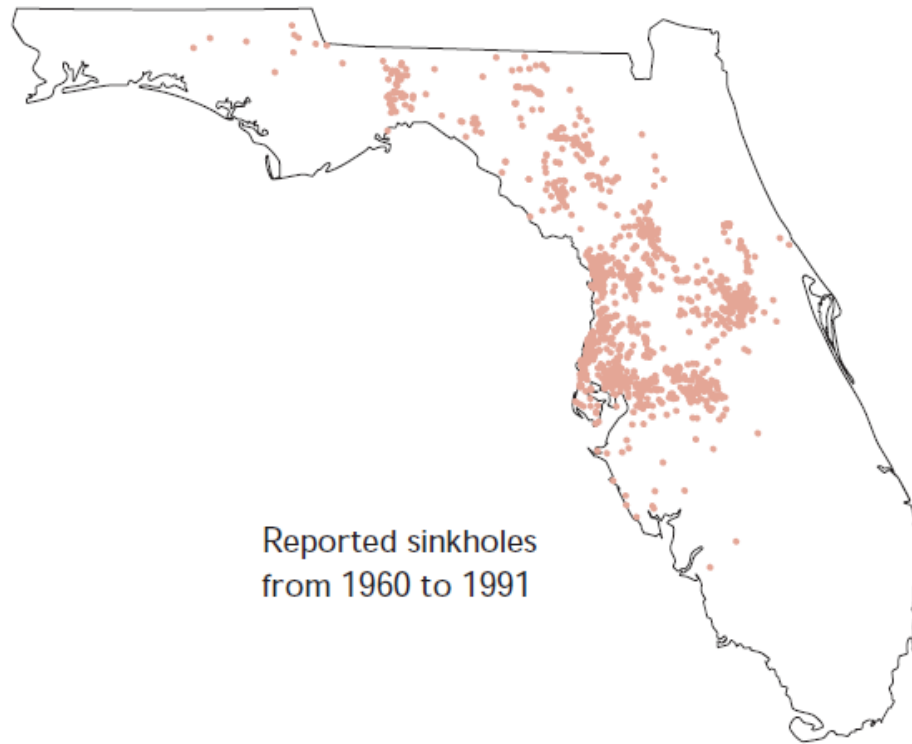
Figure 1.5. Locations of reported sinkholes in Florida between 1960 and 1991. Some of the data may be biased towards areas of high population density due to better reporting (Wilson and Shock, 1996).

One of the challenging issues currently in sinkhole investigations is determining whether or not the depressions are actively subsiding. Once materials fill in the void spaces, it is not well understood how the dissolution process continues (Tihansky, 1999). Does the newly deposited material change the dissolution rate?

A second challenge is to assess whether or not a sinkhole is hydraulically active. By hydraulically active, it is meant that the sinkhole contains low permeability zones that function as preferential flow paths for groundwater. Active sinkholes can be an important site source for water recharge into the underlying aquifers (Stewart, 1998; Stewart and

5

Parker, 1992). Improved means of imaging subsurface features and structure of sinkholes are desirable to better address these questions.

Standard Geological Investigation Methods for Sinkholes

Sinkholes are typically initially identified on the basis of their associated, often roughly conical, topographical depressions. Growing topographic expressions are often indications of sinkhole activity. Where buildings or foundation work are present, then measurements of floor elevation change or wall movement (such as cracking) can be indicators of the activity of nearby sinkholes. However these phenomena cannot be unambiguously associated with sinkhole formation, as many other factors can cause ground deformation. Other factors include tree root activity, expansive clays, and buried decomposing materials.

To further study suspected sinkholes, either to understand their precise subsurface structure or their hydrological role in recharge, more detailed geological investigation is required. Relevant information on the regional geology is helpful in setting the field site in context. Locations and morphology of other known sinkholes in the immediate area are also useful when combined with the regional geologic map. Direct geologic sampling through techniques such as drilling and boring can resolve zones of thickened overburden. With these data a local site geologic map of the subsurface can be created (e.g. Zisman et al 2005). It is important to note that such maps must with care in future investigations because of the potentially rapid (days to years) dissolution and raveling processes associated with sinkhole formation.

Hydrological data from groundwater wells can also contribute to sinkhole investigations. The information can help define the movement of local ground water, which may be influenced by sinkholes. However, direct sampling and hydrologic data are usually costly and thus seldom available until later in the investigation process.

Surface geophysical methods are commonly used for target identification and structural imaging after preliminary inspections and before any serious direct sampling methods. There are many different geophysical methods currently used to investigate various anomalous subsurface properties that are indicative of sinkholes. The majority of these methods use subsurface electrical and density properties for evaluation (Dobecki and Upchurch, 2006) such as microgravity, electrical resistivity tomography, coupled-capacitance resistivity, and seismic methods (i.e. reflection, refraction, and surface wave analysis). The Florida Geological Survey has recently detailed the use of geological, geophysical, and geotechnical procedures to be used in sinkhole investigations in the state of Florida (Schmidt, 2005). The special publication focuses on identification of sinkholes rather than assessing the levels of either subsidence or hydraulic activity. Zisman (2001) attempted to better define subsidence potential by offering a standardized investigation process based on site-specific characteristics such as soil density variance with depth, drilling properties, stratigraphic conditions, and ground water levels. Zisman (2001) emphasizes the uncertainty of the current, standard investigation procedures described briefly above. There is still a need to identify improved methods for evaluating both subsidence potential and hydraulic activity of sinkholes.

Ground-Penetrating Radar as a Modern Method to Delineate Problem

7

Of all the geophysical methods used in sinkhole investigations, ground-penetrating radar (GPR) seems to offer the highest spatial resolution (Dobecki and Upchurch, 2006). GPR is a very robust method for investigating the near-surface subsurface and has been used for many different applications (Mellett, 1995). GPR uses high-frequency electromagnetic radio waves to image subsurface structures that reflect and diffract the energy back to the surface where it is recorded. The instrumentation incorporates transmitting and receiving antennas, a recording device, power accessories, and a computer interface (Reynolds, 1997). The method is very fast and efficient when compared to most other geophysical methods, enabling individuals to rapidly collect and view field data on site at high resolution (Burger et al, 2006). Although radar wave and seismic waves respond to fundamentally different physical properties, in practice the GPR reflection method is very similar in nature to that of common-offset seismic reflection methodology and undergoes essentially the same data processing as single-receiver, common-offset seismic reflection data. One fundamental difference is that radar waves are polarized, while seismic waves are not. GPR waves travel at five orders of magnitude faster, with much shorter wavelengths (typically tens of centimeters rather tens of meters), than seismic waves. Traditionally, GPR data are collected with one transmitter and receiver antenna with a constant offset. Antennas may be unshielded or shielded to protect against electromagnetic interference. Recently new advances in resolution and positioning systems have allowed GPR surveys to become truly three-dimensional, enhancing subsurface visualization (Grasmueck et al, 2004; Grasmueck et al, 2005; Kadioglu, 2008).

8

GPR has been used in the karst of west-central Florida to identify sinkhole features with much success within the last two decades (Dobecki and Upchurch, 2006; Kruse et al, 2000; Kruse et al, 2006; Zisman et al, 2005). This methodology has also been used in other karst environments of the USA (Carpenter and Ekberg, 2006) as well as used in the karst of Jordan to identify sinkhole features (Batayneh et al, 2002). Most GPR profiles from regions of covered-kart terrain resolve the clay-rich material mantled on top of the karstified limestone bedrock. The conductive, clay-rich sediments attenuate the signal making it difficult to resolve structure beneath this mantle (Kruse et al, 2006). Even with this hindrance, GPR images of the topography of this mantled clay which can allow for a somewhat detailed analysis of the structure of the sinkhole depression. Another feature found in GPR profiles over some sinkholes are strong reflections from within a material-filling depression, most likely caused by the gradual infilling associated with sinkhole generation (Carpenter and Ekberg, 2006; Dobecki and Upchurch, 2006). On many occasions these infilling reflectors are present even when the depression itself is not, causing concern for interpretation of sinkhole structure based solely on infilling patterns that may not actually be related to sinkholes (Batayneh et al, 2002).

Truss et al (2005) imaged small dissolution sink features in Miami oolitic limestone with 3D GPR at various times during rainfall input to view their relevance as hydraulic conduits from the vadose zone to the lower surficial aquifer. The GPR profiles themselves show little in the way of conduit structure below the small depression. However, differences between "wet" and "dry" 3D data cubes helped the subsurface visualization greatly. Where water content changed the most (in the conduit) there were the greatest differences in wet and dry surfaces. Truss et al (2005) observed differences in

9

both the velocities and amplitudes. Their strategy is clearly successful in resolving flow concentrated in a conduit. However, it requires multiple surveys in wet and dry scenarios.

In this thesis, I address possible "single survey" methods for improved resolution of the "piping" or conduit structures below sinkhole depressions. Locating and imaging these structures could lead to improvements in interpretations of the current activity status of a sinkhole.

Proposed Strategies for Improved Sinkhole Resolution

This study begins with a simple attempt to understand the limitation traditional 2D surveys have for resolving sinkhole structure. Forward modeling is used to make simple model geometries to highlight the inaccuracies of 2D GPR profiles over three-dimensional features. These profiles are processed like typical 2D processing sequences, with and without migration. The results suggest that the 2D migration is unable to accurately reconstruct the structure of the three-dimensional model. Also, reflected energy from the conduit is mostly lost.

This thesis then addresses whether standard source and receiver survey geometries are optimal to resolve the difference in various structures of active sinkholes. A suite of non-traditional source and receiver survey geometries are in the modeling in order to understand if there is added value in using these types of surveys. The simple adjustment of traditional offset distance does not produce better results. Non-traditional survey geometries are proven to be as ineffective at accurately recovering reflective energy from the conduit and traditional spacing appear to be best suited even though they are limited.

10

Case studies of very high resolution 3D data of sinkholes and sinkhole-related features are shown. The data are processed using standard 3D processing methods, including 3D migration of the data. Sinkhole features from these profiles serve as examples to be compared to those of the simplified models. Results from these surveys show decent structural recovery of a small sinkhole similar in structure to that of the modeled ones. Indications of active subsidence and possible conduit structure are apparent from this data.

Finally, dense surveys serve as a benchmark to compare interpretations taken with the same surveys at lower spatial resolutions and profiles with 2D-only processing methods in order to understand errors in analysis and interpretation that are possible from 2D surveys. Two-dimensional surveys, 2D processed and migrated, show some similarity to the 3D results previously mentioned but contain more complexities and artifacts, which lead to poorer interpretation ability.

11

<center>**Modeling: Sinkhole Conduits as Difficult GPR Targets**</center>

Background Information

Numerical modeling of radar wave response to conduit structure is used to investigate optimal survey geometries and to understand artifacts of 2D profiling across 3D sinkholes. To apply this, thorough experimentation of the circumstance needs to be conducted. Numerical simulations should be conducted in three-dimensional model space and occupy volumes analogous to those of sinkhole with conduits, but simplified in order to capture first-order effects.

Radar waves are governed by Maxwell's equations. These four partial differential equations describe properties of electric and magnetic fields relative to their sources, specifically, current and charge densities (Fleisch, 2008). To model radar wave propagation these equations must be solved with respect to time and space. Simulating spatial volumes of geologic GPR surveys, including moving source and receiver, would take hundreds of hours of calculation time even with multi-core workstations. However, computational speeds permit simulations of limited numbers of transmissions.

One of the most popular computational solutions to Maxwell's equations is the finite-difference time-domain (FDTD) method (Yee, 1966; Taflove, 1980). FDTD modeling allows for conditionally stable, grid-based, and differential time-domain

<center>12</center>

numerical modeling. Given a specific dimension of unit space and a particular instance of time, Maxwell's equations may be solved with specified initial conditions and grid boundary conditions. The key to the model's ability to find realistic solutions lie in the discretization of time and space domains over which models are run.

In Yee's (1966) seminal work on FDTD methodology, he formulated what is now known as the Yee cell, which is the most basic space unit making up a multidimensional grid-based model space (see below). Key to the numerical effectiveness is the staggered positions at which electric (E) and magnetic (H) fields are calculated.
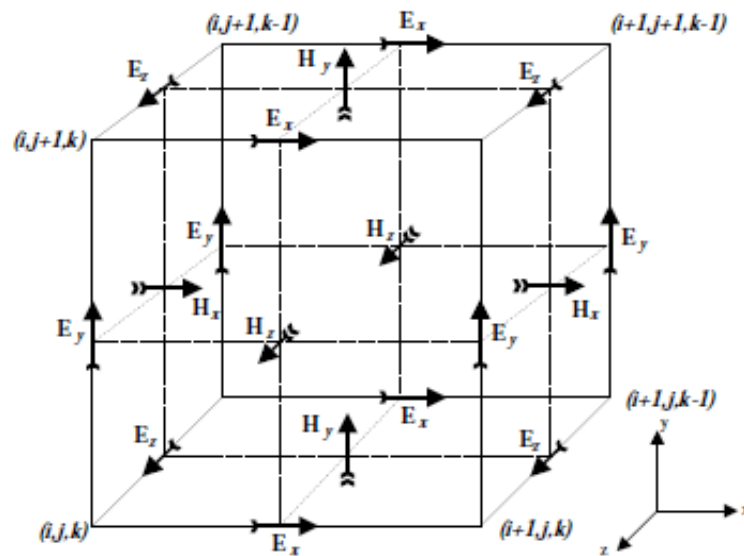
Figure 2.1. 3D FDTD Yee Cell showing electric and magnetic field directions (Yee, 1966).

In the standard Cartesian Yee cell, Maxwell's Equations may be solved in three or two dimensions at each time discretization step. In practice, almost any model geometry

13

with varying media can be specified but dipping contacts will have some "stair-case" edging at some level. Absorbing boundary conditions (ABCs) are applied to the outermost cells to ensure that the model space allows electromagnetic energy to propagate "through" the edge of the grid.

The freely available computer modeling program GPRMAX is a recently developed FDTD program specifically designed for GPR (Giannopoulos, 2005). The program allows users to produce realistic two or three dimensional models. The source code is written in C; the executable form of both of these programs may be used in Windows, Mac, or Linux operating systems installed on any standard personal computer. GPRMAX utilizes a command-line interface with ASCII text files as a means for model parameter and geometry input. The program allows users to introduce layers and shapes of almost any geologic material to be placed inside the parallelepiped model space of specified dimension. Radar transmitters and receivers can also be positioned anywhere in the model space. Repeated runs using the same model space can be performed to allow for the simulation of the typical moving scans of the transmitting and receiving antennas along a line, known as a common-offset gather. GPRMAX has been used to simulate shallow ice-covered features, rebar location in concrete structures, and dense non-aqueous phase liquids (DNAPLs) in groundwater (Brandt, 2006; Giannopoulos, 2005; Gerhard et al, 2008). Versions of the program (available from its author) allow it to access multiple processors (via OpenMP parallelization) for improved performance (Brandt, 2006).

Small conical sinkholes in covered karst terrain have diameters a few meters across at depths a few meters below the ground surface. They typically have

14

complementary depressions of sediments within them which possibly deepen as they approach the central conduit of the sinkhole. There may also be weathering layers of clay that line the top of the limestone (Parker, 1992).

Two basic models were designed to simulate simplified versions of such sinkholes. One model (Model A, seen in Figure 2.2a) contains a simple conical depression theoretically representative of a small inactive sinkhole. The other (Model B, seen in Figure 2.2b) is identical to the first model, but containing an added conduit structure that could exist in a more hydraulically active sinkhole. Models A and B have total space dimensions (xyz format, z being the depth axis) of 8.0 x 8.0 x 4.0 meters and 8.0 x 8.0 x 4.5 meters, respectively. The discretization of space (Yee cell size) in all three dimensions is set to 0.02 meter. This choice is appropriate because according to GPRMAX's rule of thumb (based on stability criterion proposed by Taflove [1980]), cell size should be at least ten times smaller than the smallest wavelength of the propagating electromagnetic field. A 250 MHz frequency antenna (common to geologic investigations of this scale) generates a wavelength of 0.12 m for velocities in saturated sediments. Models A and B are composed of more than 30 million Yee cells.

The basic geologic structure of both models, from the base up, is a block layer of clay 2.5 to 3.0 m in thickness (Figure 2.2). Above the clay is a 1.0 m thick sand surface horizon. Above the sand layer (ground level) is a 0.5 m thick layer of air. The sinkhole is simulated by a series of progressively-smaller thin cylinders to make a conical section. The cylinders are one Yee cell (0.02 m) in thickness. The cylinders are made of sand and start at the base of the sand layer and protrude into the clay layer below producing a three-dimensional conical breach of sand 2.0 meters deep and 4.0 meters across at the

15

top. The added conduit in Model B is introduced inside the original sand cone where its width is 1.0 m across and steeply descends another 1.0 m down into the clay. All GPRMAX model input text files are shown in Appendix A.

16
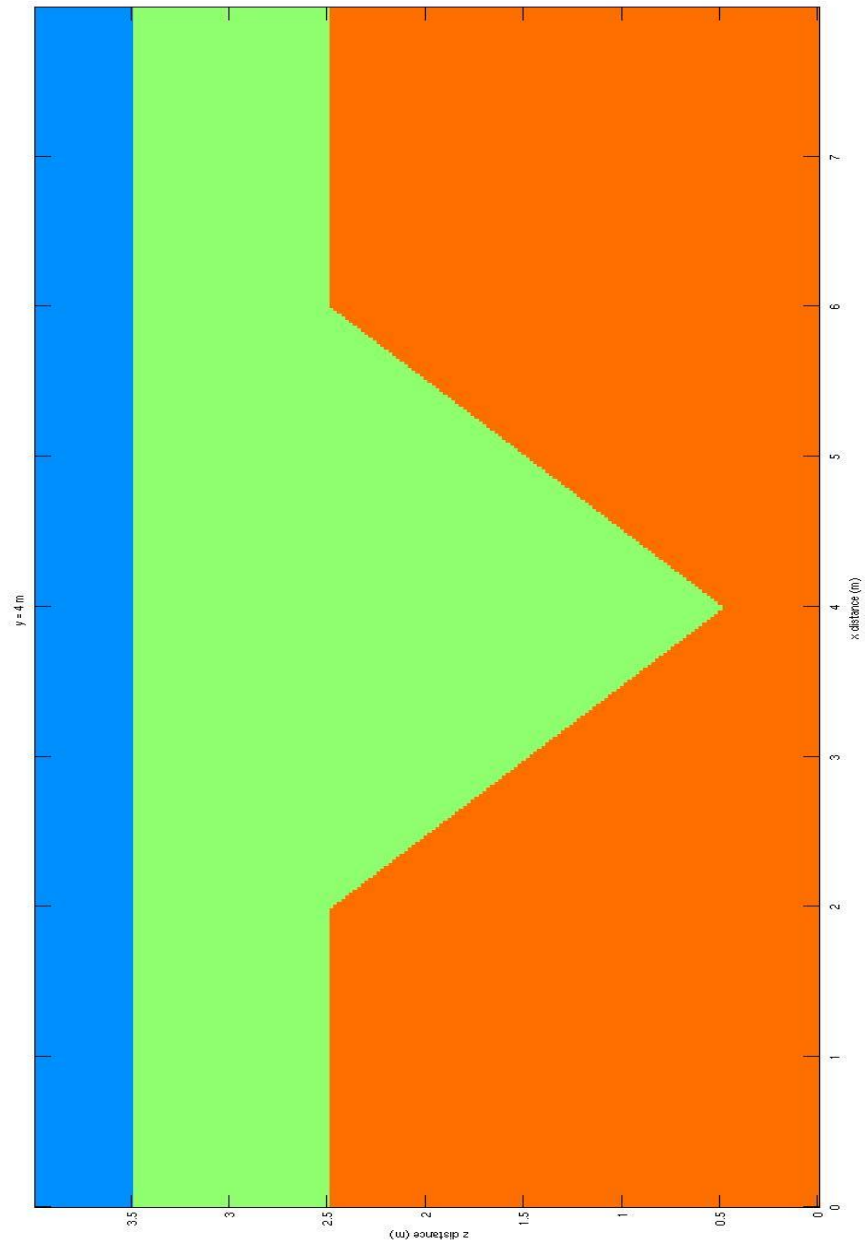
Figure 2.2a

Figure 2.2b
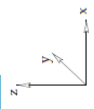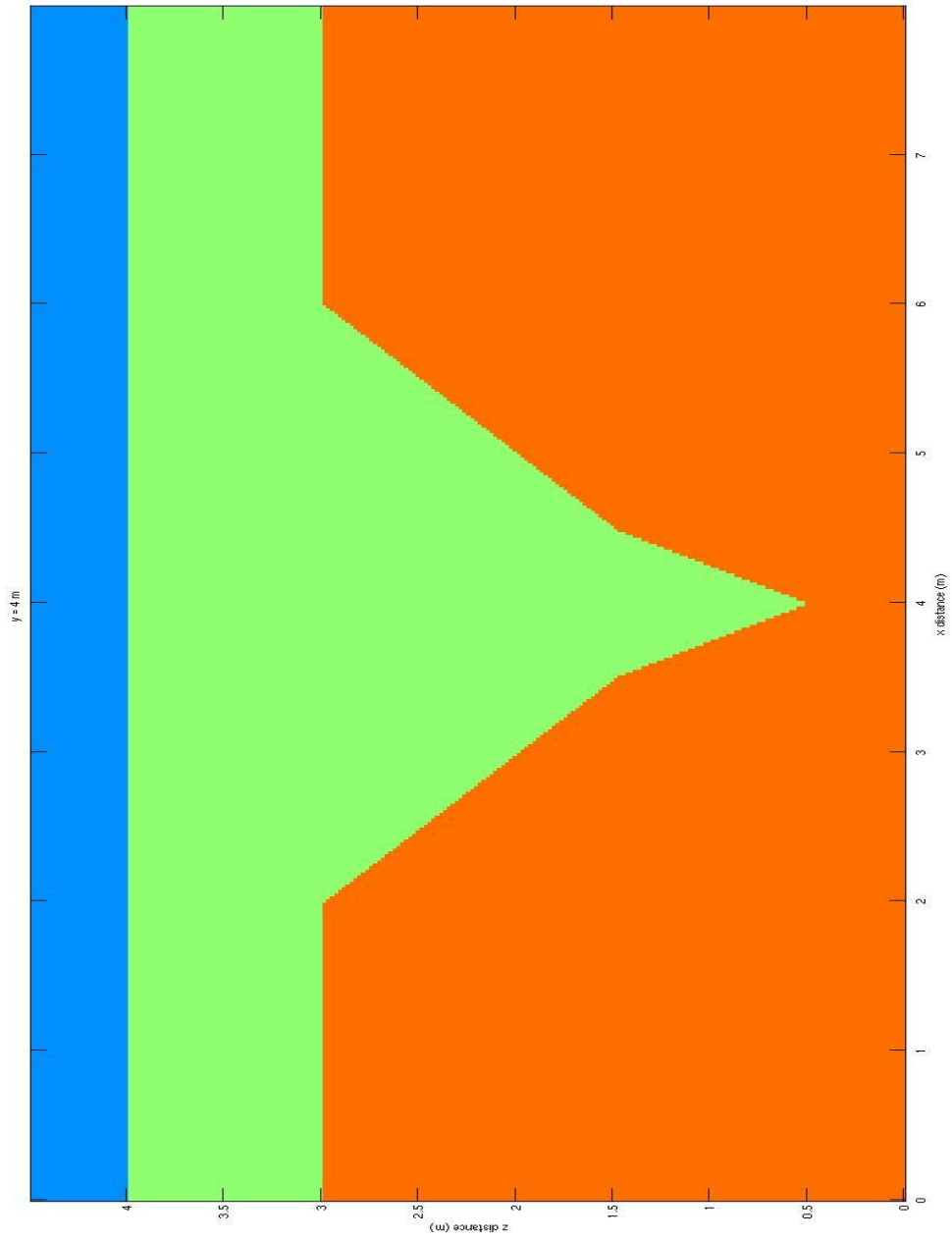
Figure 2.2a. Model A: Vertical slice through three-dimensional model space at midpoint (y=4.0m). Orange material represents clay; green, sand; and blue, free space. Values for distance given as model coordinate values where (0.0, 0.0, 0.0) represents lower left forward-most point and (8.0, 8.0, 4.0) is the upper right back-most point in the model space.

Figure 2.2b. Model B: Vertical slice through three-dimensional model space at midpoint (y=4.0 m). Orange material represents clay; green, sand; and blue, free space. Values for distance given as model coordinate values where (0.0, 0.0, 0.0) represents lower left forward-most point and (8.0, 8.0, 4.5) is the upper right back-most point in the model space. The MATLAB codes used to create these figures and all others in this work, unless otherwise specified, may be found in Appendix B.

The physical parameters used for sand are 9.0 for the DC (static) relative permittivity, 0.005 Siemens/m for the DC (static) conductivity, and 1.0 for the relative magnetic permeability. The physical parameters used for clay are 25.0 for the DC (static) relative magnetic permittivity, 0.05 Siemens/m for the DC (static) conductivity, and 1.0 for the relative magnetic permeability. The values for the air layer are those of free space. Limestone, although the basis for sinkhole genesis, is not used in the modeling because the GPR waves rarely penetrate past the clay layer as they attenuate almost completely in the clay before reaching the limestone reflecting surface.

The antenna specifications chosen for the models are a reasonable approximation of a 250 MHz shielded antenna. In the GPRMAX program this is chosen by selecting

19

model parameters of a Hertzian dipole with unit amplitude (1.0) and a center frequency of a Ricker wavelet of 250 MHz. This command technically simulates an infinitesimal dipole (although it does have a very small, but not nearly infinitesimal in length) which is not exactly used in shielded systems but allows a decent approximation nonetheless. Polarization directions may either be in x or y orientations. In this particular model the polarization is in the x-direction. The total transmitting time was set so that the two-way travel time for radar waves propagating from one end of the surface to the bottom of the conical depression of sand could be recorded. The total recording time was 100 nanoseconds (ns) for Model A and 120 ns for Model B. When working in the time domain, the time iteration of the model is governed by the discretization of space so it cannot be independently assigned. Rather, for the FDTD method to be conditionally stable numerically, it must satisfy the Courant, Fredrichs, and Lewy (CFL) condition (see below).

$$\Delta t \leq \frac{1}{c\sqrt{\frac{1}{(\Delta x)^2} + \frac{1}{(\Delta y)^2} + \frac{1}{(\Delta z)^2}}}$$

Equation 2.1. The CFL condition, where *c* is the speed of light and *t* is the time discretization based on the values of the space discretization in the *x*, *y*, and *z* directions.

In this particular model case, the time discretization is approximately 38.5 picoseconds (ps) given a space discretization of 0.02 meters. Using this time step, 2597 iterations for Model A and 3116 iterations for Model B are required for each transmitter

20

location. In order to acquire GPR trace imaging along the lines of realistic surveying, model runs must be repeated, moving transmitting and receiving antennas (spaced 0.3 m apart) pair almost 150 times at 0.04 m increments to simulate a transect crossing the sinkhole.

To simulate a single profile, this required solving Maxwell's Equations in three dimensions for each of the approximately 30 million cells for each iteration at each transmitting location. A single processor (~2.5 GHz) on a computer requires over a month of total run time. Also, the amount of memory (Random Access Memory, RAM) required for the model to run was about 700-1500 Megabytes (Mb) in size. Total binary output files sizes for models could be anywhere in size from a few hundred Mb to tens of Gigabytes (Gb), depending on the number of receivers included in the model. Fortunately, by utilizing the Open MP commands built into the source code of GPRMAX and recompiling the program, GPRMAX could be used with many more processors to speed up run times for the models. Using a desktop workstation containing dual CPU sockets with Quad-core processors (for a total of 8 processors) and 16 Gb of RAM, run times for acquired profiles were shortened from over a month to about four to five days.

21

Standard 2D Geometry Survey

Here we examine what users may miss or misinterpret with 2D profiling and data processing over conical sinkholes. Models were simulated in both 2D and 3D versions of models A and B (see Figure 2.2), utilizing the same parameters as those described in the previous section. All of the model results were processed as typical field GPR data would be treated using the software package ReflexW (Sandmeier). This package allows for standard 2D and 3D data processing including filtering, statics, gaining, and migration. Although GPRMAX outputs results of the six components of the electromagnetic fields (Ex, Ey, Ez, Hx, Hy, and Hz) as well as the currents (Ix, Iy, and Iz) calculated as the curl of the magnetic fields at each electric field location, only the Ex values are used for processing. These values are the same as those collected in the field with both standard shielded antennas oriented in the x-direction while recording along the y-direction. Examples of unprocessed Ex, Ey, and Ez field data for 3D model A can be compared in Figures 2.3a, 2.3b, and 2.3c.

22

Figure 2.3a

Figure 2.3b

23

Figure 2.3c

Ez
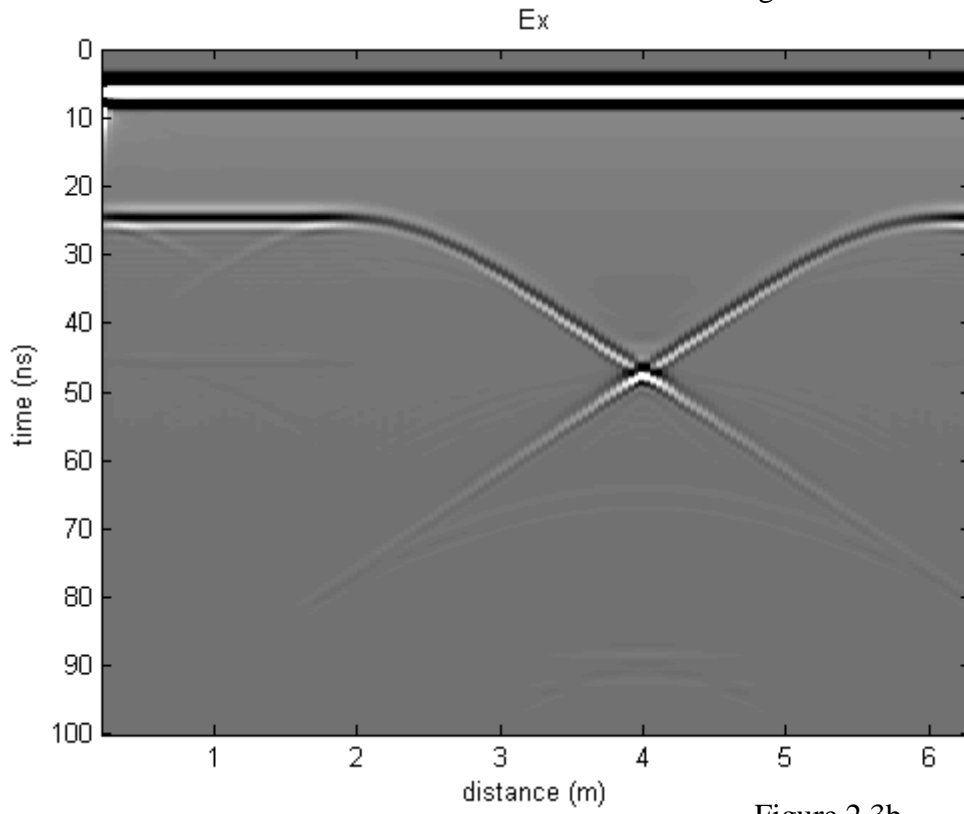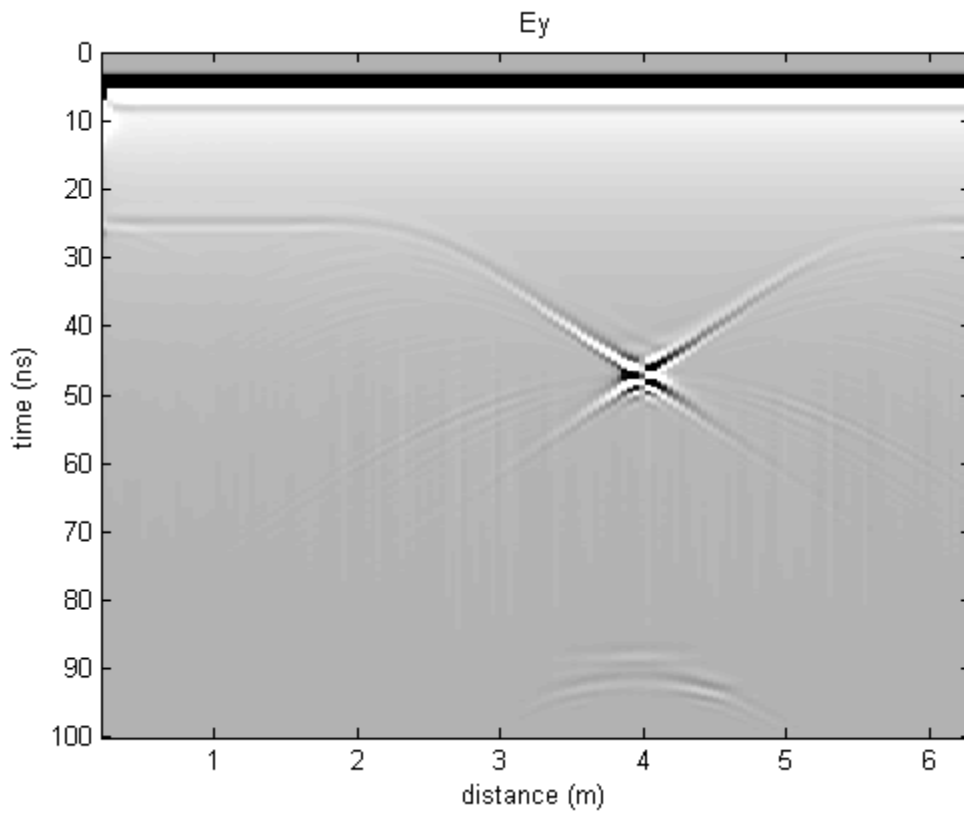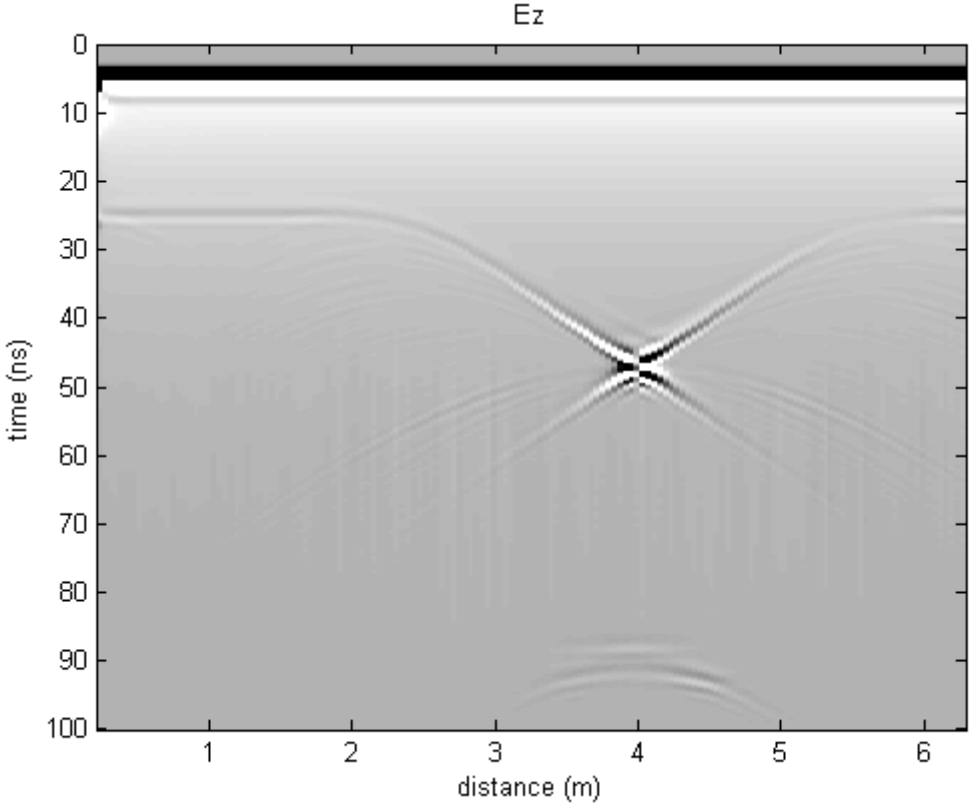
Figure 2.3a. This is an example of unprocessed results from 3D model A Ex field data. Time in ns is given on the y-axis (z-axis in model coordinates) and distance along the simulated survey line is given in m along the x-axis (y-axis in model coordinates) for all three figures.

Figure 2.3b. This is an example of unprocessed results from 3D model A Ey field data.

Figure 2.3c. This is an example of unprocessed results from 3D model A Ez field data. Notice that the Ex field having a particularly strong and symmetric signal over the other fields, making it the choice field of study.

It is clear that 2D profiles will record out-of-plane features from 3D structures. We also seek to understand artifacts associated with 2D migrations of out-of-plane features. Here, the raw profiles over 2D and 3D models are shown (Figures 2.4-2.7), along with the results of 2D migrations of each. All of the 2D and 3D models generally produce similar synthetic profiles. When the 2D model A data are migrated (diffraction stack, time-to-depth conversion of 0.1 m/ns), it produces an image that perfectly mimics the model geometry it is given (Figure 2.4b). This confirms that the 2D migration process is robust for this 2D geometry. However, it is clear that there are artifacts associated with the 2D migration of the 3D structure (Figure 2.5b). These artifacts are associated with features outside the viewing plane and the 3D nature of the wave, in this case, the side of the conical sink. The 3D results of model A give an unexpected curvature through an area at about the middle of the conical area of the modeled sinkhole (Figure 2.5b), which are the implied out-of-plane effects of the conical sinkhole. The bottom of the sinkhole

25

feature is still visible and able to be located as in the 2D migrated results. However, there are also some unexplained strong reflecting artifacts below the sinkhole feature, which may be complex wave reflections. Both the 2D and 3D pre-migrated results of model B look very similar to those of model A's (Figures 2.4a & 2.5a) except that they are slightly more 'noisy' in appearance, most likely from numerical artifacts associated with the GPRMAX simulation (see Figures 2.6a & 2.7a). The reason for the increase in noise level in model B simulations is not clear. The migrated results of the 2D model B resemble those of model A's in that there is the same basic larger depression, but the added conduit in model B (Figure 2.6b) appears as a loss of reflected energy and imperfectly migrated weak returns. The migrated results of the 3D model B data look similar to the 3D model A's data in that there is the same conical out-of-plane artifact and basic depression expected (Figure 2.7b). There is also a loss in the reflective energy at the mouths of the conduit. It is clear from these simple models that out-of-plane returns can dominate 2D profile and introduce significant artifacts during migration. Acquiring data in three dimensions is a necessary step in improved sinkhole structure imaging.

26

Figure 2.4a

DEPTH [METER] at v=0.1[m/s]

Figure 2.5a

DEPTH [METER] at v=0.1[m/s]

29
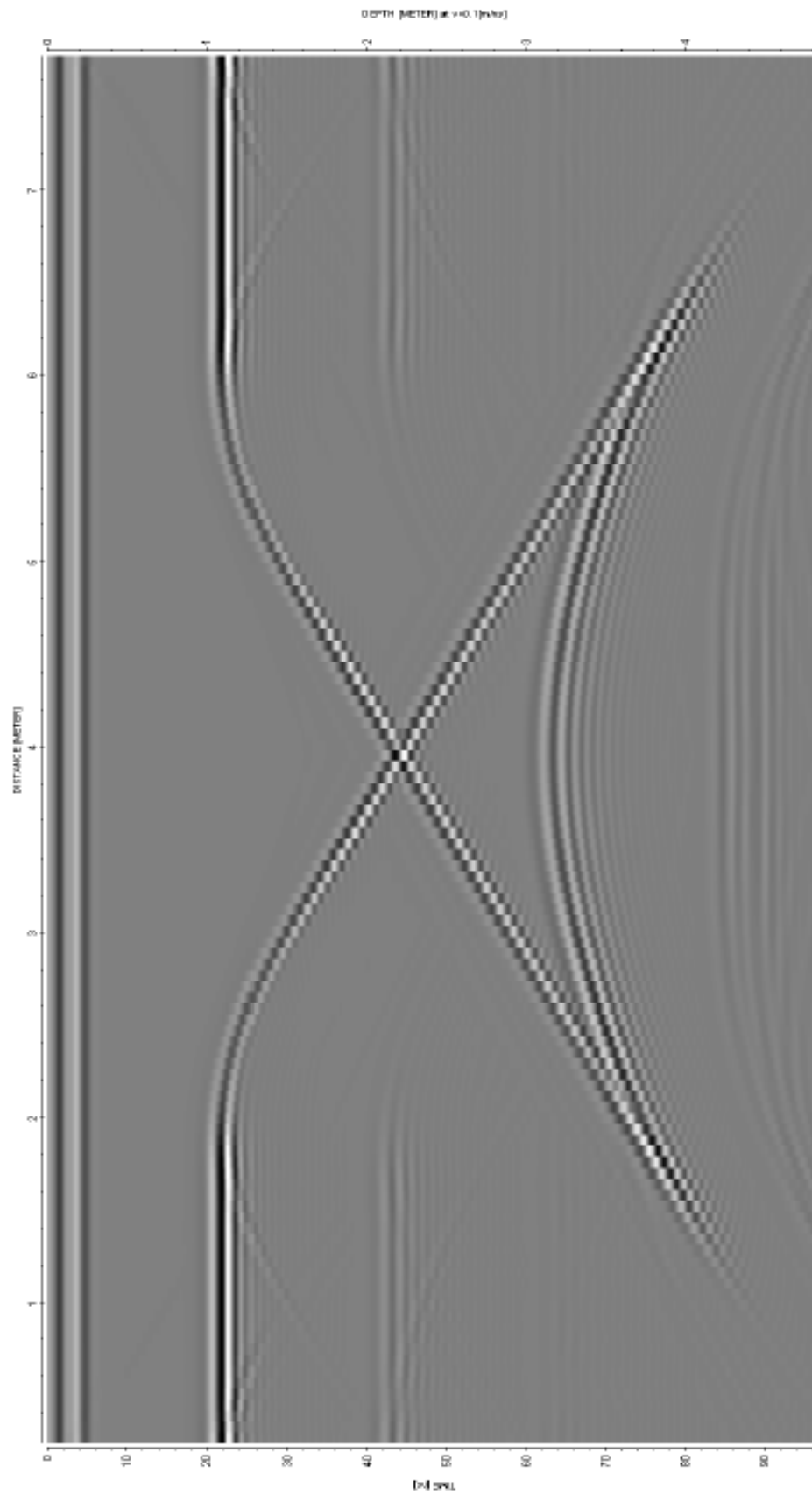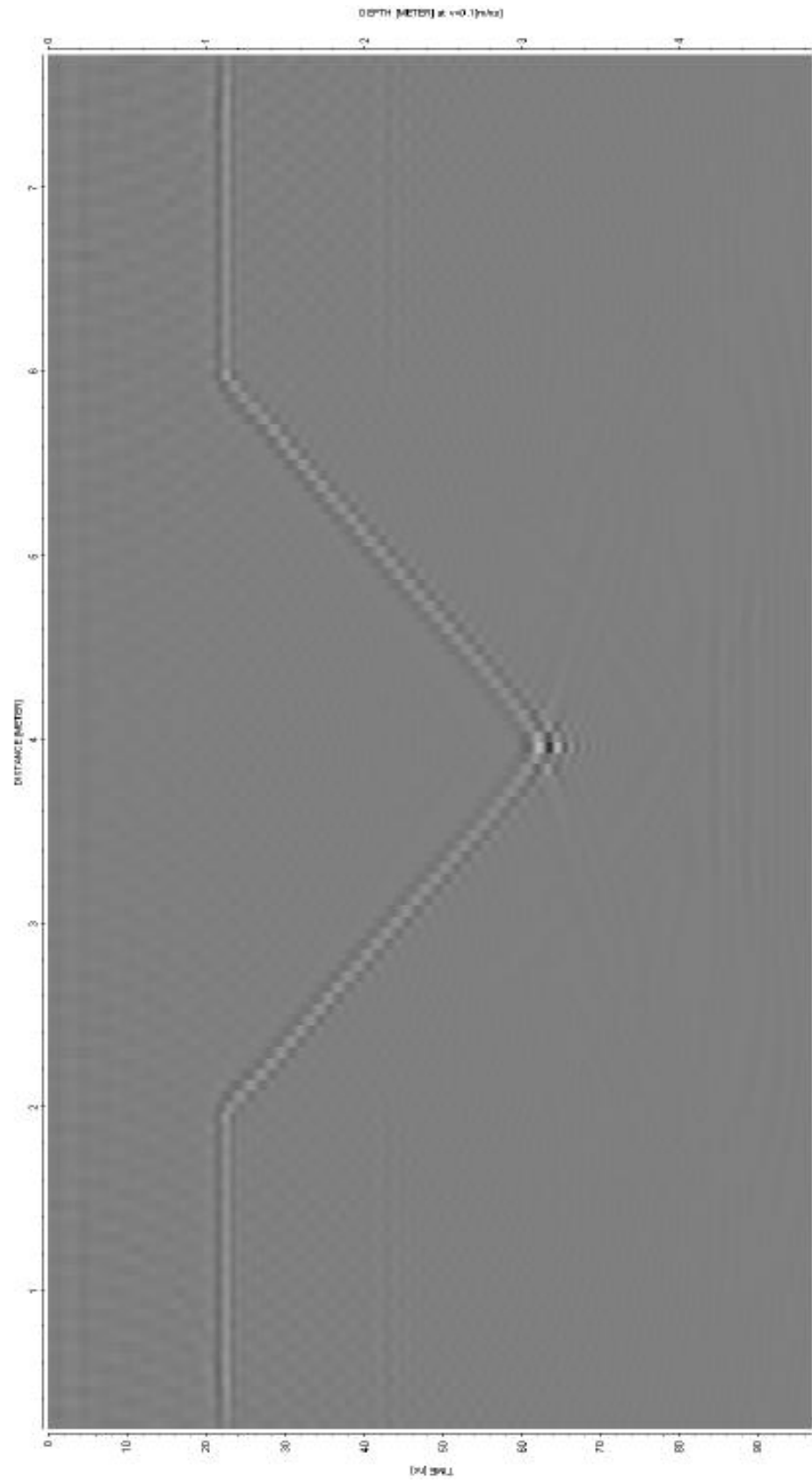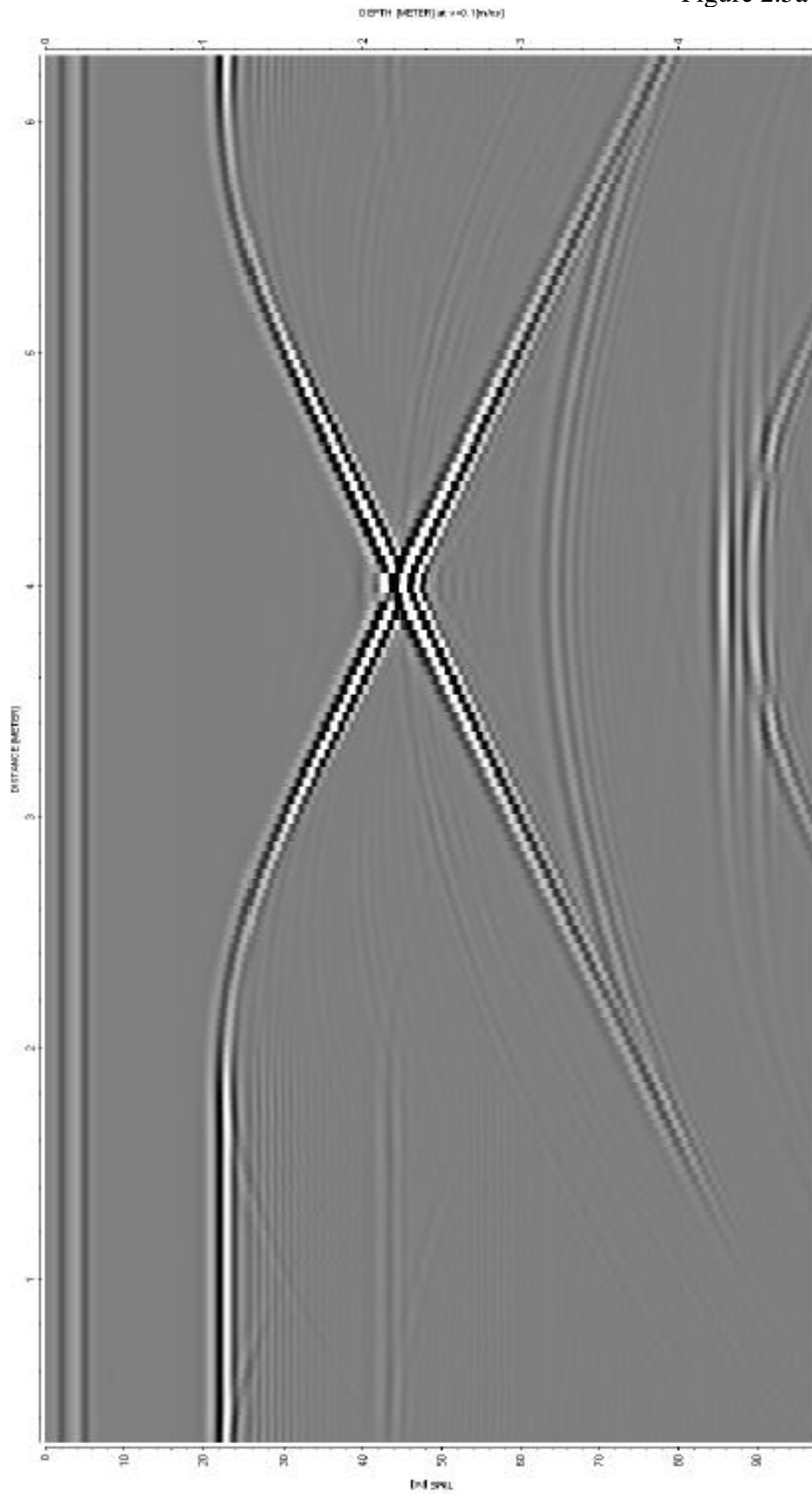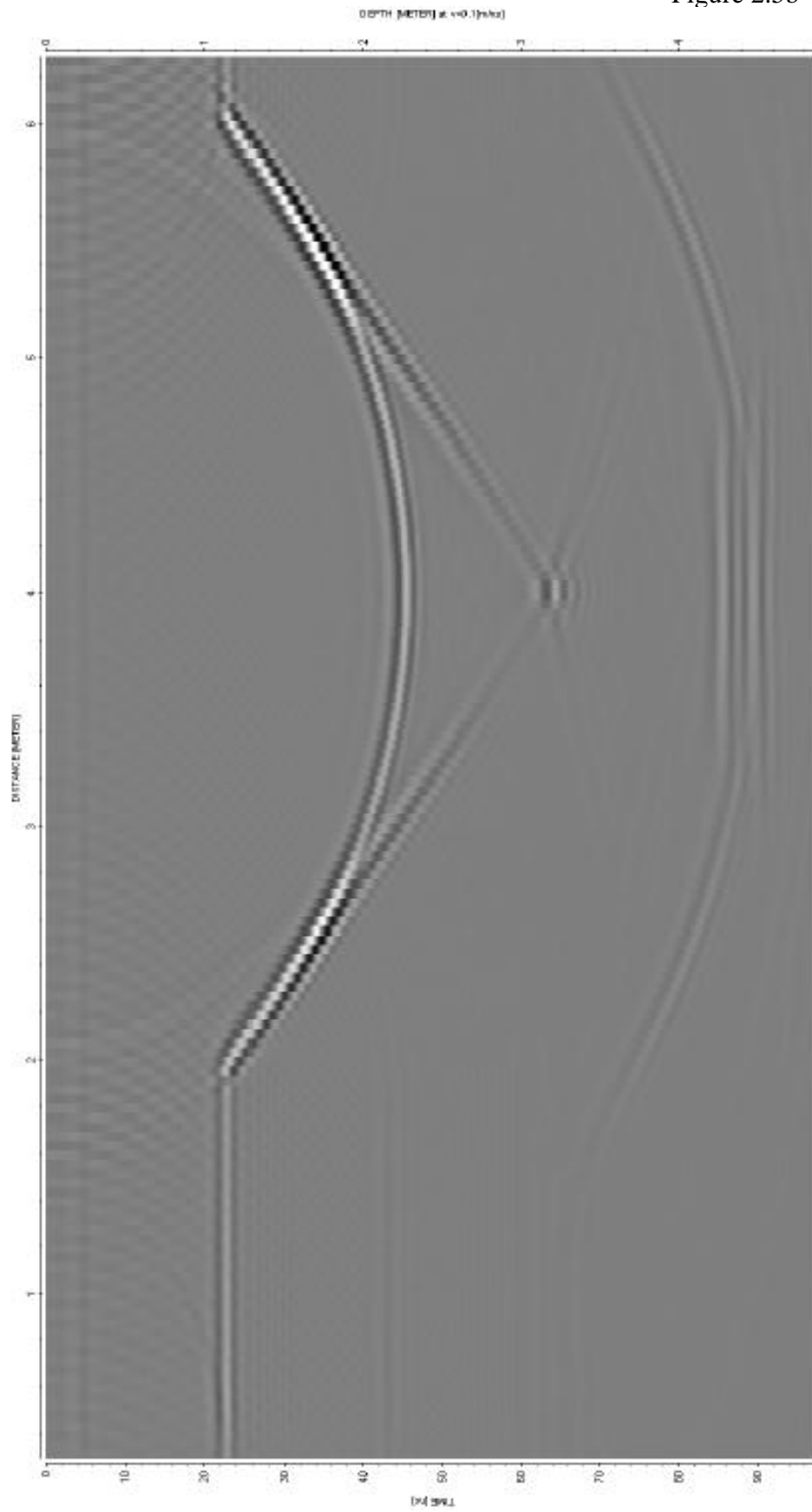
Figure 2.5b
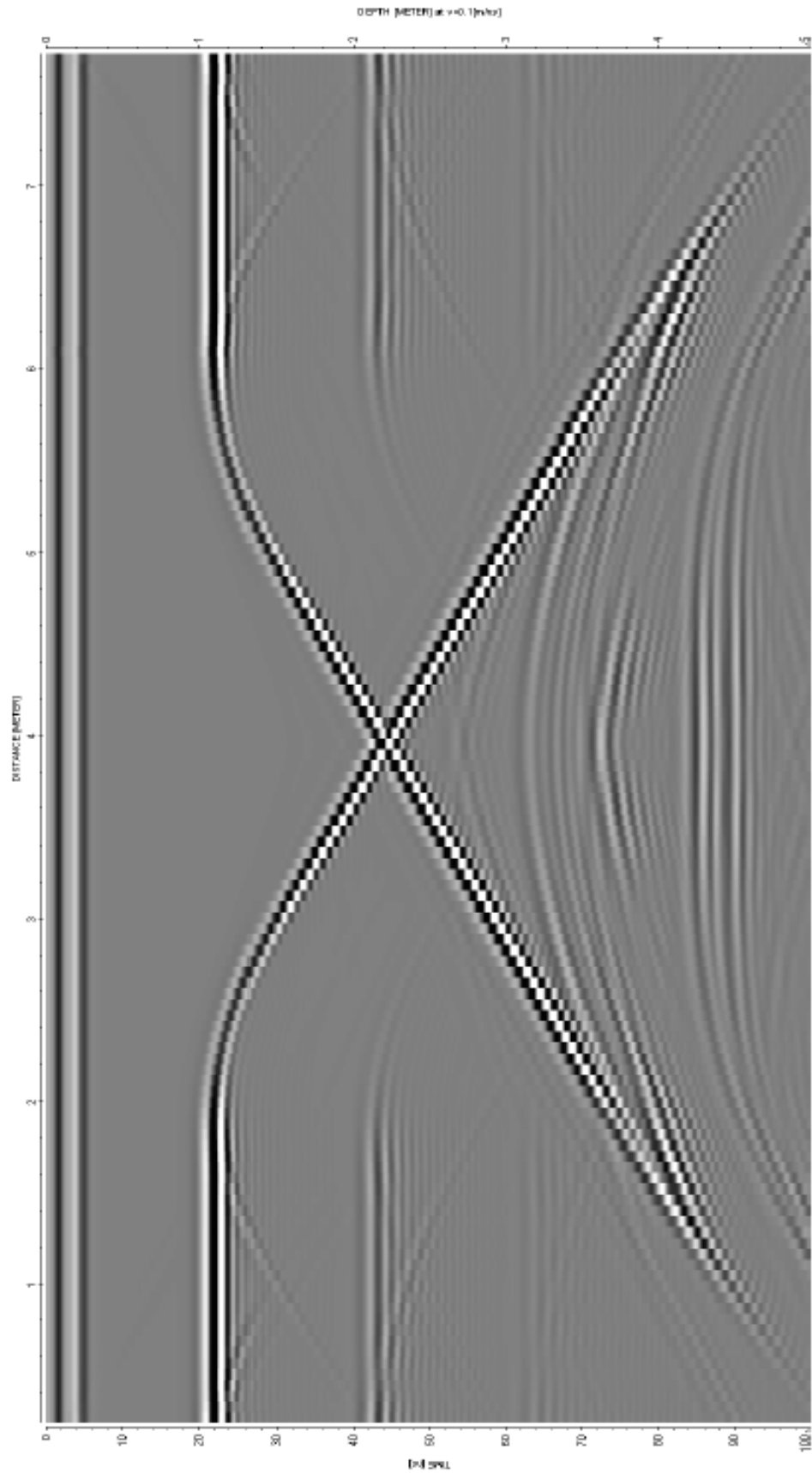
Figure 2.6a

Figure 2.6b
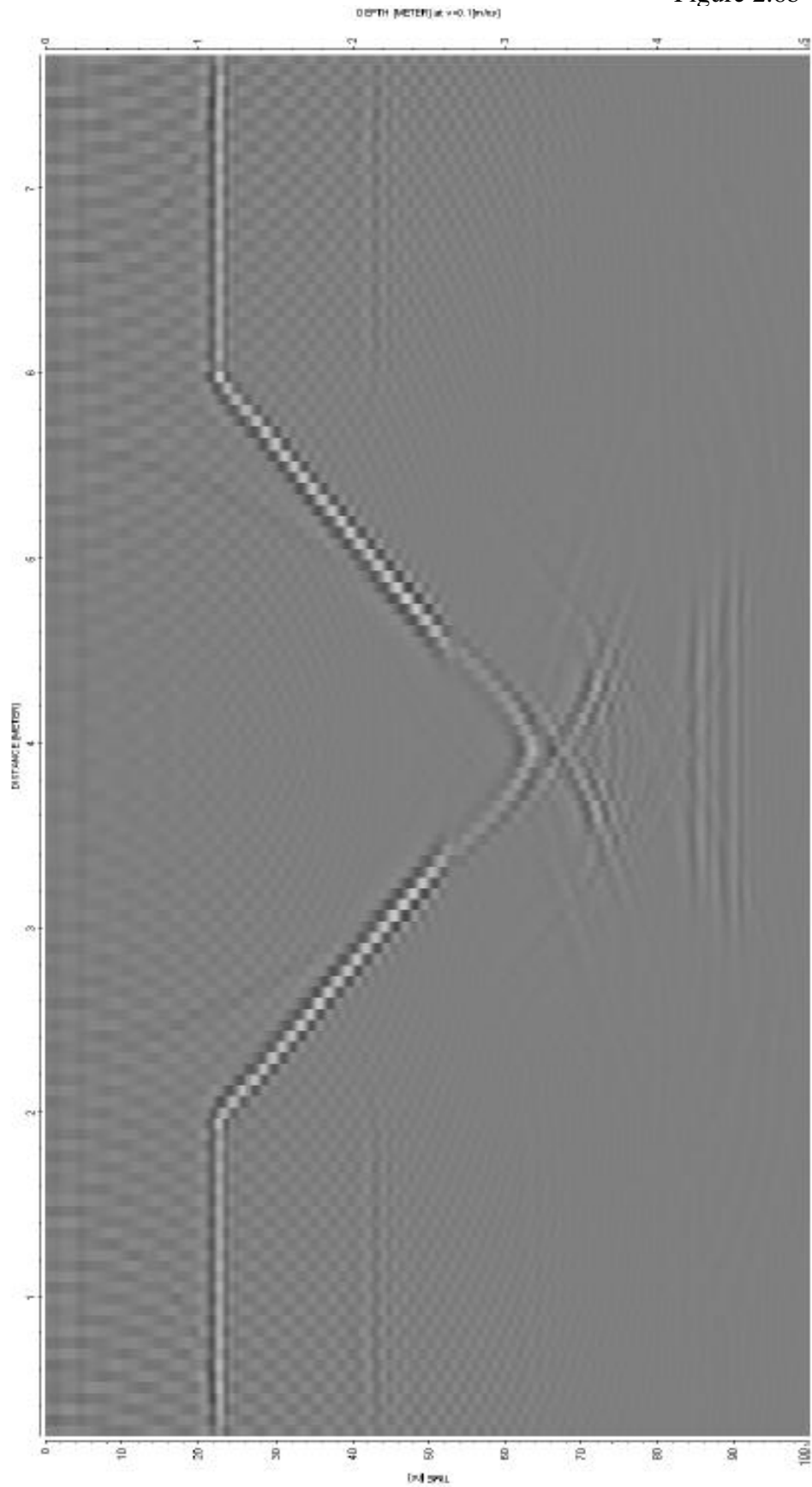
Figure 2.7a
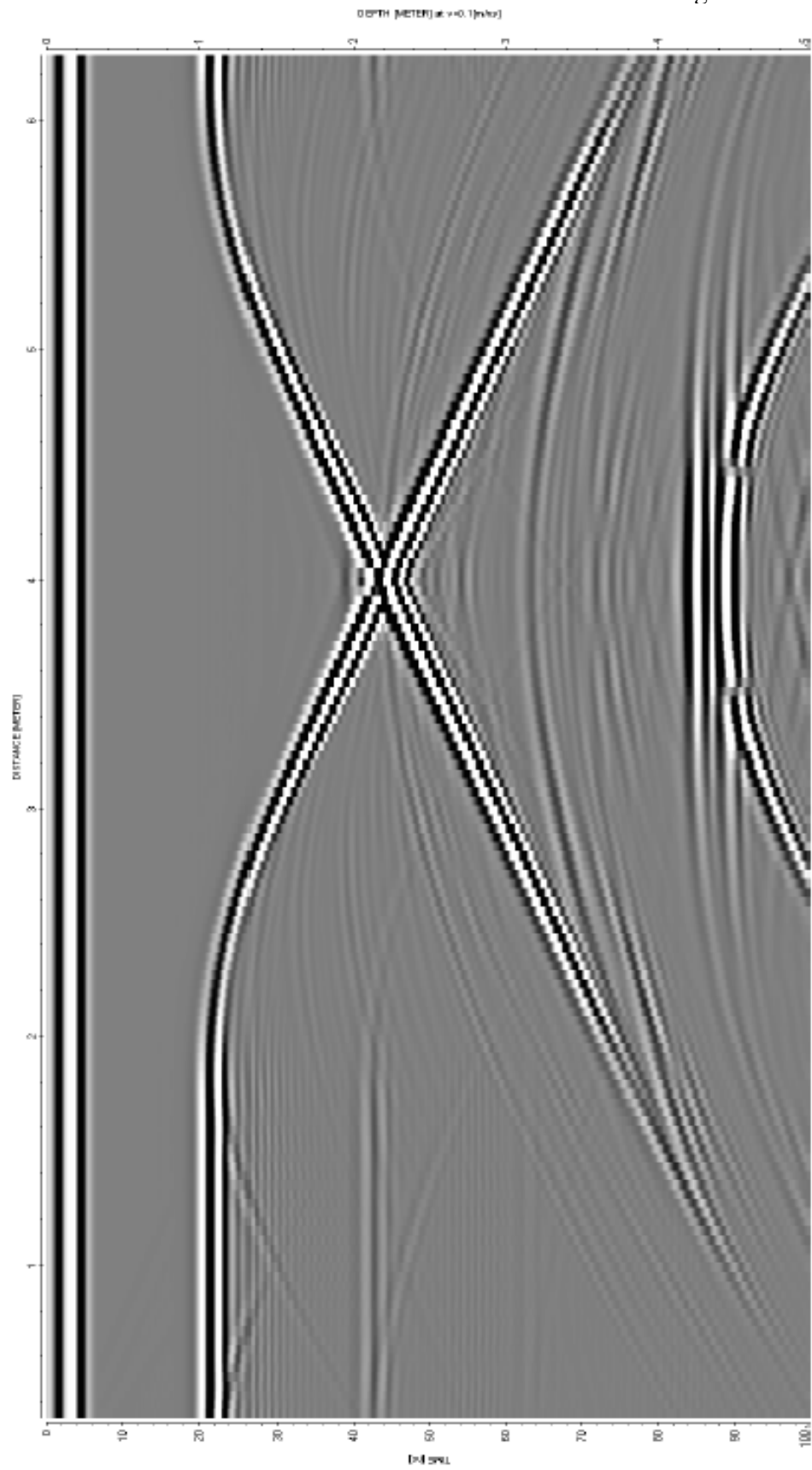
Figure 2.7b
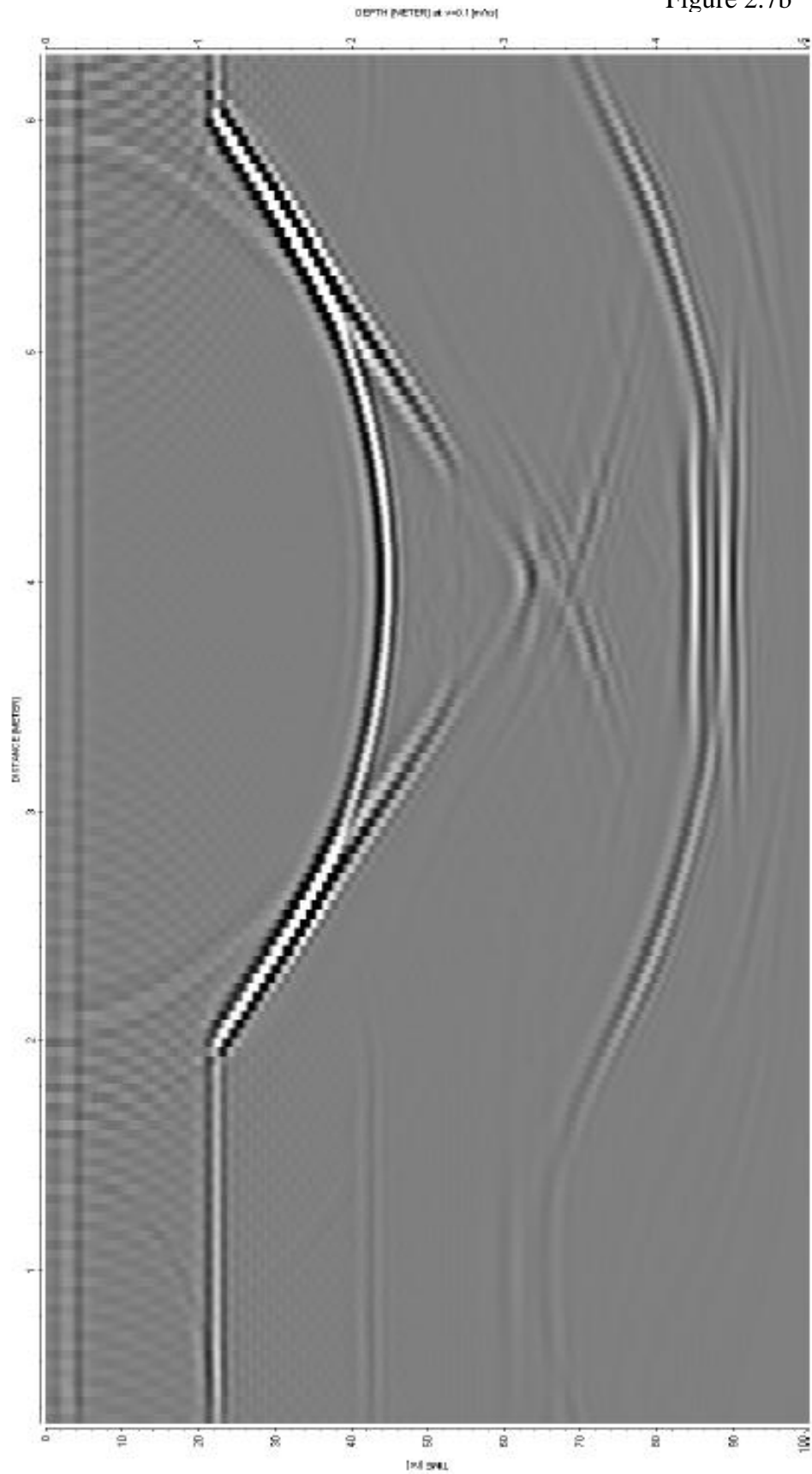
Note on previous figures: All model data was processed with custom static and gain filters. The diffraction stack migration (2D) used a constant time-to-depth conversion of 0.1 m/ns. All these figures have both a time axis (y-axis) in ns and a secondary y-axis with depth (conversion 0.1 m/ns). Also, all common-offset spacings are 0.3 meters.

Figure 2.4a. Model A 2D results processed and displayed as profile; unmigrated.

Figure 2.4b. Model A 2D results processed and displayed as profile; migrated.

Figure 2.5a. Model A 3D results processed and displayed as profile; unmigrated.

Figure 2.5b. Model A 3D results processed and displayed as profile; migrated.

Figure 2.6a. Model B 2D results processed and displayed as profile; unmigrated.

Figure 2.6b. Model B 2D results processed and displayed as profile; migrated.

Figure 2.7a. Model B 3D results processed and displayed as profile; unmigrated.

Figure 2.7b. Model B 3D results processed and displayed as profile; migrated.

To see whether non-traditional transmitter-receiver offsets might better resolve conduit geometry, model B was run with one transmitter that moved along the center line of the simulated sinkhole. As discussed previously, there was also a receiver at a fixed distance (0.3 m) from the transmitter, also along the same survey line. In addition to this initial receiver, 15 others were placed in line spaced at 0.1 m intervals. This spacing can simulate various offsets for common-offset surveys. Specific intervals used for comparison were the 0.3, 1.0, and 1.8 m offset spacings. Comparison of the unprocessed results of each of these offset lengths may be seen in Figures 2.8a-c. It can be seen that there is not much initial difference among these three unprocessed profiles. In order to

35

understand the differences that could occur, the modeling results must be processed, including migration. Only the maximum and minimum offset spacing were used to observe the greatest difference in varying the offset. The processed results (both migrated and unmigrated) of the minimum 0.3 m offset spacing were previously displayed in Figures 2.7a and 2.7b.

Figure 2.8a

Figure 2.8b

37

Figure 2.8c

offset = 1.8 m
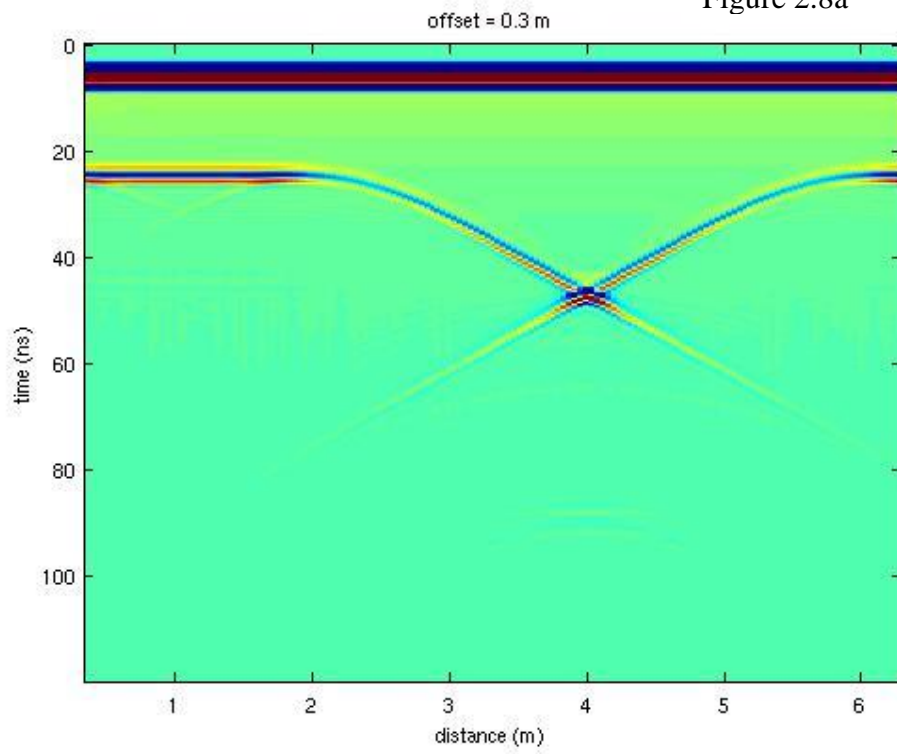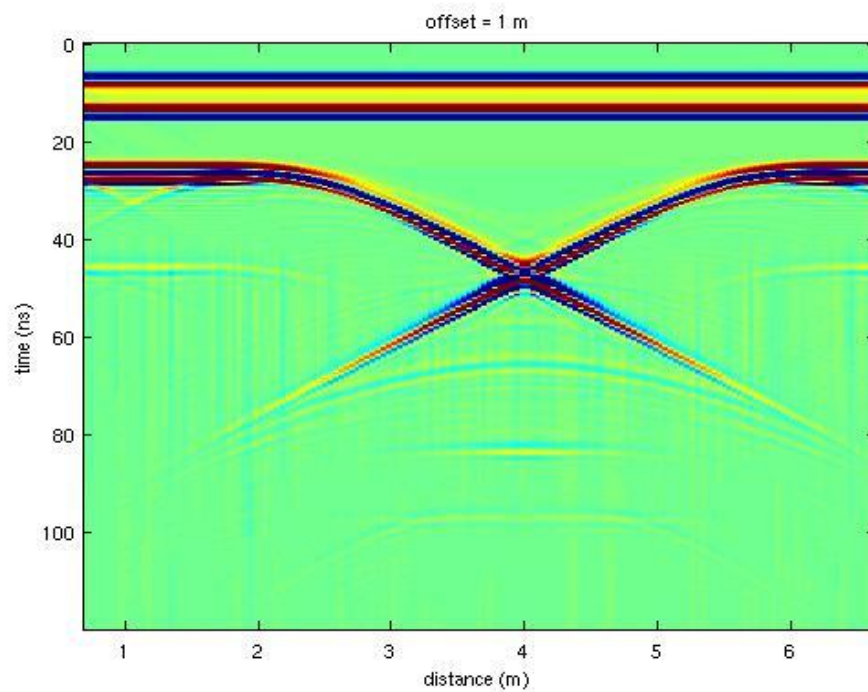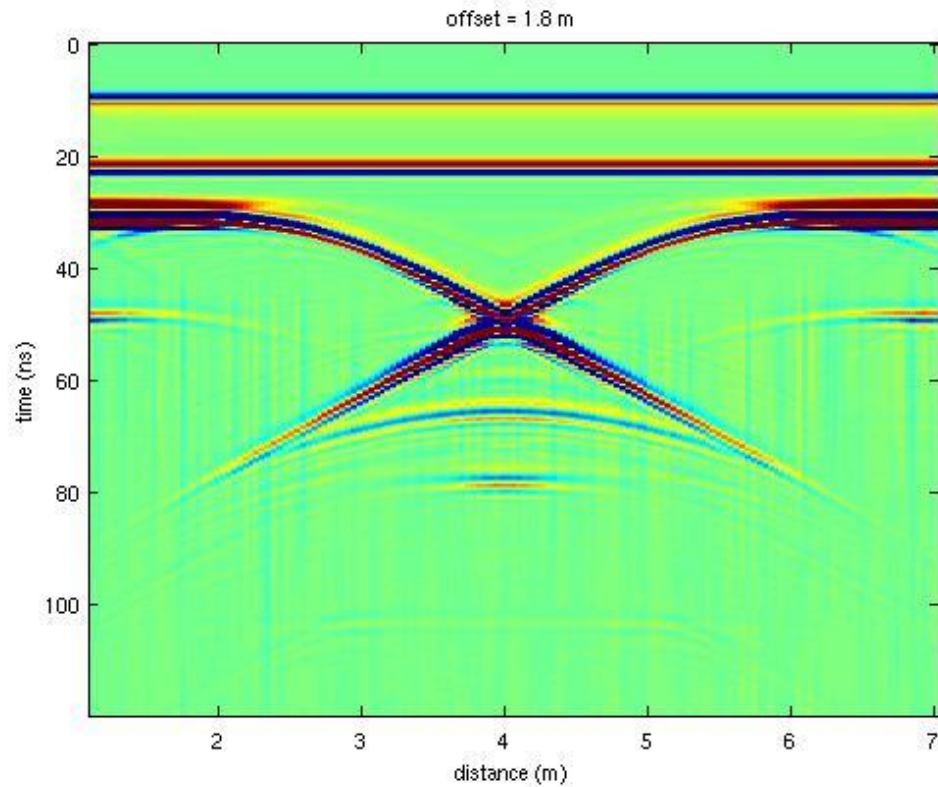
Figure 2.8a. Top, previous page. Model B 3D unprocessed results with 0.3 m common offset.

Figure 2.8b. Bottom, previous page. Model B 3D unprocessed results with 1.0 m common offset.

Figure 2.8c. Top, current page. Model B 3D unprocessed results with 1.8 m common offset.

Note: in constructing the profiles the length of the obtainable profile decreases as the offset spacing increases. Also, increasing offset distance increases travel time for reflections. These two things account for the greatest discrepancies in similarity of the figures.

Figure 2.9a

DEPTH [METER] at v=0.1[m/n]

Figure 2.9b

DISTANCE [METER]

TIME [x]

40
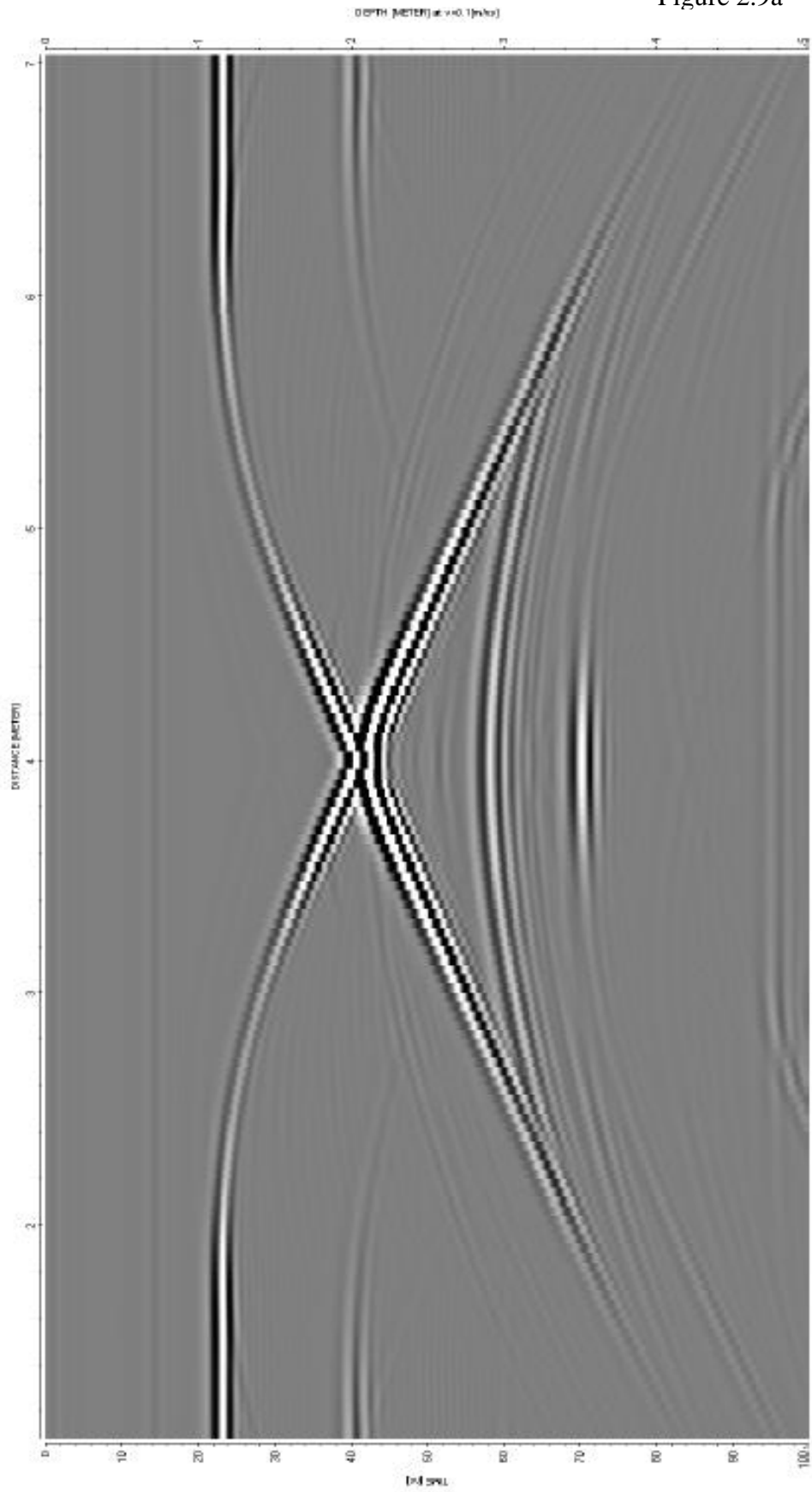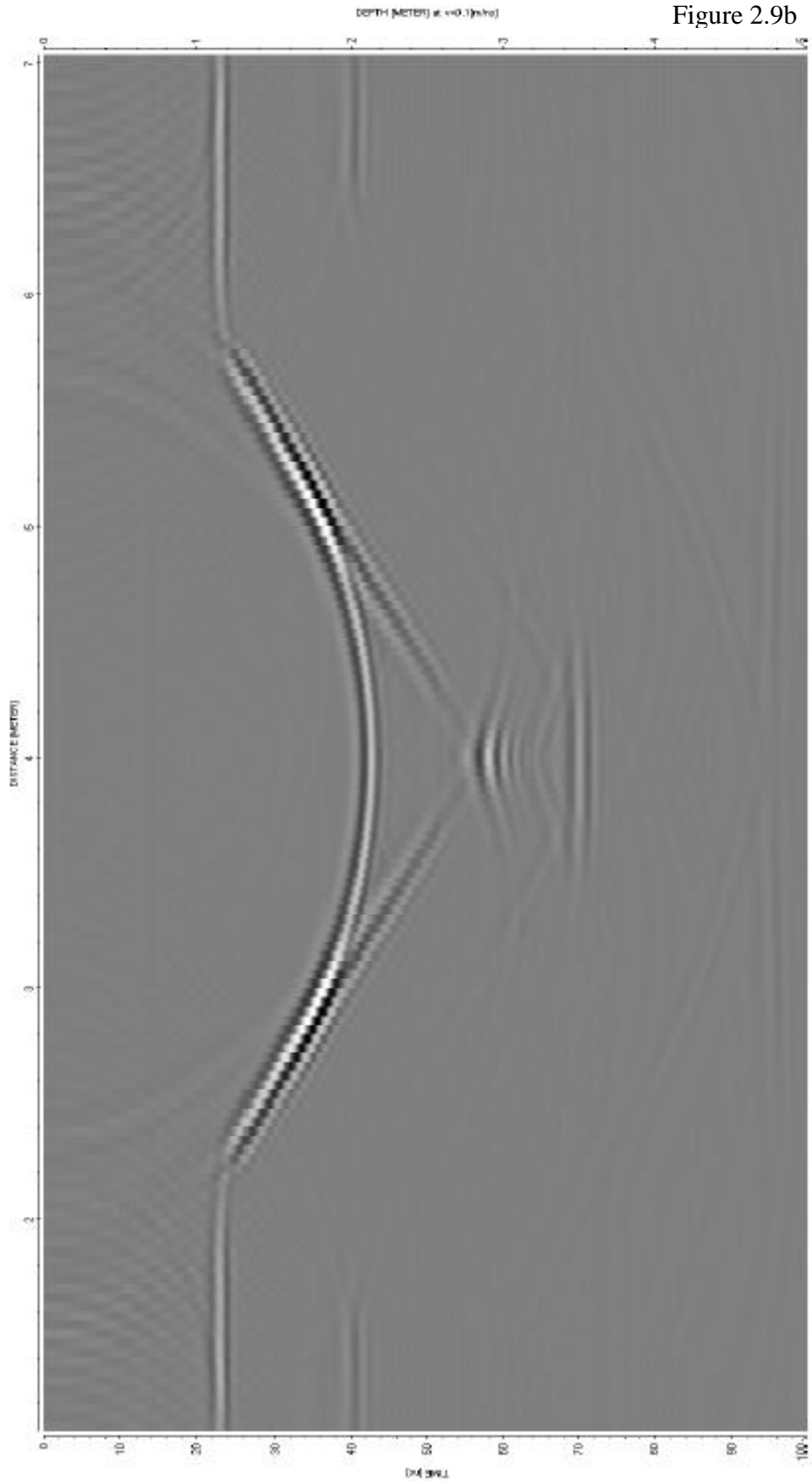
Figure 2.9a. Model B 3D results processed and displayed as profile; unmigrated.

Figure 2.9b. Model B 3D results processed and displayed as profile; migrated.

Both figures have a common-offset spacing of 1.8 m and Figure 2.9b was

diffraction-stack migrated with a constant time-to-depth conversion of 0.1 m/ns.

The processed results (both migrated and unmigrated) of the maximum 1.8 m offset spacing are displayed in Figures 2.9a&b.

In comparison, the two different offsets give similar profiles but are definitely not the same. It is clear from the processed results that the shorter offset has a better signal strength than the wider offset. This is most likely due to there being a more direct return of reflected energy to the receiver than if traveling on a longer path. Also, the reflection coefficient depends on the angle of incidence. The migrated results suggest that the shorter offset will allow for better reconstruction of a subsurface depression. The shorter offset also gives a stronger return of artifacts below the sand-clay interface. The wider offset has an overall weaker return on reflected energy, which is an expected result of the longer travel path through matter. What was not expected was the anomalous pattern of reflected energy where the conduit should exist. The larger offsets were no better than traditional smaller ones at reconstructing the steep, narrow conduit geometry of the model.

In order to gain better insight into how radar energy propagates and reflects inside the model space, a 3D method similar to 2D ray tracing was employed. GPRMAX allows its user the ability to save model volume information at specified time instants, known as snapshots. Specifying many snapshots over time allows for detailed analysis of the radar

41

wave as it propagates through the media similar to ray tracing methods. This type of analysis is useful for understanding how the radar energy interacts with the narrow conduit geometry at the base of the modeled sinkhole. This process could be useful for understanding which receiver positions would record the strongest reflected energy from the conduit and interpreting the profiles.

One arbitrary transmission location (specifically at [4.5,4.0,4.0]) was chosen from the simulated survey line (center-line) from model B. Snapshots were collected from 5 ns to 120 ns at 5 ns intervals and can be viewed in three orthogonal planes. These snapshots may be compared directly to Figure 2.9a&b's profile at 4.8 meters (4.5 m plus 0.3 m spacing). Shown following this section are snapshots at 20 to 70 ns (Figures 2.10abc- 2.20abc). Following the initial contacts of the first reflections on the larger depression, the radar waves begin to enter the conduit structure after 30 nanoseconds (Figure 2.12ab). The energy as it enters the conduit, is sharply diminished (Figure 2.13ab). Most of the returned energy that is received is from the slope-break at the neck of the conduit (Figure 2.14ab), which is why the record indicates no conduit but a weak-bottomed basic-form depression (Figure 2.7ab). For the remaining time record, reflection multiples can be clearly seen but none of which seem to originate from the conduit structure. These later- time intervals are useful for identifying strong reflections after first arrivals seen in Figure 2.7ab. The snapshot function demonstrates that no direct or indirect returns from the conduit boundary arrive at the surface.

42

Figure 2.10a

Ex at x=3.5m

Figure 2.10b

Ex at y=3.9m

43

Figure 2.10c

Ex at z=3.5m
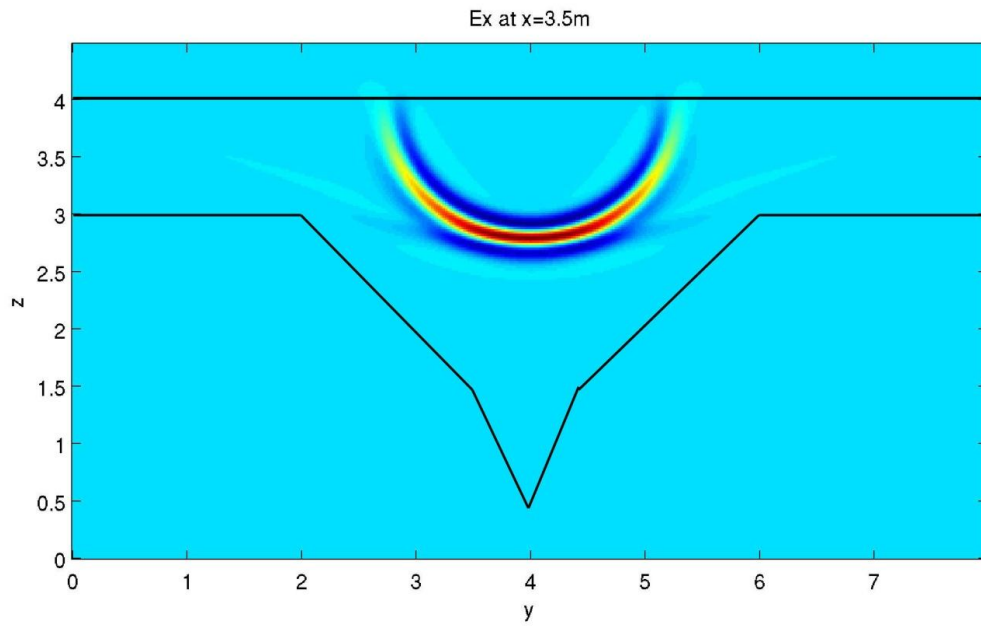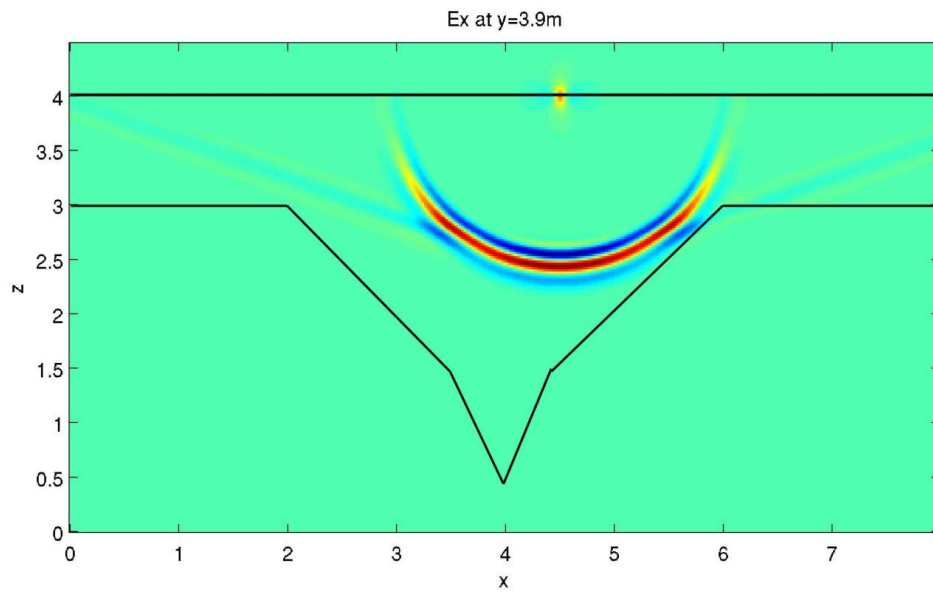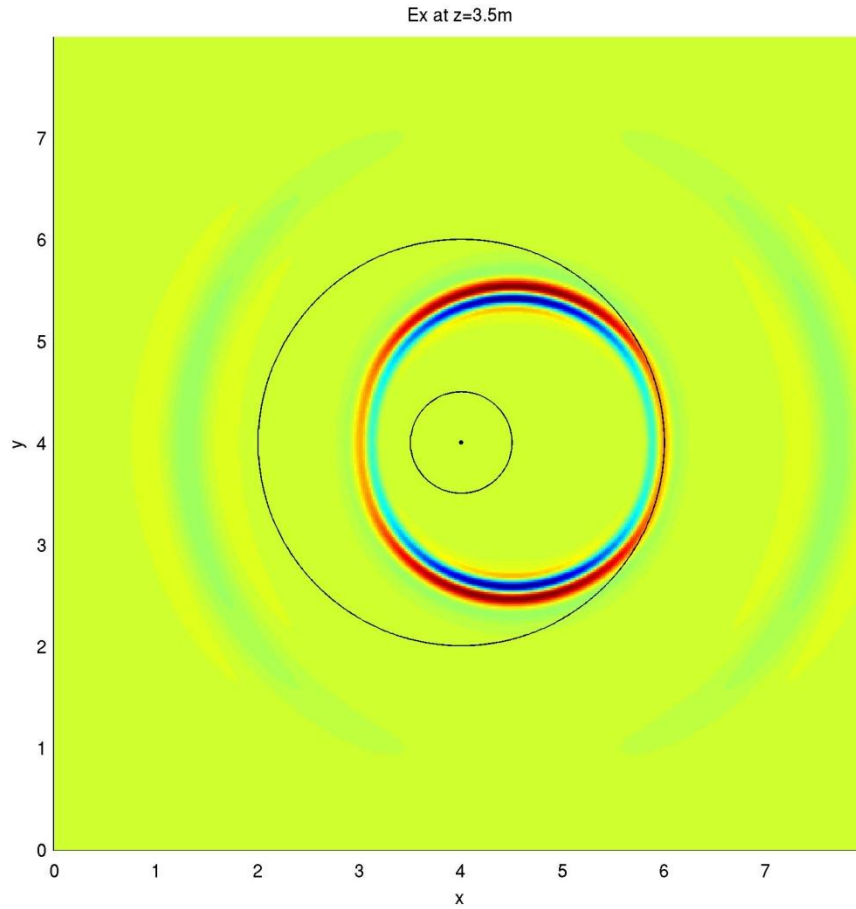
Figure 2.10a. Top, previous page. Snapshot at 20 ns in x-plane. Media boundaries drawn in for visual assistance. Distances are in meters for all snapshots.

Figure 2.10b. Bottom, previous page. Snapshot at 20 ns in y-plane. Transmitter location visible at surface, (4.5,4.0,4.0).

Figure 2.10c. Top, current page. Snapshot at 20 ns in z-plane, specifically at surface. Center point of model, outer rim of conduit, and outer rim of larger depression superimposed on image.

44

Figure 2.11a

Ex at x=3.5m

Figure 2.11b

Ex at y=3.9m

45

Figure 2.11c

Ex at z=3.5m
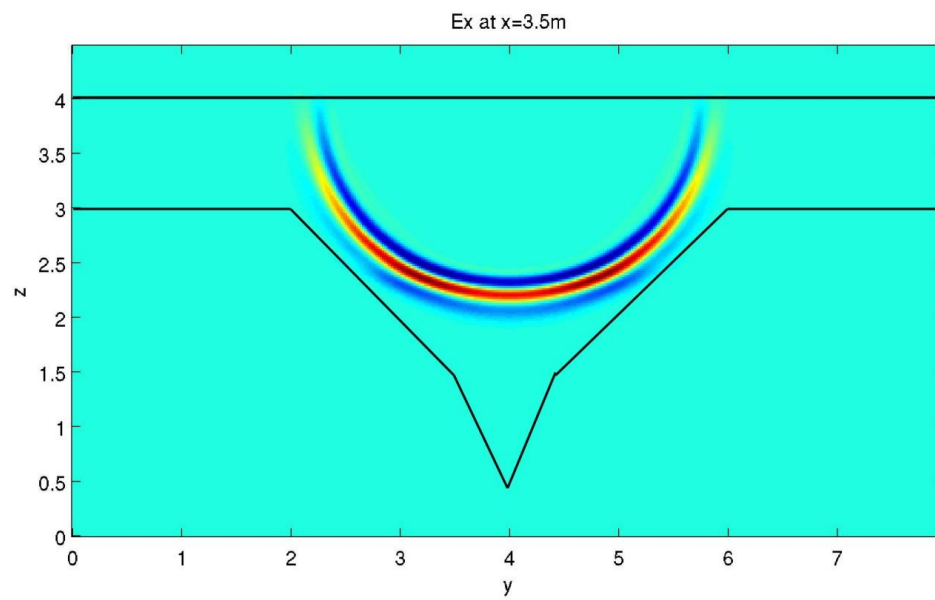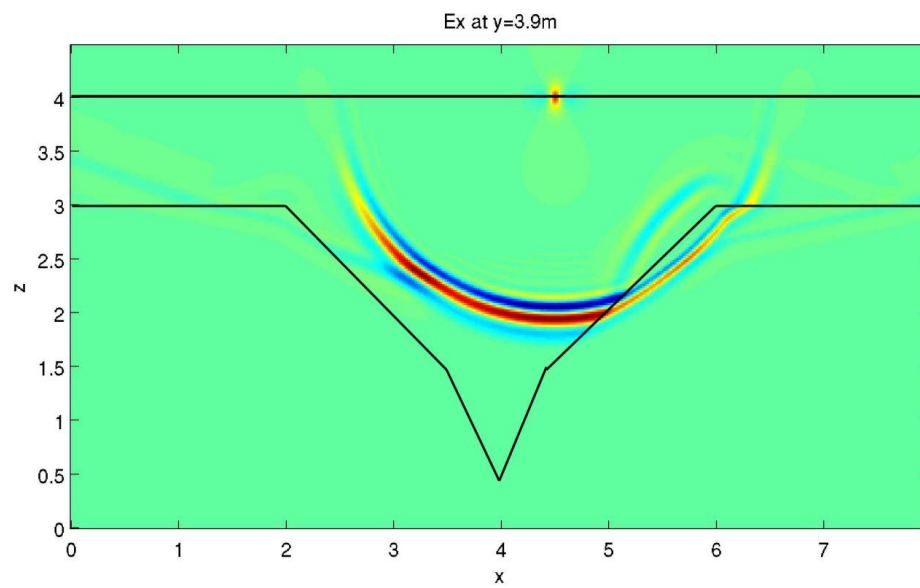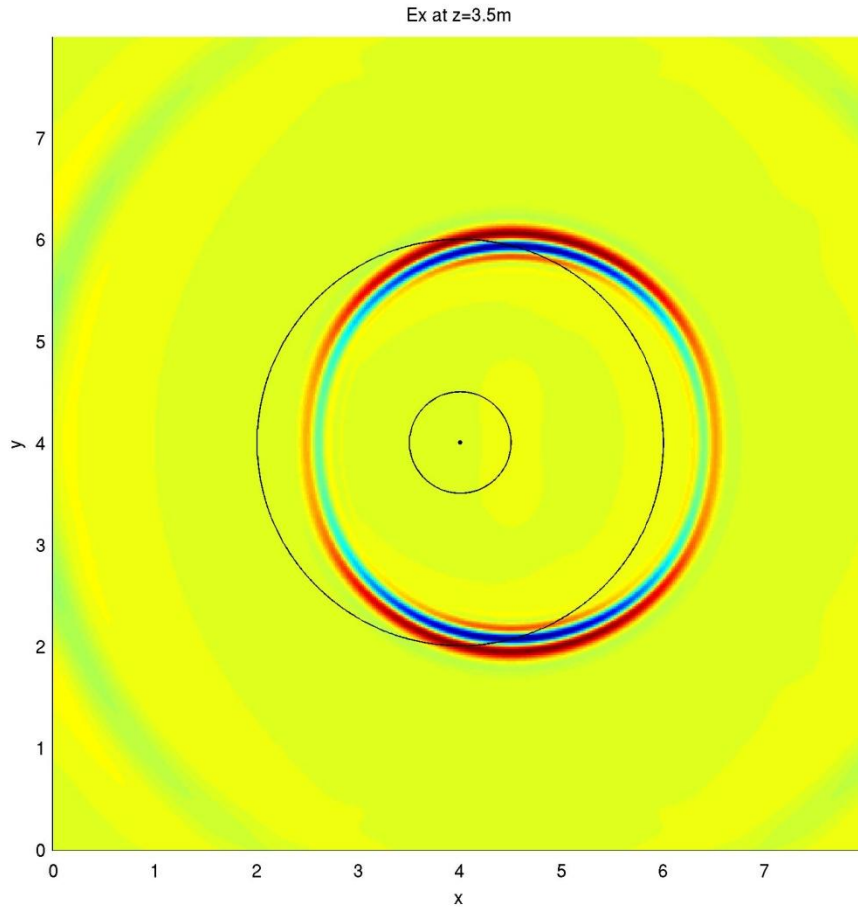
Figure 2.11a. Top, previous page. Snapshot at 25 ns in x-plane. Media boundaries drawn in for visual assistance. Distances are in meters for all snapshots.

Figure 2.11b. Bottom, previous page. Snapshot at 25 ns in y-plane. Transmitter location visible at surface, (4.5,4.0,4.0).

Figure 2.11c. Top, current page. Snapshot at 25 ns in z-plane, specifically at surface. Center point of model, outer rim of conduit, and outer rim of larger depression superimposed on image.

46

Figure 2.12a

Ex at x=3.5m

Figure 2.12b

Ex at y=3.9m

Figure 2.12c

Ex at z=3.5m
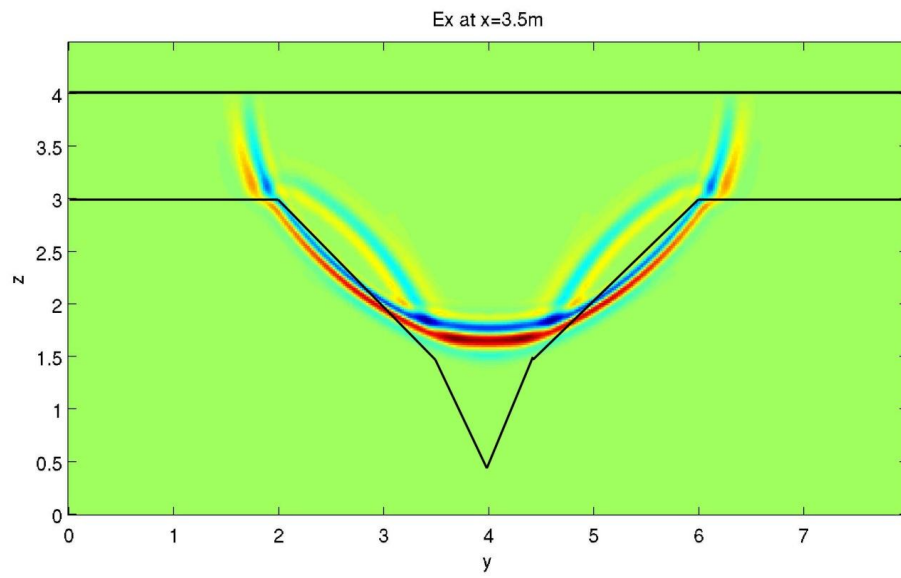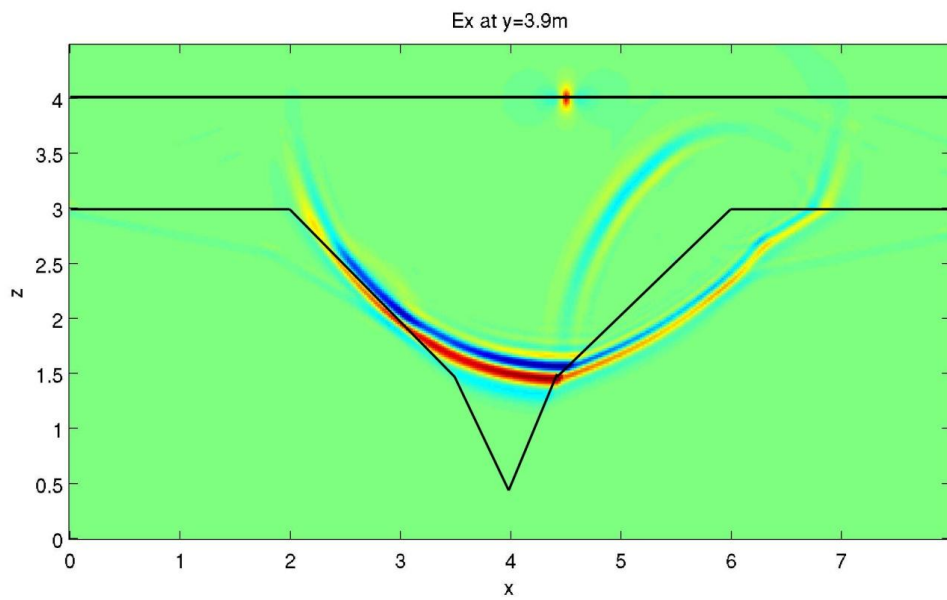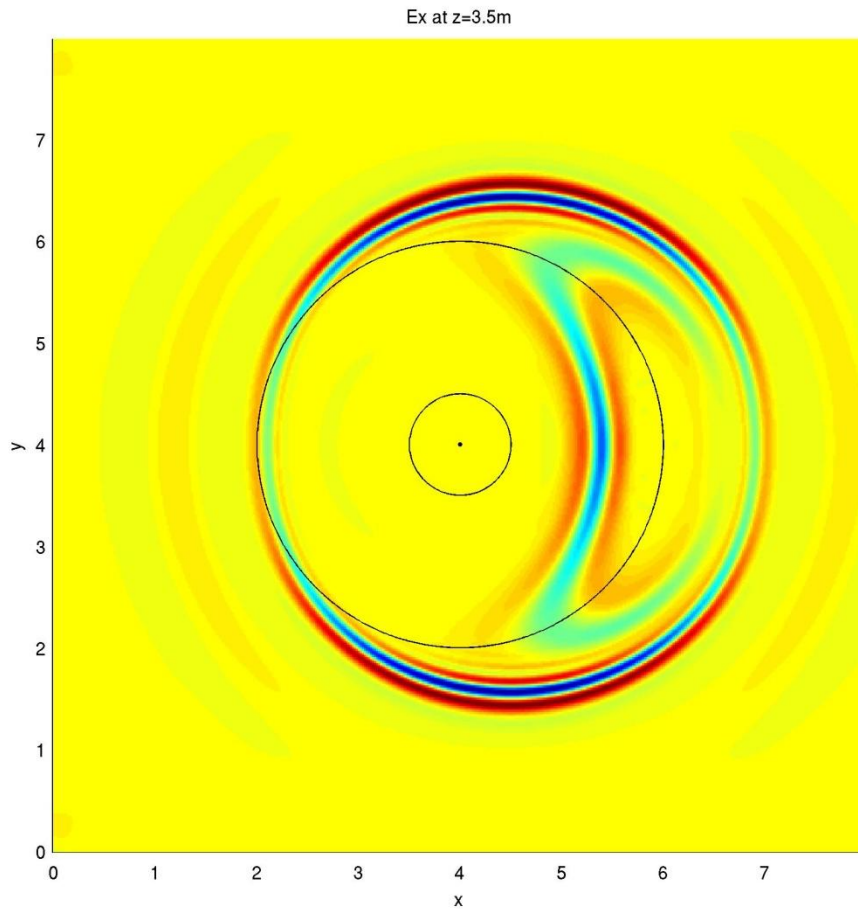
Figure 2.12a. Top, previous page. Snapshot at 30 ns in x-plane. Media boundaries

drawn in for visual assistance. Distances are in meters for all snapshots.

Figure 2.12b. Bottom, previous page. Snapshot at 30 ns in y-plane. Transmitter

location visible at surface, (4.5,4.0,4.0).

Figure 2.12c. Top, current page. Snapshot at 30 ns in z-plane, specifically at

surface. Center point of model, outer rim of conduit, and outer rim of larger

depression superimposed on image.

48

Figure 2.13a

Ex at x=3.5m

Figure 2.13b

Ex at y=3.9m

49

www.manaraa.com

Ex at z=3.5m
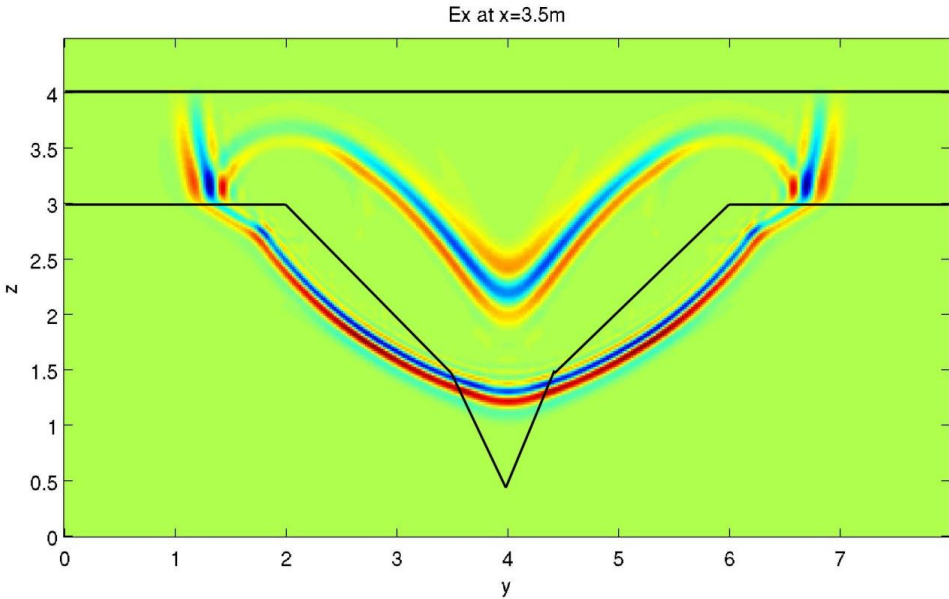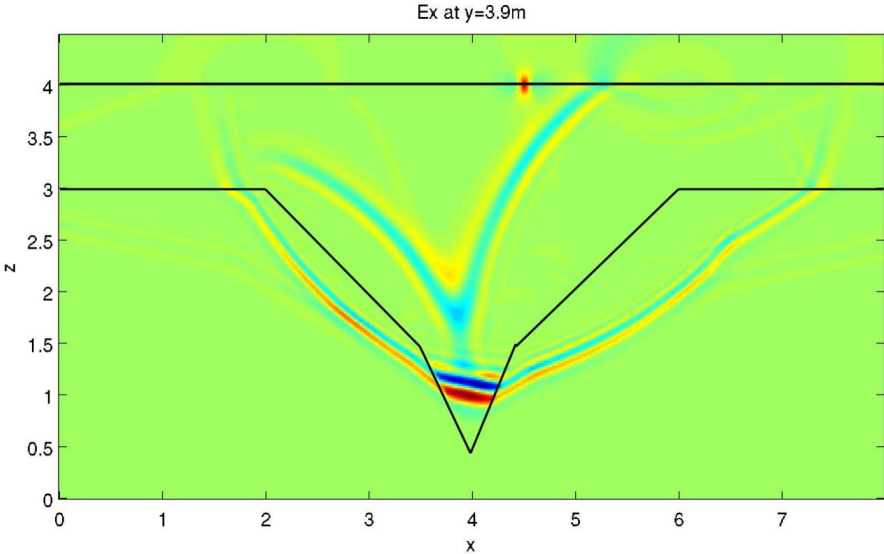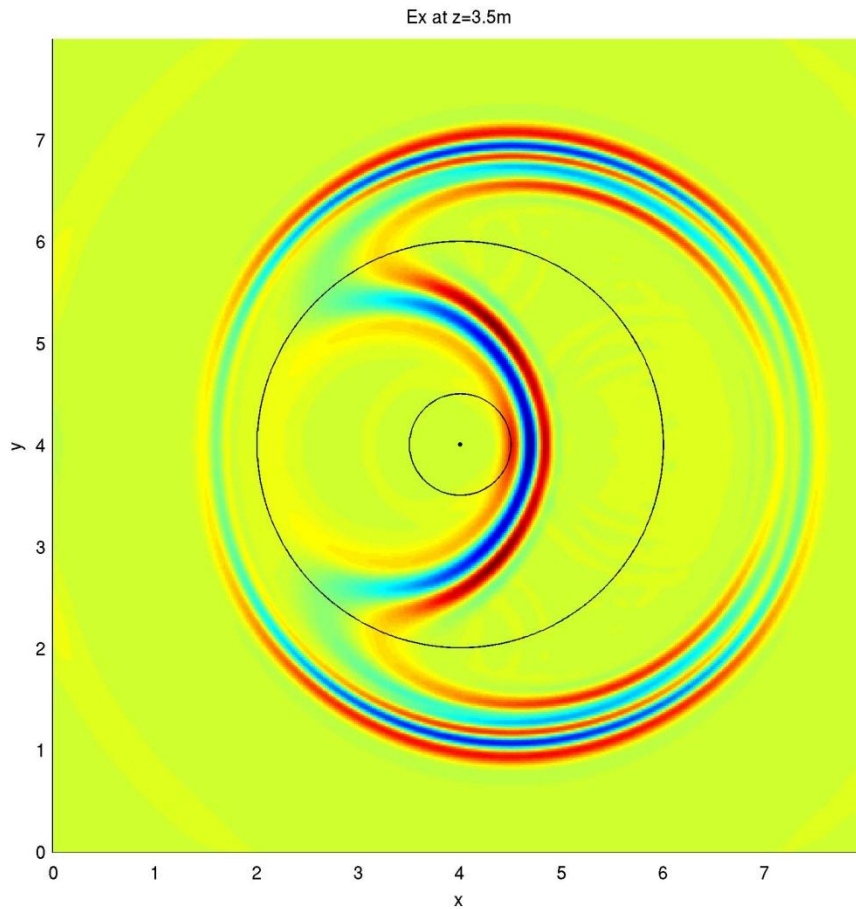
Figure 2.13a. Top, previous page. Snapshot at 35 ns in x-plane. Media boundaries drawn in for visual assistance. Distances are in meters for all snapshots.

Figure 2.13b. Bottom, previous page. Snapshot at 35 ns in y-plane. Transmitter location visible at surface, (4.5,4.0,4.0).

Figure 2.13c. Top, current page. Snapshot at 35 ns in z-plane, specifically at surface. Center point of model, outer rim of conduit, and outer rim of larger depression superimposed on image.

50

Figure 2.14a

Ex at x=3.5m

Figure 2.14b

Ex at y=3.9m

51

Figure 2.14c

Ex at z=3.5m
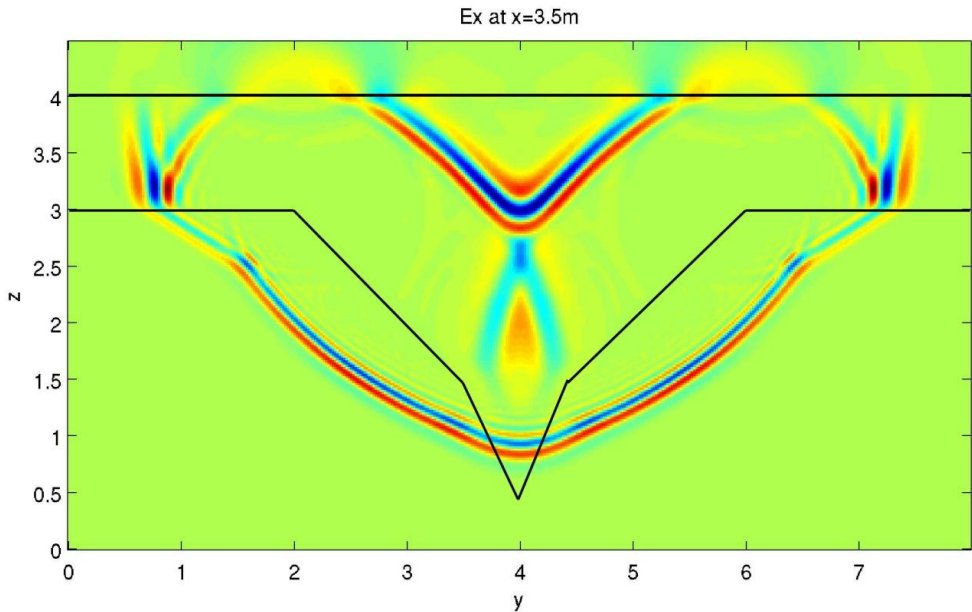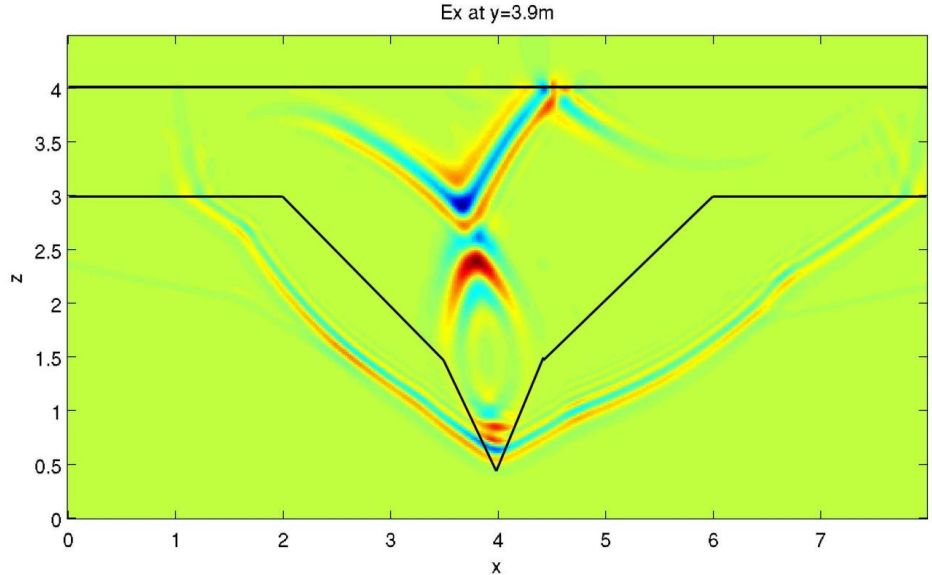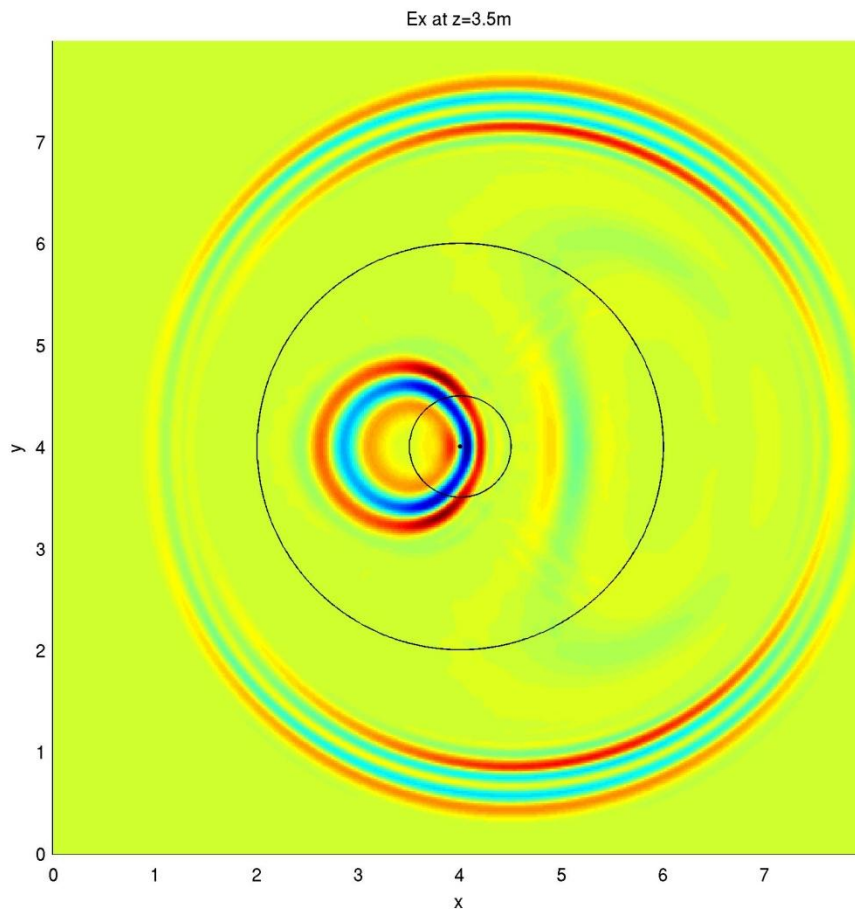
Figure 2.14a. Top, previous page. Snapshot at 40 ns in x-plane. Media boundaries drawn in for visual assistance. Distances are in meters for all snapshots.

Figure 2.14b. Bottom, previous page. Snapshot at 40 ns in y-plane. Transmitter location visible at surface, (4.5,4.0,4.0).

Figure 2.14c. Top, current page. Snapshot at 40 ns in z-plane, specifically at surface. Center point of model, outer rim of conduit, and outer rim of larger depression superimposed on image.

52

Figure 2.15a

Ex at x=3.5m

Figure 2.15b

Ex at y=3.9m

53

Figure 2.15c

Ex at z=3.5m
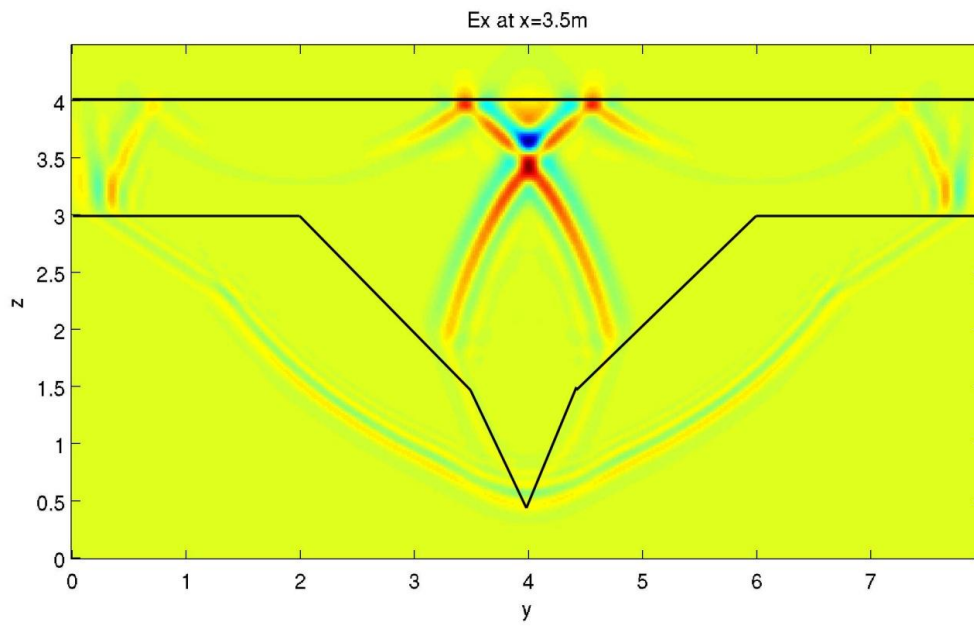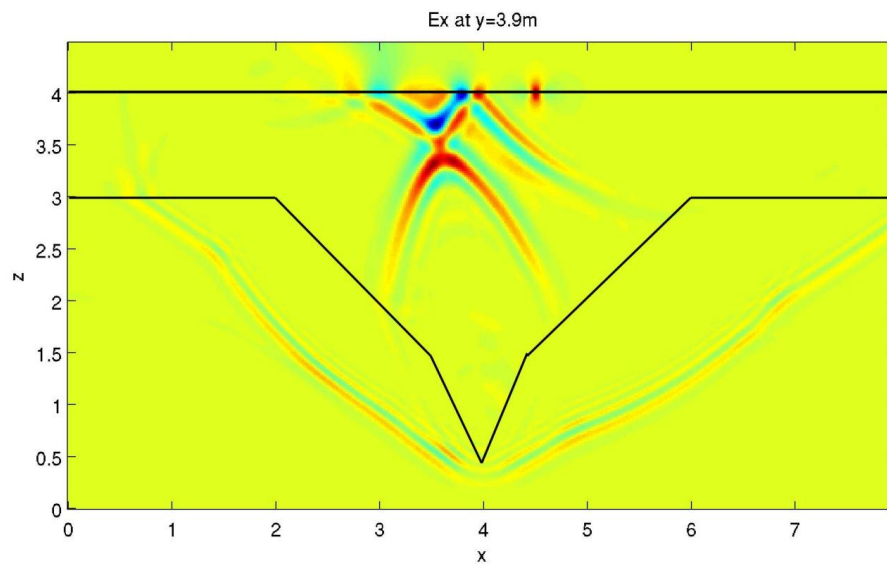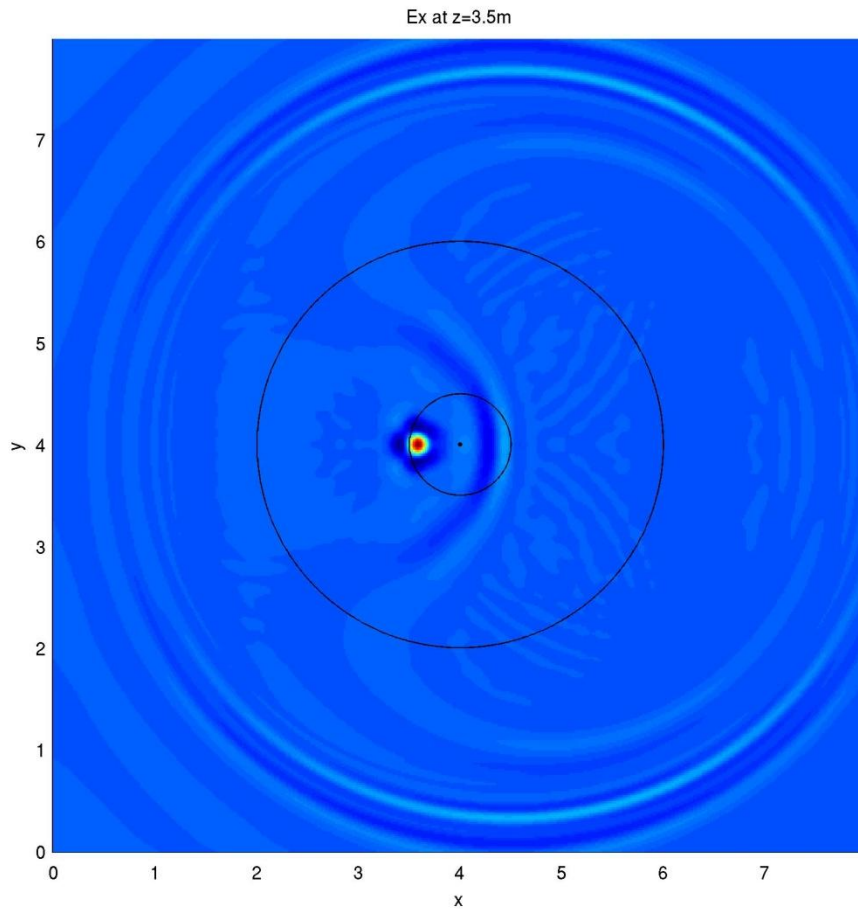
Figure 2.15a. Top, previous page. Snapshot at 45 ns in x-plane. Media boundaries drawn in for visual assistance. Distances are in meters for all snapshots.

Figure 2.15b. Bottom, previous page. Snapshot at 45 ns in y-plane. Transmitter location visible at surface, (4.5,4.0,4.0).

Figure 2.15c. Top, current page. Snapshot at 45 ns in z-plane, specifically at surface. Center point of model, outer rim of conduit, and outer rim of larger depression superimposed on image.

54

Figure 2.16a

Ex at x=3.5m

Figure 2.16b

Ex at y=3.9m

55

Figure 2.16c

Ex at z=3.5m
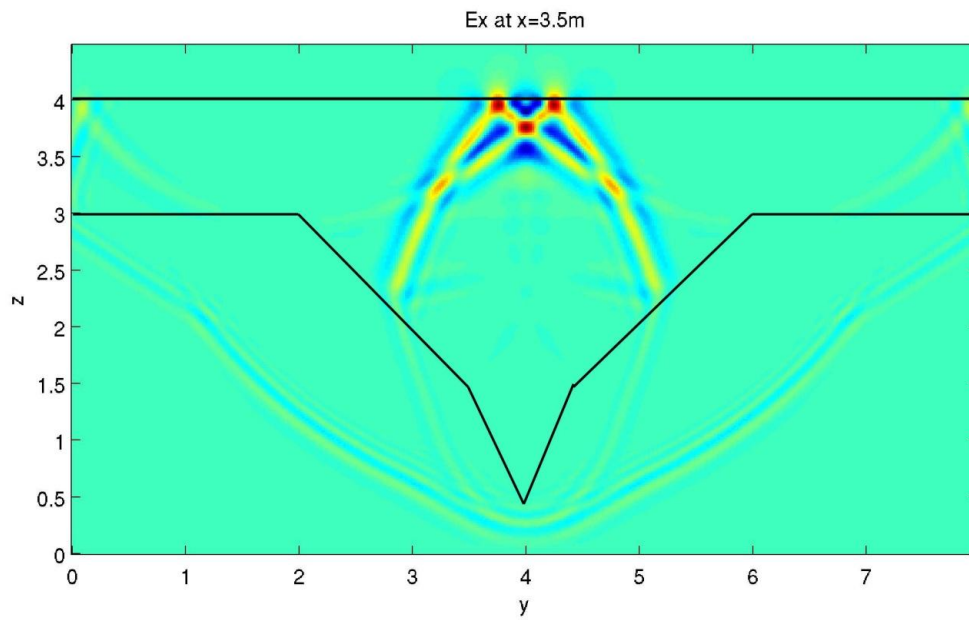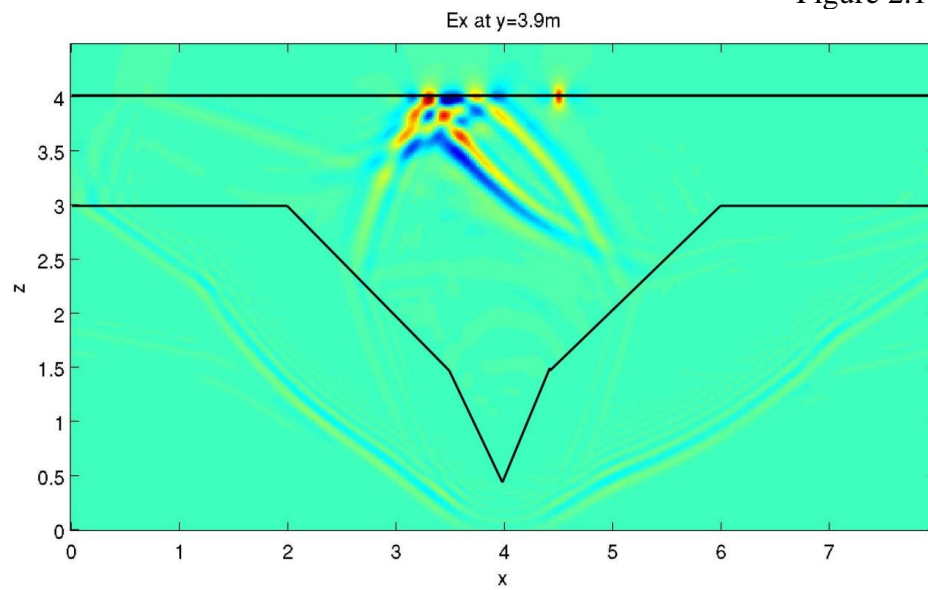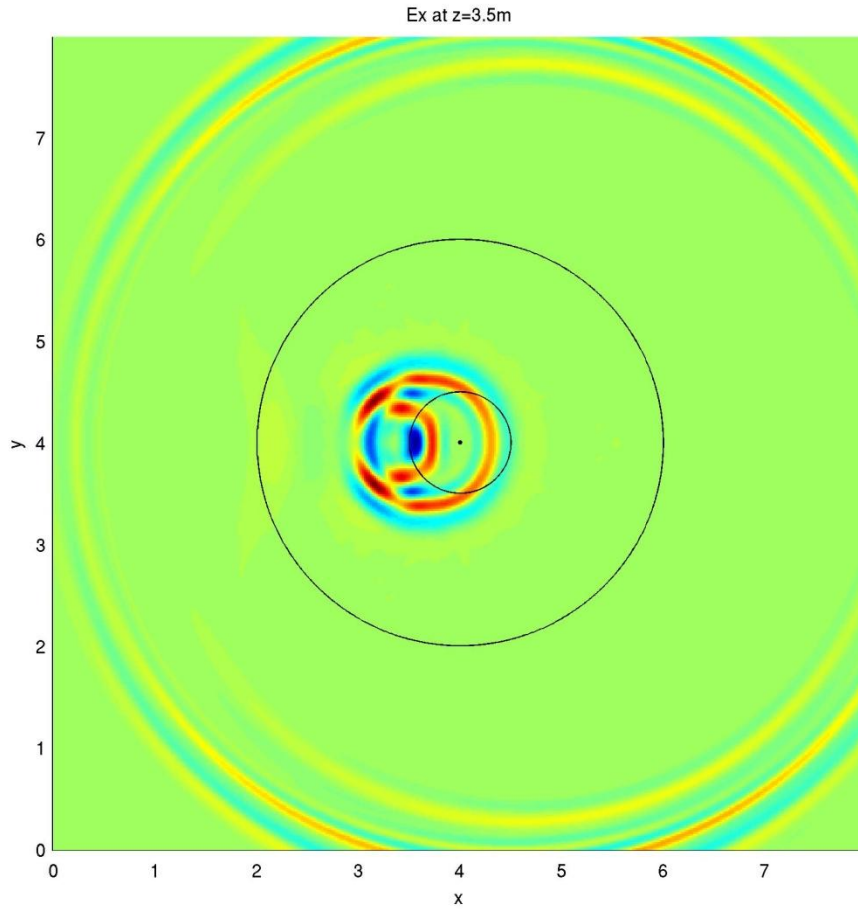
Figure 2.16a. Top, previous page. Snapshot at 50 ns in x-plane. Media boundaries drawn in for visual assistance. Distances are in meters for all snapshots.

Figure 2.16b. Bottom, previous page. Snapshot at 50 ns in y-plane. Transmitter location visible at surface, (4.5,4.0,4.0).

Figure 2.16c. Top, current page. Snapshot at 50 ns in z-plane, specifically at surface. Center point of model, outer rim of conduit, and outer rim of larger depression superimposed on image.

56

Figure 2.17a

Ex at x=3.5m

Figure 2.17b

Ex at y=3.9m

57

Figure 2.17c

Ex at z=3.5m

Figure 2.17a. Top, previous page. Snapshot at 55 ns in x-plane. Media boundaries
drawn in for visual assistance. Distances are in meters for all snapshots.

Figure 2.17b. Bottom, previous page. Snapshot at 55 ns in y-plane. Transmitter
location visible at surface, (4.5,4.0,4.0).

Figure 2.17c. Top, current page. Snapshot at 55 ns in z-plane, specifically at
surface. Center point of model, outer rim of conduit, and outer rim of larger
depression superimposed on image.

58

Figure 2.18a

Ex at x=3.5m

Figure 2.18b

Ex at y=3.9m

59

Figure 2.18c

Ex at z=3.5m

Figure 2.18a. Top, previous page. Snapshot at 60 ns in x-plane. Media boundaries
drawn in for visual assistance. Distances are in meters for all snapshots.

Figure 2.18b. Bottom, previous page. Snapshot at 60 ns in y-plane. Transmitter
location visible at surface, (4.5,4.0,4.0).

Figure 2.18c. Top, current page. Snapshot at 60 ns in z-plane, specifically at
surface. Center point of model, outer rim of conduit, and outer rim of larger
depression superimposed on image.

60

Figure 2.19a

Ex at x=3.5m

Figure 2.19b

Ex at y=3.9m

61

Figure 2.19c

Ex at z=3.5m

Figure 2.19a. Top, previous page. Snapshot at 65 ns in x-plane. Media boundaries

drawn in for visual assistance. Distances are in meters for all snapshots.

Figure 2.19b. Bottom, previous page. Snapshot at 65 ns in y-plane. Transmitter

location visible at surface, (4.5,4.0,4.0).

Figure 2.19c. Top, current page. Snapshot at 65 ns in z-plane, specifically at

surface. Center point of model, outer rim of conduit, and outer rim of larger

depression superimposed on image.

Figure 2.20a

Ex at x=3.5m

Figure 2.20b

Ex at y=3.9m

Figure 2.20c

Ex at z=3.5m
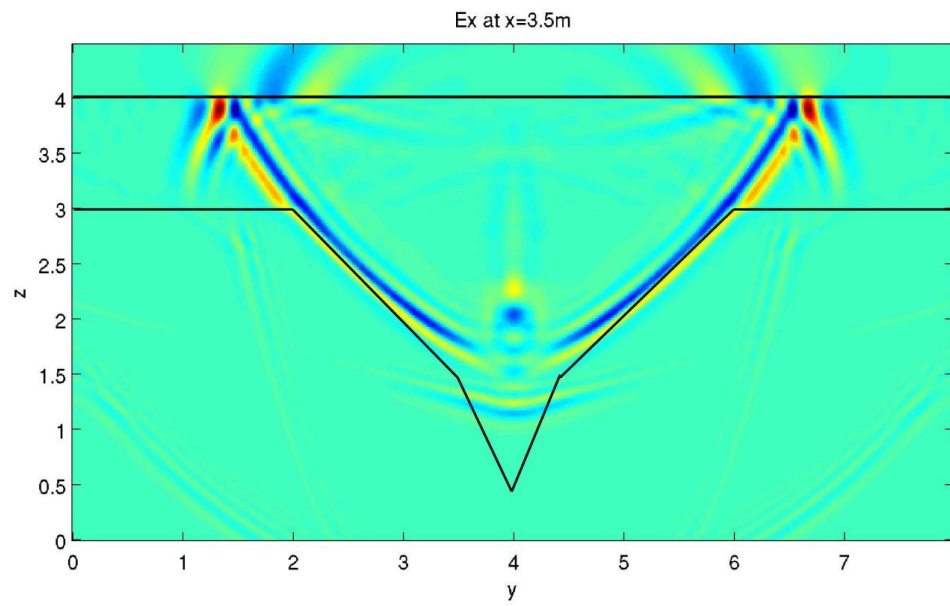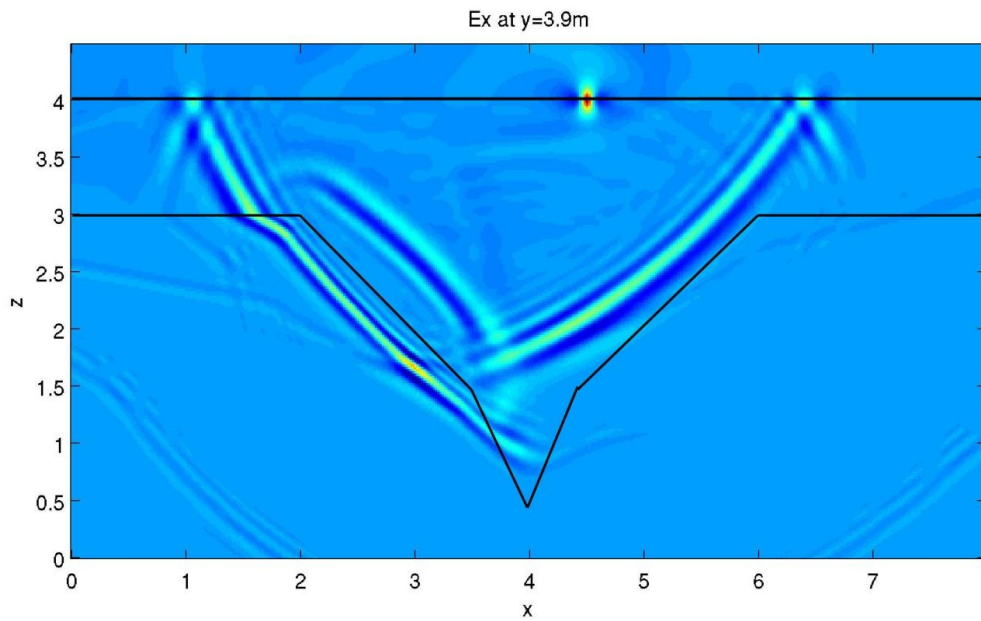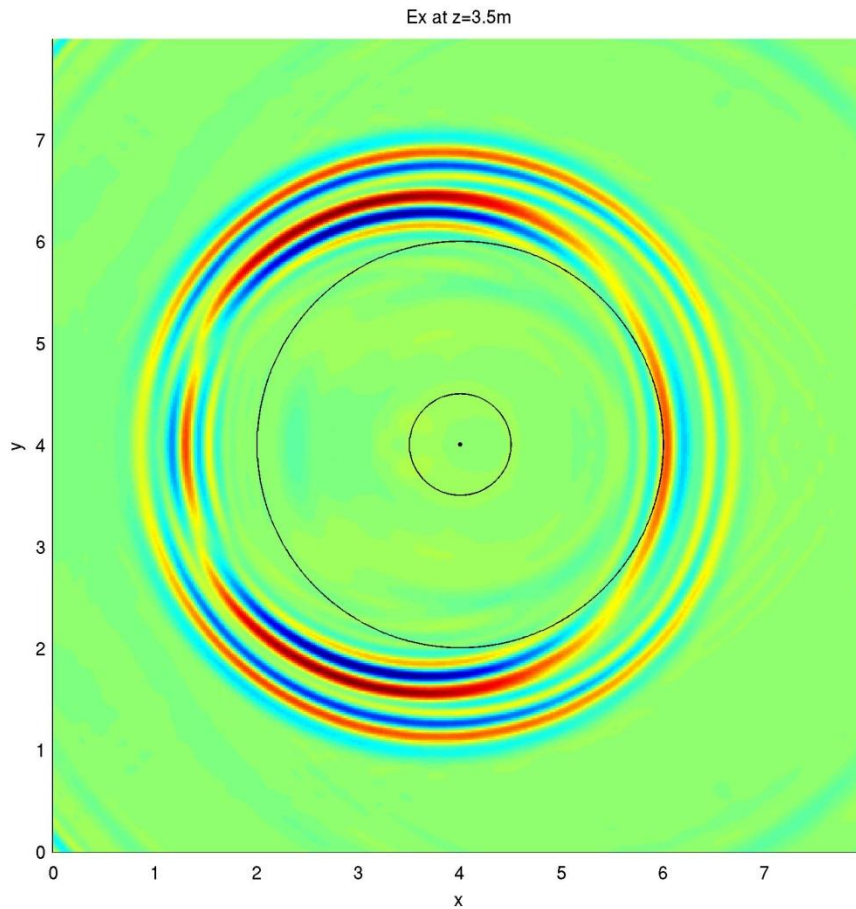
Figure 2.20a. Top, previous page. Snapshot at 70 ns in x-plane. Media boundaries
drawn in for visual assistance. Distances are in meters for all snapshots.

Figure 2.20b. Bottom, previous page. Snapshot at 70 ns in y-plane. Transmitter
location visible at surface, (4.5,4.0,4.0).

Figure 2.20c. Top, current page. Snapshot at 70 ns in z-plane, specifically at
surface. Center point of model, outer rim of conduit, and outer rim of larger
depression superimposed on image.

64

Modeling: Non-Standard Acquisition Geometries for Improved Conduit Detection

Differences in Receiver Field in XY Plane at Surface (z=0)

One advantage of the modeling software GPRMAX is that it efficiently simulates nontraditional data collection methods. The key feature is the ability to place any number of receivers virtually any place in the model space. The rx_box command enables the user to define a 2D box of evenly spaced receivers over specified dimensions. Each of the receivers in this grid will record all the of the available EM information over time for each transmission. This process can lead to very large storage space requirements when large numbers of receivers are positioned in larger-size models.

Two different rx_box models (based on the previously described models A and B) were created to identify transmitter-receiver locations most sensitive to the presence/absence of the conduit. Rx_box model A and B are identical to model A and B except that they are slightly trimmed around the edges to save processing time and storage space. The new models have dimensions of 5.0 x 7.0 x 4.0 meters and 5.0 x 7.0 x 4.5 meters, respectively (Figures 3.1a and 3.1b). The receiver field used was an evenly spaced grid only on the modeled ground surface with a receiver every 0.1 meter in both the x- and y-directions (Figure 3.2).

Figure 3.1a

Figure 3.1b

66
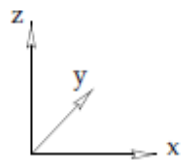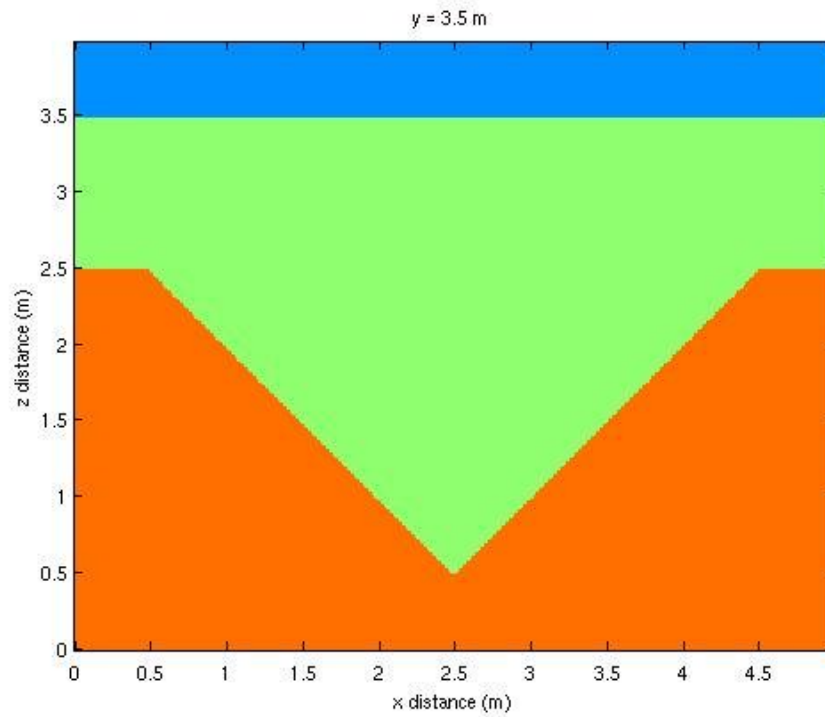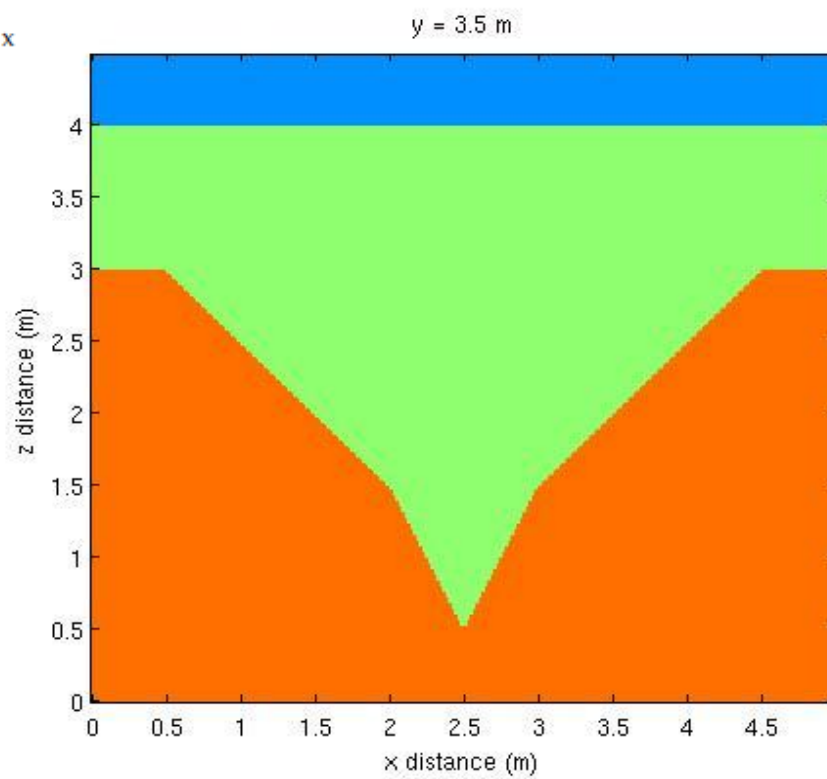
Figure 3.1a. Top of previous page, Model A: Vertical slice through three-dimensional model space at midpoint (y=3.5m). Orange material represents clay; green, sand; and blue, free space. Values for distance given as model coordinate values where (0.0, 0.0, 0.0) represents lower left forward-most point and (5.0, 7.0, 4.0) is the upper right back-most point in the model space.

Figure 3.1b. Bottom of previous page, Model B: Vertical slice through three-dimensional model space at midpoint (y=3.5m). Orange material represents clay; green, sand; and blue, free space. Values for distance given as model coordinate values where (0.0, 0.0, 0.0) represents lower left forward-most point and (5.0, 7.0, 4.5) is the upper right back-most point in the model space.

Figure 3.2

67
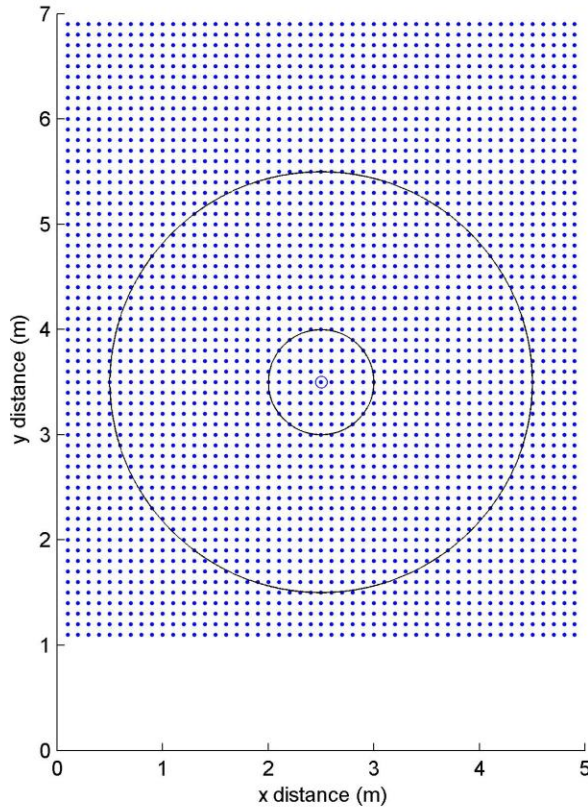
Figure 3.2. Bottom, previous page. Receiver positions used in both models. Receiver spread on modeled ground surface only. Outer rims of both conical features superimposed on the image.

The first test examined receiver field results for receivers oriented in the same direction as the transmitter (Ex) in the model (note: this is the same as used in previous sections). The data for the first 100 ns from one model is subtracted from the other. The absolute values of this difference trace are summed to capture a single value representative of the total difference between models A and B at that receiver location. These difference values are then displayed as a contour map over receiver locations (e.g. Figure 3.3). Transmitter locations along the same survey line as used in the previous models are used for the rx_box models. This entire process is then repeated for different transmitter positions (Figures 3.3-3.18). Ideally, this process could yield areas on the surface where difference in the two model's subsurface geometry is the greatest. Finding these locations could help plan where to place receivers when trying to maximize sensitivity to conduit presence/absence.

Select contour images from a total of 145 transmitter locations can be seen in Figures 3.3-3.18. Although the output images should be symmetric from symmetric model geometry, computational instabilities produced some distortion in the images. The basic patterns are still visible and useful in determining areas of greatest difference in the receiver field between conduit and no-conduit models. There is a pattern that suggests the curvature of depression and conduit cause some of the symmetric distortion (Figures 3.3,

68

3.14-3.18). Also, some of the difference appears on the opposite side of the conduit when the transmitter approaches the center but this pattern is not stable (Figures 3.7-3.9). In most cases, the strongest difference occurs for receiver locations closest to the transmitter. Thus, the principal conclusion of this modeling is that traditional acquisition geometries, in which the receiver antenna is close to the transmitting antenna, maximize sensitivity to the presence or absence of the modeled conduit.

69

Figure 3.3. Ex Difference plot at transmitter location 1 (displayed as a star on plot). The x-axis refers to the x-direction at the surface and is in meters. Likewise, the y-axis refers to the y-direction at the surface. Color bar units are relative differences with red being more different and blue being less different. Outer rims of both conical depressions are superimposed on plot.

70

Figure 3.4. Ex Difference plot at transmitter location 15 (displayed as a star on plot). The x-axis refers to the x-direction at the surface and is in meters. Likewise, the y-axis refers to the y-direction at the surface. Color bar units are relative differences with red being more different and blue being less different. Outer rims of both conical depressions are superimposed on plot.

71
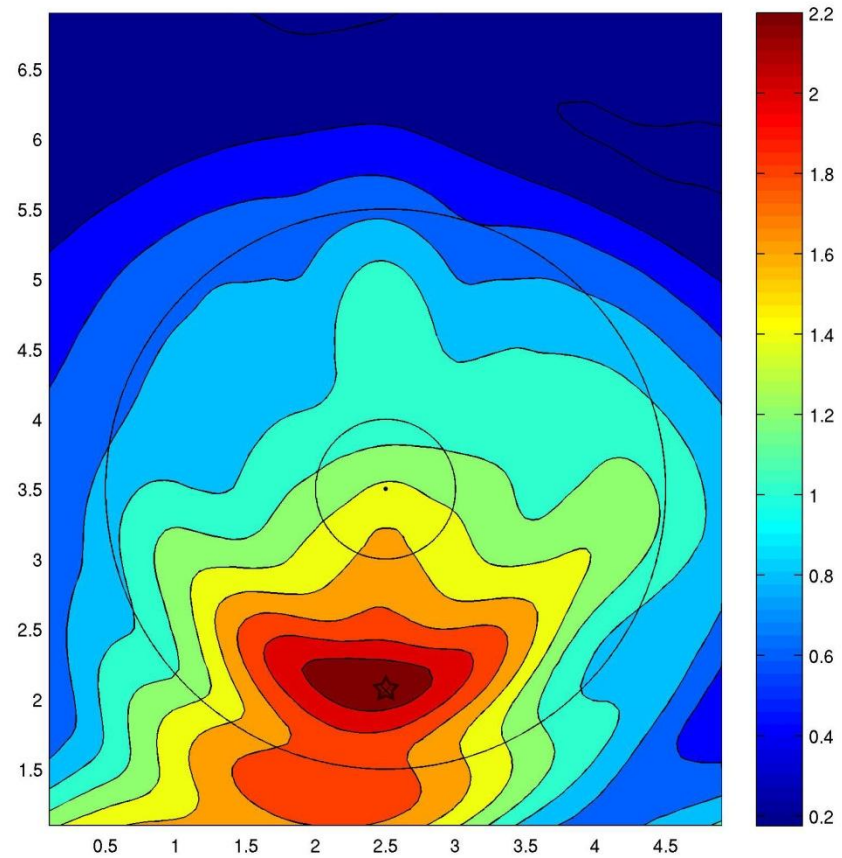
Figure 3.5. Ex Difference plot at transmitter location 25 (displayed as a star on plot). The x-axis refers to the x-direction at the surface and is in meters. Likewise, the y-axis refers to the y-direction at the surface. Color bar units are relative differences with red being more different and blue being less different. Outer rims of both conical depressions are superimposed on plot.

72
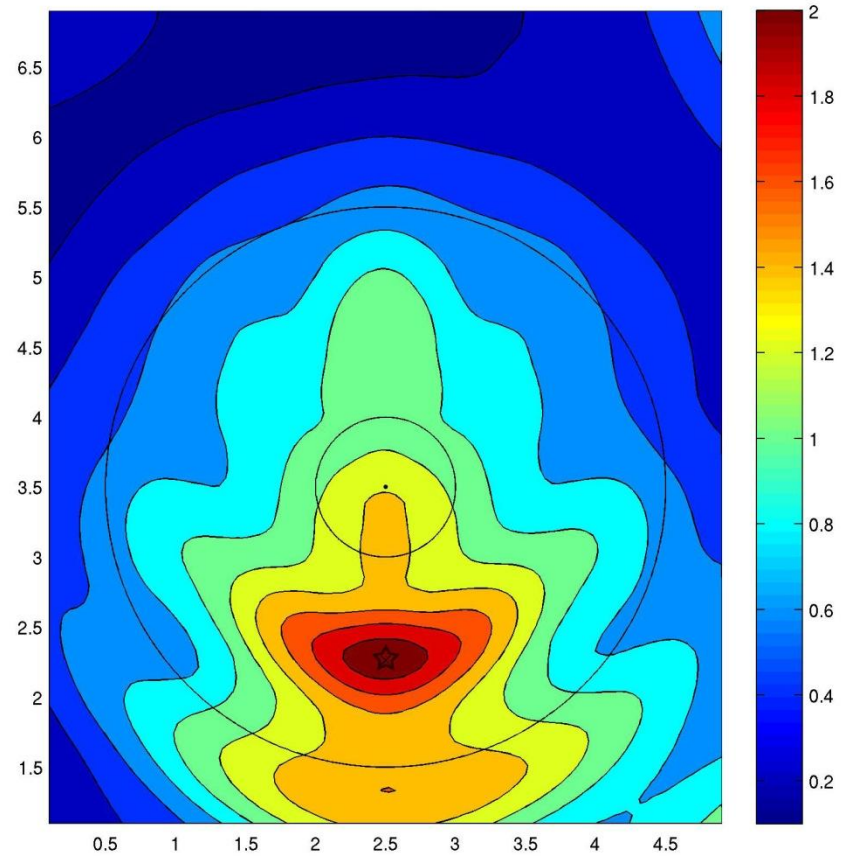
Figure 3.6. Ex Difference plot at transmitter location 30 (displayed as a star on plot). The x-axis refers to the x-direction at the surface and is in meters. Likewise, the y-axis refers to the y-direction at the surface. Color bar units are relative differences with red being more different and blue being less different. Outer rims of both conical depressions are superimposed on plot.

73
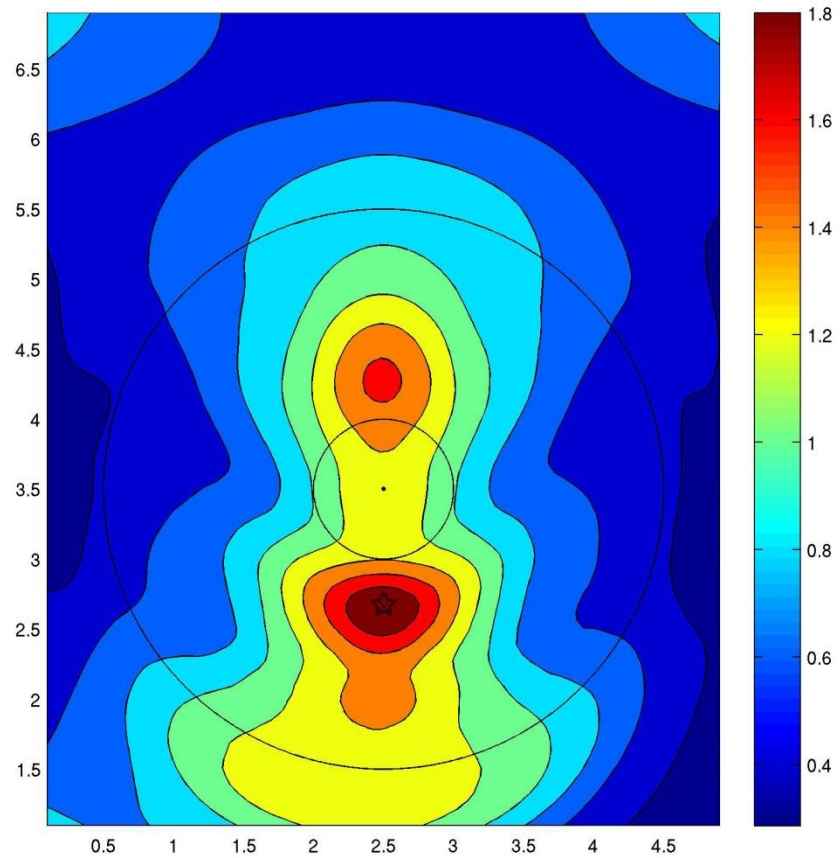
Figure 3.7. Ex Difference plot at transmitter location 40 (displayed as a star on plot). The x-axis refers to the x-direction at the surface and is in meters. Likewise, the y-axis refers to the y-direction at the surface. Color bar units are relative differences with red being more different and blue being less different. Outer rims of both conical depressions are superimposed on plot.

74
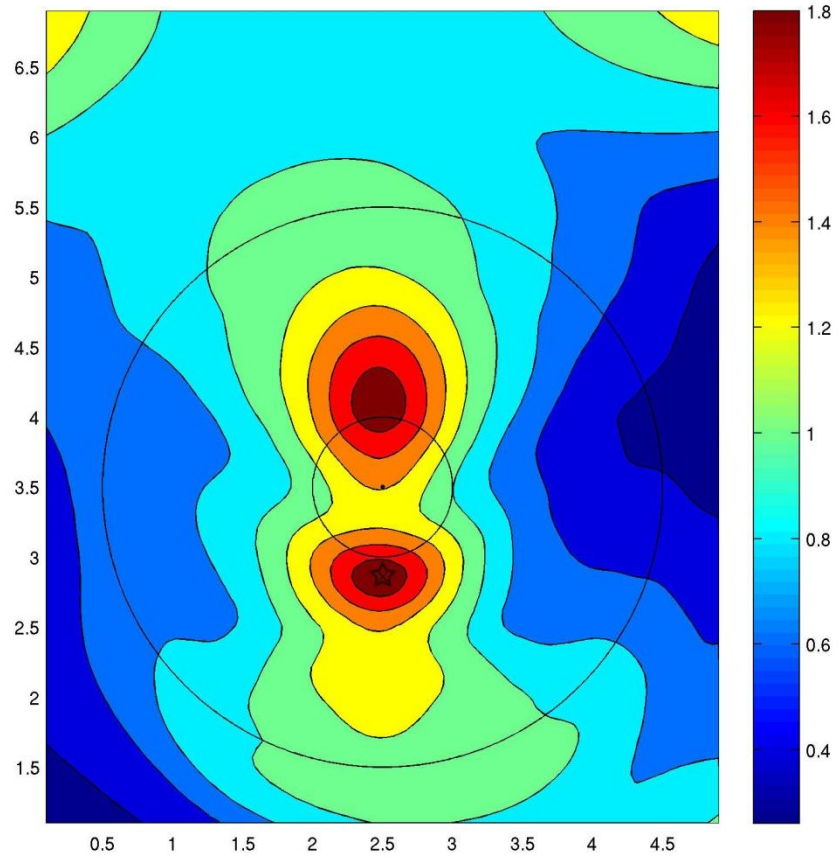
Figure 3.8. Ex Difference plot at transmitter location 45 (displayed as a star on plot). The x-axis refers to the x-direction at the surface and is in meters. Likewise, the y-axis refers to the y-direction at the surface. Color bar units are relative differences with red being more different and blue being less different. Outer rims of both conical depressions are superimposed on plot.
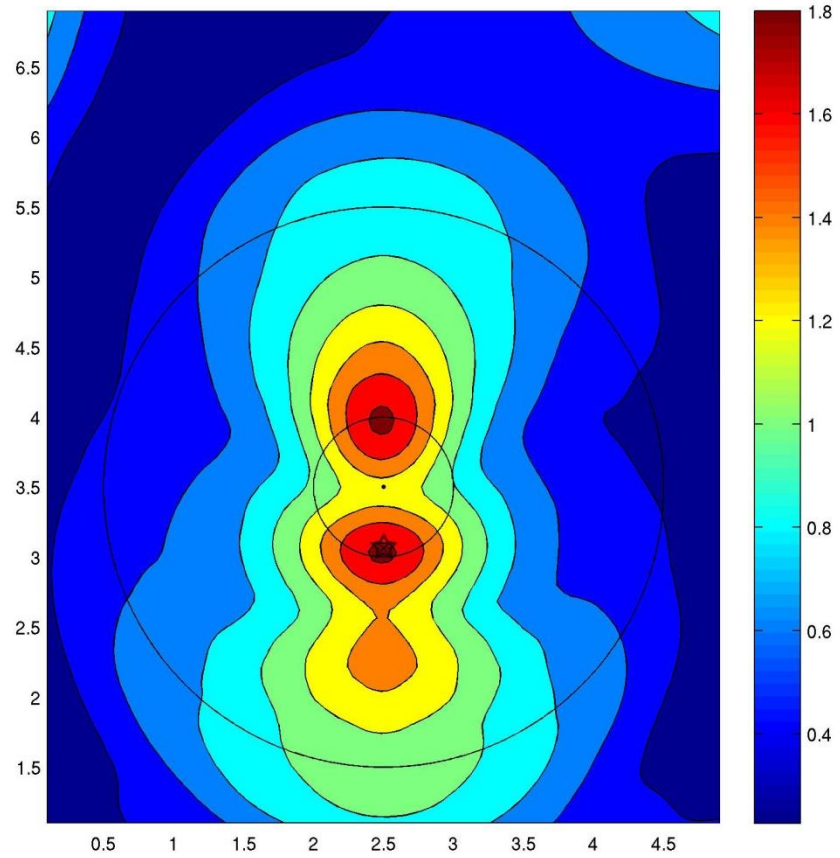
Figure 3.9. Ex Difference plot at transmitter location 50 (displayed as a star on plot). The x-axis refers to the x-direction at the surface and is in meters. Likewise, the y-axis refers to the y-direction at the surface. Color bar units are relative differences with red being more different and blue being less different. Outer rims of both conical depressions are superimposed on plot.

76
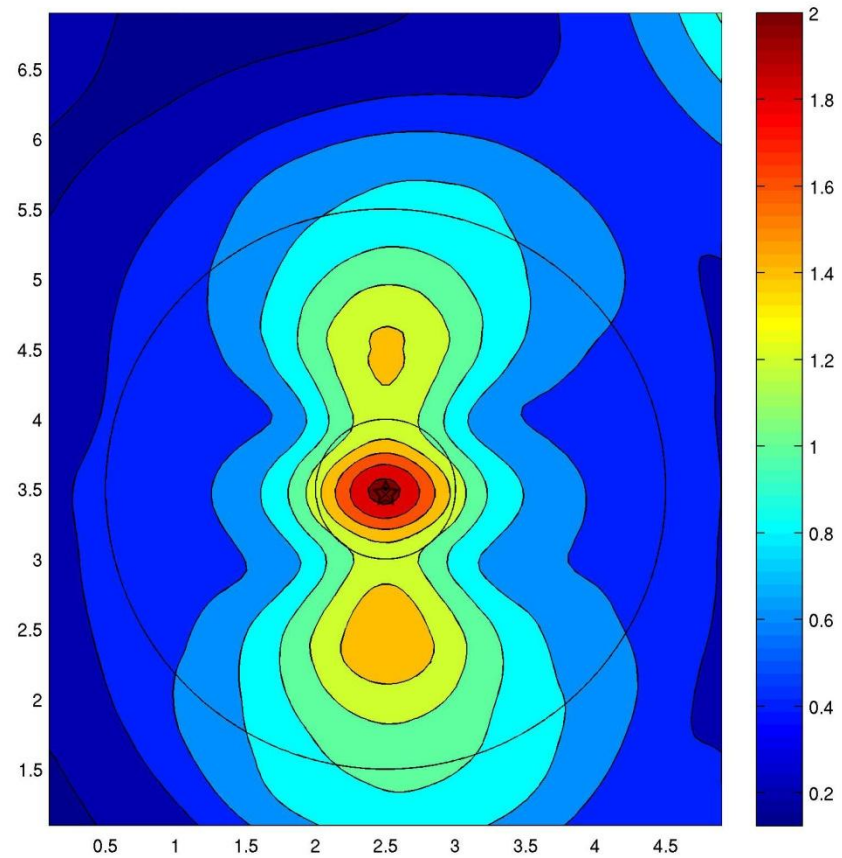
Figure 3.10. Ex Difference plot at transmitter location 60 (displayed as a star on plot). The x-axis refers to the x-direction at the surface and is in meters. Likewise, the y-axis refers to the y-direction at the surface. Color bar units are relative differences with red being more different and blue being less different. Outer rims of both conical depressions are superimposed on plot.

77
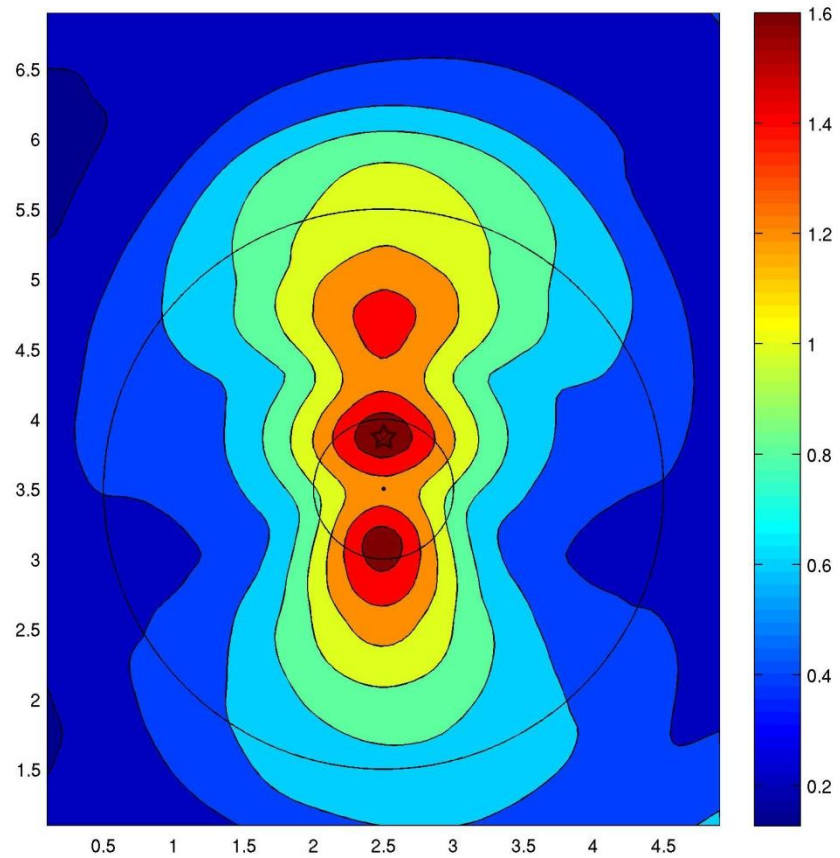
Figure 3.11. Ex Difference plot at transmitter location 70 (displayed as a star on plot). The x-axis refers to the x-direction at the surface and is in meters. Likewise, the y-axis refers to the y-direction at the surface. Color bar units are relative differences with red being more different and blue being less different. Outer rims of both conical depressions are superimposed on plot.

78
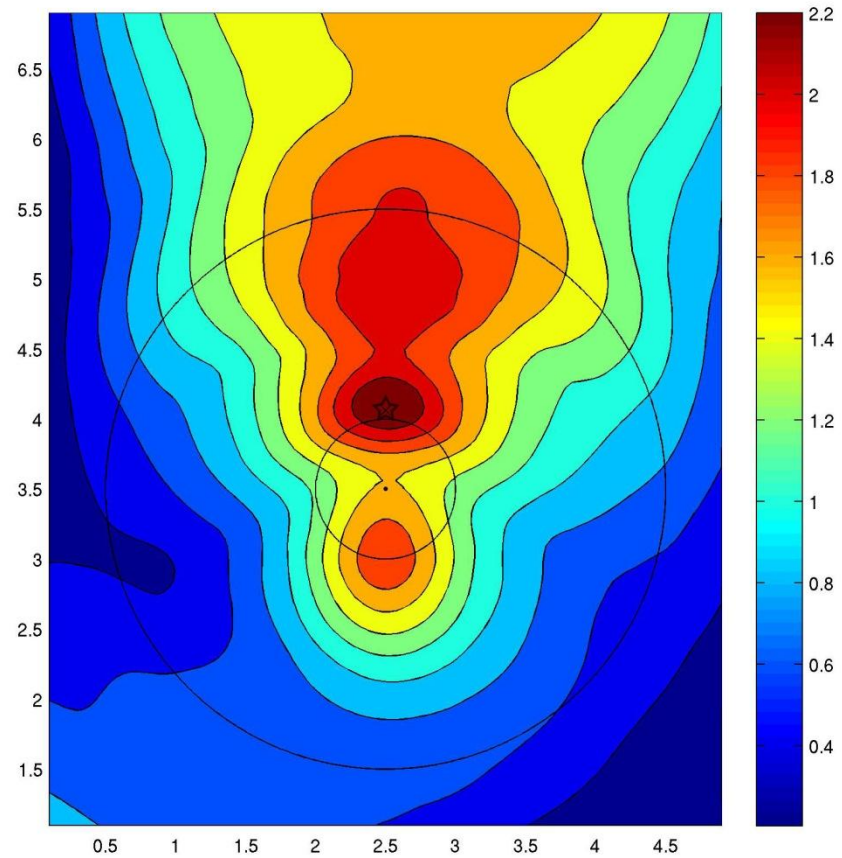
Figure 3.12. Ex Difference plot at transmitter location 75 (displayed as a star on plot). The x-axis refers to the x-direction at the surface and is in meters. Likewise, the y-axis refers to the y-direction at the surface. Color bar units are relative differences with red being more different and blue being less different. Outer rims of both conical depressions are superimposed on plot.

79
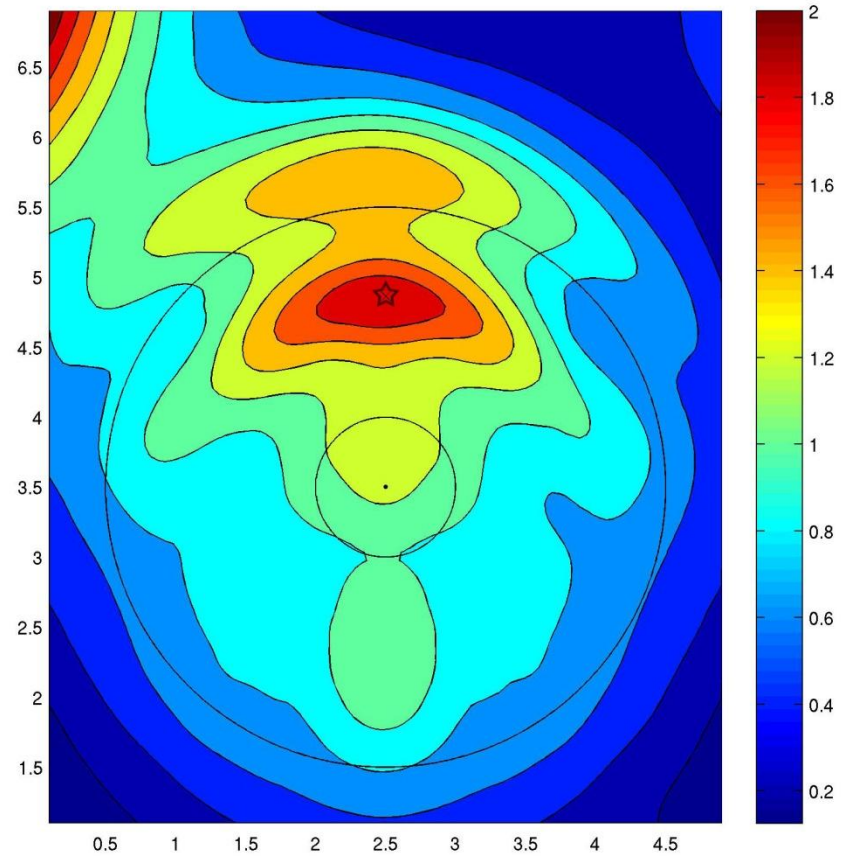
Figure 3.13. Ex Difference plot at transmitter location 95 (displayed as a star on plot). The x-axis refers to the x-direction at the surface and is in meters. Likewise, the y-axis refers to the y-direction at the surface. Color bar units are relative differences with red being more different and blue being less different. Outer rims of both conical depressions are superimposed on plot.

80
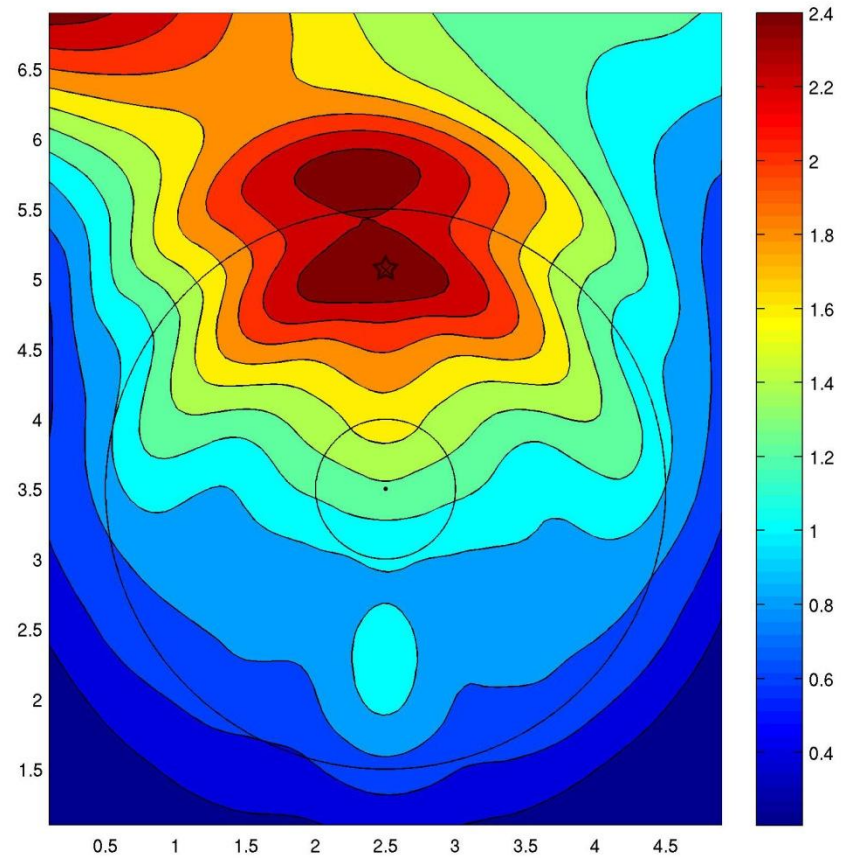
Figure 3.14. Ex Difference plot at transmitter location 100 (displayed as a star on plot). The x-axis refers to the x-direction at the surface and is in meters. Likewise, the y-axis refers to the y-direction at the surface. Color bar units are relative differences with red being more different and blue being less different. Outer rims of both conical depressions are superimposed on plot.

81
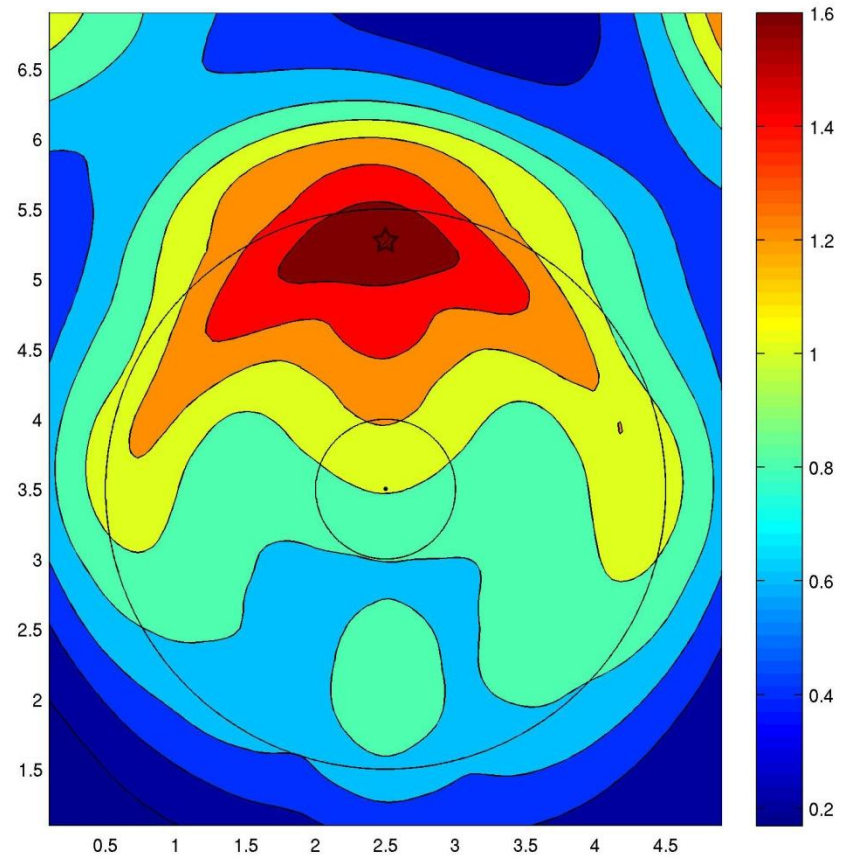
Figure 3.15. Ex Difference plot at transmitter location 105 (displayed as a star on plot). The x-axis refers to the x-direction at the surface and is in meters. Likewise, the y-axis refers to the y-direction at the surface. Color bar units are relative differences with red being more different and blue being less different. Outer rims of both conical depressions are superimposed on plot.

82
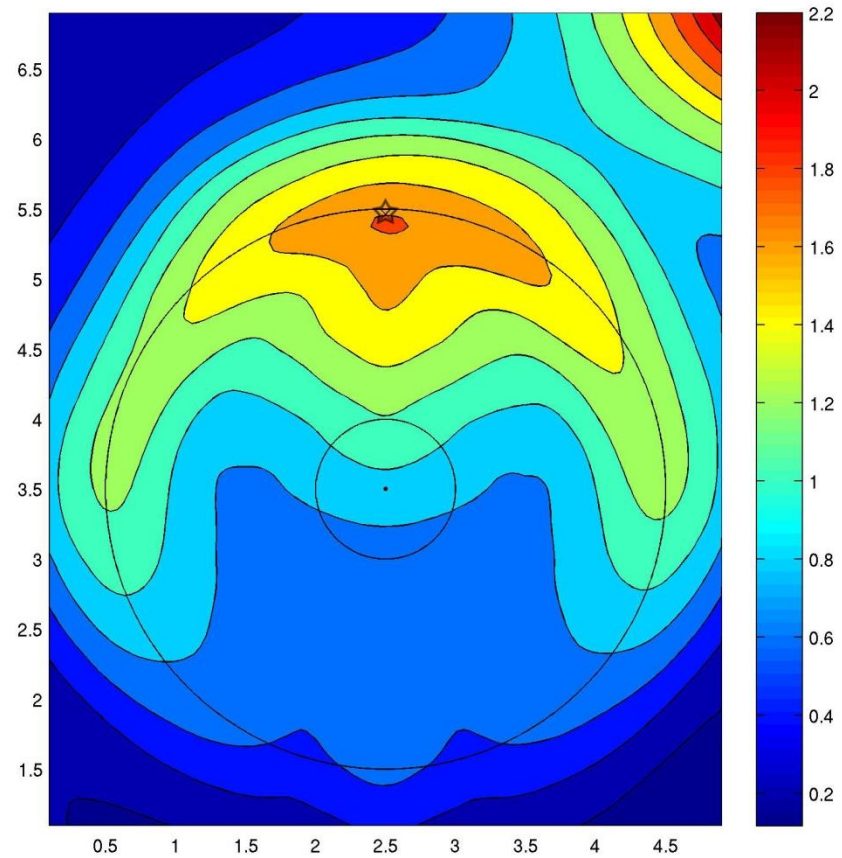
Figure 3.16. Ex Difference plot at transmitter location 110 (displayed as a star on plot). The x-axis refers to the x-direction at the surface and is in meters. Likewise, the y-axis refers to the y-direction at the surface. Color bar units are relative differences with red being more different and blue being less different. Outer rims of both conical depressions are superimposed on plot.

83
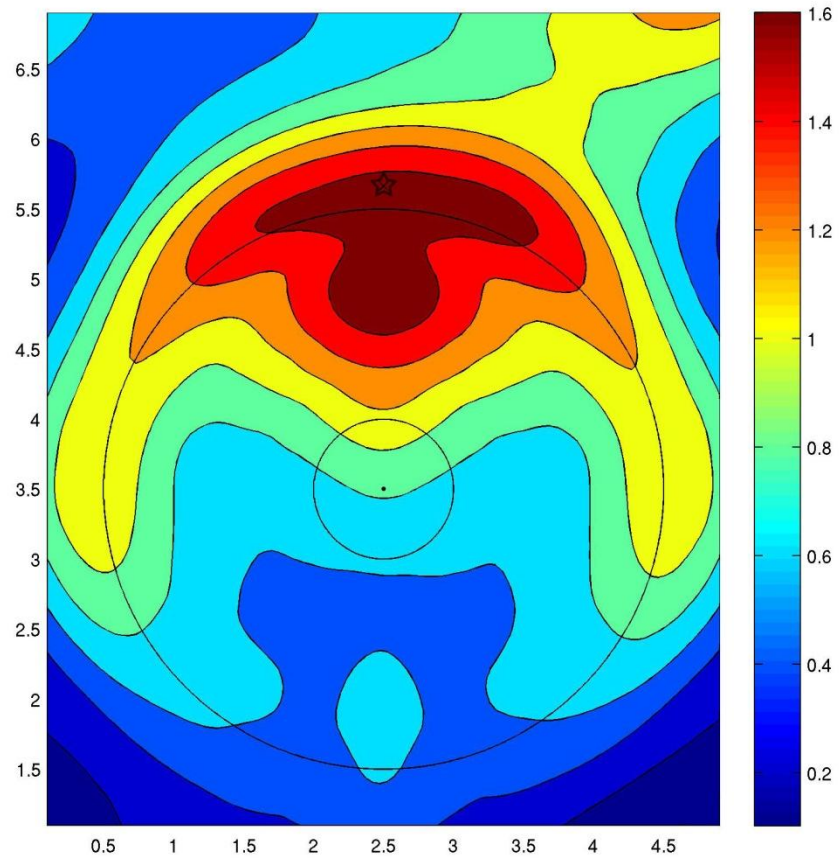
Figure 3.17. Ex Difference plot at transmitter location 115 (displayed as a star on plot). The x-axis refers to the x-direction at the surface and is in meters. Likewise, the y-axis refers to the y-direction at the surface. Color bar units are relative differences with red being more different and blue being less different. Outer rims of both conical depressions are superimposed on plot.
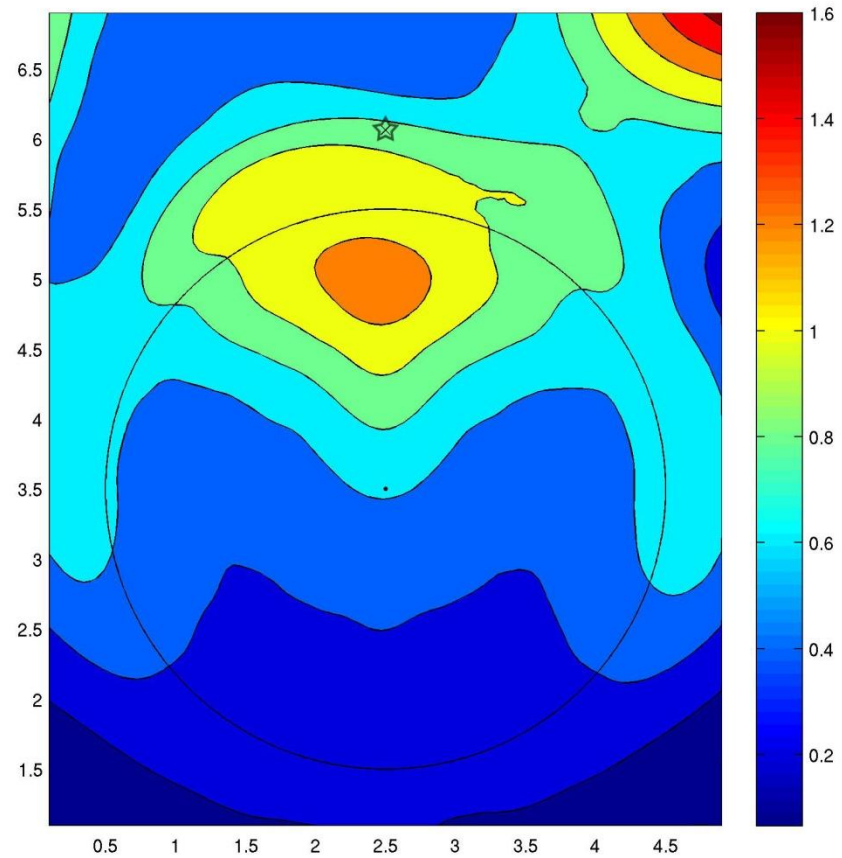
Figure 3.18. Ex Difference plot at transmitter location 125 (displayed as a star on plot). The x-axis refers to the x-direction at the surface and is in meters. Likewise, the y-axis refers to the y-direction at the surface. Color bar units are relative differences with red being more different and blue being less different. Outer rims of both conical depressions are superimposed on plot.

85

An additional receiver geometry examined here is the case in which the receiving antenna is oriented perpendicular to the transmitting antenna. This methodology has been described in previous studies (e.g. Lutz et al, 2003; Orlando and Slob, 2009). This receiver geometry response can be extracted from the GPRMAX models from the computed component of the E field in the y-direction at the surface. Once again, select figures from the total available 145 transmitting locations are displayed in Figures 3.19-3.31. The results show that there is almost no difference between the two models records near the transmitter at any location. Also, the greatest differences appear strongest as the transmitter enters the area above the outer rim of the sinkhole depression. Once inside this area, the locations of greatest differences seem to be isolated in quadrants at 45 degree angles to the lines parallel to the x- and y-axes resembling somewhat of a 'butterfly' pattern (see Figure 3.25). Although it is possible to record a stronger E_y signal from the conduit, it would not be feasible to implement it because the difference quadrants wander as the transmitter is moved along its survey line (x = 2.5 m). This means that having perpendicular receivers set at specified distances 45 degrees off axis would not have a constant record of the conduit's signal due to the wander of the difference magnitudes. Not to mention, that trying to employ this method when subsurface conditions are unknown would be entirely guesswork and prove to be ineffective. Simply put, there is not a simple, different transmitter-receiver arrangement that will improve resolution over the standard one.

86
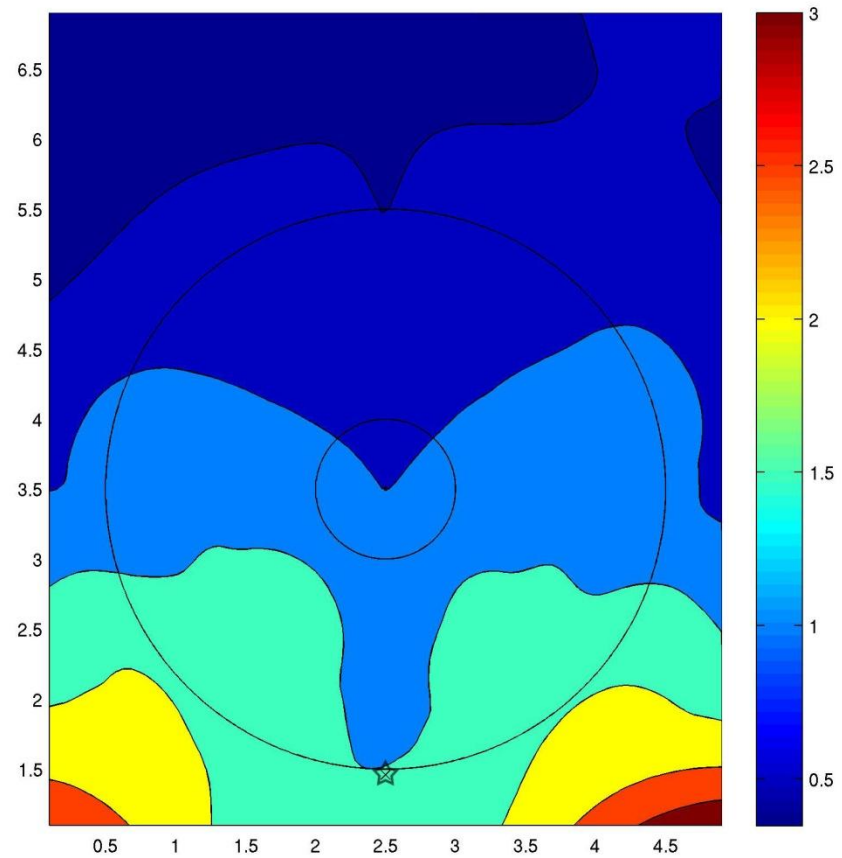
Figure 3.19. Ey Difference plot at transmitter location 10 (displayed as a star on plot). The x-axis refers to the x-direction at the surface and is in meters. Likewise, the y-axis refers to the y-direction at the surface. Color bar units are relative differences with red being more different and blue being less different. Outer rims of both conical depressions are superimposed on plot.

87
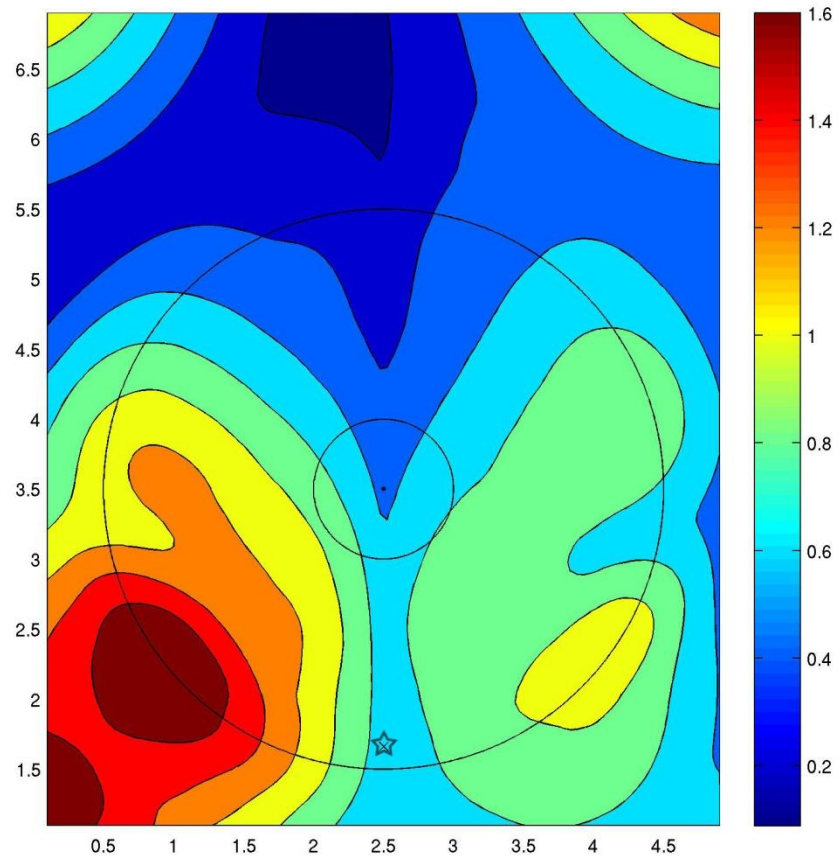
Figure 3.20. Ey Difference plot at transmitter location 15 (displayed as a star on plot). The x-axis refers to the x-direction at the surface and is in meters. Likewise, the y-axis refers to the y-direction at the surface. Color bar units are relative differences with red being more different and blue being less different. Outer rims of both conical depressions are superimposed on plot.

88
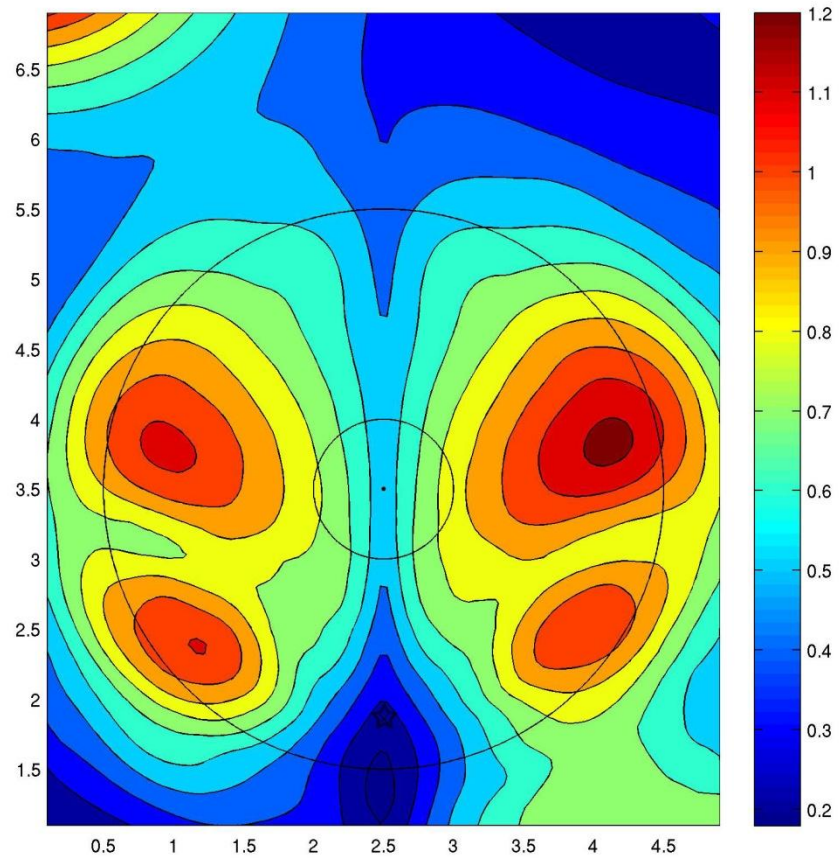
Figure 3.21. Ey Difference plot at transmitter location 20 (displayed as a star on plot). The x-axis refers to the x-direction at the surface and is in meters. Likewise, the y-axis refers to the y-direction at the surface. Color bar units are relative differences with red being more different and blue being less different. Outer rims of both conical depressions are superimposed on plot.

89
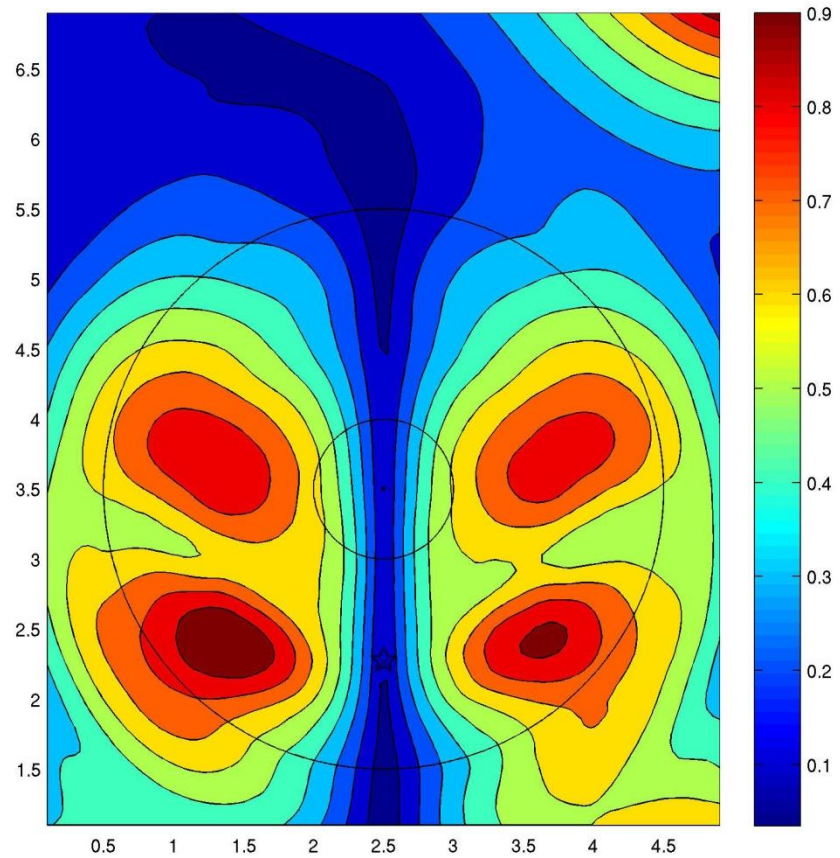
Figure 3.22. Ey Difference plot at transmitter location 30 (displayed as a star on plot). The x-axis refers to the x-direction at the surface and is in meters. Likewise, the y-axis refers to the y-direction at the surface. Color bar units are relative differences with red being more different and blue being less different. Outer rims of both conical depressions are superimposed on plot.

90
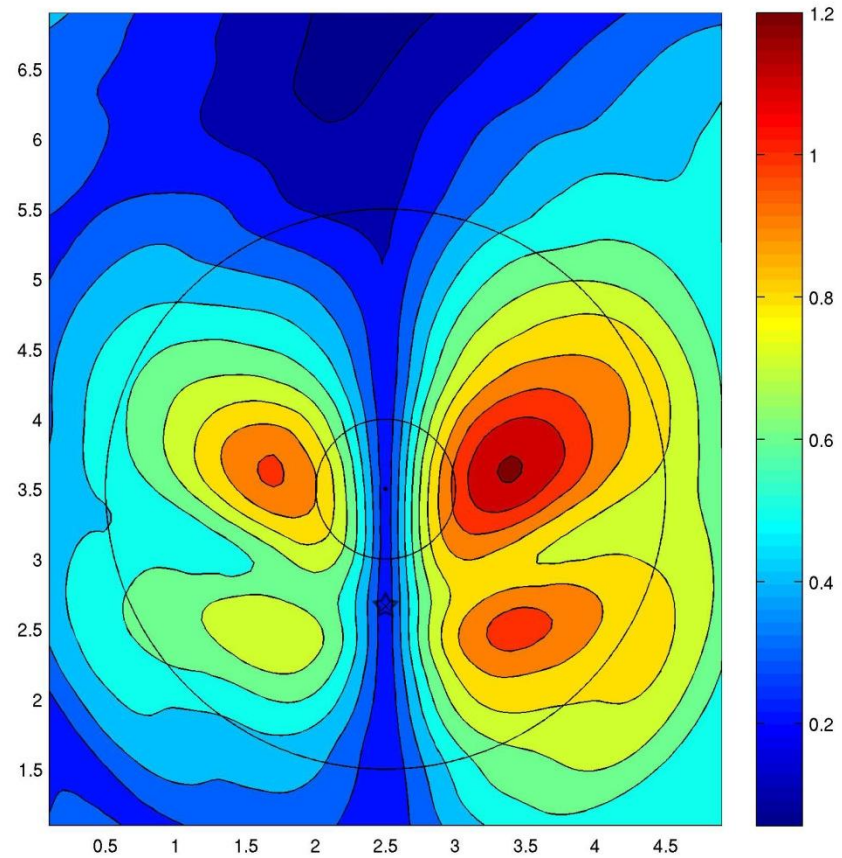
Figure 3.23. Ey Difference plot at transmitter location 40 (displayed as a star on plot). The x-axis refers to the x-direction at the surface and is in meters. Likewise, the y-axis refers to the y-direction at the surface. Color bar units are relative differences with red being more different and blue being less different. Outer rims of both conical depressions are superimposed on plot.

91
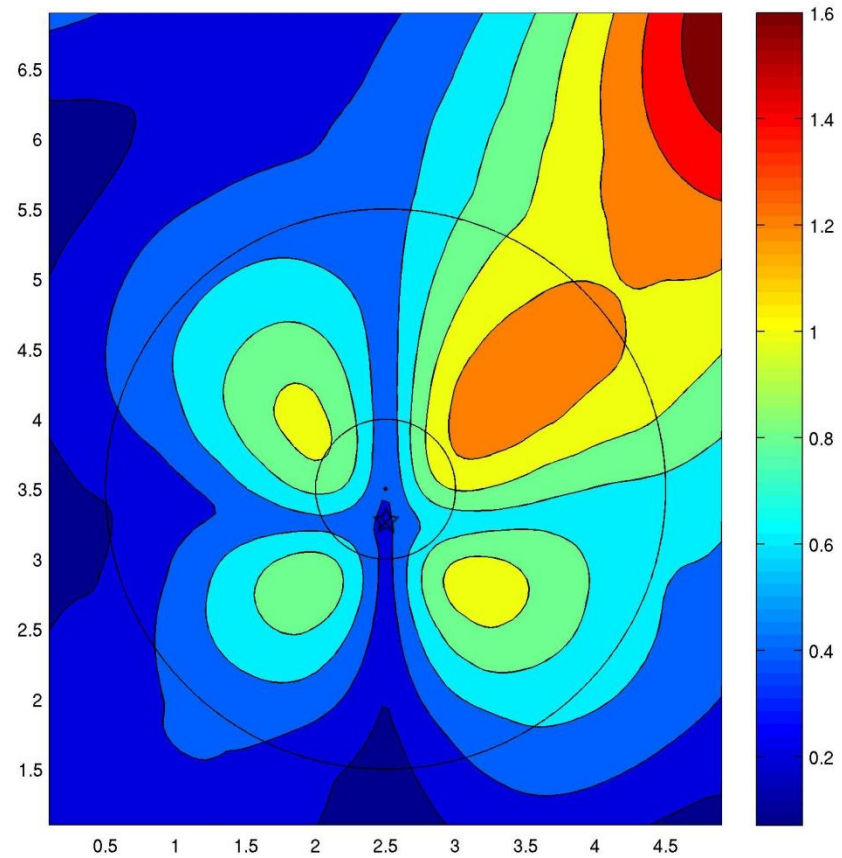
Figure 3.24. Ey Difference plot at transmitter location 55 (displayed as a star on plot). The x-axis refers to the x-direction at the surface and is in meters. Likewise, the y-axis refers to the y-direction at the surface. Color bar units are relative differences with red being more different and blue being less different. Outer rims of both conical depressions are superimposed on plot.

92
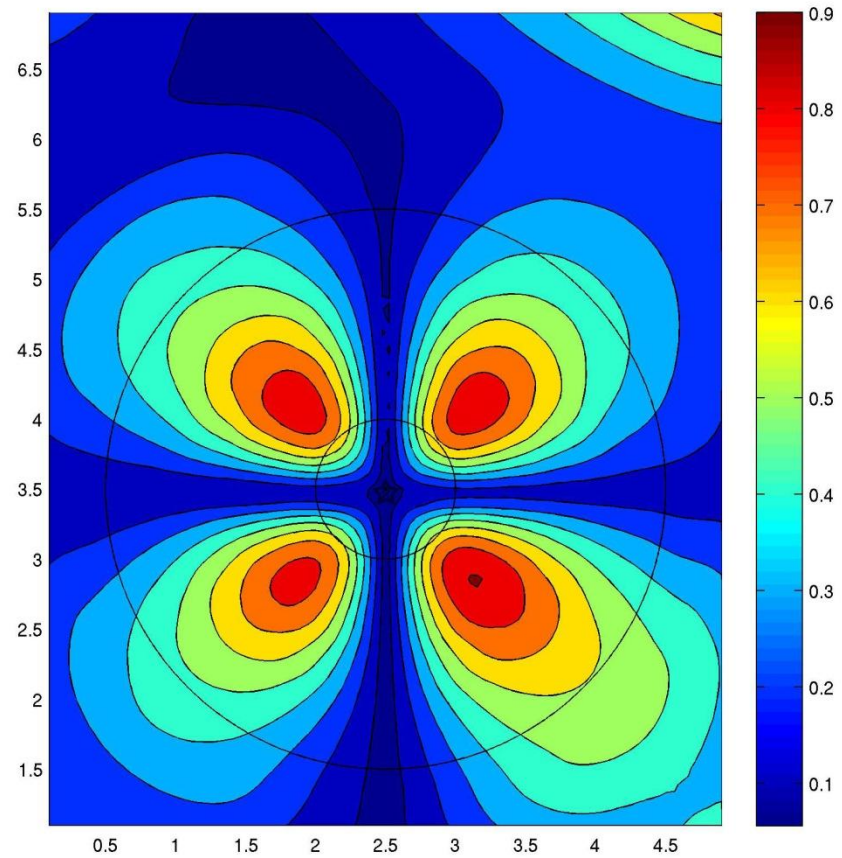
Figure 3.25. Ey Difference plot at transmitter location 60 (displayed as a star on plot). The x-axis refers to the x-direction at the surface and is in meters. Likewise, the y-axis refers to the y-direction at the surface. Color bar units are relative differences with red being more different and blue being less different. Outer rims of both conical depressions are superimposed on plot.

93
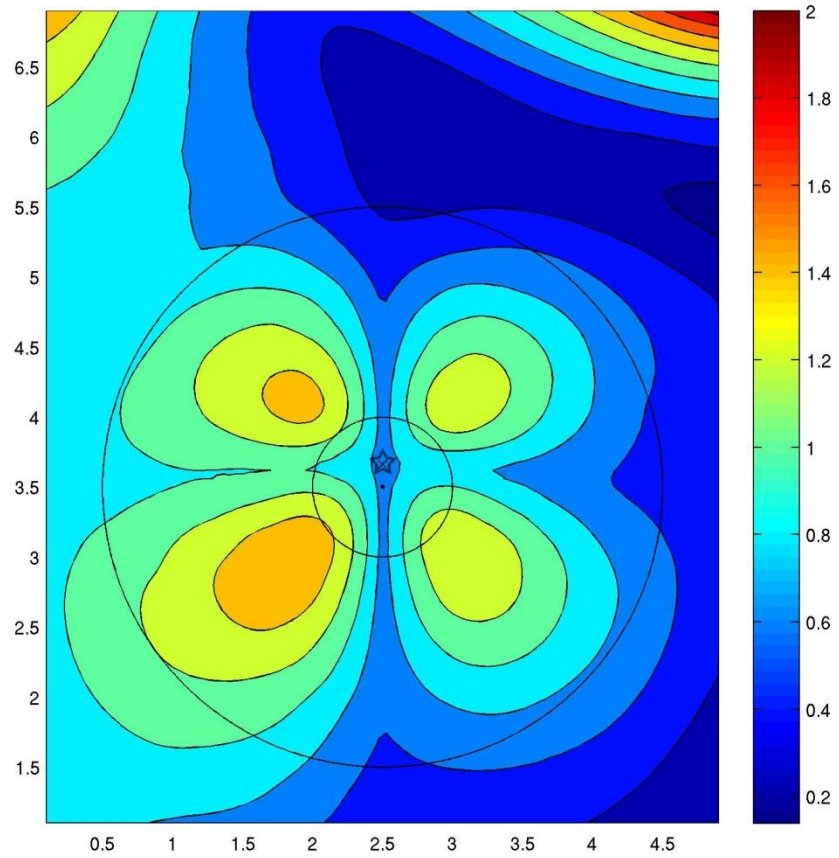
Figure 3.26. Ey Difference plot at transmitter location 65 (displayed as a star on plot). The x-axis refers to the x-direction at the surface and is in meters. Likewise, the y-axis refers to the y-direction at the surface. Color bar units are relative differences with red being more different and blue being less different. Outer rims of both conical depressions are superimposed on plot.

94
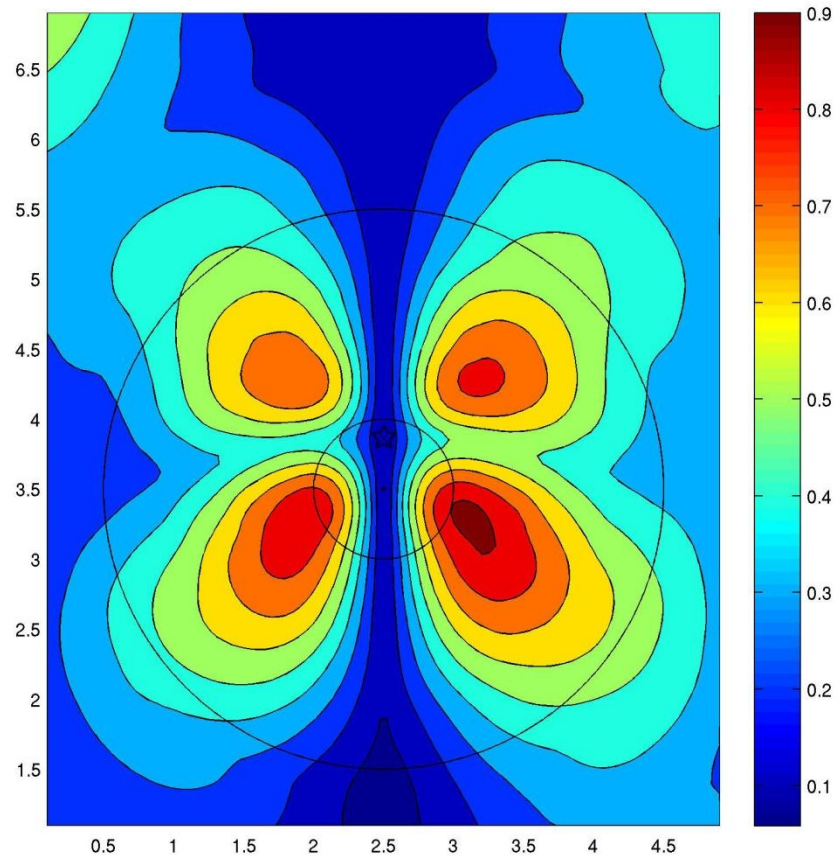
Figure 3.27. Ey Difference plot at transmitter location 70 (displayed as a star on plot). The x-axis refers to the x-direction at the surface and is in meters. Likewise, the y-axis refers to the y-direction at the surface. Color bar units are relative differences with red being more different and blue being less different. Outer rims of both conical depressions are superimposed on plot.

95
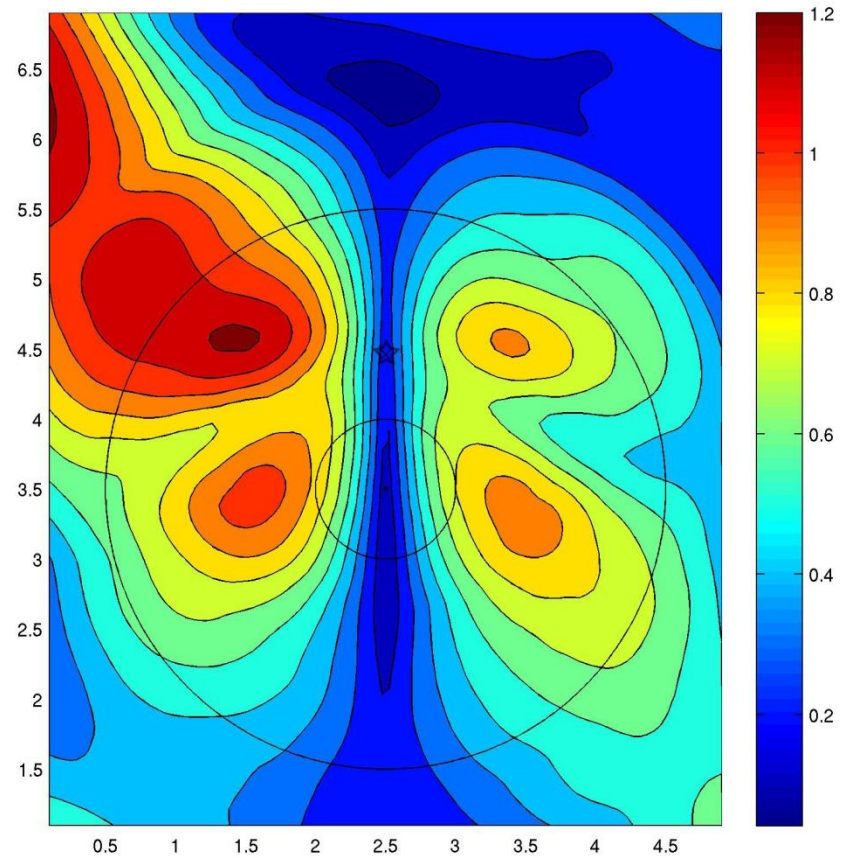
Figure 3.28. Ey Difference plot at transmitter location 85 (displayed as a star on plot). The x-axis refers to the x-direction at the surface and is in meters. Likewise, the y-axis refers to the y-direction at the surface. Color bar units are relative differences with red being more different and blue being less different. Outer rims of both conical depressions are superimposed on plot.
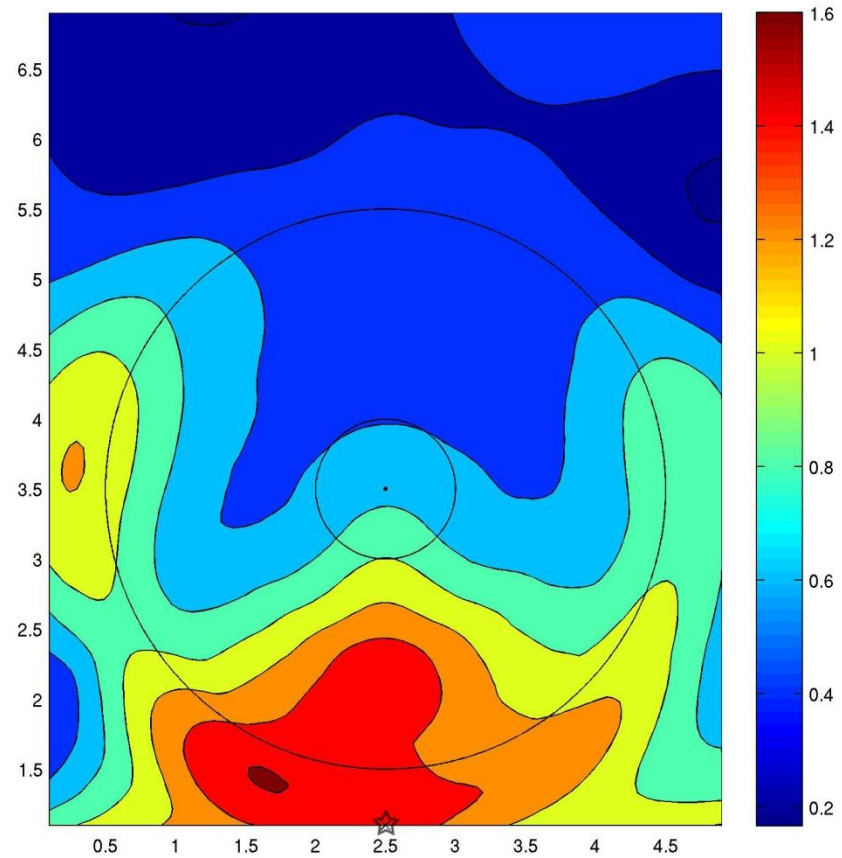
96
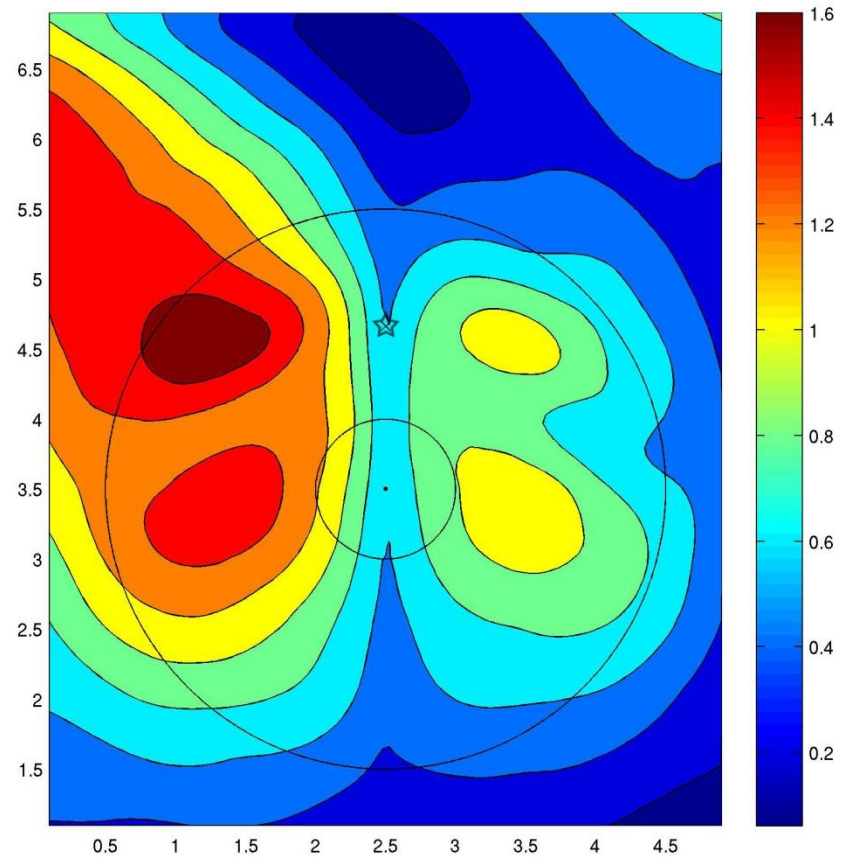
Figure 3.29. Ey Difference plot at transmitter location 90 (displayed as a star on plot). The x-axis refers to the x-direction at the surface and is in meters. Likewise, the y-axis refers to the y-direction at the surface. Color bar units are relative differences with red being more different and blue being less different. Outer rims of both conical depressions are superimposed on plot.
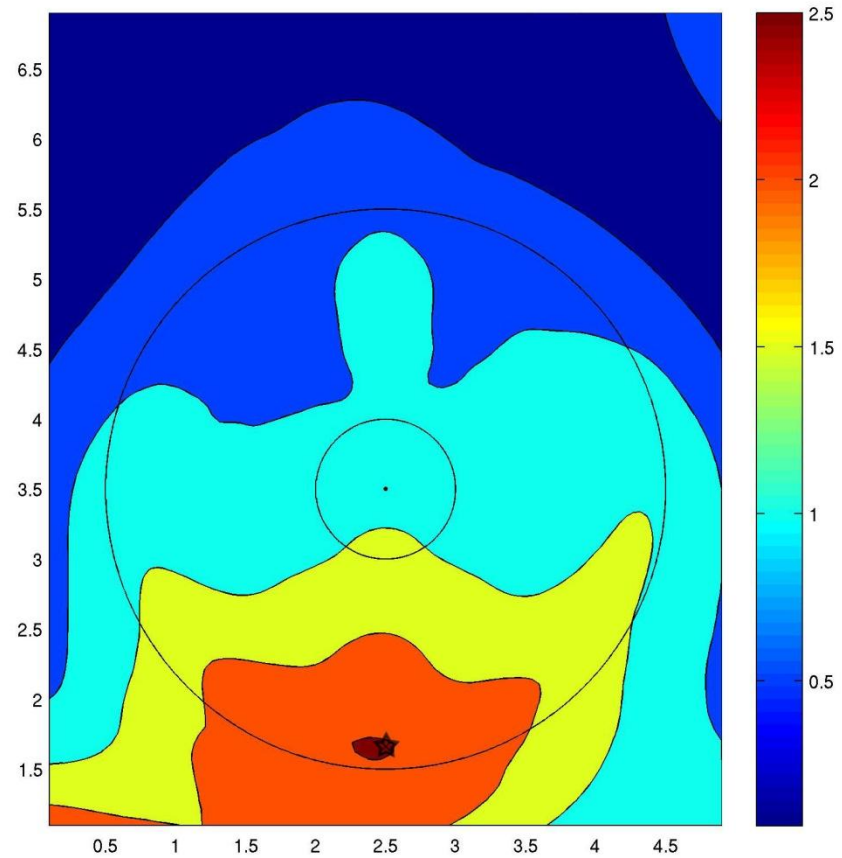
97
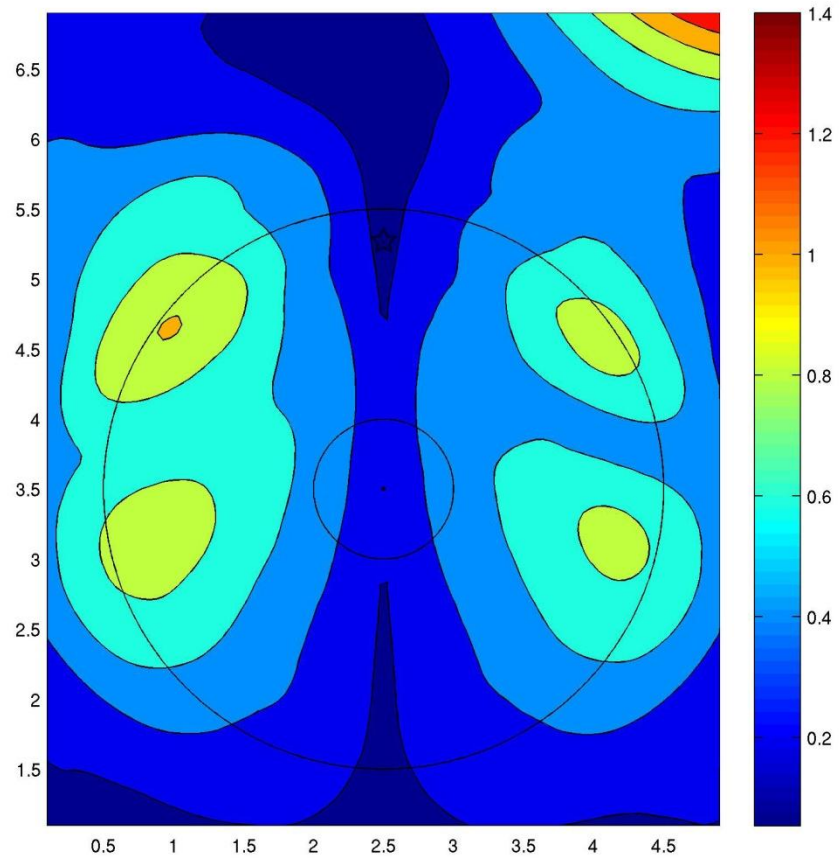
Figure 3.30. Ey Difference plot at transmitter location 105 (displayed as a star on plot). The x-axis refers to the x-direction at the surface and is in meters. Likewise, the y-axis refers to the y-direction at the surface. Color bar units are relative differences with red being more different and blue being less different. Outer rims of both conical depressions are superimposed on plot.

98
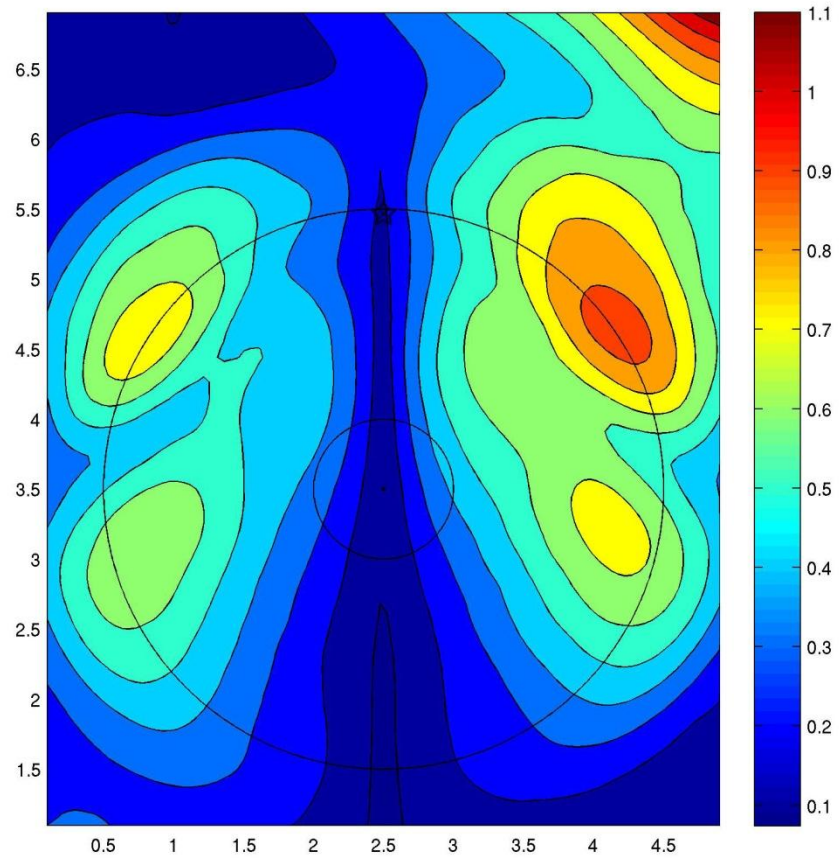
Figure 3.31. Ey Difference plot at transmitter location 110 (displayed as a star on plot). The x-axis refers to the x-direction at the surface and is in meters. Likewise, the y-axis refers to the y-direction at the surface. Color bar units are relative differences with red being more different and blue being less different. Outer rims of both conical depressions are superimposed on plot.

99

Field Data from GeoPark, Tampa, FL

High Resolution 3D GPR Grids

In order to better understand the connection between the modeled results and real-world structure, high-resolution 3D GPR data was collected from an area with sinkholes and karstic features of dimensions comparable to the sinkhole models. The field site is located in the Geopark on the campus of the University of South Florida in Tampa, Florida (see Figure 4.1). The site is a covered-karst terrain with high sinkhole density (Stewart and Parker, 1992). Figure 4.2 shows a generalized geology of the GeoPark with 1-2 m of unconsolidated sands underlain by a 2-3 m sequence of fining sands to clays. Below that, limestone that varies from very-weathered on top to a less-weathered limestone underneath. Mapped sinkholes in the area range in diameter from a few meters across to approximately 15 meters (see Figure 4.2).

In October, 2008, a 3D GPR survey (250 MHz) was collected in order to obtain a 3D data set in an area of the GeoPark that had not been previously studied at high resolution. A year later, in October, 2009, another 3D GPR survey (500 MHz) was acquired to look at a specific section of that area in more detail. The locations of these survey areas are in Figure 4.1. The 3D surveys were conducted by collecting GPR data along parallel lines in a "mowing the lawn" fashion. The first survey (250 MHz) covered

100

an area of approximately 35 m by 13 m and used 0.10 m in-line spacing (trace interval, 0.05 m). The second survey (500 MHz) covered an area of approximately 16 m by 9 m (inside the previous survey area) and used 0.05 m in-line spacing (trace interval, 0.025 m). The specific radar system used for both surveys was manufactured by MALÅ Geoscience.
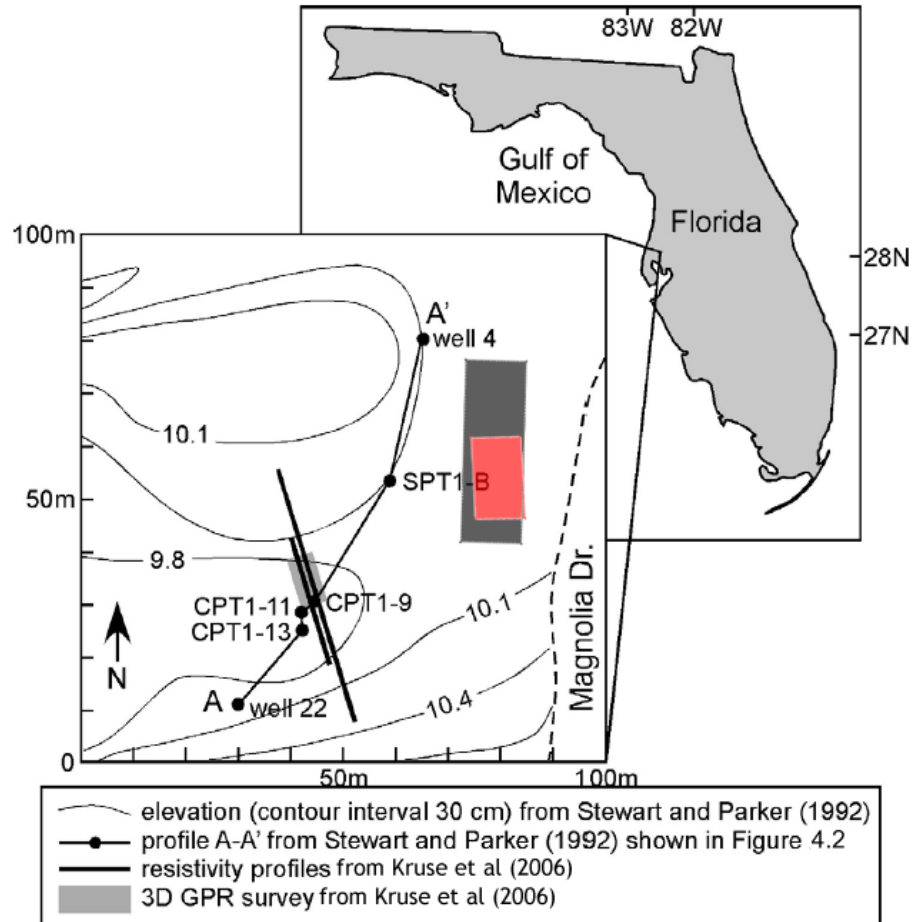
Figure 4.1. Figure modified from Kruse et al (2006) showing approximate locations of previous studies conducted in the USF GeoPark. In addition, the black-shaded area represents the approximate location of the 250 MHz 3D GPR grid and the red-shaded, the 500 MHz grid.

101
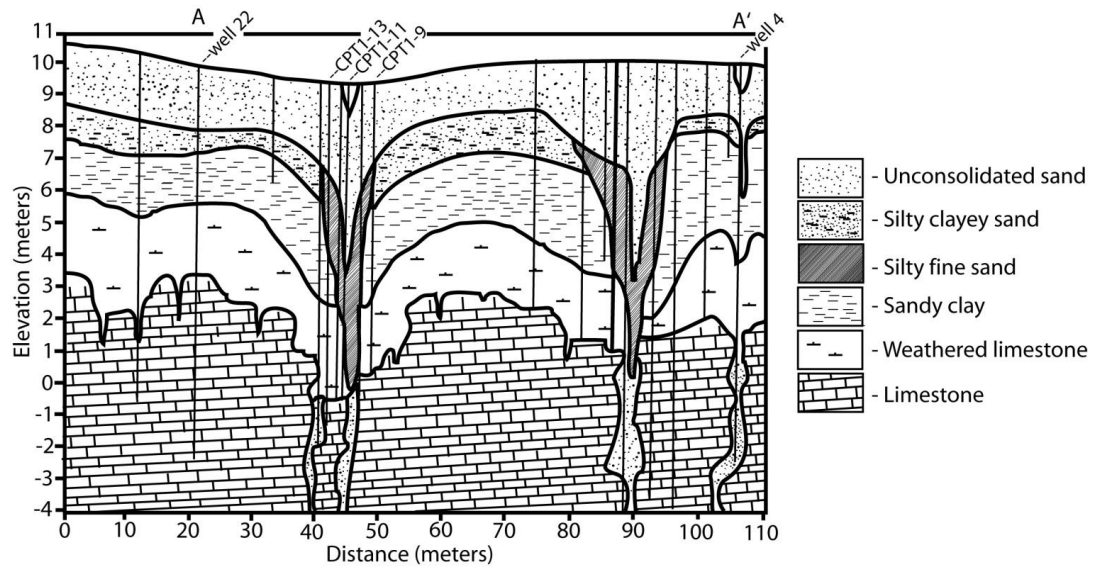
Figure 4.2. Figure showing near-surface geology of USF GeoPark from Kruse et al (2006), originally from Stewart and Parker (1992). Data compiled from CPT and well data at sites along profile A-A' shown in Figure 4.1.

Processing the GPR data first required the flipping and fitting of each line of data to minimize offset jitters due to the errors of switching direction at the end of each line. Data were then processed with the program ReflexW (Sandmeier). Both data sets were processed by dewowing, statics, background removal, custom gain functions, and fk filtering. The data were also 3D migrated after this using ReflexW's constant-velocity diffraction stack migrations. The 250 MHz data were processed with a velocity of 0.10 m/ns and the 500 MHz data with 0.12 m/ns; found by applying a best-fitting velocity

Figure 4.3, 250 MHz, depth = 0.94 m
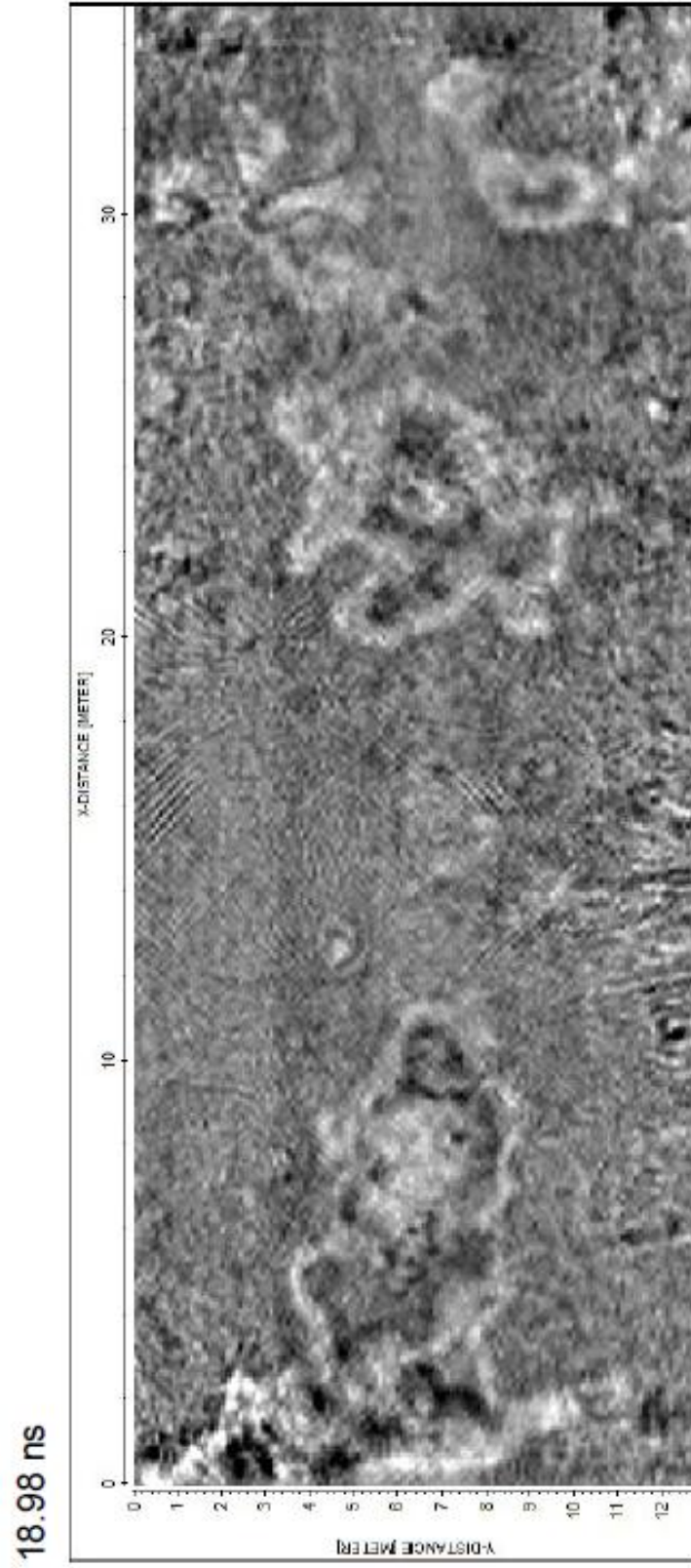
Figure 4.4, 250 MHz, depth = 1.19 m
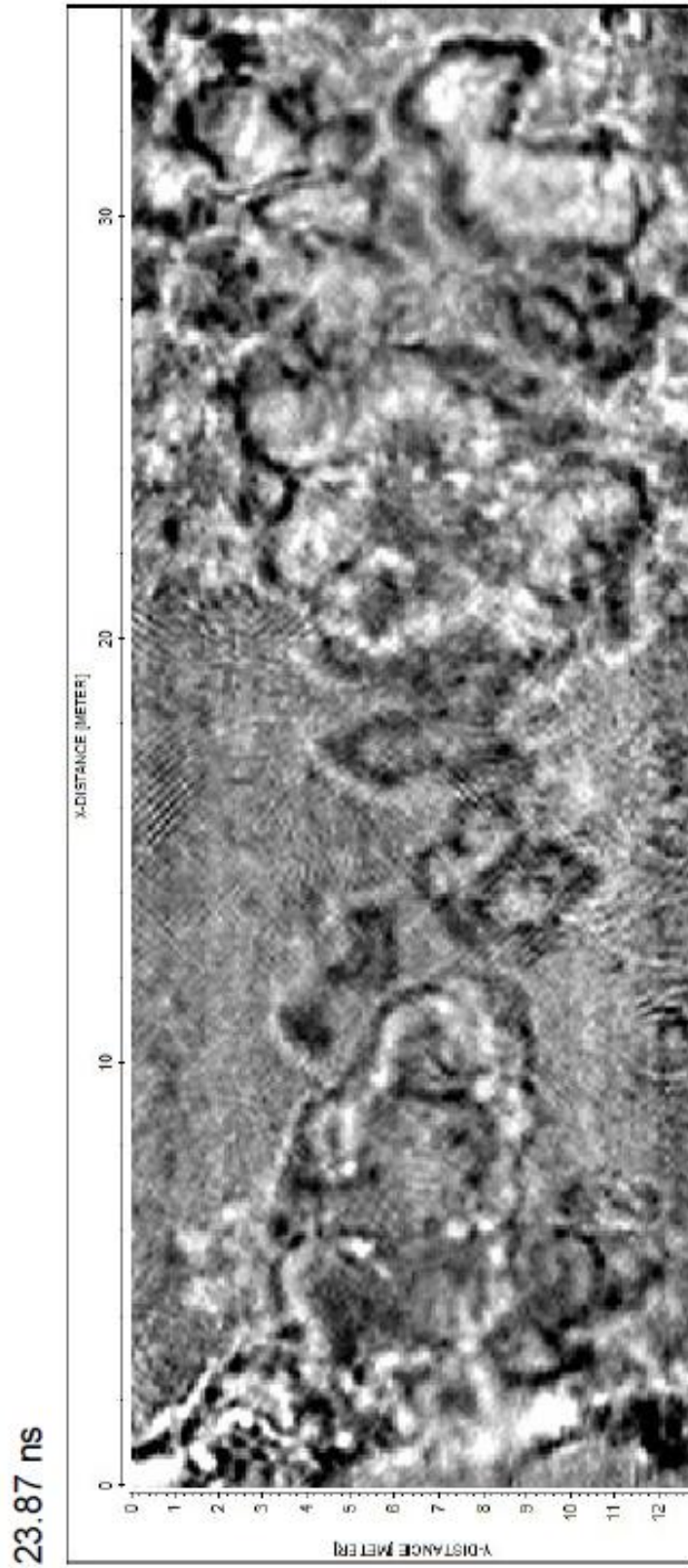
Figure 4.5, 250 MHz, depth = 1.48 m

105
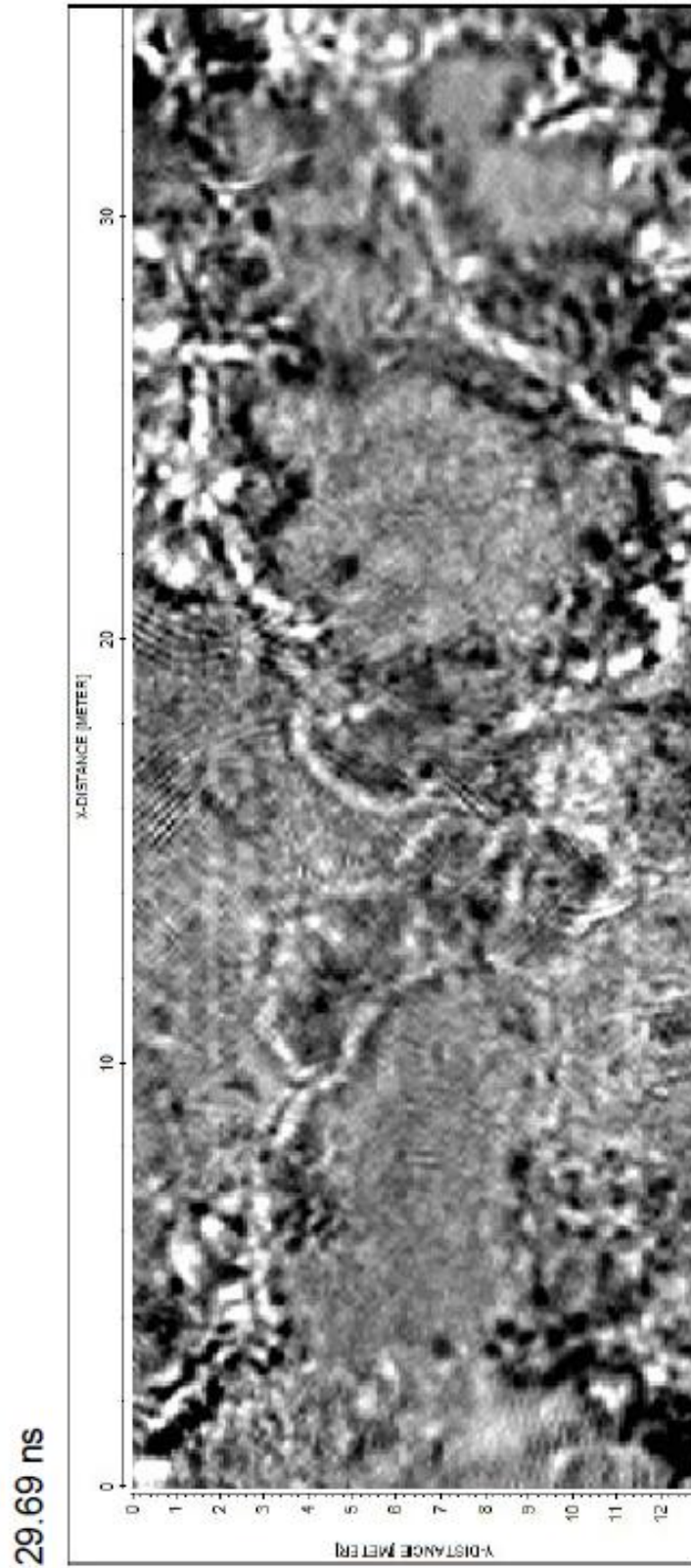
Figure 4.6, 250 MHz, depth = 1.70 m

33.97 ns
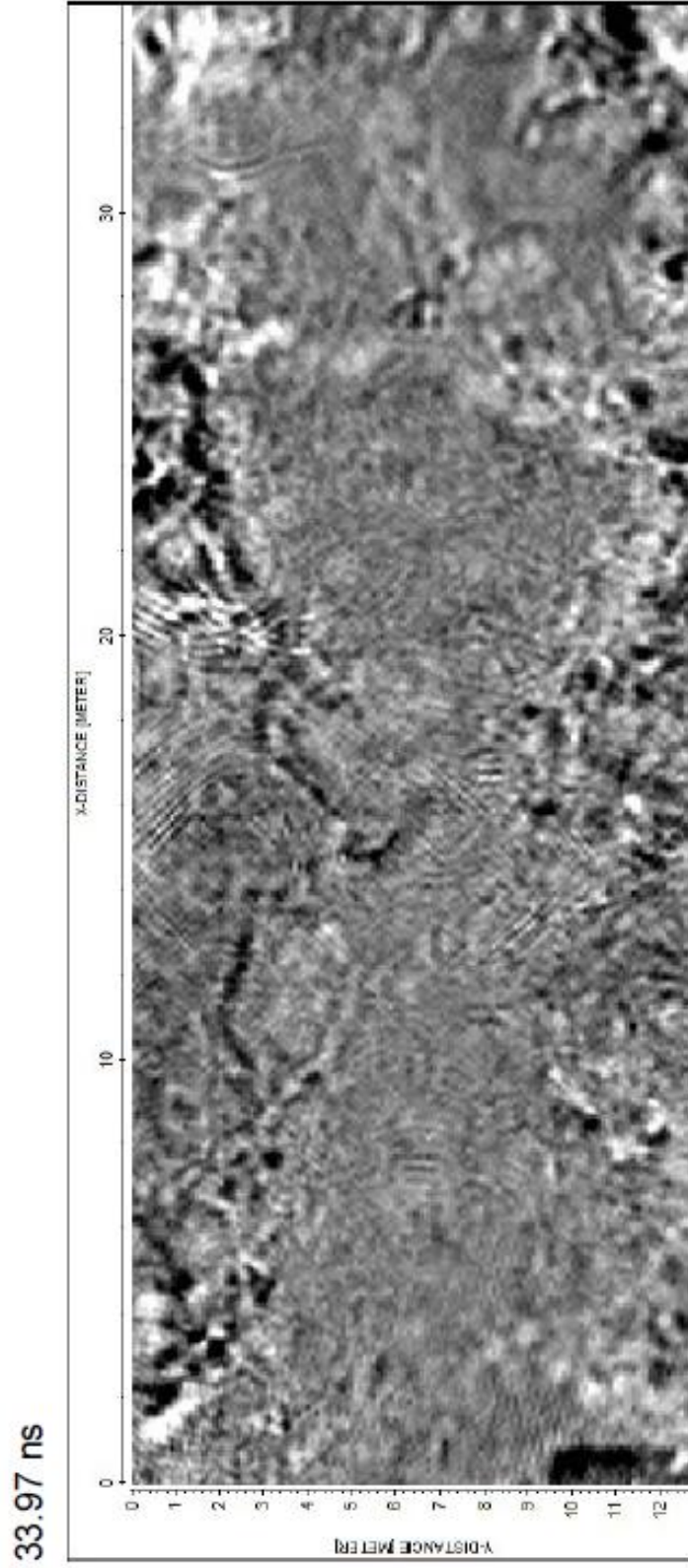
Figures 4.3-4.6. Migrated time slice 3D GPR (250 MHz) data oriented in the same position as that of the black-shaded area it is represented by in Figure 4.1. Figure numbers also increase with time.

analysis to various diffraction hyperbolas in the profiles. The differing velocities are presumably due to varying water content in the ground on different dates. Profiles were acquired along the long axis of the survey grid and those produced from the cross-lines are interpolated when making the 3D cube. The cross-line profiles are less sharp in appearance than the in-line profiles acquired for this reason, as well as, the fact the spatial sampling is half as dense in the cross-line direction.

The 250 MHz GPR shows the prominent features (Figures 4.3-4.6). First, there are two general areas of higher hill-like reflection surfaces that gradually deepen with time. These are most likely the tops of the silty clayey sand horizon which follows the topography of the deeper geologic structure. The structure appears to trend North-South with a sag in the middle and steeper drop-offs to the east and west. The second feature of interest is a small sinkhole in the mid-to-lower SE section of the grid.

Only certain selected lines from the entire 3D data cube have been displayed to emphasis certain features and to save space in this publication. The entire area of the sinkhole was not surveyed (the sinkhole lies partially off the grid) but enough of it existed on record due to its symmetry to analyze and interpret it as a sinkhole. The small sinkhole, as it appears in the 250 MHz data (see Figure 4.7-4.21), is roughly a circular

107

Figure 4.7, 250 MHz, depth = 1.90 m

108
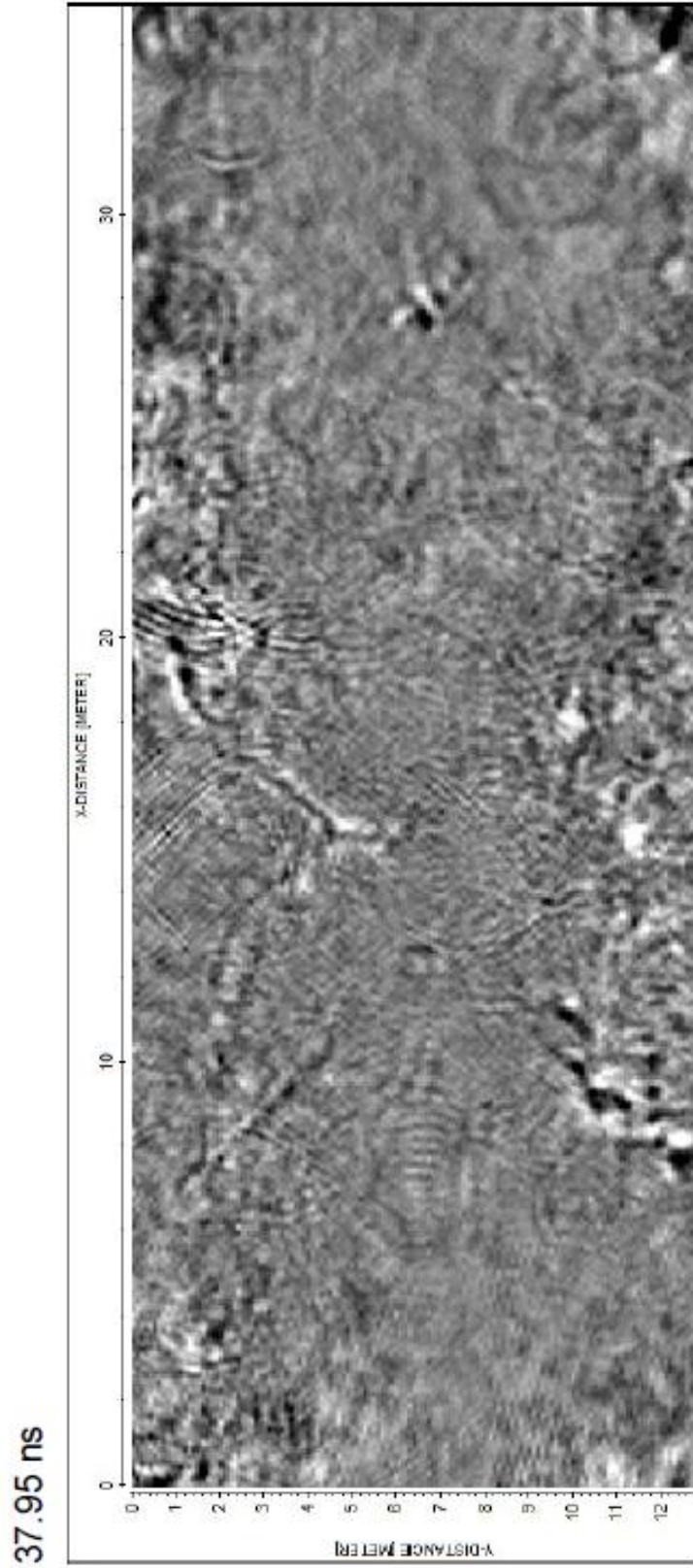
Figure 4.8, 250 MHz, depth = 2.19 m

109
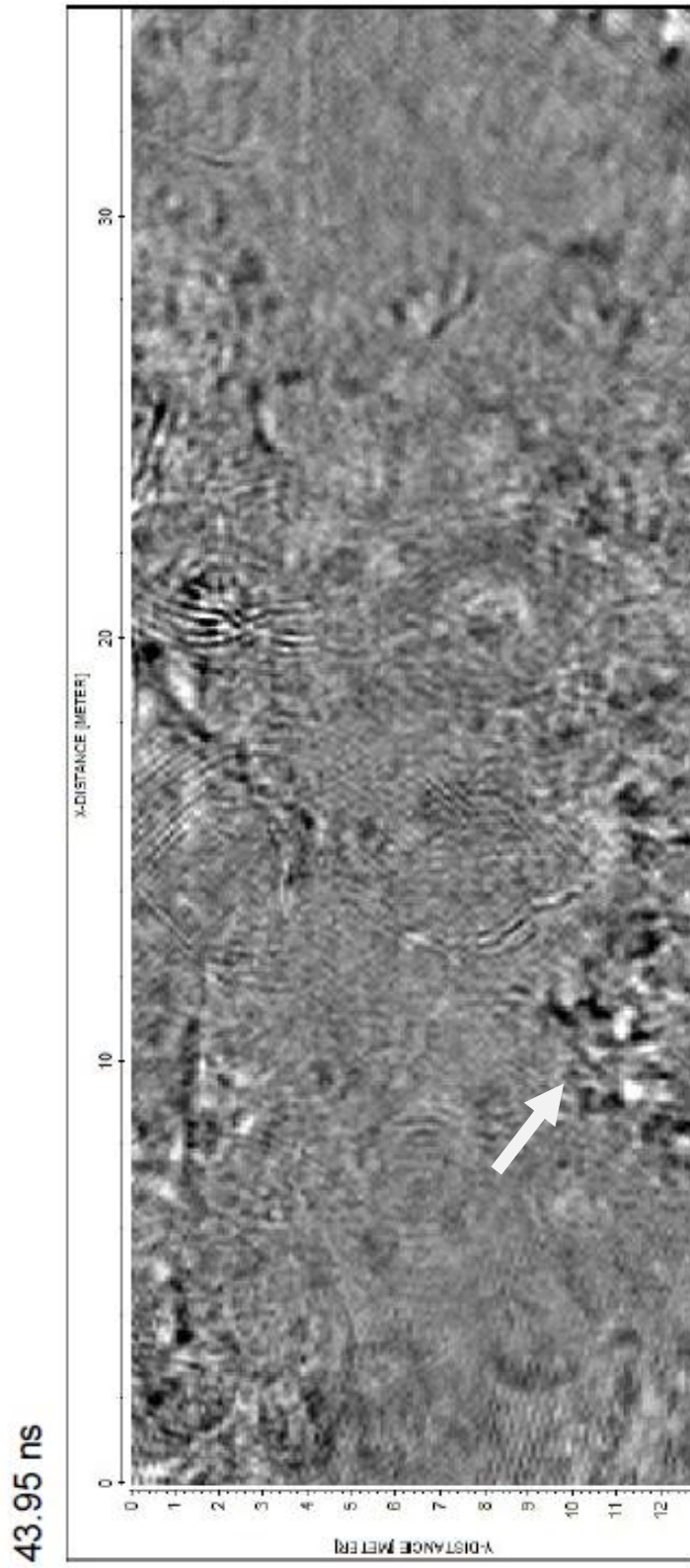
Figure 4.9, 250 MHz, depth = 2.30 m
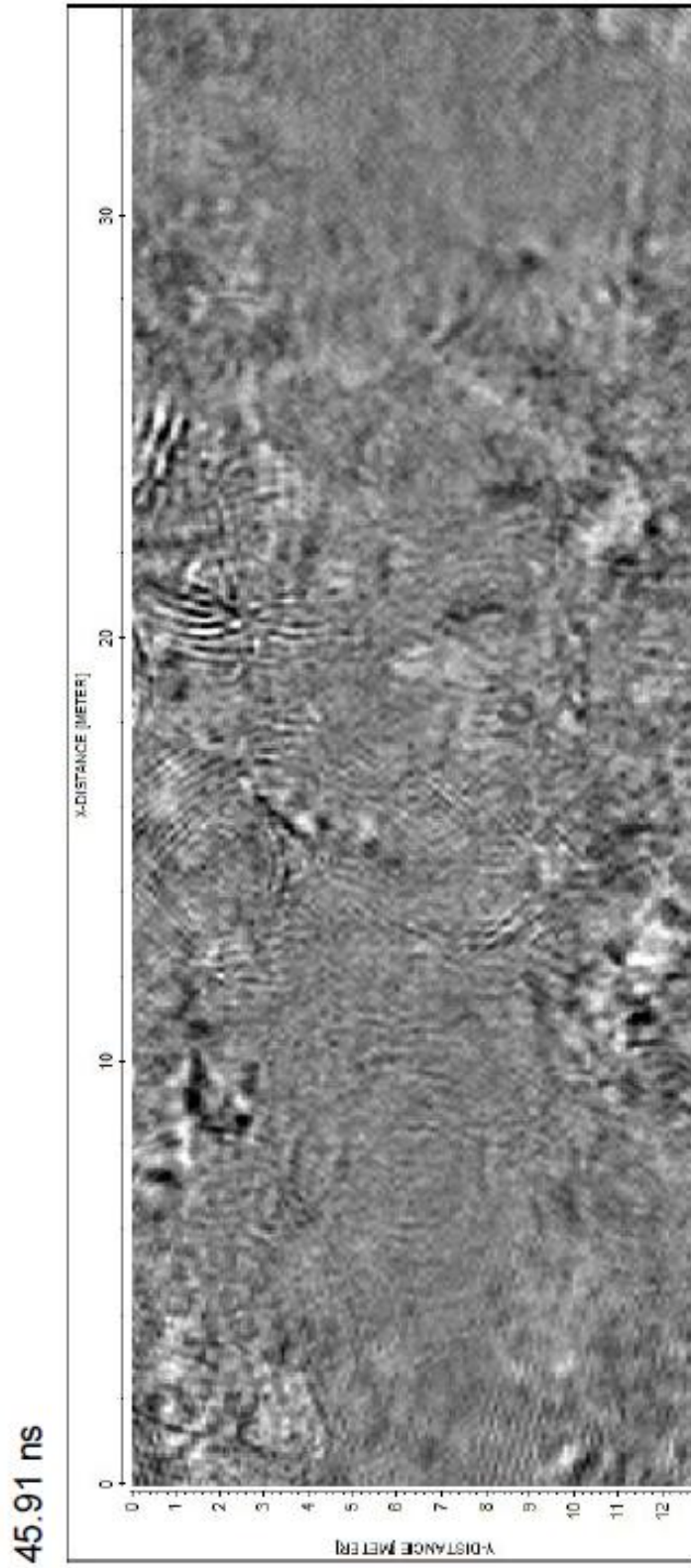
Figure 4.10, 250 MHz, depth = 2.50 m

111
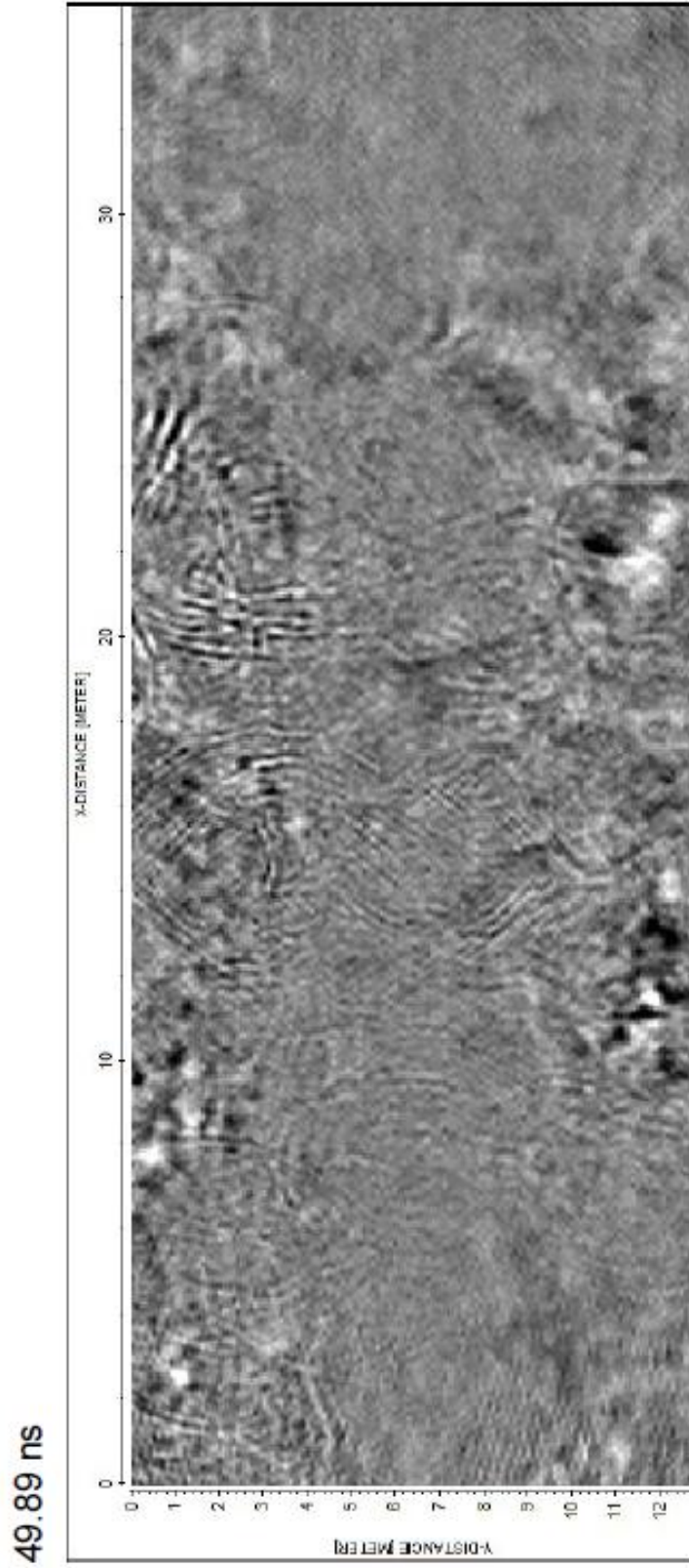
Figure 4.11, 250 MHz, depth = 2.60 m
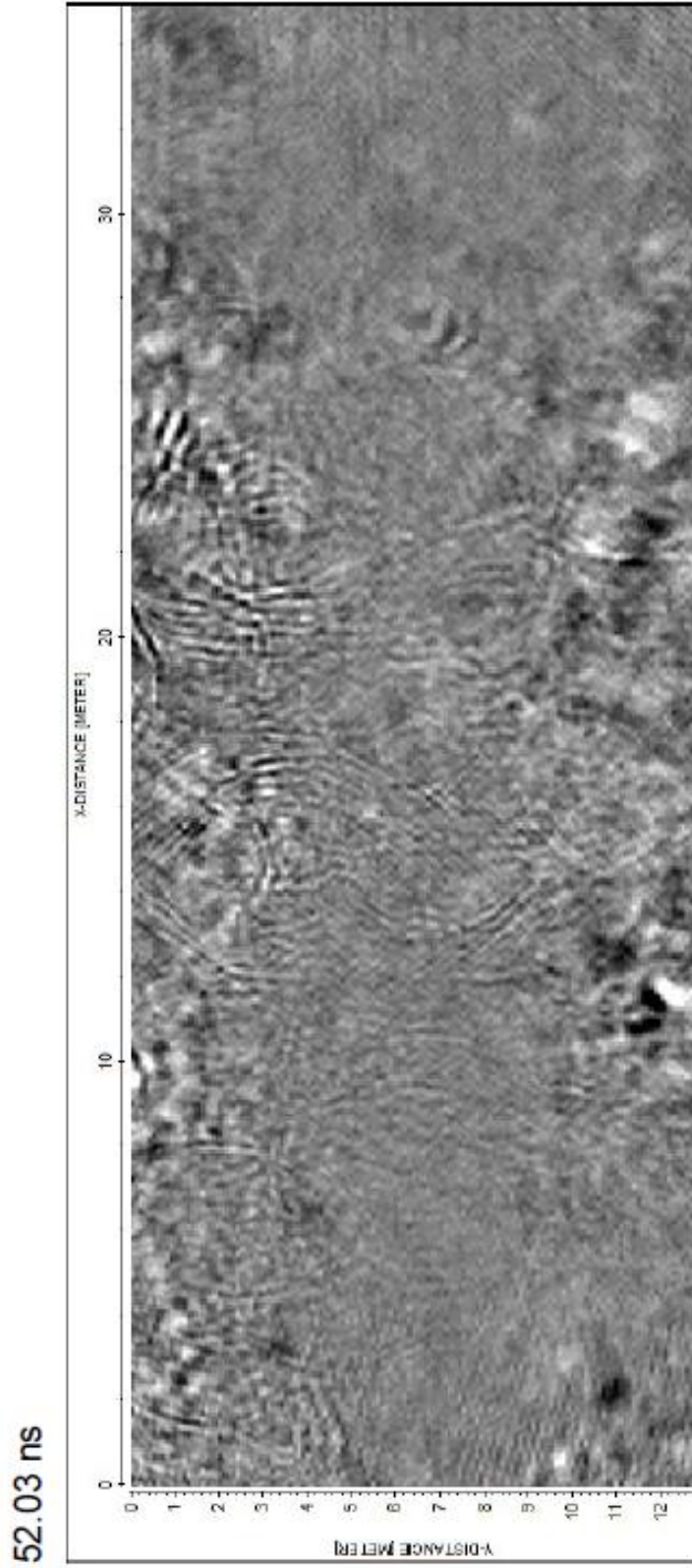
Figures 4.7-4.11. Migrated time slice 3D GPR (250 MHz) data oriented in the
same position as that of the black-shaded area it is represented by in Figure 4.1.
Figure numbers also increase with time.

feature about 4-6 m across (Figure 4.8) and about 2 m deep (Figure 4.14 & 4.20). In all of

the GPR figures, the structure can be seen to form from a general sloping of the

topography. These two objects are the most prominent identifiable features acquired with

the 250 MHz GPR antenna frequency. Anything else that may appear on the profiles is

most likely highly complex, near-surface features or data artifacts, possibly from

migration.

The 500 MHz data grid was collected in a smaller area within the previous survey

mapped with the 250 MHz antenna system. The grid location of the high frequency data

can be seen in Figure 4.1. As with the previous survey, the in-line data were collected

along the long axis of the grid (~N-S). The selected figures can be seen in Figures 4.22-

4.35. Overall, the data from the 500 MHz system are generally of a higher resolution than

those of the 250 MHz system so the data appear sharper. The prominent features in this

3D survey are essentially the same as those in the other data set. The mound-like

structure of the first major reflection surface between the surface sands and underlying

clay-rich sands are visible in the near-surface (Figures 4.22 & 4.23). They are similar in

form when compared to that of the previous survey (Figures 4.3 & 4.4). The sinkhole is

once again visible in the mid-to-lower right hand (E) side of the survey grid (Figure 4.24)

and becomes visible at about 40 ns in time slice view. The sinkhole is about

113

Figure 4.12, 250 MHz

114

Figure 4.13, 250 MHz

9.035 m

115
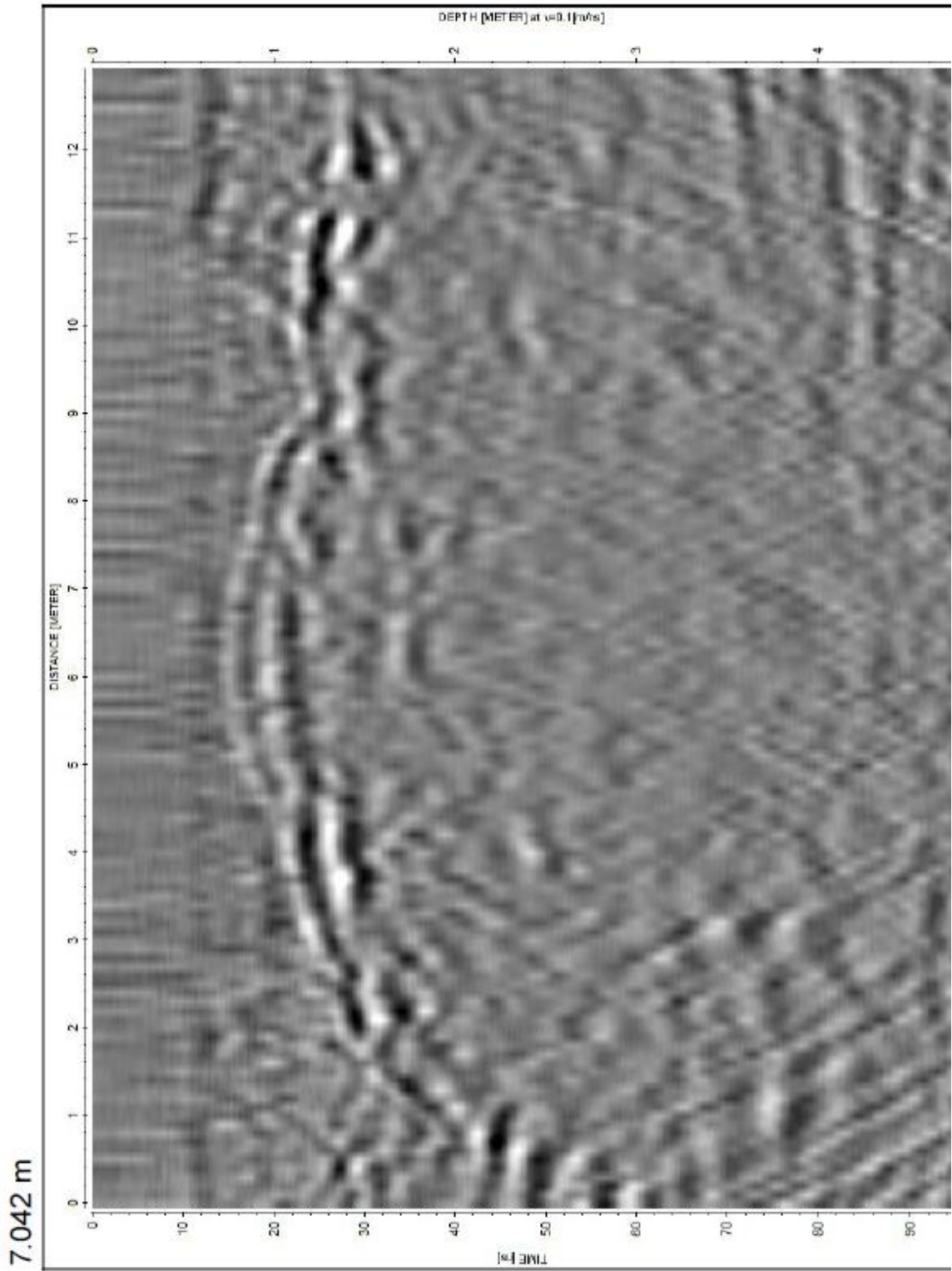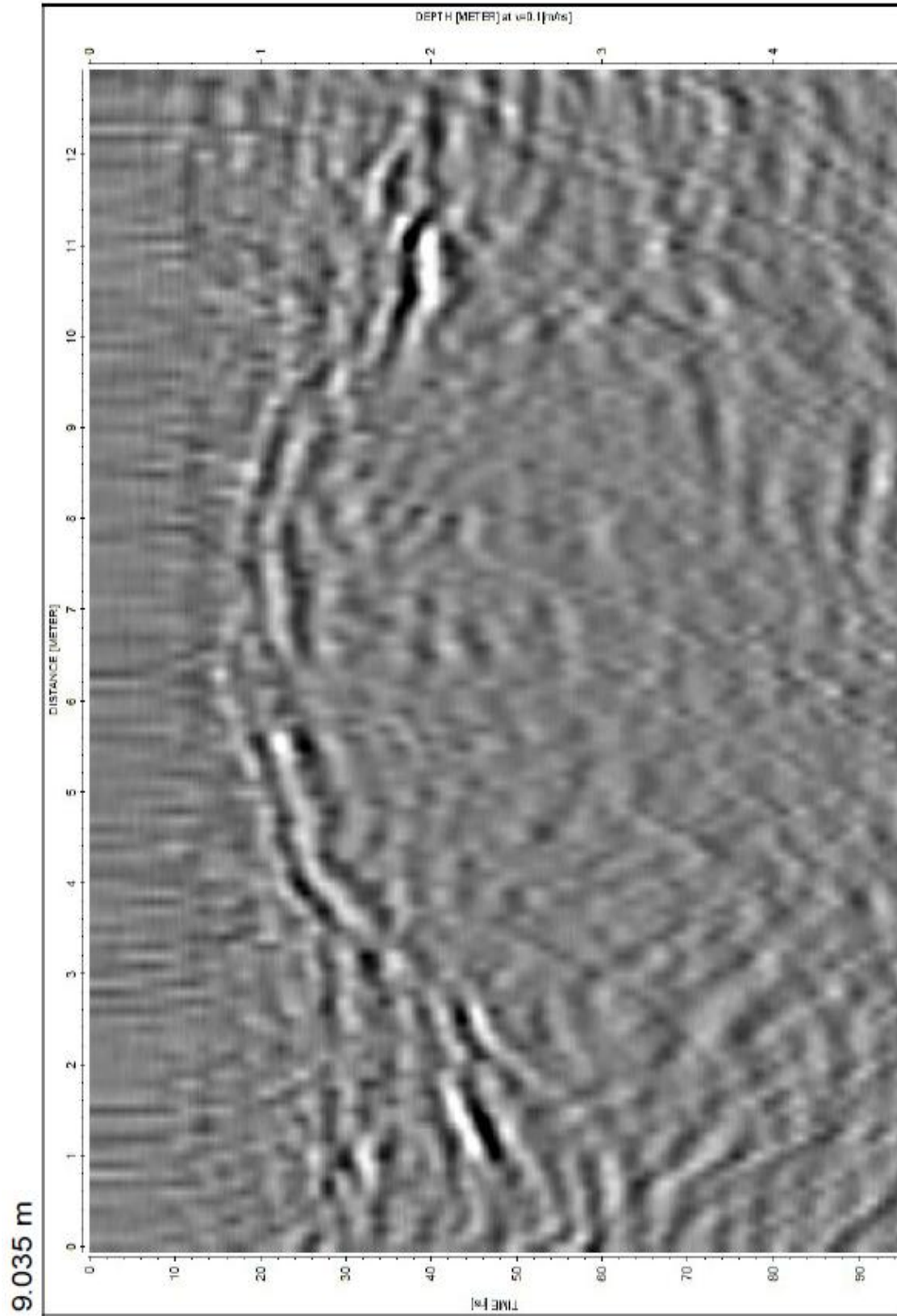
Figure 4.14, 250 MHz
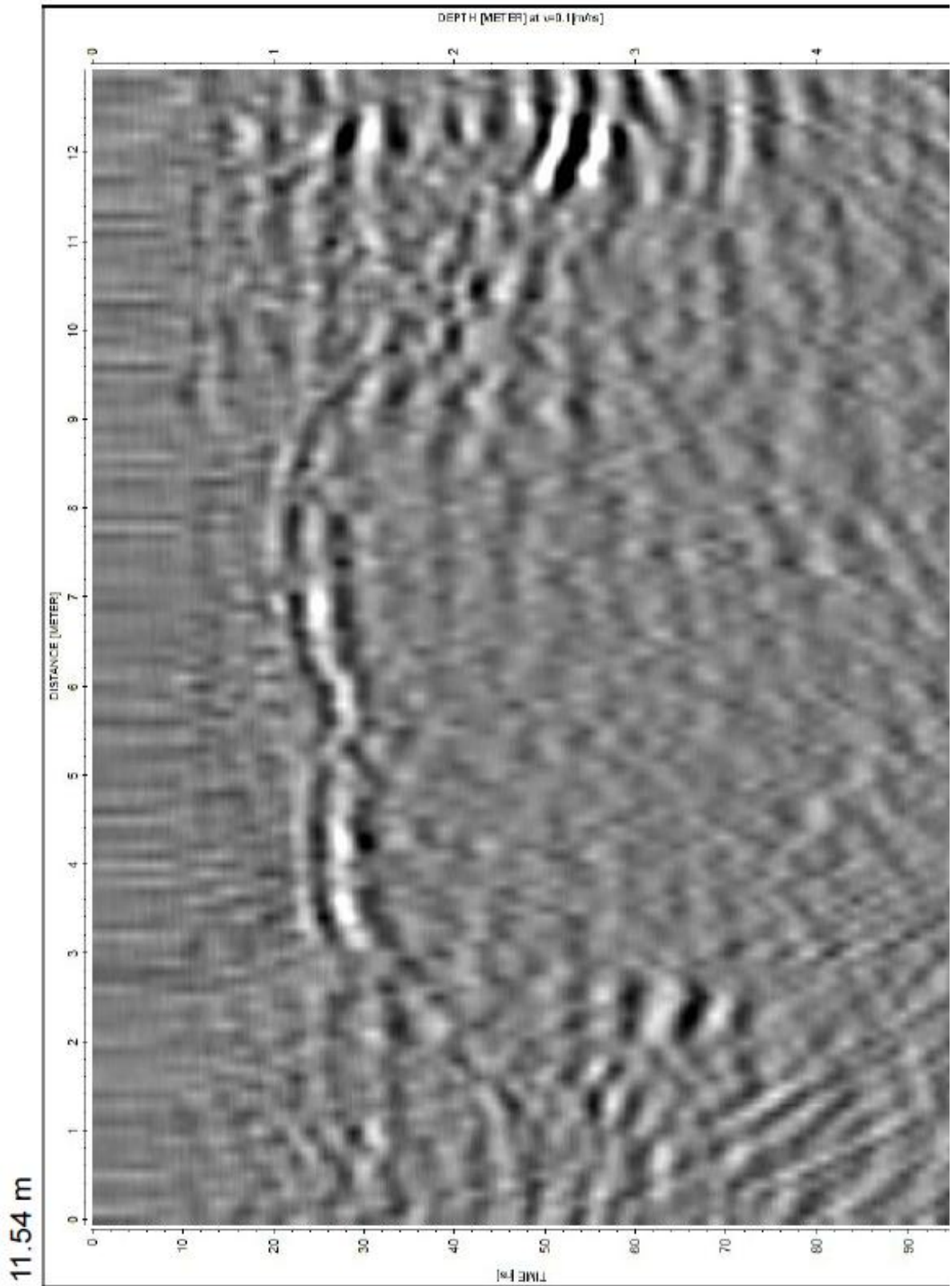
Figures 4.12-4.14. Migrated (time-to-depth correction of 0.1 m/ns) 3D GPR (250 MHz) cross-line data. Data interpolated across in-line profiles and extends across the y-distance on the time slice plots.

5 m across (Figure 4.24) and about 2 m deep (Figures 4.30 & 4.35). Even with an imprecise migration time-to-depth (as seen in diffraction artifacts in the migrated image), the conical sinkhole collapses to a point and completely disappears in the time record appropriately for typical sinkholes (Carpenter and Ekberg, 2006; Truss et al, 2005).

This particular sinkhole geometry is comparable to the model geometry seen in the previous chapters. Results from the models show that steep conduit walls will not be recoverable in the GPR record but shallower slopes will show up. It is also possible that if the base of the sinkhole gradually steepens, the last part of the recoverable slope will appear as the bottom of the sinkhole in the data profile. This could be the case for an example like that in Figure 4.35 where a slope break exists near the bottom of the sink at about 6.5 m along the profile. Comparing that figure to Figure 4.34 shows that there might be conduit structure below the bottom due to the bright reflections beneath the inferred bottom reflections. However, it is not possible to definitively determine whether or not this sinkhole has active sediment piping or not in the sense that it has well-defined conduit structure. Although some studies (Carpenter and Ekberg, 2006; Dobecki and Upchurch, 2006; Batayneh et al, 2002) suggest that more active sinkholes could contain a bright spot of reflections from sediment infilling, this particular sinkhole does not appear to have any sign of it. Any dense collection of reflectors in the top layer of this data are

Figure 4.15, 250 MHz

118

Figure 4.16, 250 MHz

119
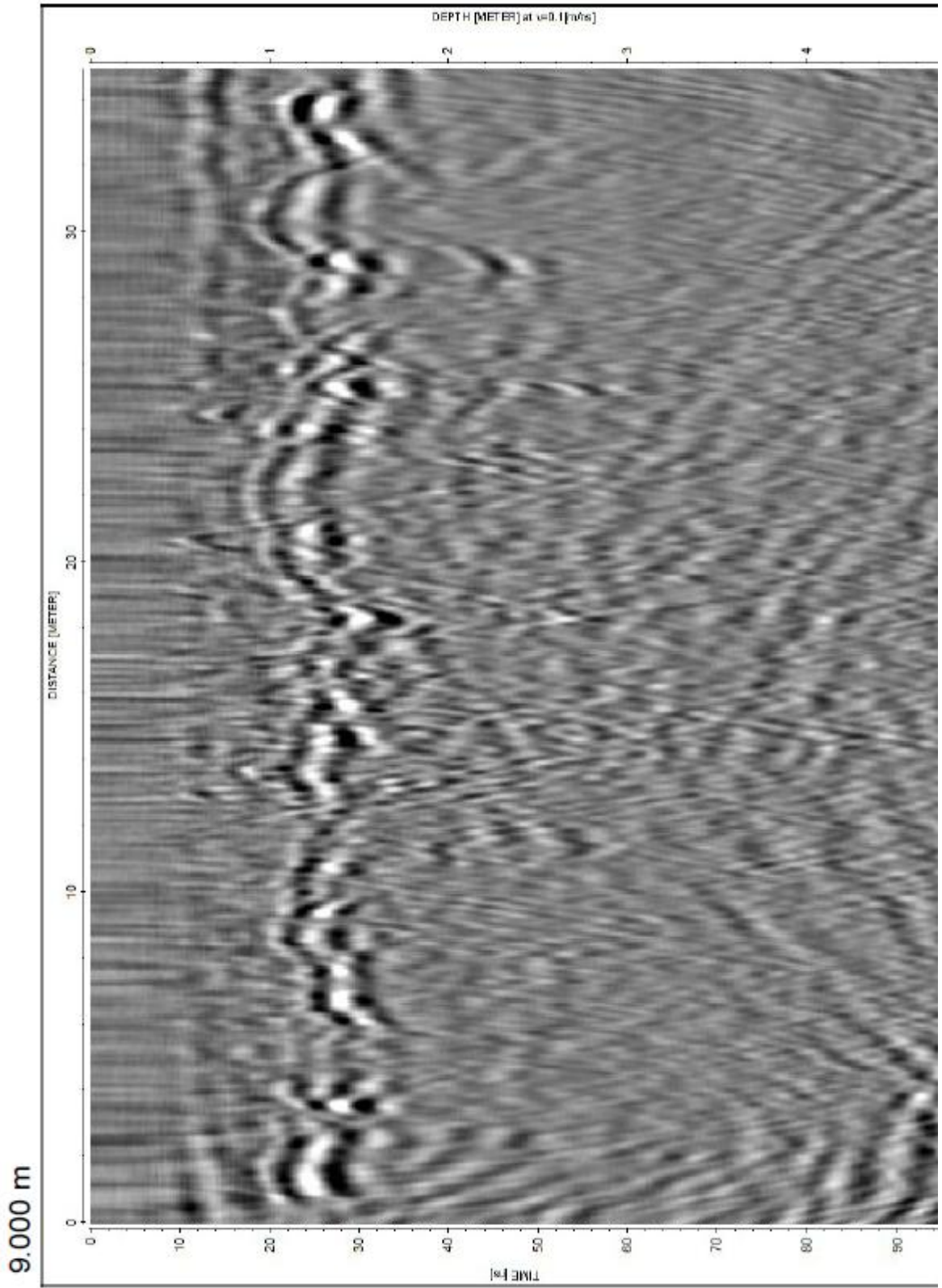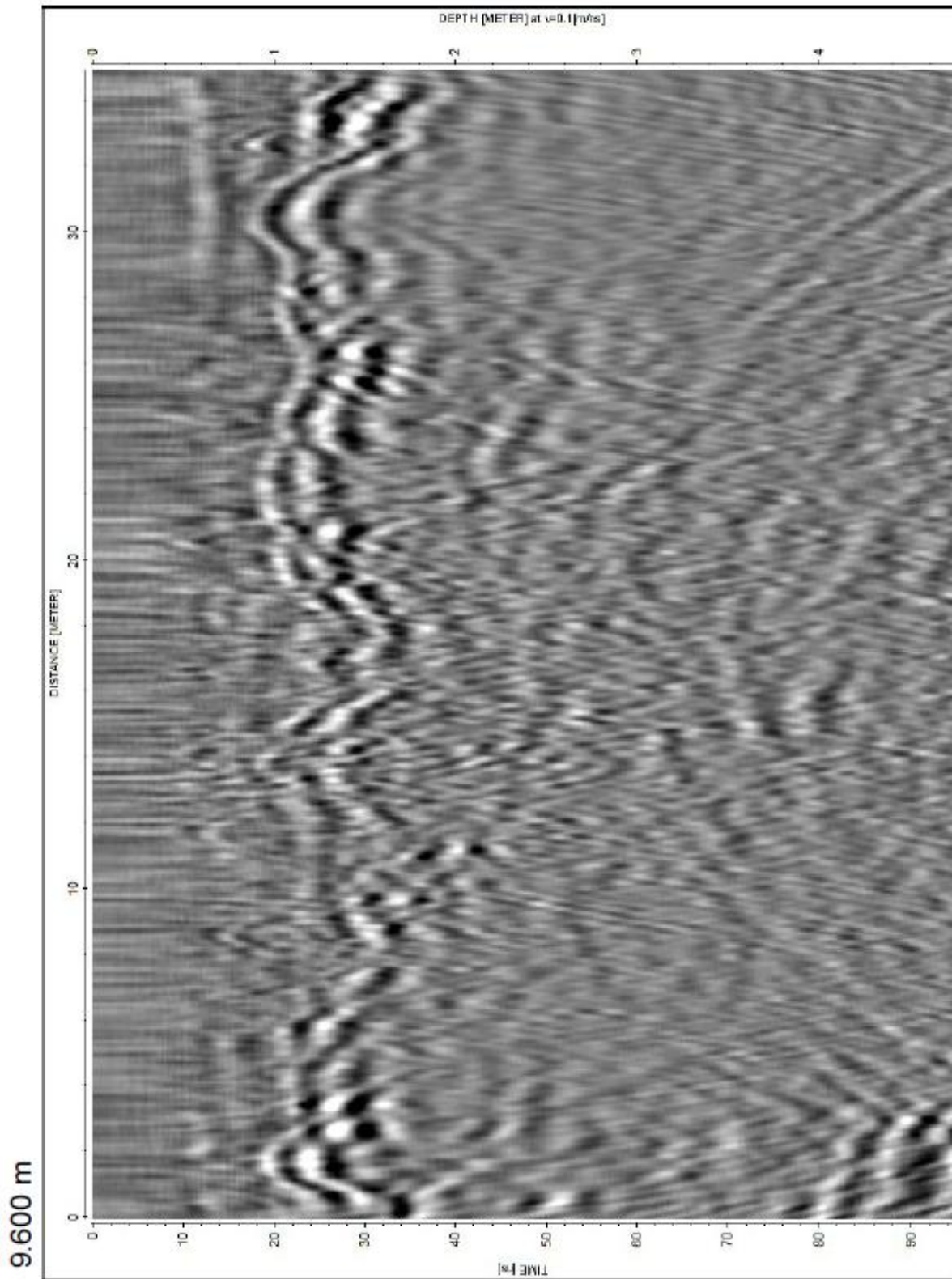
Figure 4.17, 250 MHz

Figure 4.18, 250 MHz

121
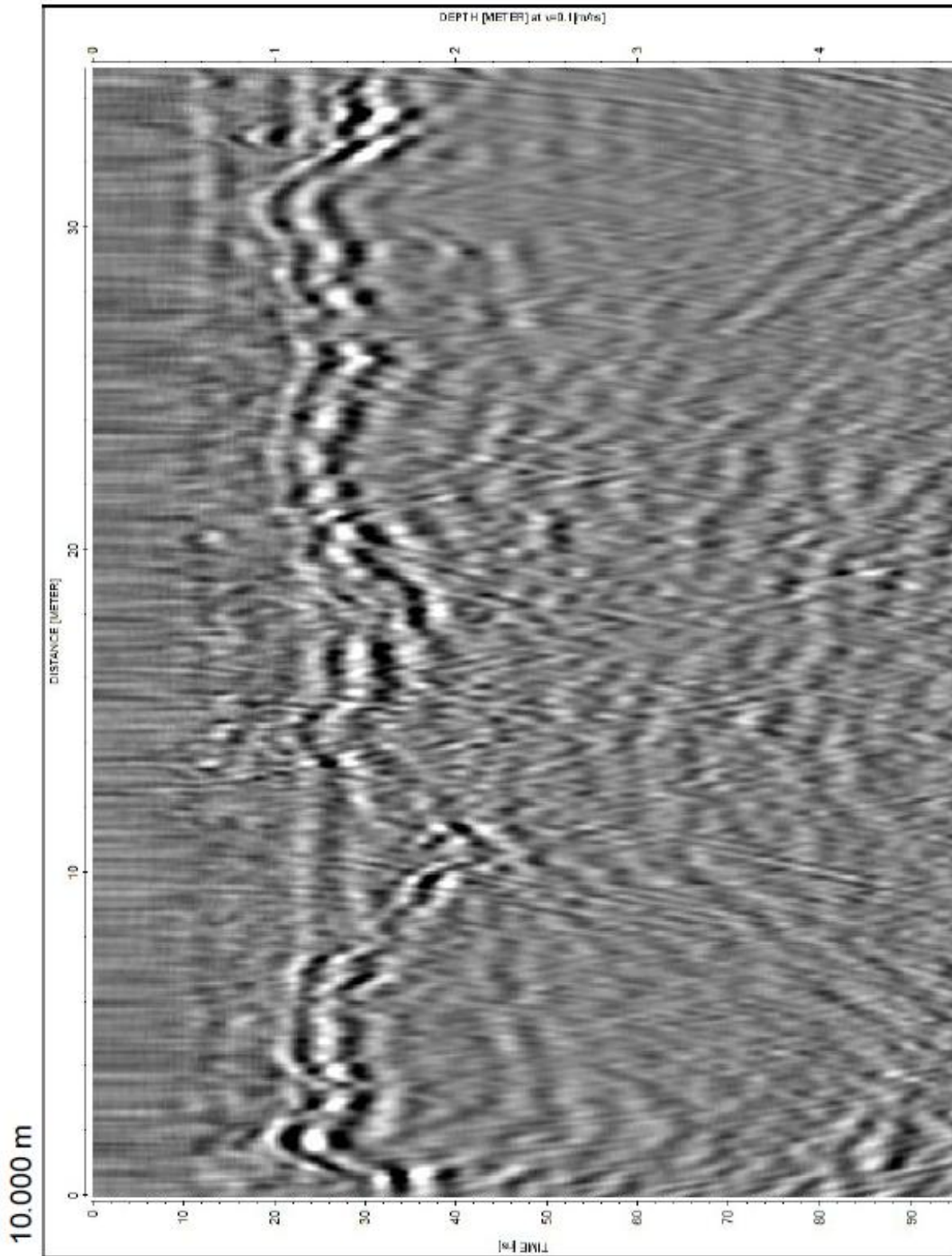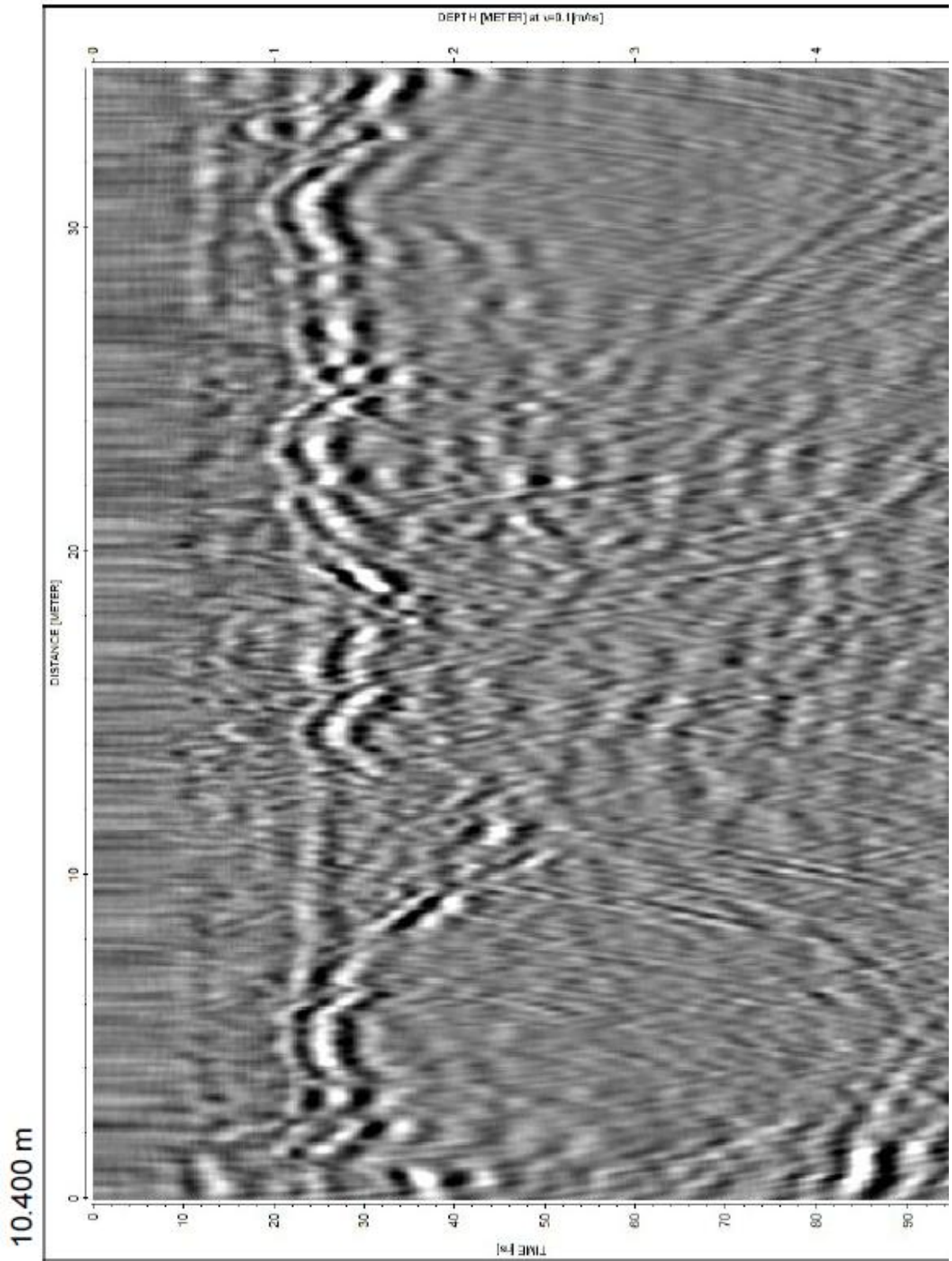
Figure 4.19, 250 MHz
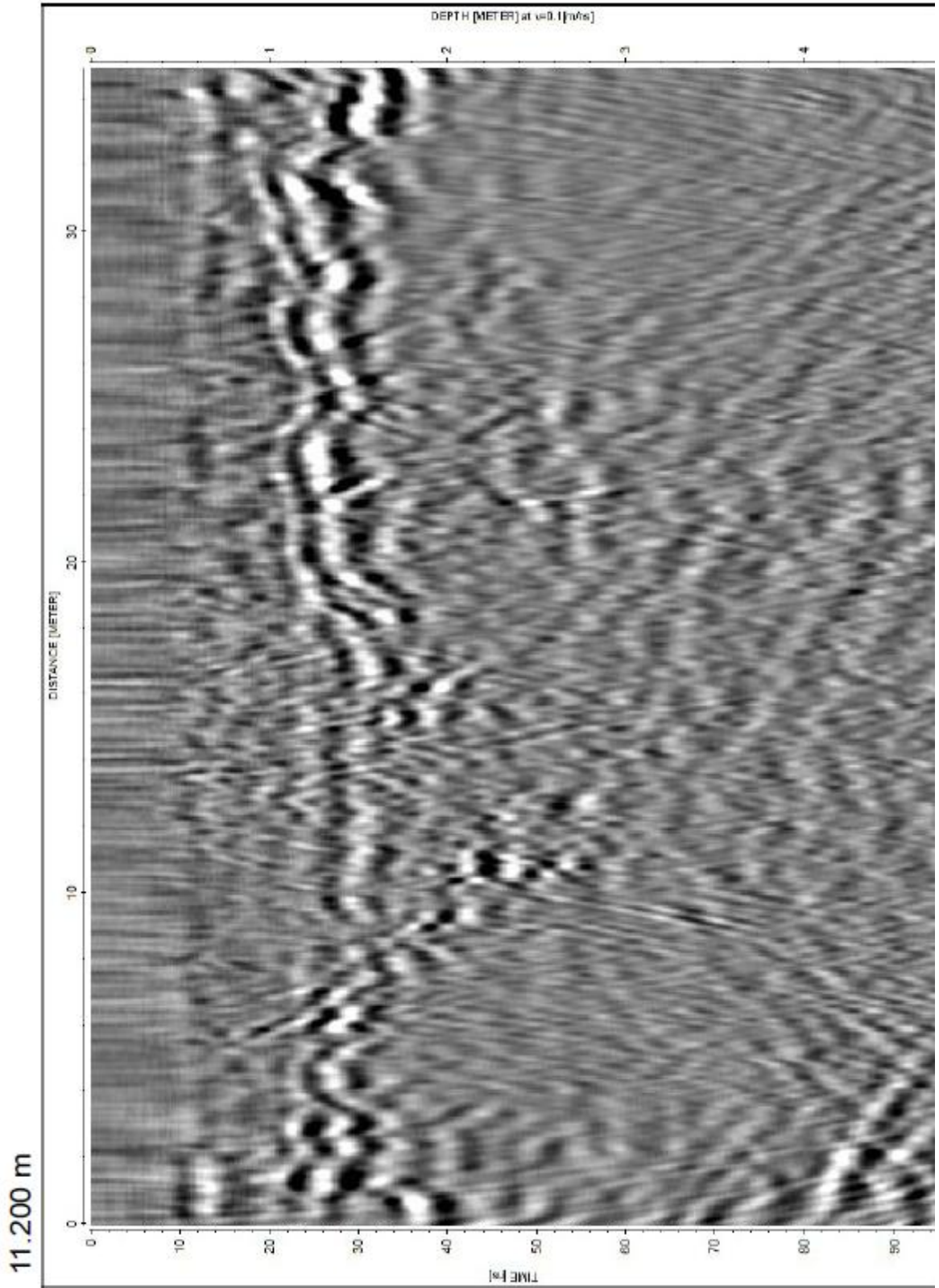
Figure 4.20, 250 MHz

Figure 4.21, 250 MHz

124
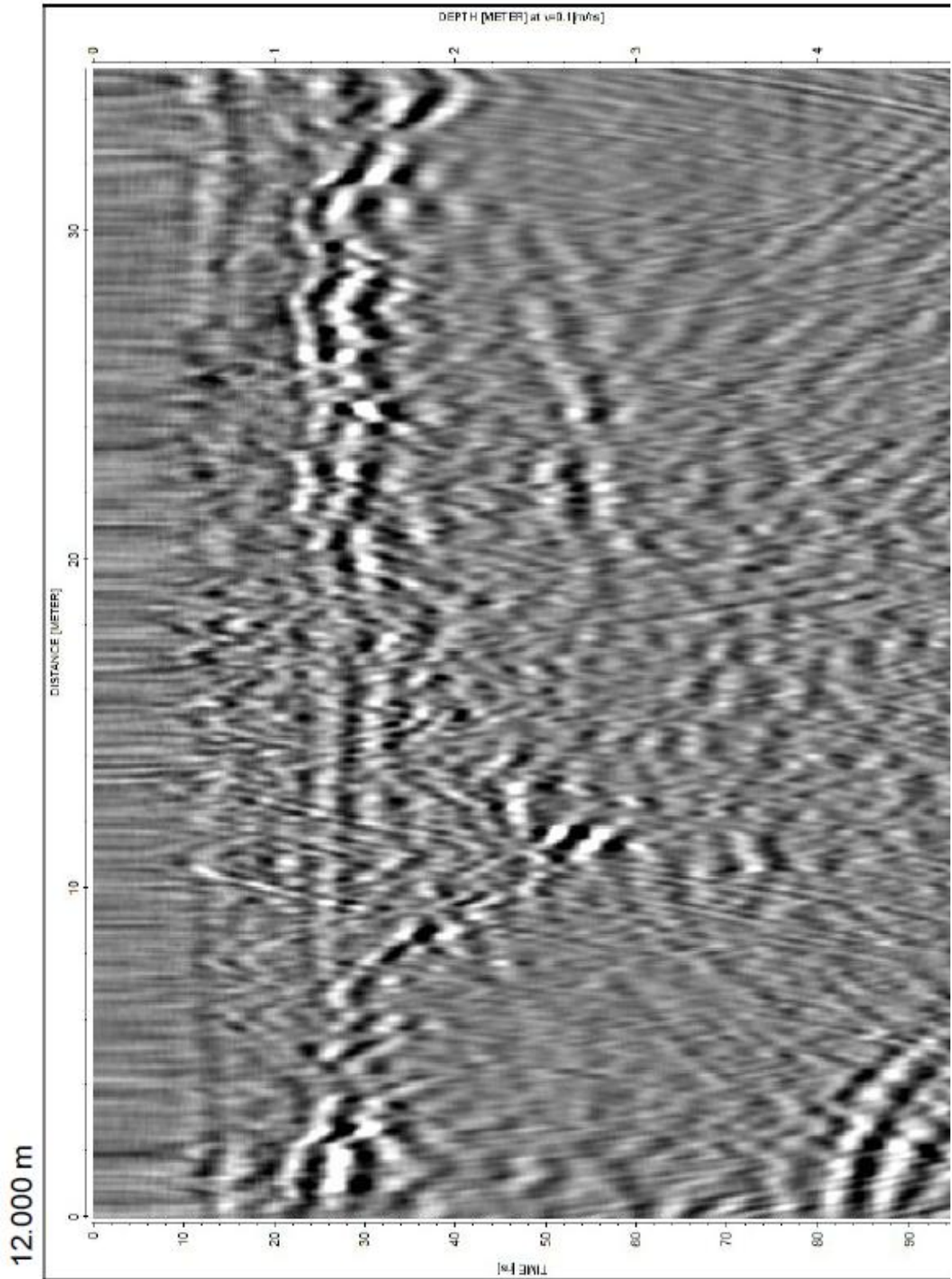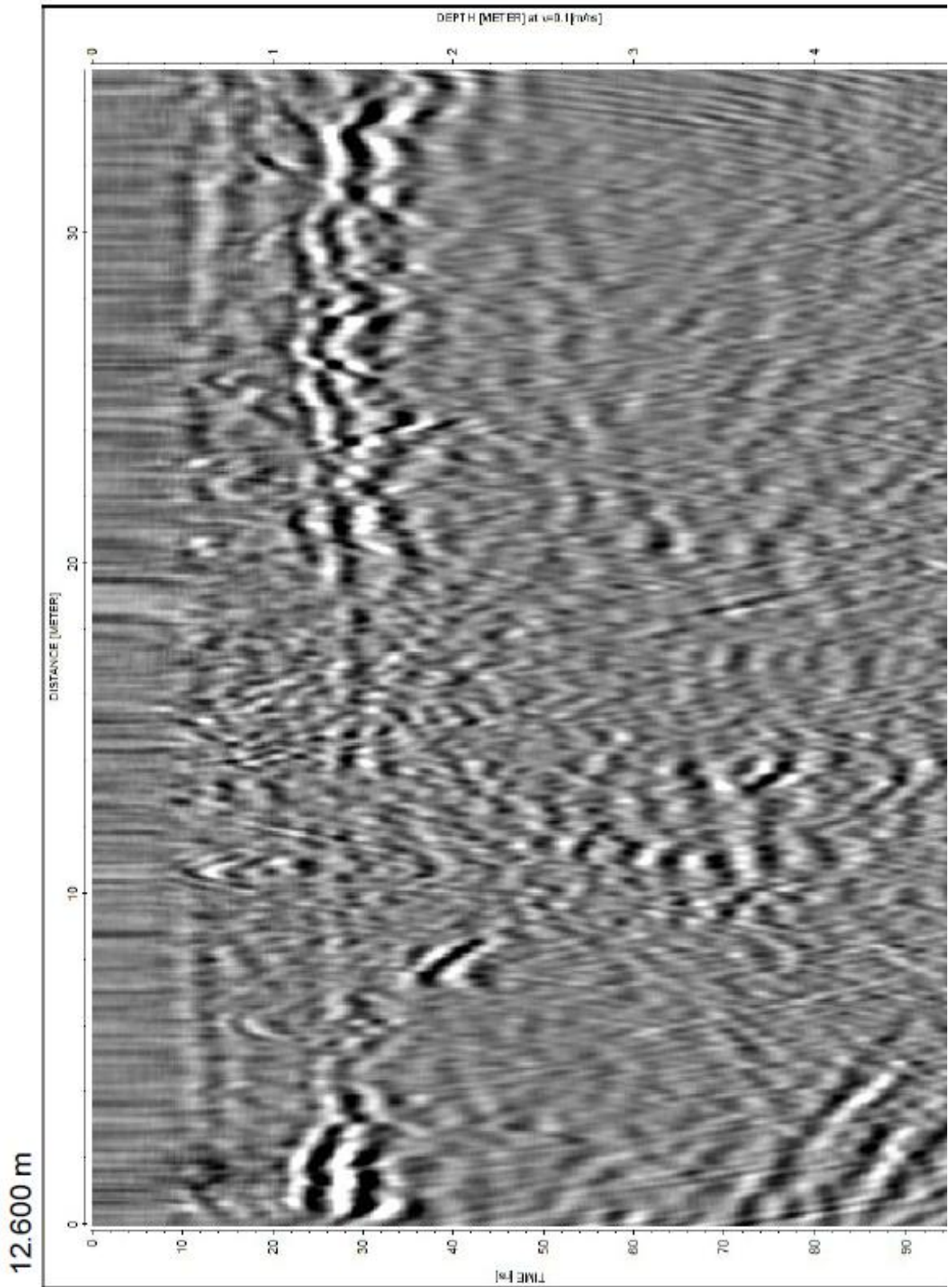
Figures 4.15-4.21. Migrated (time-to-depth correction of 0.1 m/ns) 3D GPR (250 MHz) in-line data. Data extends across the x-distance on the time slice plots.

mostly small buried objects, roots, and small slump features that can be collapsed to points with varying migration parameters. On the whole this sinkhole may be considered more of a plugged type.

The 500 MHz data show many more small anomalous features than the 250 MHz data. The first is a noticeable concentric ring-like structure that can be seen in the time slice images (Figures 4.25-4.27). This is an artifact from a buried bundle of wires currently being used for a self-potential experiment taking place in the same study area. Many small circular rings abound in the near surface, but are actually small diffractions from buried objects that have been migrated with the wrong time-to-depth conversion (in this case, too high for being shallow, dry sands). As they are mainly very shallow features, they were not the focus of this study and not given a best-fitting value for migration.

It is good practice to identify and analyze features that exist in both data sets and not give much attention to those that exist only in one or the other. This consistency of appearance with varying frequencies is definitely a good method for determining subsurface structures. The feature's structure appears very similar to others seen in GPR profiles collected elsewhere (Carpenter and Ekberg, 2006; Truss et al, 2005). These

125

Figure 4.22, 500 MHz, depth = 1.14 m

18.95 ns

126
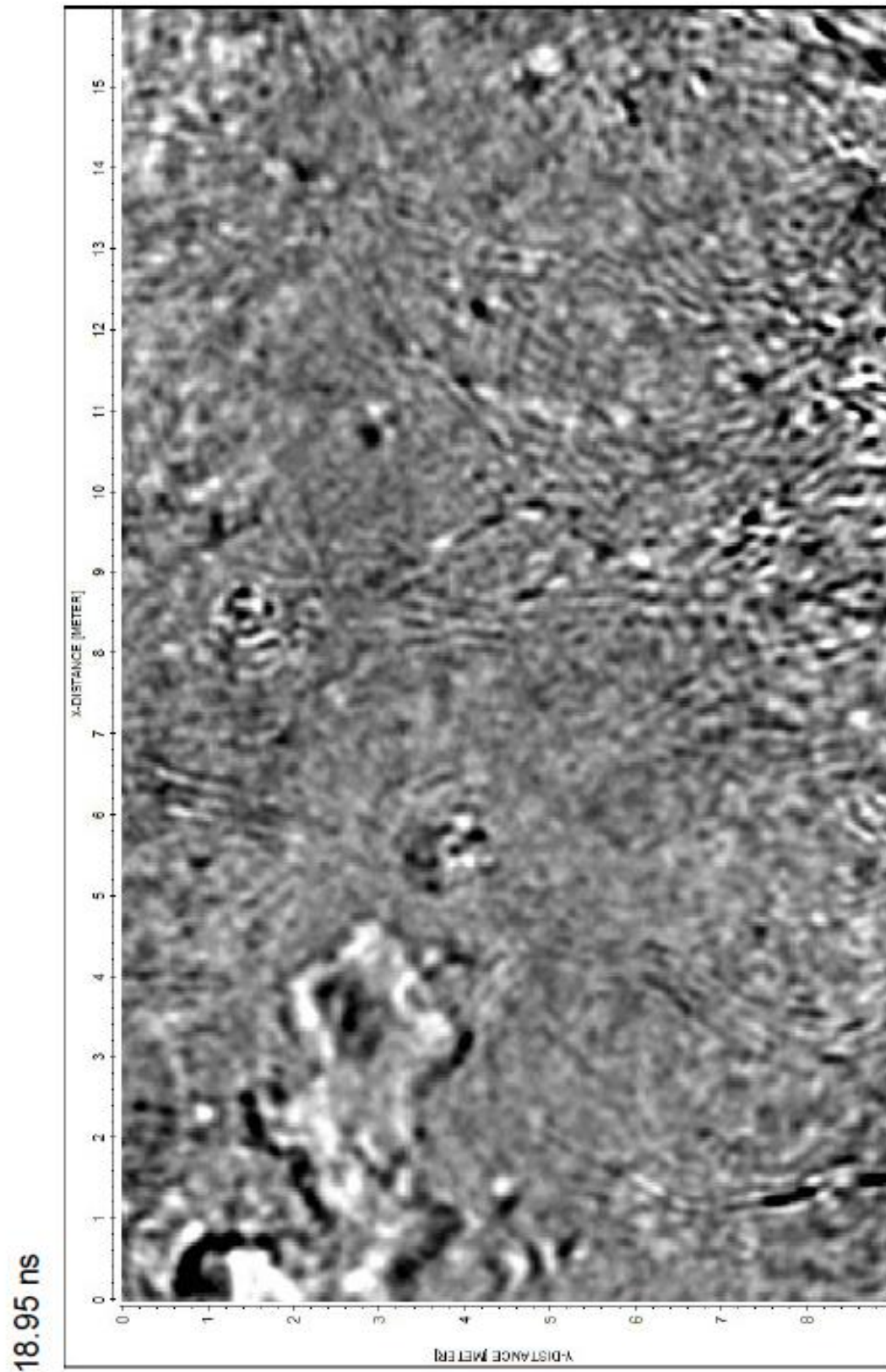
Figure 4.23, 500 MHz, depth = 1.79 m

29.75 ns

127
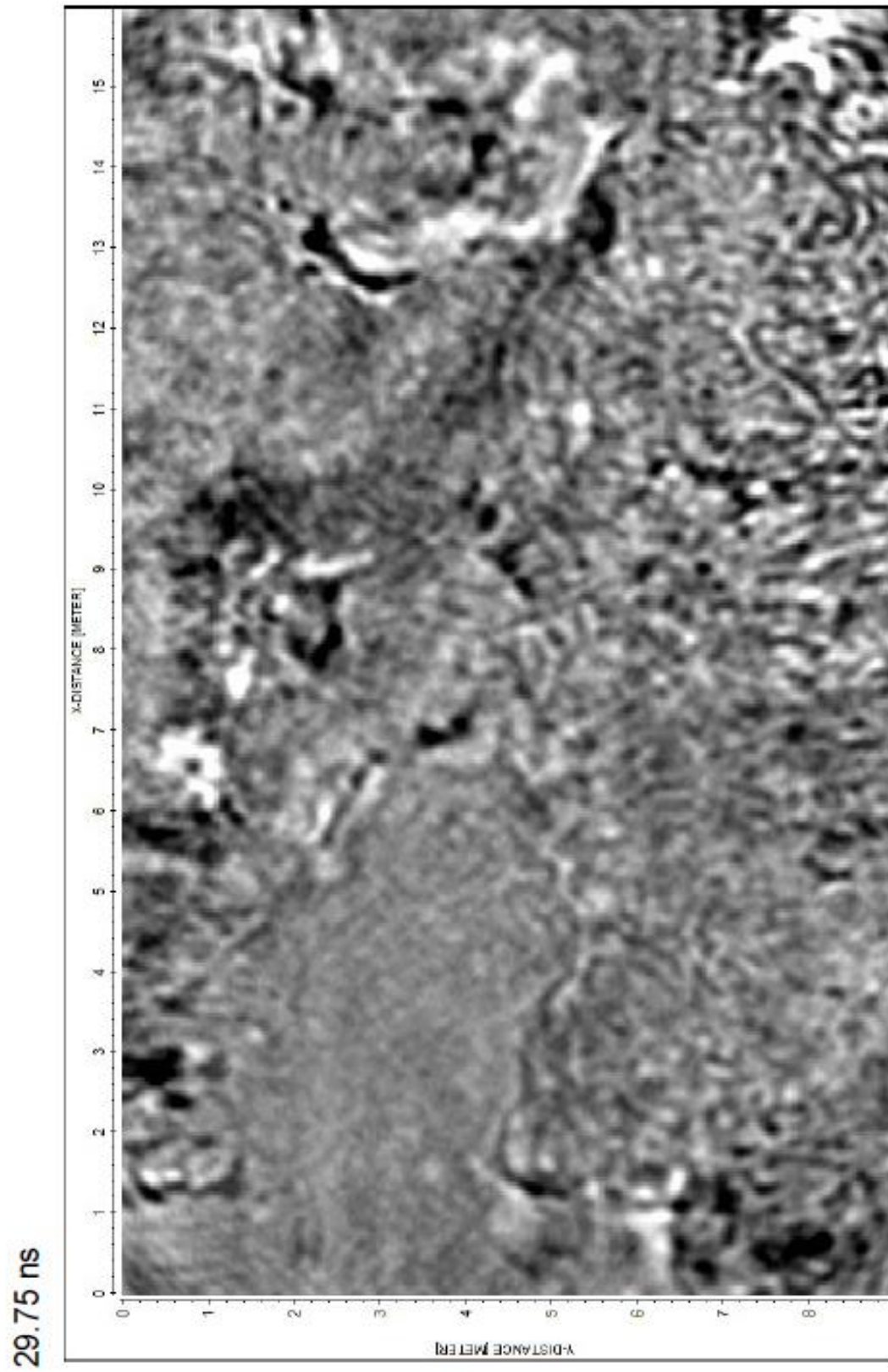
Figure 4.24, 500 MHz, depth = 2.52 m

42.05 ns
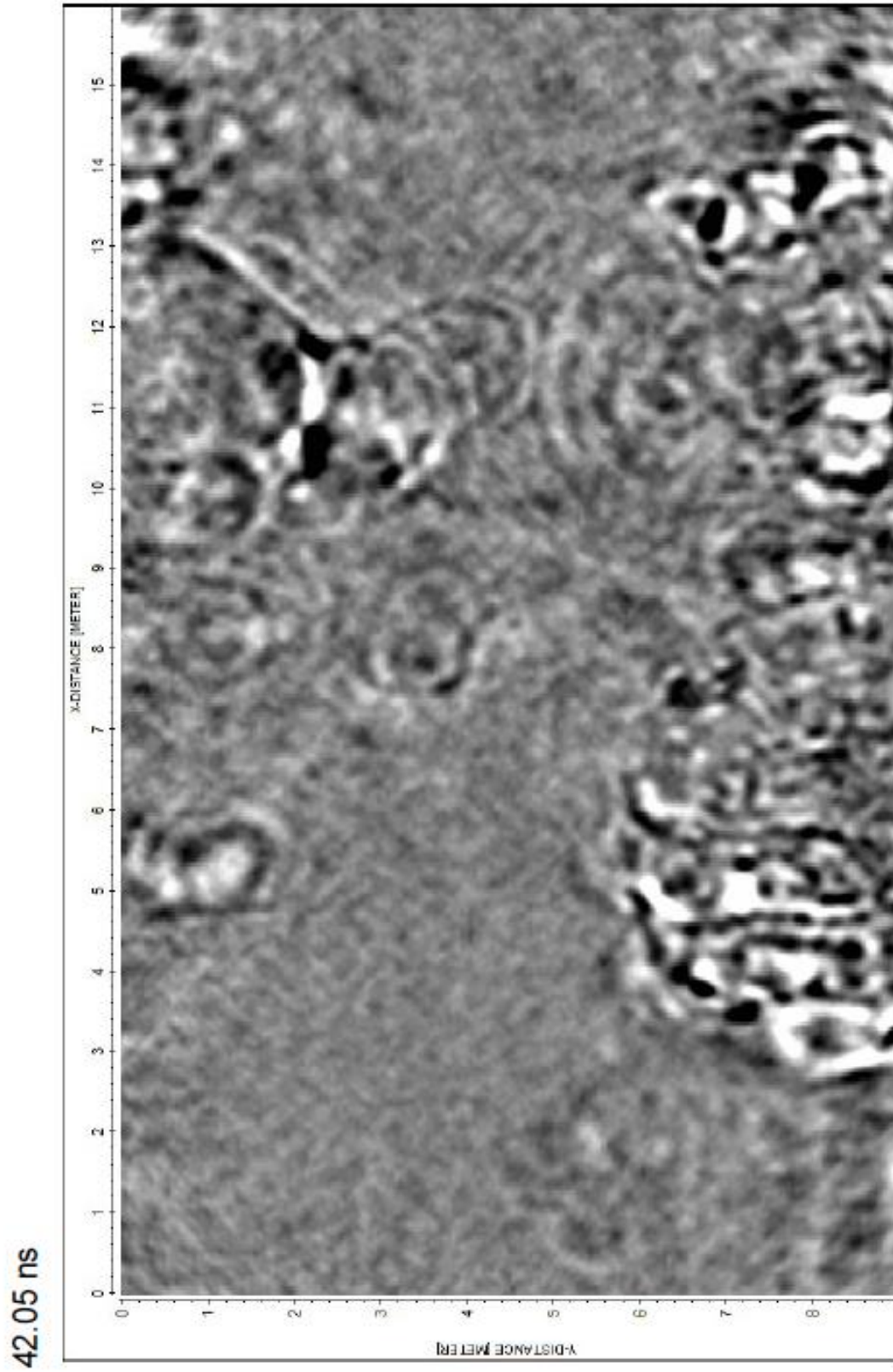
Figure 4.25, 500 MHz, depth = 3.12 m
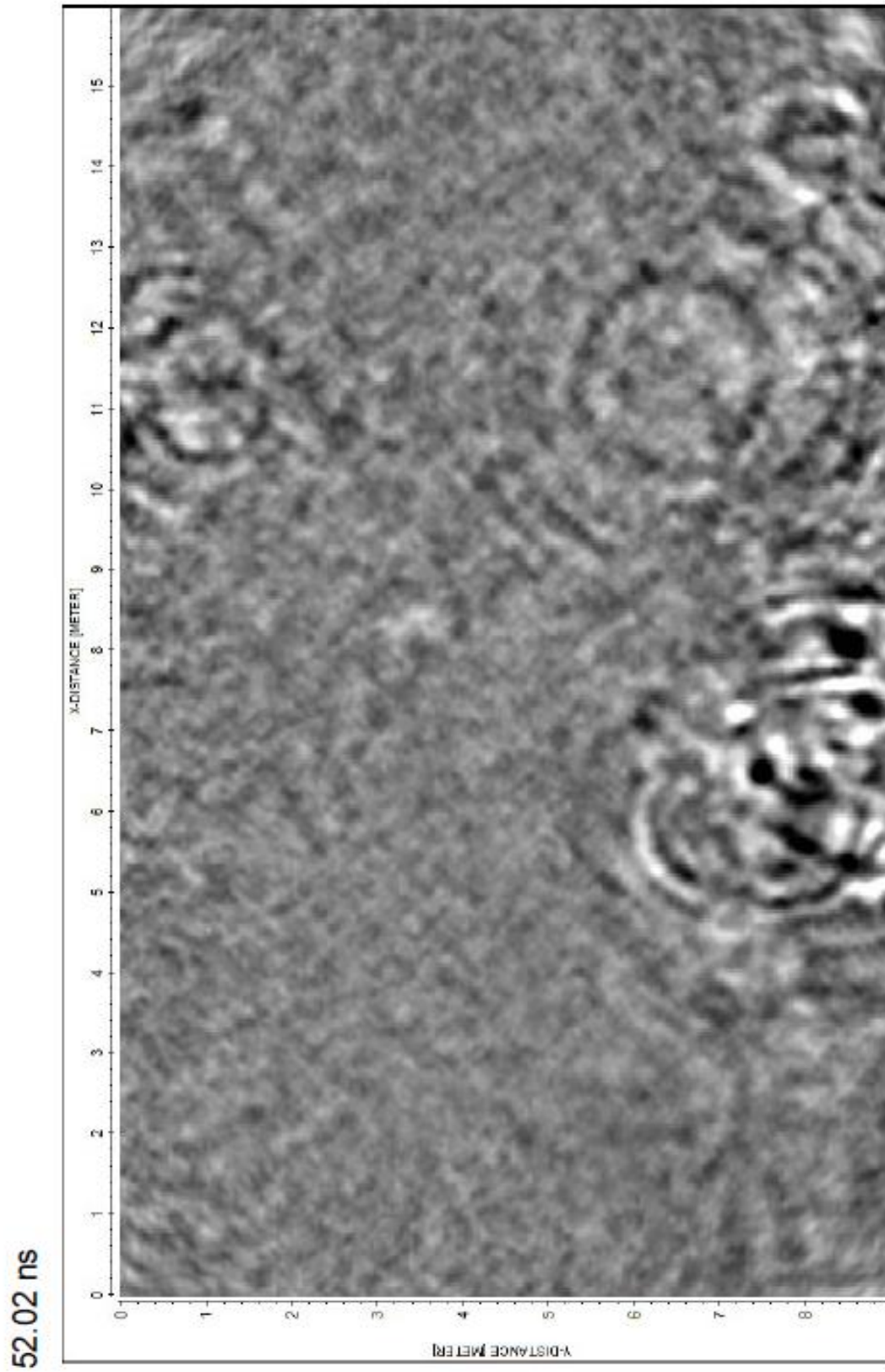
Figure 4.26, 500 MHz, depth = 3.48 m
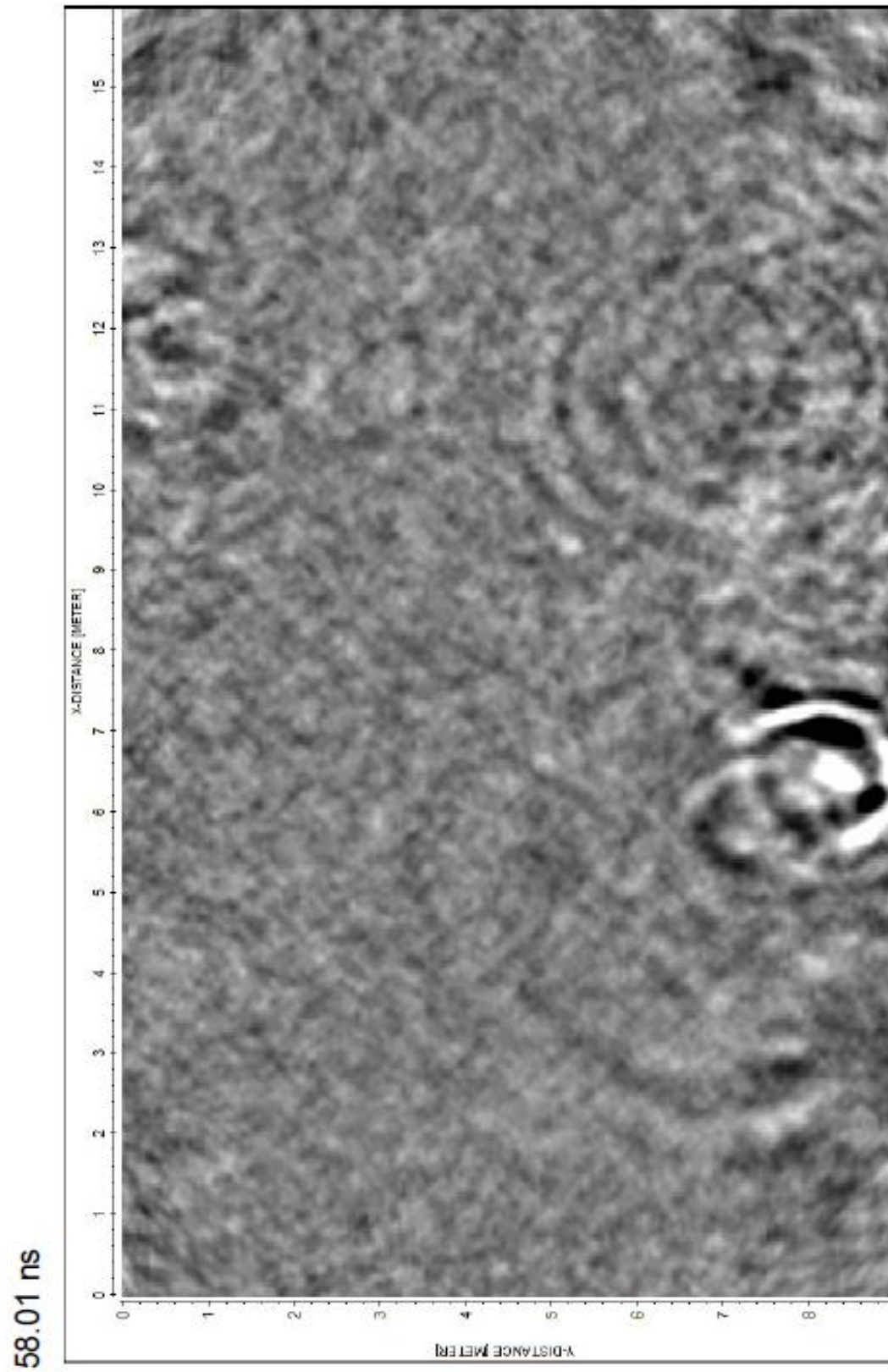
Figure 4.27, 500 MHz, depth = 3.96 m
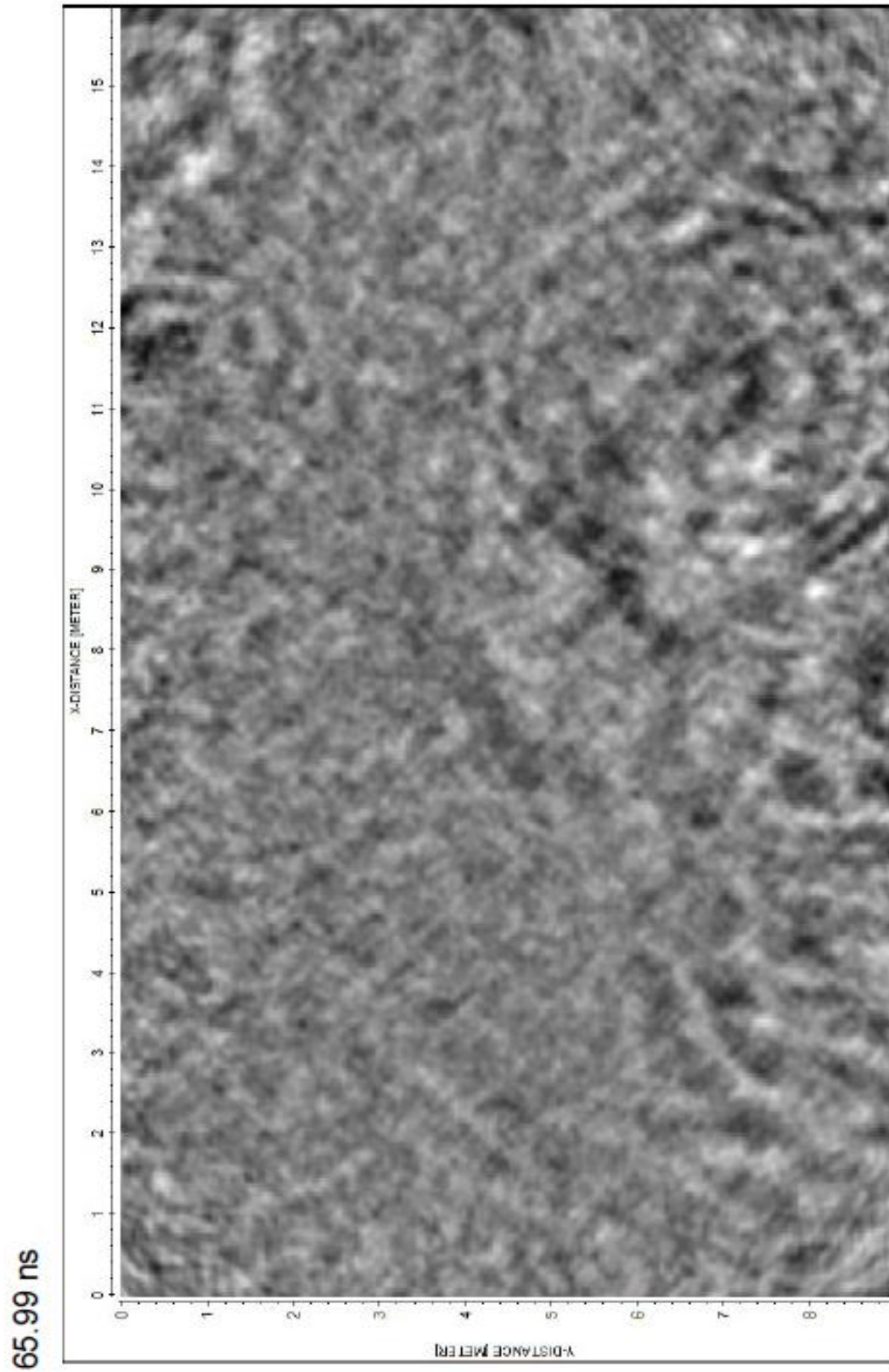
Figures 4.22-4.27. Migrated time slice 3D GPR (500 MHz) data oriented in the same position as that of the red-shaded area it is represented by in Figure 4.1. Figure numbers also increase with time

sinkhole images may even contain evidence for conduit structure recovery (Figure 4.20-21) with stronger amplitude reflections below the center of the sinkhole. Although the results cannot be definitive, this particular sinkhole does not seem to be aggressively forming but may be technically active regardless of showing no signs of surface activity (e.g. depression).

132

Figure 4.28, 500 MHz

133

Figure 4.29, 500 MHz

134
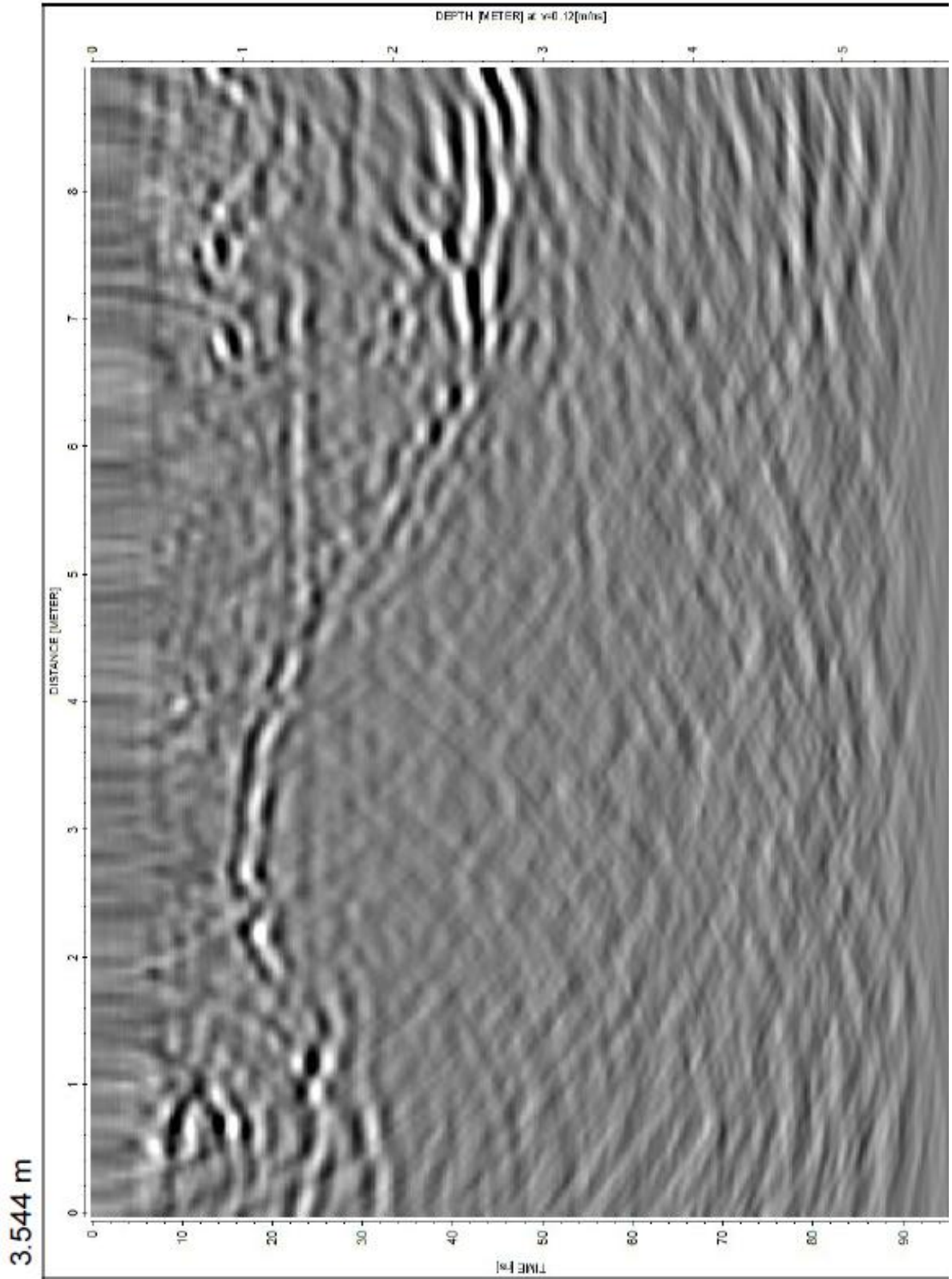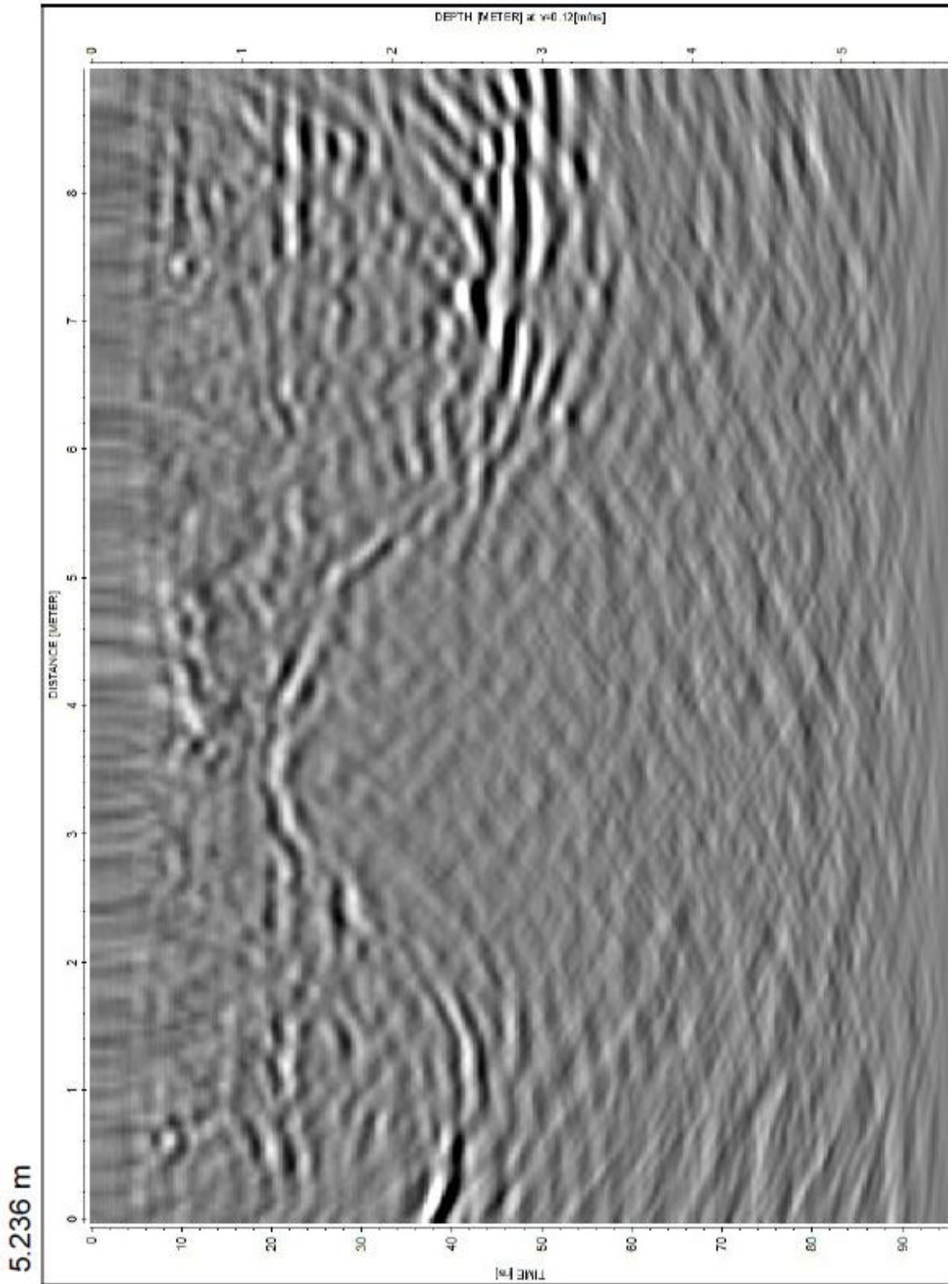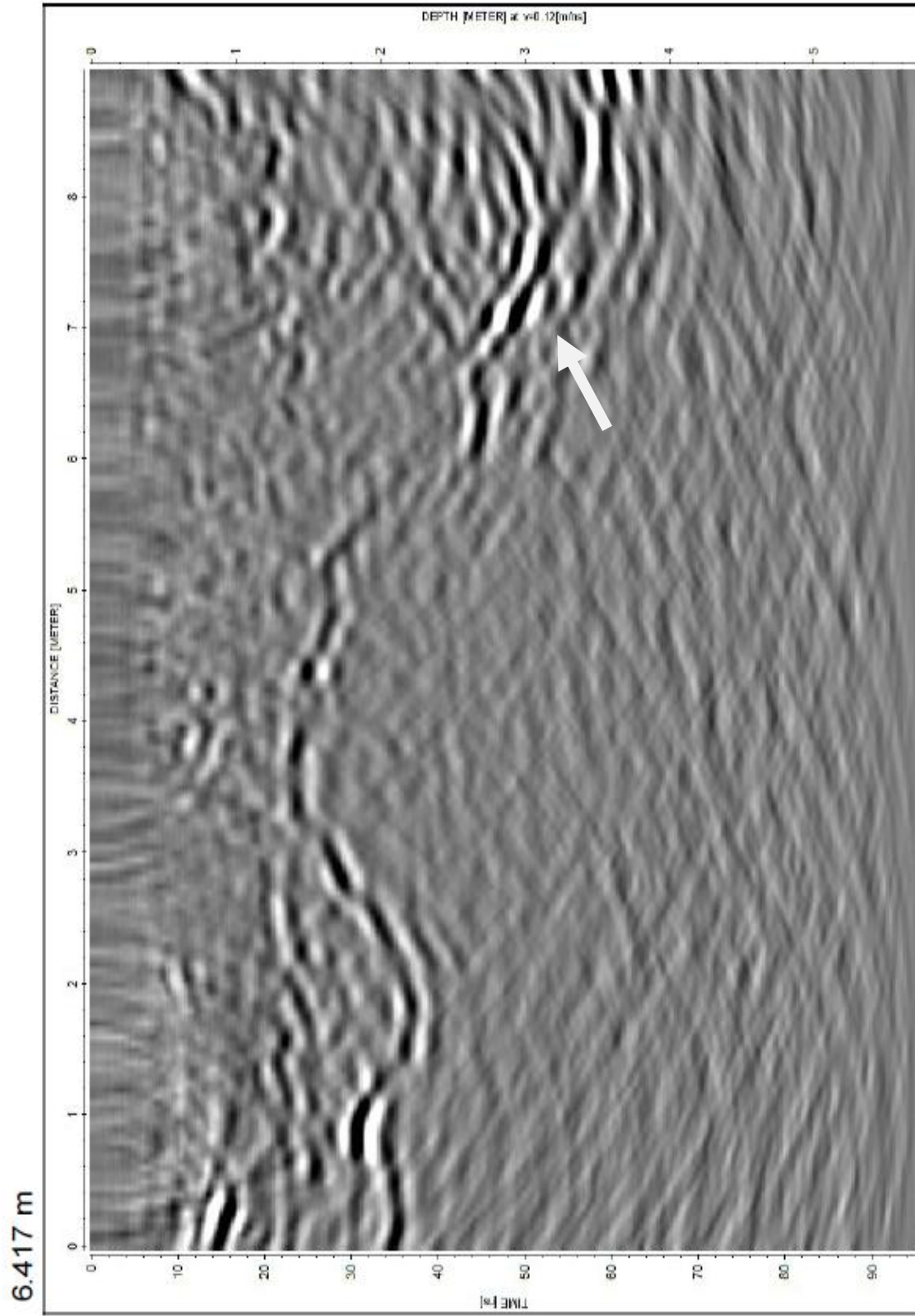
Figure 4.30, 500 MHz

Figure 4.31, 500 MHz
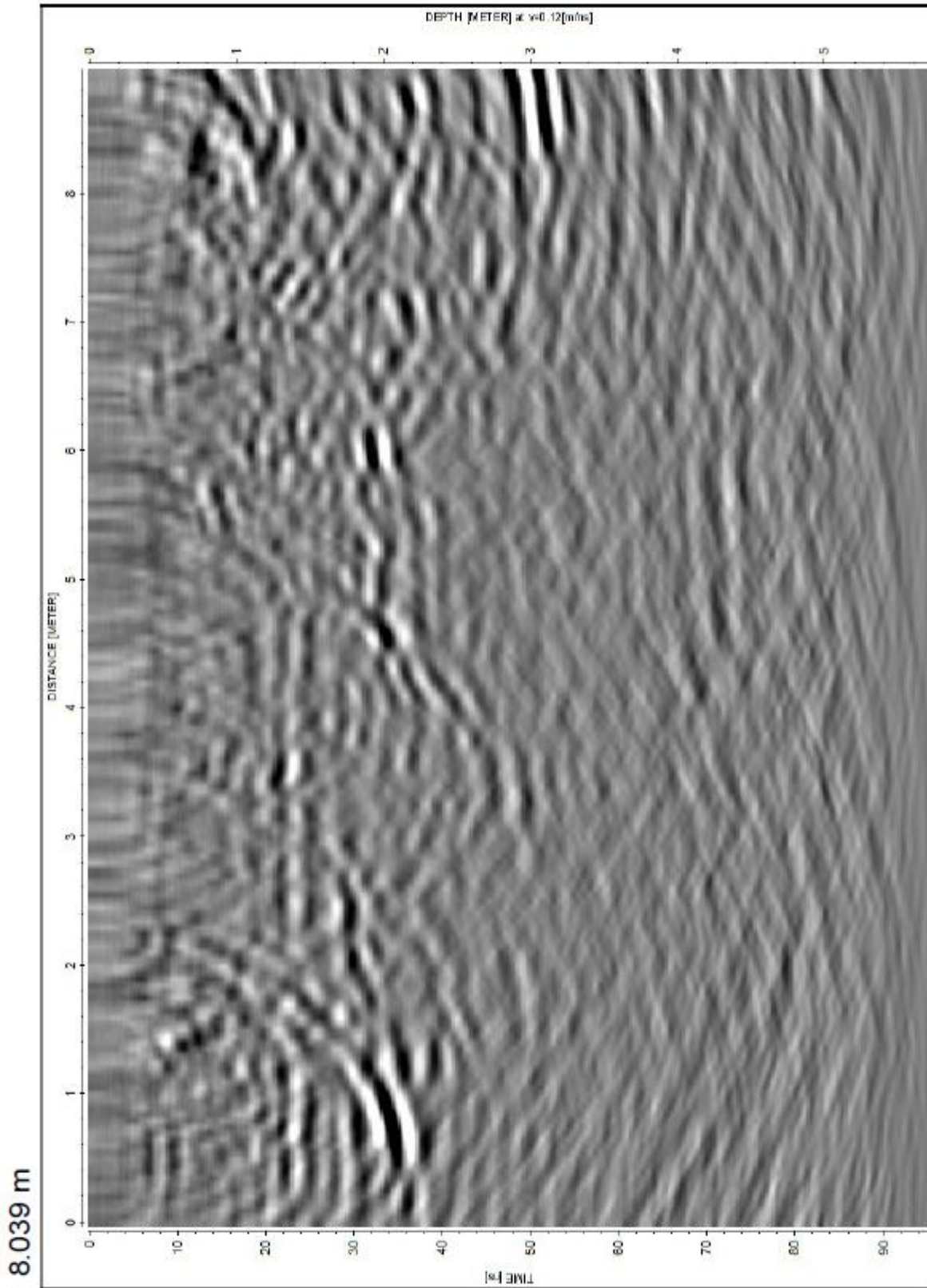
Figures 4.28-4.31. Migrated (time-to-depth correction of 0.12 m/ns) 3D GPR (500 MHz) cross-line data. Data interpolated across in-line profiles and extends across the y-distance on the time slice plots.

137

Figure 4.32, 500 MHz

138

Figure 4.33, 500 MHz

139
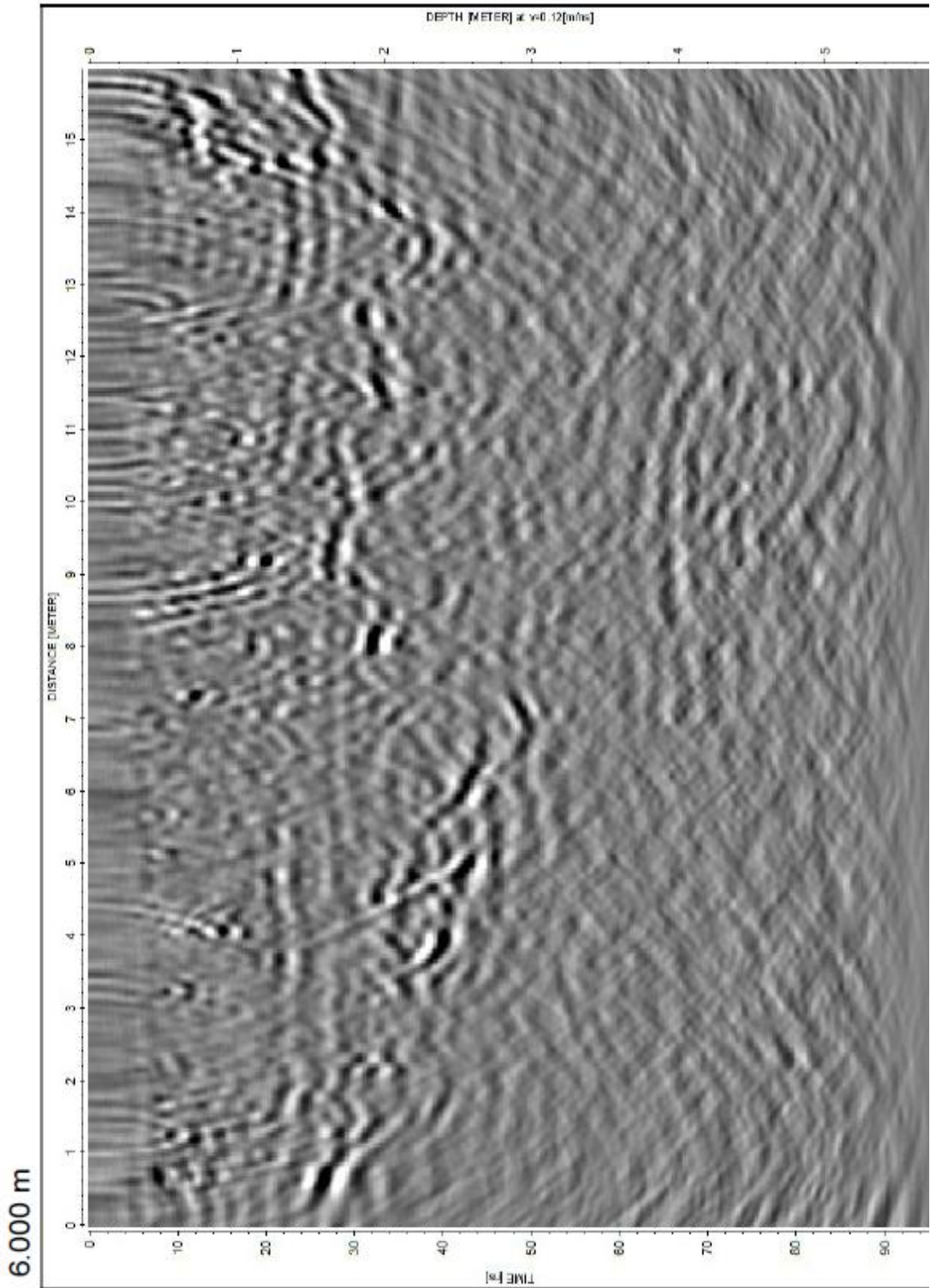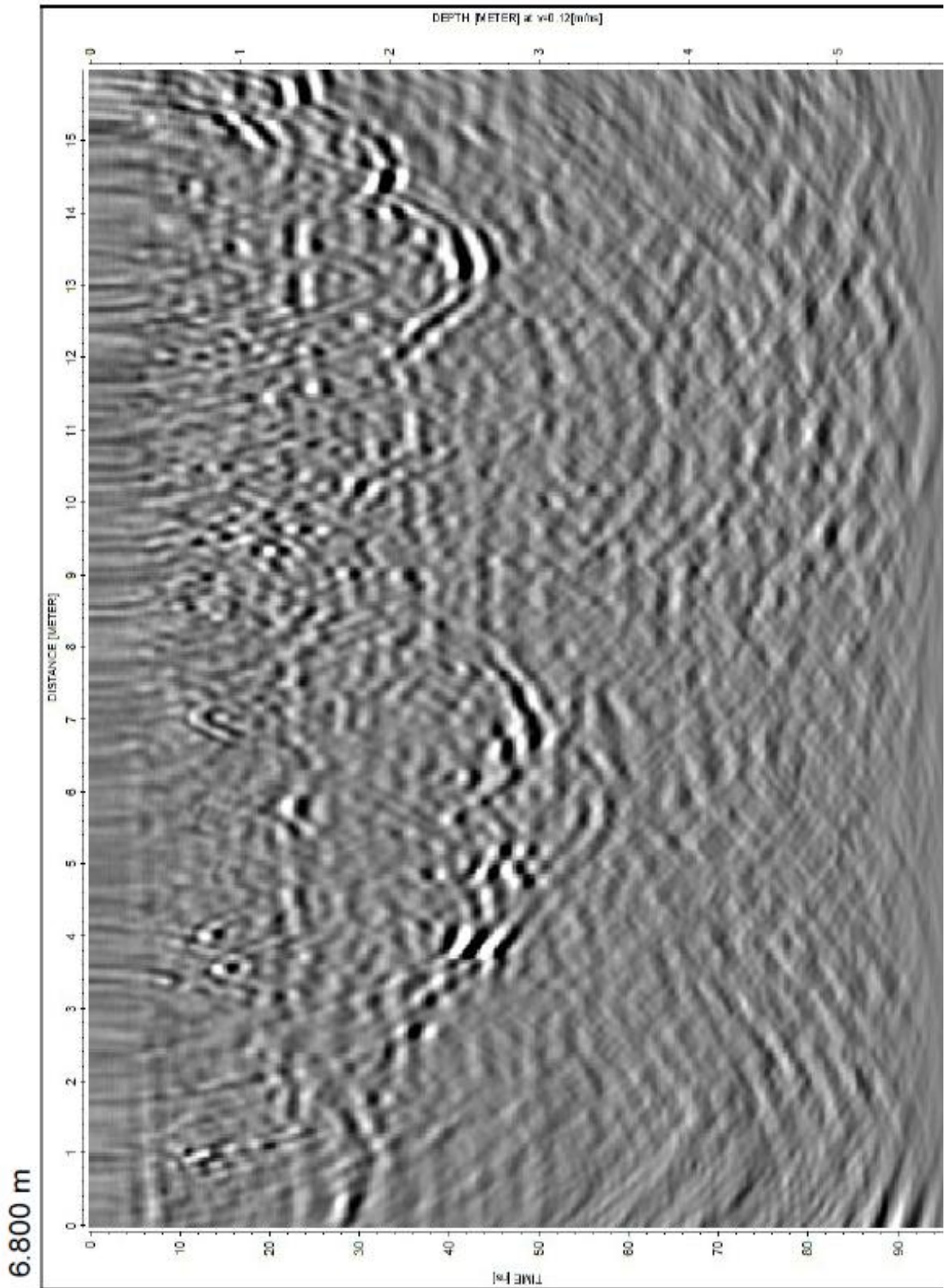
Figure 4.34, 500 MHz

Figure 4.35, 500 MHz

141
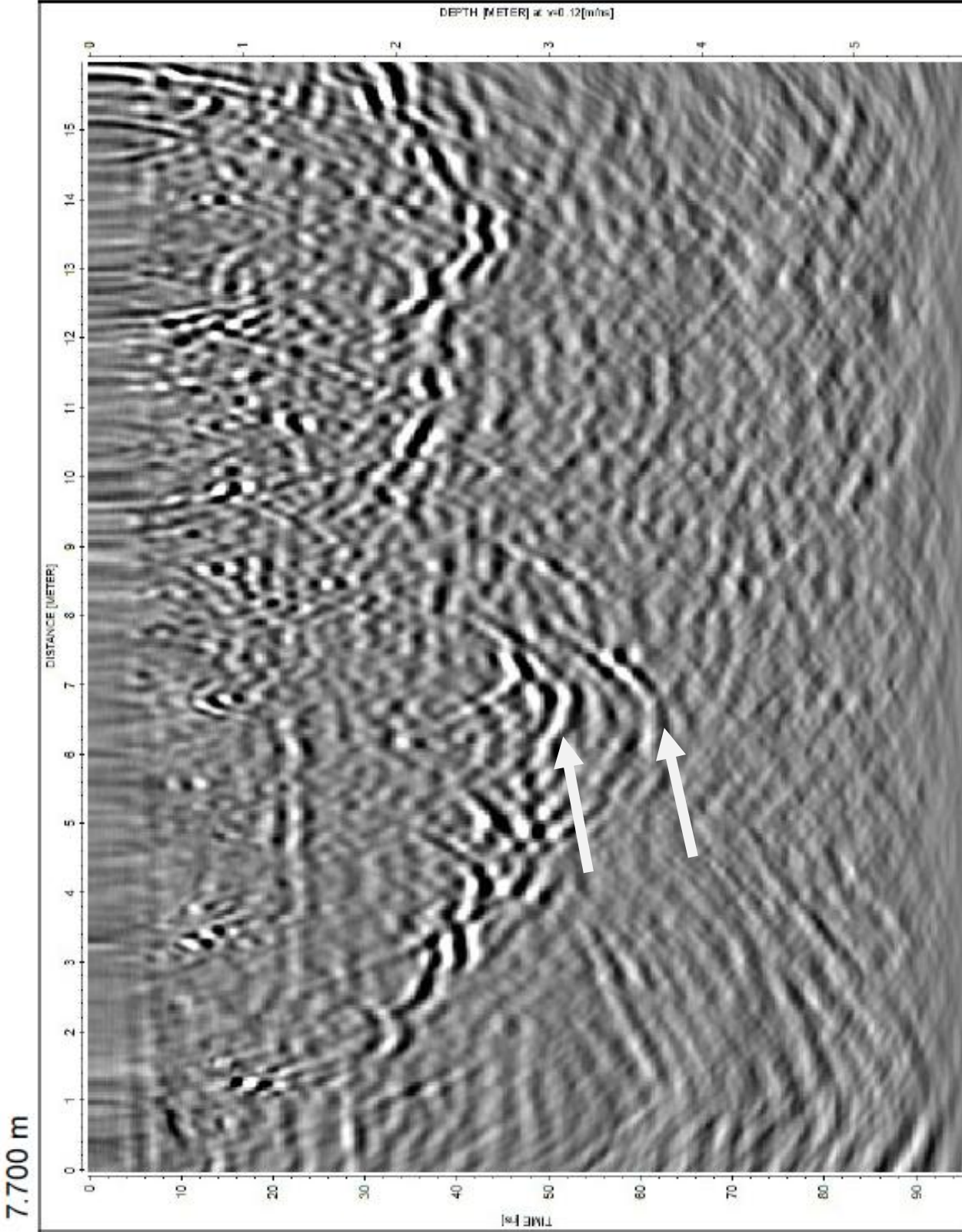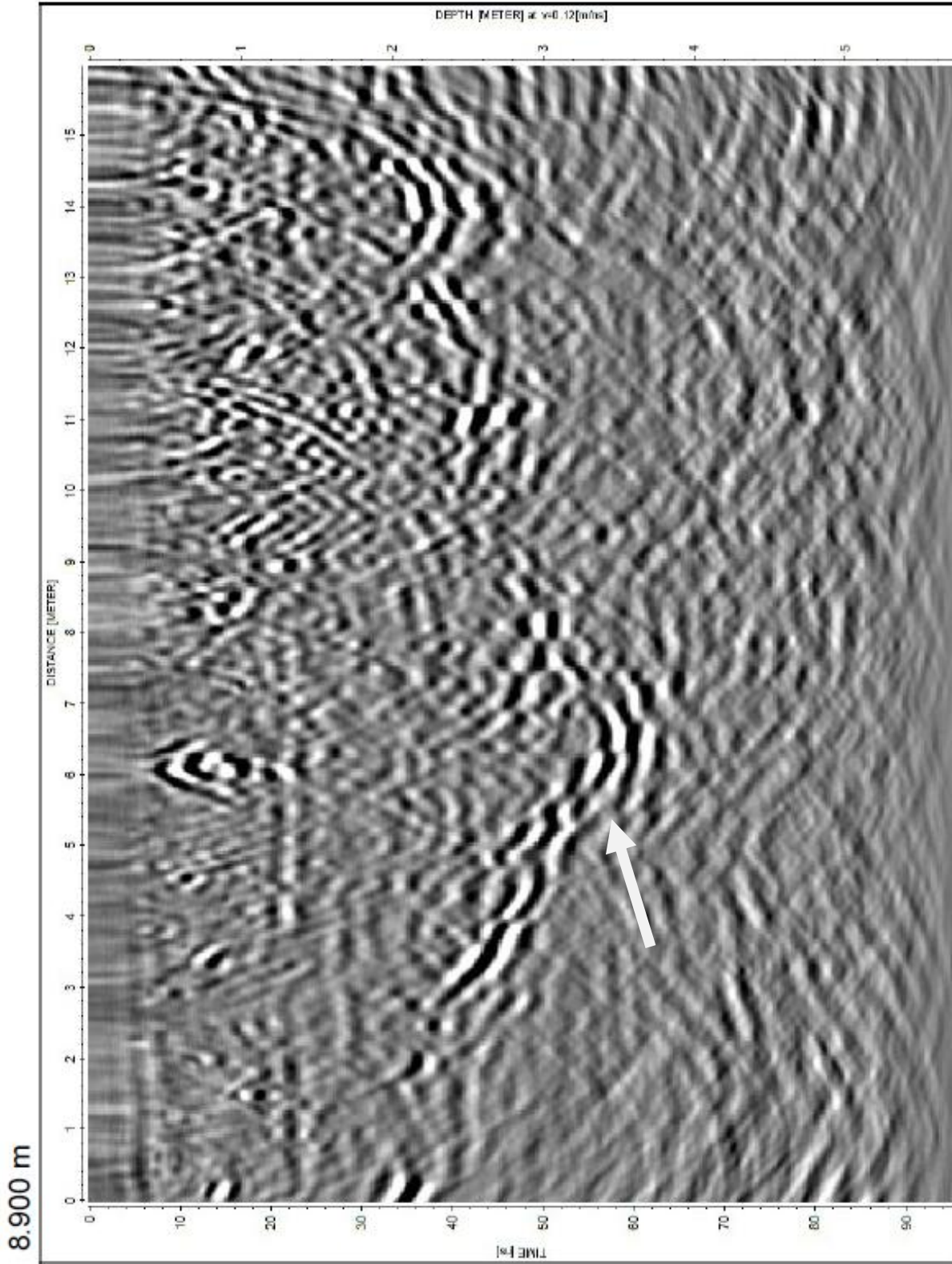
Figures 4.32-4.35. Migrated (time-to-depth correction of 0.12 m/ns) 3D GPR (500

MHz) in-line data. Data extends across the x-distance on the time slice plots.

Effects on Interpretation by Decreased Resolution

Typically, spatial GPR sinkhole investigations in the Tampa, FL area are not conducted at the high resolution of the surveys shown here (grid spacings may be on the order of meters). In order to understand what this might do to survey interpretations, the 500 MHz 3D GPR data to spacing between lines of 0.50 m instead of 0.05 meter.

Migration was not performed on the down-sampled cube as it typically would not be performed on such a sparse data set. A few specific profiles were selected to compare to those displayed in the previous section. The first is a time slice at 42.05 ns (in Figures 4.24 & 4.36) which shows the maximum depression of the sinkhole previously discussed in detail earlier. Figure 4.36 displays the grid with lower resolution. Even with the bright spot in the same position as the sinkhole, it is no longer possible to claim any sort of sinkhole or depression-like feature in the same area with this time slice. Diffraction hyperbolas are also not visible with this spacing interval. The lower resolution cross-line profile at 6.510 m (Figure 4.37) cannot provide any useful information when compared to its higher-resolution equivalent at 6.417 m (Figure 4.30). The in-line profiles should provide a little more useful information since data was collected at this interval and because it has the greatest resolution compared to the other viewing planes. The in-line profile at 6.00 m (Figure 4.38) is in fact clearer than the other viewing planes but is still very hard to interpret because of its noisy appearance, due to a high density of shallow diffractions. In some spots the lower reflection horizon clearly visible in Figure 4.32 can be seen in the lower resolution profile but they are not as noticeable or well-connected when viewing the higher resolution profile. Collecting, processing, and interpreting 3D

143

Figure 4.36, 500 MHz, depth = 2.52 m

144
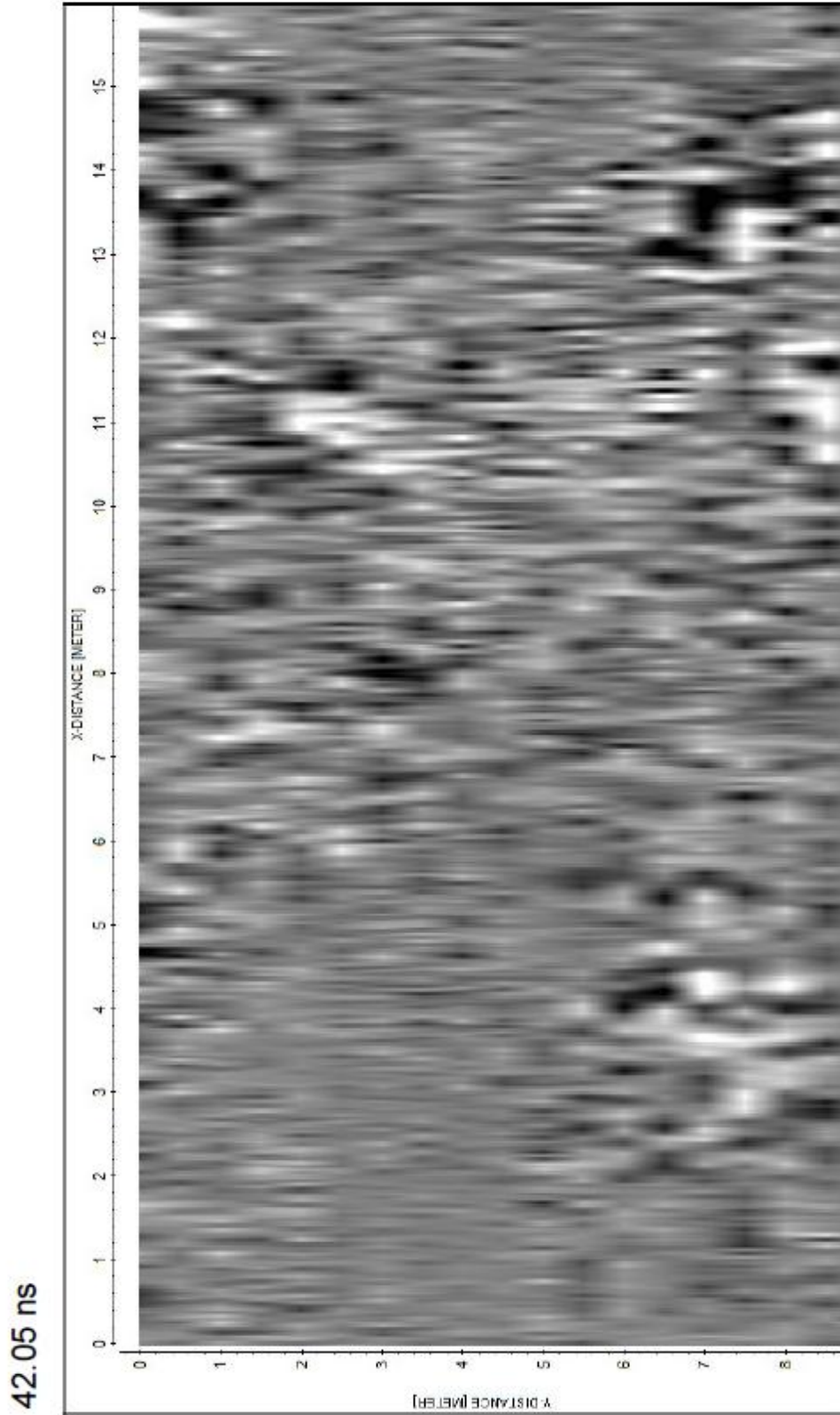
Figure 4.37, 500 MHz

Figure 4.38, 500 MHz

146
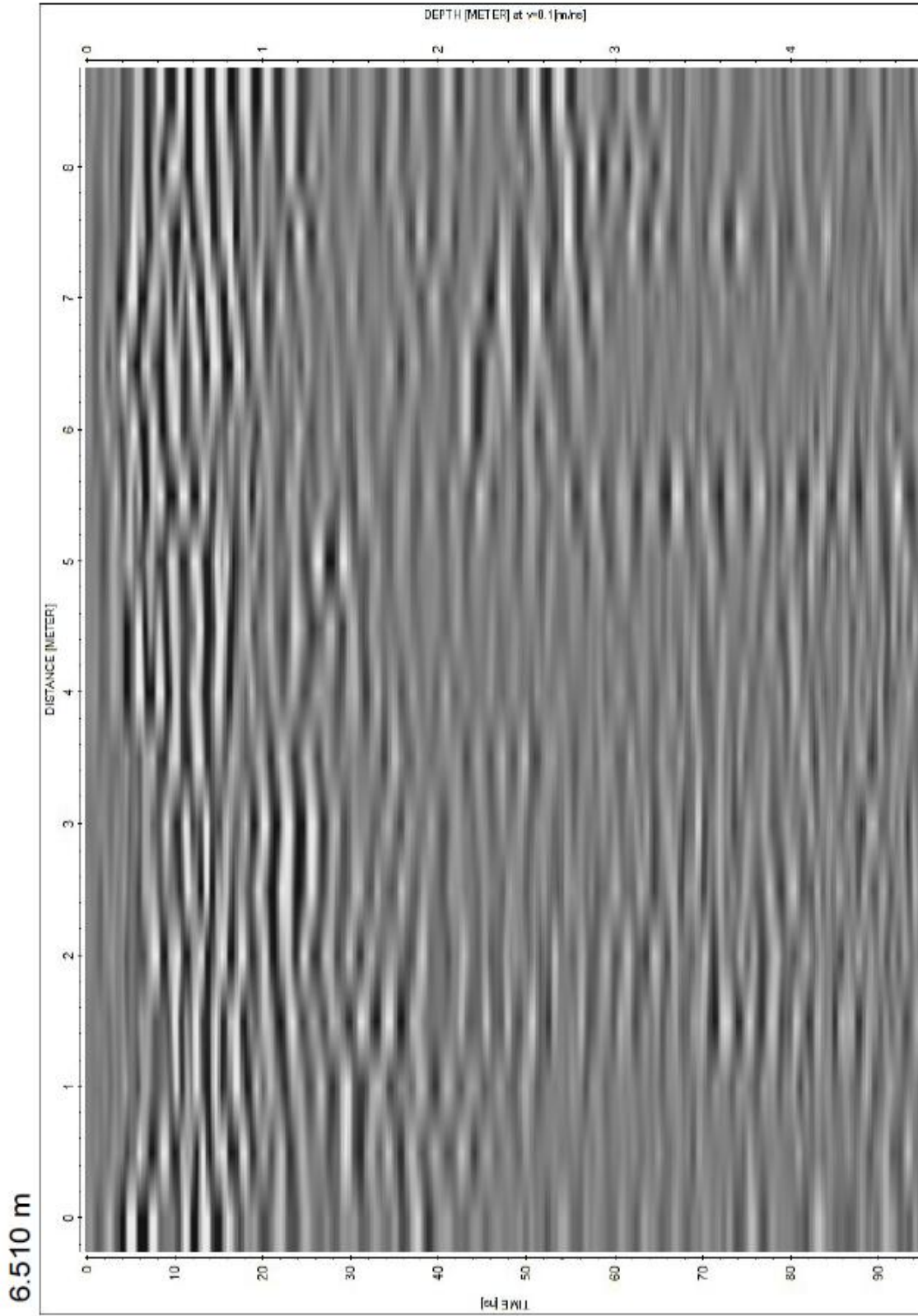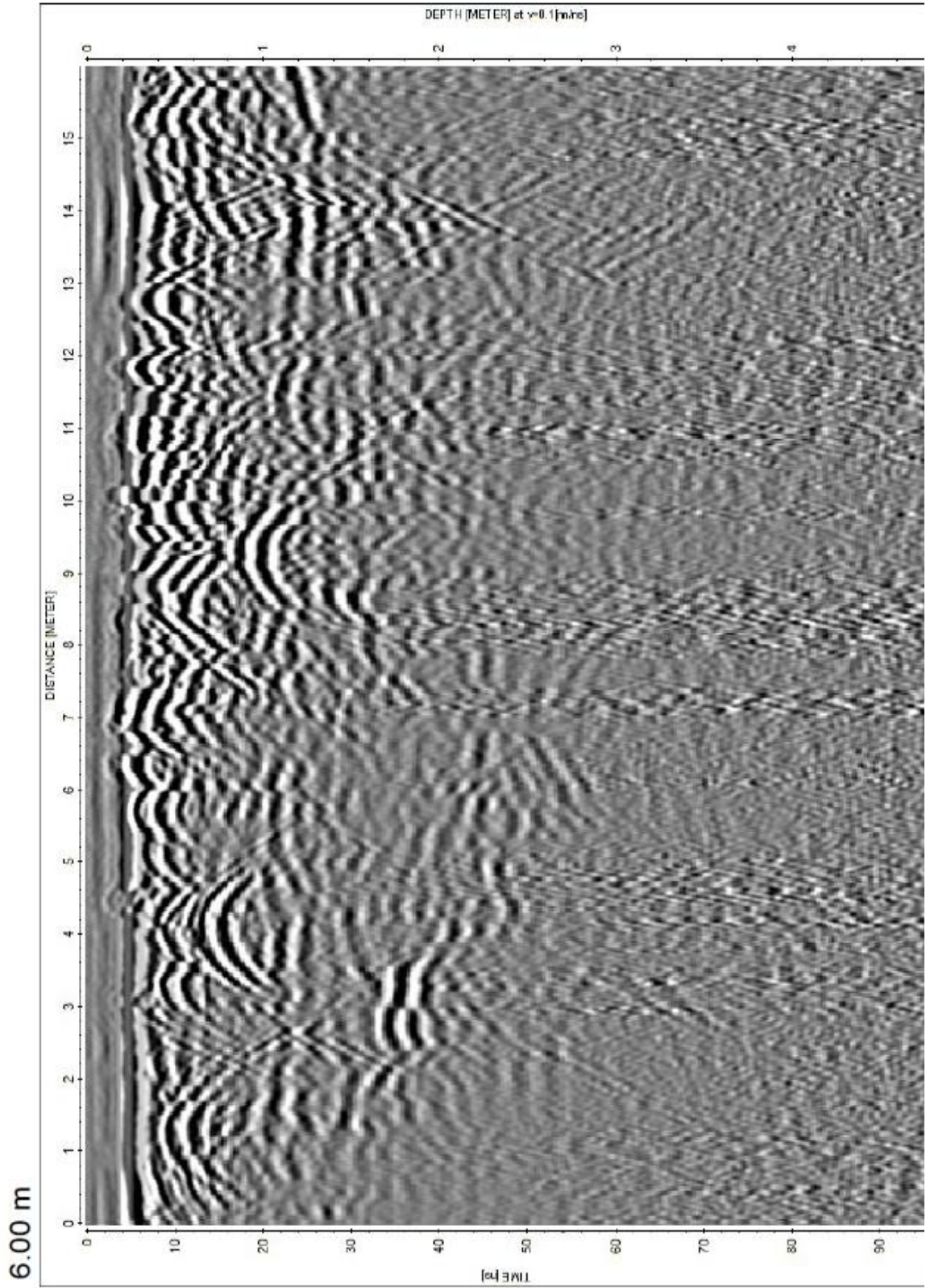
Figures 4.36-4.38. Selected viewing planes from a lower-resolution migrated 3D GPR data cube. [Figure 4.36, Figure 4.37 (y-distance profile on Figure 4.36), Figure 4.38 (x-distance profile on Figure 4.36)].

GPR data volumes at this low resolution is not appropriate for sinkholes analysis at this scale. This experiment proves how necessary it is to use such a small interval spacing (0.05 m for 500 MHz) to process 3D data volumes with 3D processing techniques.

Here we compare the effective level of interpretation of a 3D GPR data set to conventional 2D processing of a sparse grid. Usually, sparsely-spaced GPR profiles are interpreted without any sort of data migration. To see the effect on interpretation, sample profiles from the 500 MHz data cube were taken and left unmigrated, but processed in every other way exactly the same, in order to compare them to ones with a 3D migration applied. Figure 4.39 displays in-line data at the 6.80 m interval which has not been migrated but shows a time-to-depth conversion of 0.12 m/ns just as the 3D-migrated profile seen in Figure 4.33. The lower bright reflector is still visible without migration. Above the lower reflection, there are a great deal of shallow diffractions that are very densely packed together and even give the impression of some sort of shallow structure towards the right edge of the profile. They also blur what could be inferred as a water table at 20 nanoseconds. Figure 4.40 displays a similar result except that the continuous

147
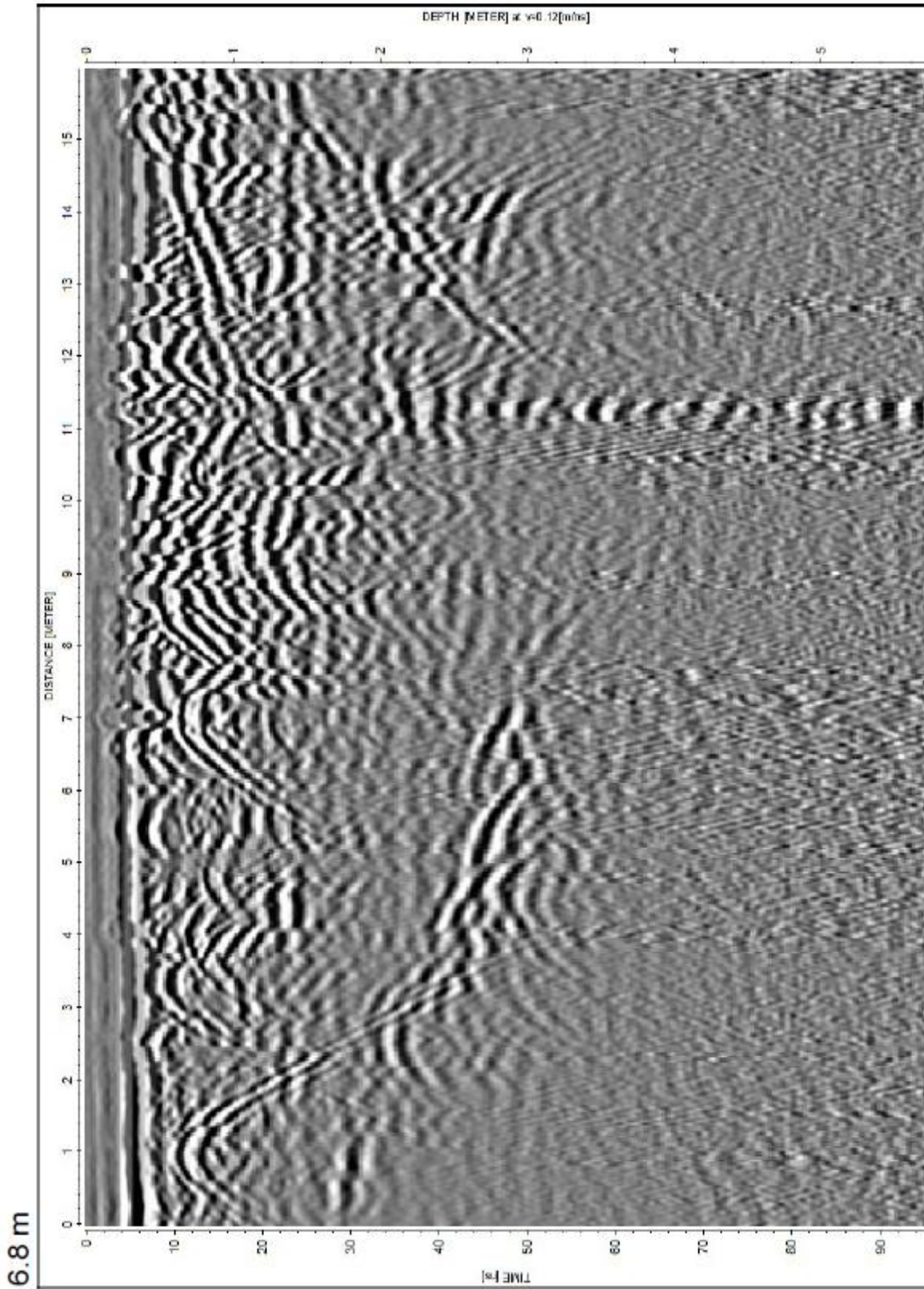
Figure 4.39, 500 MHz

Figure 4.40, 500 MHz
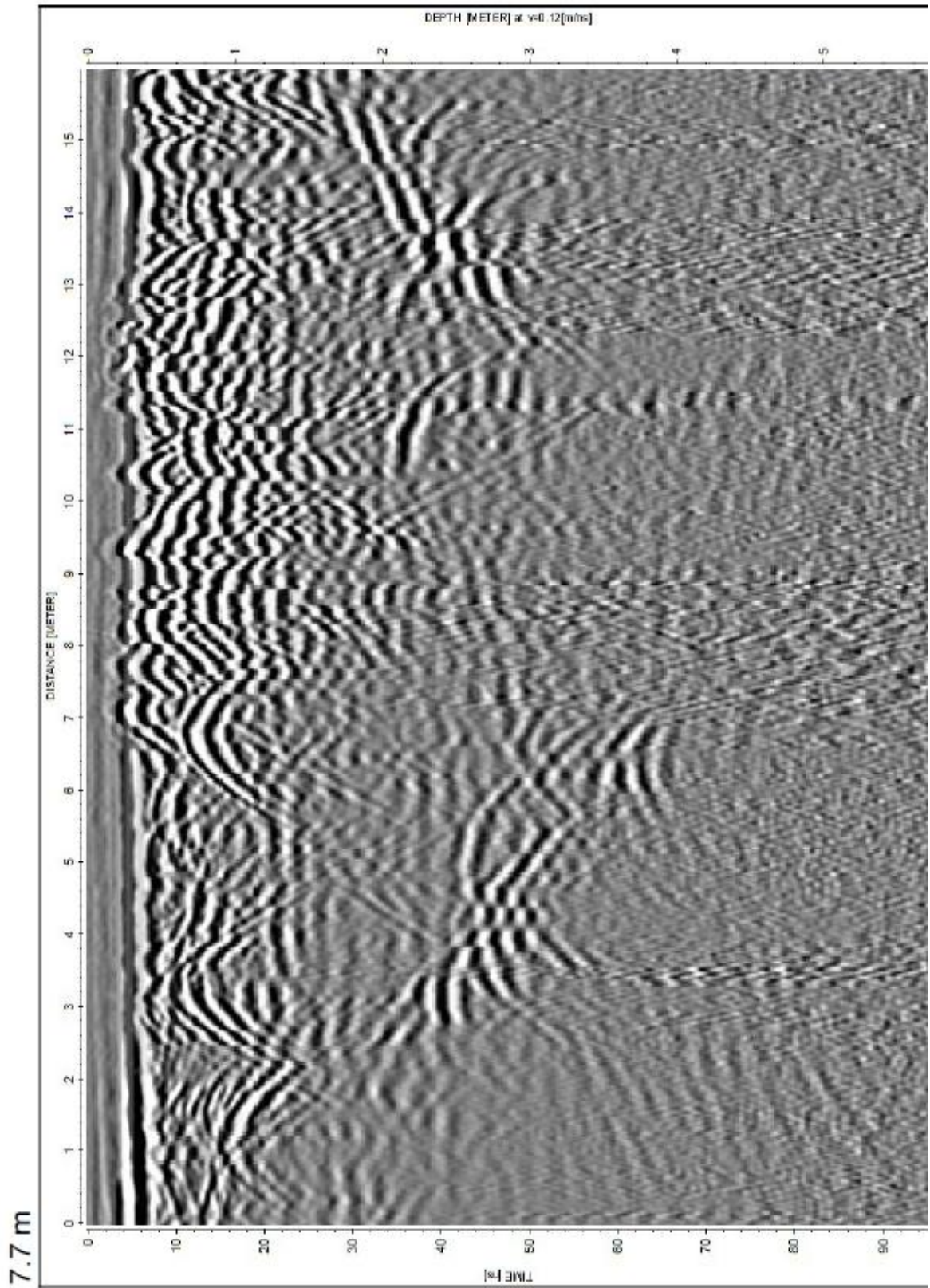
Figures 4.39-4.40. Figures 4.39 and 4.40 represent unmigrated versions of Figures 4.33 and 4.34, respectively.

lower reflection seen in Figure 4.34 is not as well observed. In fact, without the 3D migration, the lower reflection may not even be interpreted as much more than some buried objects with larger diffractions. Clearly without the 3D migration, the semi-continuity of this reflecting horizon is lost.

Another approach to working with sparse GPR data sets is to migrate the data in only two dimensions. Although the validity of this 2D method was deemed inappropriate for recovering 3D structures in Chapter 2, the method may still offer some improvement in interpretation of non-3D grid data sets. Figure 4.41 once again looks at the in-line data at the 6.80 m interval but has been 2D migrated with a 0.12 m/ns time-to-depth conversion. The 2D migration does a decent job at clearing the densely packed diffractions above the lower reflector but actually produces false structure in the upper right hand corner which is not produced in the 3D migration in Figure 4.33. The lower reflector is recovered similar to that in the 3D migration but is less connected overall. Figure 4.42 displays the in-line profile at the 7.70 m interval and has been 2D migrated the same as the previous figure. The 2D migration in this profile did a good job at reducing the dense diffractions above the lower reflector. It did not do as well at recovering the continuous structure of the lower reflector as the 3D migration did.

It seems that 2D migrations on data over 3D structures can recovery some real subsurface structure but can also just as easily introduce new false structures, as the models in Chapter 2 document. Nevertheless it is still probably best to 2D migrate data in hopes of understanding basic subsurface structure when 3D migrations are not possible due to insufficient data volumes.

Figure 4.41, 500 MHz

Figure 4.42, 500 MHz

153
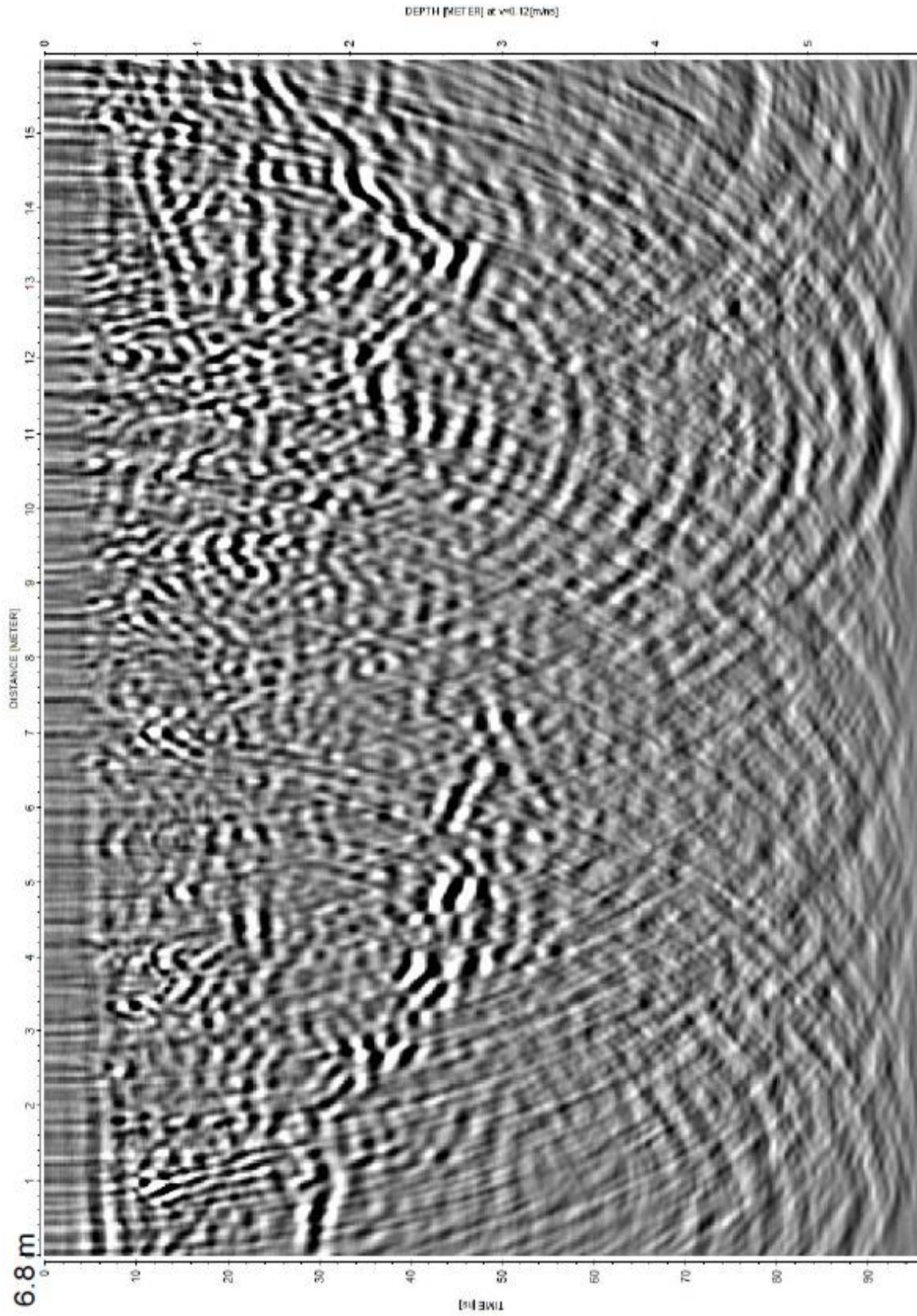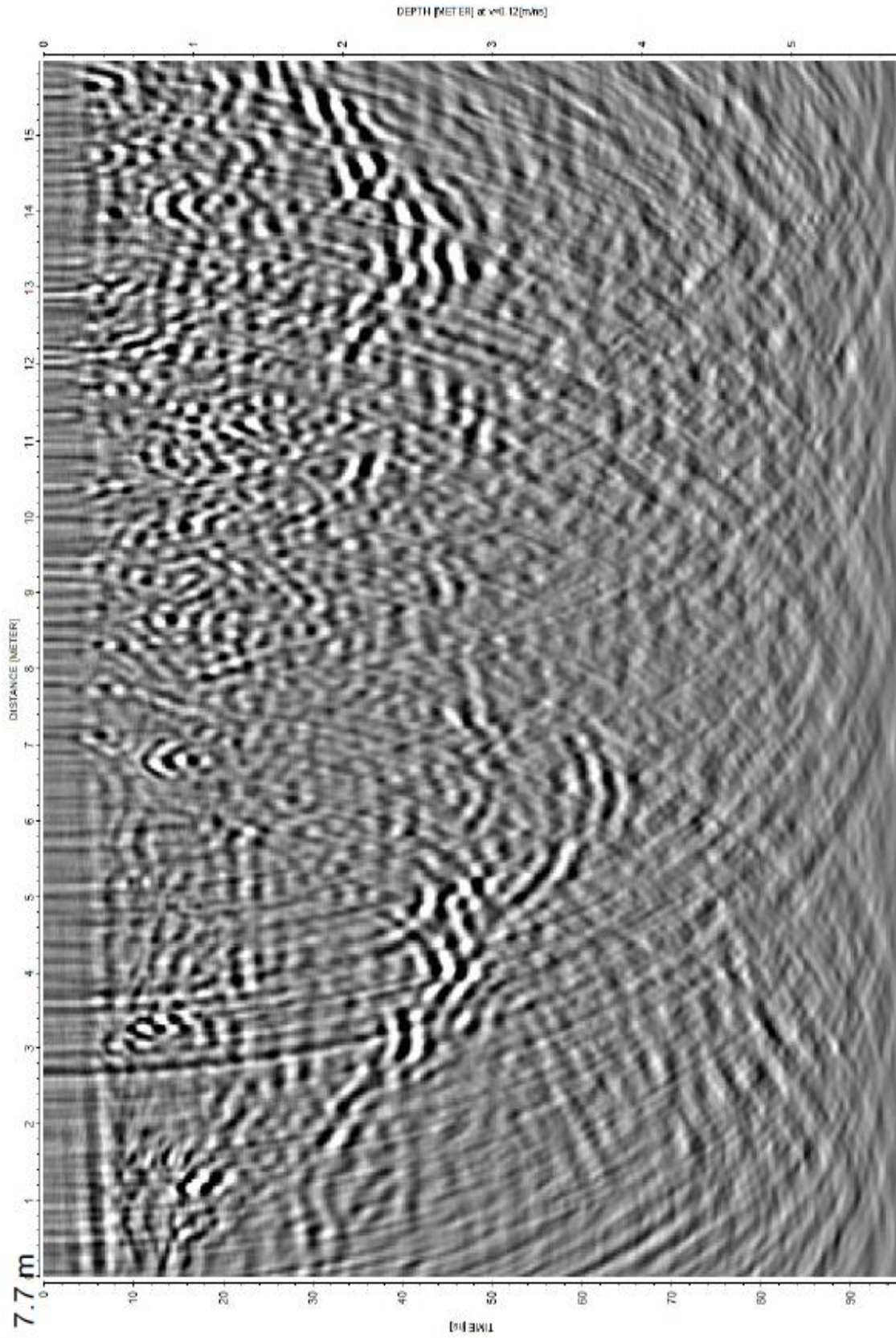
Figures 4.41-4.42. Figures 4.41 and 4.42 represent 2D-migrated versions of Figures 4.33

and 4.34, respectively.

154

Conclusions

This study started with a simple attempt to understand the limitation traditional 2D surveys for resolving sinkhole structure. Forward modeling was used to make simple model geometries to highlight the inaccuracies of 2D GPR profiles over three-dimensional features. These profiles were processed like typical 2D processing sequences, with and without migration. The results suggest that the 2D migration was unable to accurately reconstruct the structure of the three-dimensional model. Also, reflected energy from the conduit was mostly lost.

This thesis then addressed whether standard source and receiver survey geometries were optimal to resolve the difference in various structures of active sinkholes. A suite of non-traditional source and receiver survey geometries were used in the modeling in order to understand if there was added value in using these types of surveys. The simple adjustment of traditional offset distance did not produce better results. Non-traditional survey geometries were proven to be as ineffective at accurately recovering reflective energy from the conduit and traditional spacing appeared to be best suited even though they are limited.

Case studies of very high resolution 3D data of sinkholes and sinkhole-related features were then shown. The data were processed using standard 3D processing methods, including 3D migration of the data. Sinkhole features from these profiles served

155

as examples compared to those of the simplified models. Results from these surveys showed decent structural recovery of a small sinkhole similar in structure to that of the modeled ones. Indications of active subsidence and possible conduit structure were apparent from this data.

Finally, the dense surveys served as a benchmark to compare interpretations taken with the same surveys at lower spatial resolutions and profiles with 2D-only processing methods in order to understand errors in analysis and interpretation that are possible from 2D surveys. Two-dimensional surveys, 2D processed and migrated, showed some similarity to the 3D results previously mentioned but contained more complexities and artifacts, which led to poorer interpretation ability.

Future work in this specific field of research should include a wider range of model geometries in order to obtain a better understanding of the robustness of traditional offset GPR's ability to resolve conduit structure. By varying the lengths and grades of the conduit slope breaks, it may be possible to see if there is any sort of "breaking point" at which the radar energy is still returned from the bottom of the conduit. Also, producing more model geometries that incorporate simplified versions of complex infilling patterns seen in real world examples of sinkholes would be helpful in the understanding of what those patterns may suggest about the activity of the sinkholes below them.

156

References

Batayneh, A., Abueladas, A., & Moumani, K. A. (2002). *Use of ground-penetrating radar for assessment of potential sinkhole conditions: an example from Ghor al Haditha area, Jordan*. Environmental Geology 41:977–983.

Brandt, O., Langley, K., Giannopoulos, A., & Kohler, J. (2006). *3D Modelling of EM Waves in High Arctic Glaciers (II)*. HPC-Europa report.

Burger, H. R., Sheehan, A., & Jones, C. (2006). *Introduction to applied geophysics: exploring the shallow subsurface*. W.W. Norton.

Carpenter, P. J. & Ekberg, D. W. (2006). Identification of buried sinkholes, fractures and soil pipes using ground-penetrating radar and 2D electrical resistivity tomography. In Anderson, N.L. (Editor), *Proceedings of the 2006 Highway Geophysics – NDE Conference*, 437-449.

Dobecki, T. L. & Upchurch, S. B. (2006). *Geophysical applications to detect sinkholes and ground subsidence*. Leading Edge 25:336–341.

Ford, D. C. & Williams, P. W. (1989). *Karst Geomorphology and Hydrology*. Unwin Hyman, London, UK.

Gerhard, J. I., Power, C., Wilson, V., Giannopoulos, A., & Grant, G., (2008*). DNAPL Mapping by Ground Penetrating Radar Investigated via Numerical Simulation*. Eos Trans. AGU, 89(53), Fall Meet. Suppl., Abstract H51G-0923.

Grasmueck, M., Weger, R., & Horstmeyer, H. (2004). *Three dimensional ground-penetrating radar imaging of sedimentary structures, fractures, and archaeological features at submeter resolution*. Geology, 32(11), 933–936.

Grasmueck, M., Weger, R., & Horstmeyer, H. (2005). *Full-resolution 3-D GPR imaging*. Geophysics, vol. 70, no. 1, pp. K-12–K-19.

Giannopoulos, A. (2005a). *Modelling of ground penetrating radar using GprMax*. Construction and Building Materials, 19, pp. 755–762.

157

Giannopoulos, A. (2005b). *GPRMax User Guide V2*. Available from
http://www.gprmax.org/.

Kadioglu, S. (2008) *Photographing layer thicknesses and discontinuities in a marble quarry with 3D GPR visualization*. Journal of Applied Geophysics, vol. 64, 109–14.

Kruse, S. E., Schneider, J. C., Campagna, D. J., Inman, J. A., & Hickey, T. D. (2000). *Ground penetrating radar imaging of cap rock, caliche and carbonate strata*. Journal of Applied Geophysics, vol. 43, pp. 239–249.

Kruse, S., Grasmueck, M., Weiss, M., Viggiano, D. (2006). *Sinkhole structure imaging in covered Karst terrain*. Geophysical Research Letters 33: L16405. DOI: 10.1029/2006GL026975.

Mellet, J. (1995). *Ground penetrating radar applications in engineering, environmental management, and geology*. Journal of Applied Geophysics, vol. 33, pp. 157–166.

Orlando, L., Slob, E., (2009). *Using multicomponent GPR to monitor cracks in a historical building*, Journal of Applied Geophysics, vol. 67, iss. 4, p. 327-334.

Parker, J. W. (1992). *Surficial Aquifer Hydrogeology in a Covered-Karst Terrane*. Masters Thesis, University of South Florida, 228pp.

Reynolds, J. M. (1997). *An Introduction to Applied and Environmental Geophysics*. Wiley, Chichester.

Schmidt, W. (2005). *Geological and Geotechnical Investigation Procedures for Evaluation of the Causes of Subsidence Damage In Florida*, Florida Geological Survey, Special Publication No. 57.

Sinclair, W. C., & Stewart, J. W. (1985). *Sinkhole type, development, and distribution in Florida*. Florida Bureau of Geology, Map series No. 11.

Sandmeier, K.J. (2005) Software, Reflexw. Available from http://www.sandmeier-geo.de/.

Stewart, M. & Parker, J. (1992). *Localization and seasonal variation of recharge in a covered karst aquifer system, Florida, USA*. International Contributions Hydrogeology, vol. 13, pp. 443–460.

Stewart, M. T. (1998). *The Florida water wars: A geologic perspective*, Geotimes, vol. 43, pp. 24–27.

Taflove, A. (1995). *The Finite Difference in Time Domain Method*, Artech House, Boston, London.

Tihansky, A. B. (1999). *Sinkholes, west-central Florida, in Land Subsidence in the United States*, edited by D. Galloway et al., U.S. Geologic Survey Circular, 1182, 121–140.

Truss, S., Grasmueck, M., Vega, S., & Viggiano, D. A. (2007). *Imaging rainfall drainage within the Miami oolitic limestone using high-resolution time-lapse ground-penetrating radar*. Water Resour. Res., 43, W03405.

Wilson, W. L. & Shock, E. J. (1996). New sinkhole data spreadsheet manual (v1.1): Winter Springs, Fla., Subsurface Evaluations, Inc., 31 p. 3, app., 1 disk.

Yee, K. S. (1966). *Numerical solution of initial boundary value problems involving Maxwell's equations in isotropic media*. IEEE Trans. Antennas Propagat., vol. AP-14, pp. 302–307.

Zisman, E. D. (2001). *A standard method for sinkhole detection in the Tampa, Florida area.* Environmental Engineering Geoscience, vol. 7(1):31–50.

Zisman, E. D., Wightman, M. J., & Taylor, C. (2005). *The Effectiveness of GPR in Sinkhole Investigations*, ASCE Conf. Proc. 177, 65, DOI:10.1061/40796(177)65.

Appendices

160

Appendix A: GPRMAX input files

Geopark 2D Model A GPRMAX input file

#medium: 9.0 0.0 0.0 0.005 1.0 0.0 sand_geopark
#medium: 25.0 0.0 0.0 0.05 1.0 0.0 clay_geopark

#domain: 8.0 4.0
#dx_dy: 0.02 0.02
#time_window: 100e-9

#box: 0.0 0.0 8.0 2.5 clay_geopark
#box: 0.0 2.5 8.0 3.5 sand_geopark
#box: 0.0 3.5 8.0 4.0 free_space

#triangle: 2.0 2.5 4.0 0.5 6.0 2.5 sand_geopark

#line_source: 1.0 250e6 ricker MyLineSource

#analysis: 128 geopark2_2D.out a
#tx: 0.0 3.5 MyLineSource 0.0 100e-9
#rx: 0.3 3.5
#tx_steps: 0.05 0.0
#rx_steps: 0.05 0.0
#end_analysis:

#geometry_file: geopark2_2D.geo
#title: geopark 1 sink in 2D
#messages: y

Geopark 2D Model B GPRMAX input file
#medium: 9.0 0.0 0.0 0.005 1.0 0.0 sand_geopark
#medium: 25.0 0.0 0.0 0.05 1.0 0.0 clay_geopark

#domain: 8.0 4.5
#dx_dy: 0.02 0.02
#time_window: 100e-9

161

Appendix A (Continued)

```
-----------------------------------------------------------------------
#box: 0.0 0.0 8.0 3.0 clay_geopark
#box: 0.0 3.0 8.0 4.0 sand_geopark
#box: 0.0 4.0 8.0 4.5 free_space
-----------------------------------------------------------------------
#triangle: 2.0 3.0 4.0 1.0 6.0 3.0 sand_geopark
#triangle: 3.5 1.5 4.0 0.5 4.5 1.5 sand_geopark
-----------------------------------------------------------------
#line_source: 1.0 250e6 ricker MyLineSource
-----------------------------------------------------------------
#analysis: 128 geopark3_2D.out a
#tx: 0.0 4.0 MyLineSource 0.0 100e-9
#rx: 0.3 4.0
#tx_steps: 0.05 0.0
#rx_steps: 0.05 0.0
#end_analysis:
----------------------------------------------------------
#geometry_file: geopark3_2D.geo
#title: geopark 3 sink in 2D
#messages: y
```

Geopark 3D Model A GPRMAX input file

```
#medium: 9.0 0.0 0.0 0.005 1.0 0.0 sand_geopark
#medium: 25.0 0.0 0.0 0.05 1.0 0.0 clay_geopark
-----------------------------------------------------------------------
#domain: 8.0 8.0 4.0
#dx_dy_dz: 0.02 0.02 0.02
#time_window: 100e-9
-----------------------------------------------------------------------
#box: 0.0 0.0 0.0 8.0 8.0 2.5 clay_geopark
#box: 0.0 0.0 2.5 8.0 8.0 3.5 sand_geopark
#box: 0.0 0.0 3.5 8.0 8.0 4.0 free_space
-----------------------------------------------------------------------
#cylinder: z 2.480 2.500 4.000 4.000 2.000 sand_geopark
#cylinder: z 2.460 2.480 4.000 4.000 1.980 sand_geopark
#cylinder: z 2.440 2.460 4.000 4.000 1.960 sand_geopark
#cylinder: z 2.420 2.440 4.000 4.000 1.940 sand_geopark
```

162

Appendix A (Continued)

```
#cylinder: z 2.400 2.420 4.000 4.000 1.920 sand_geopark
#cylinder: z 2.380 2.400 4.000 4.000 1.900 sand_geopark
#cylinder: z 2.360 2.380 4.000 4.000 1.880 sand_geopark
#cylinder: z 2.340 2.360 4.000 4.000 1.860 sand_geopark
#cylinder: z 2.320 2.340 4.000 4.000 1.840 sand_geopark
#cylinder: z 2.300 2.320 4.000 4.000 1.820 sand_geopark
#cylinder: z 2.280 2.300 4.000 4.000 1.800 sand_geopark
#cylinder: z 2.260 2.280 4.000 4.000 1.780 sand_geopark
#cylinder: z 2.240 2.260 4.000 4.000 1.760 sand_geopark
#cylinder: z 2.220 2.240 4.000 4.000 1.740 sand_geopark
#cylinder: z 2.200 2.220 4.000 4.000 1.720 sand_geopark
#cylinder: z 2.180 2.200 4.000 4.000 1.700 sand_geopark
#cylinder: z 2.160 2.180 4.000 4.000 1.680 sand_geopark
#cylinder: z 2.140 2.160 4.000 4.000 1.660 sand_geopark
#cylinder: z 2.120 2.140 4.000 4.000 1.640 sand_geopark
#cylinder: z 2.100 2.120 4.000 4.000 1.620 sand_geopark
#cylinder: z 2.080 2.100 4.000 4.000 1.600 sand_geopark
#cylinder: z 2.060 2.080 4.000 4.000 1.580 sand_geopark
#cylinder: z 2.040 2.060 4.000 4.000 1.560 sand_geopark
#cylinder: z 2.020 2.040 4.000 4.000 1.540 sand_geopark
#cylinder: z 2.000 2.020 4.000 4.000 1.520 sand_geopark
#cylinder: z 1.980 2.000 4.000 4.000 1.500 sand_geopark
#cylinder: z 1.960 1.980 4.000 4.000 1.480 sand_geopark
#cylinder: z 1.940 1.960 4.000 4.000 1.460 sand_geopark
#cylinder: z 1.920 1.940 4.000 4.000 1.440 sand_geopark
#cylinder: z 1.900 1.920 4.000 4.000 1.420 sand_geopark
#cylinder: z 1.880 1.900 4.000 4.000 1.400 sand_geopark
#cylinder: z 1.860 1.880 4.000 4.000 1.380 sand_geopark
#cylinder: z 1.840 1.860 4.000 4.000 1.360 sand_geopark
#cylinder: z 1.820 1.840 4.000 4.000 1.340 sand_geopark
#cylinder: z 1.800 1.820 4.000 4.000 1.320 sand_geopark
#cylinder: z 1.780 1.800 4.000 4.000 1.300 sand_geopark
#cylinder: z 1.760 1.780 4.000 4.000 1.280 sand_geopark
#cylinder: z 1.740 1.760 4.000 4.000 1.260 sand_geopark
#cylinder: z 1.720 1.740 4.000 4.000 1.240 sand_geopark
#cylinder: z 1.700 1.720 4.000 4.000 1.220 sand_geopark
#cylinder: z 1.680 1.700 4.000 4.000 1.200 sand_geopark
#cylinder: z 1.660 1.680 4.000 4.000 1.180 sand_geopark
#cylinder: z 1.640 1.660 4.000 4.000 1.160 sand_geopark
```

Appendix A (Continued)

```
#cylinder: z 1.620 1.640 4.000 4.000 1.140 sand_geopark
#cylinder: z 1.600 1.620 4.000 4.000 1.120 sand_geopark
#cylinder: z 1.580 1.600 4.000 4.000 1.100 sand_geopark
#cylinder: z 1.560 1.580 4.000 4.000 1.080 sand_geopark
#cylinder: z 1.540 1.560 4.000 4.000 1.060 sand_geopark
#cylinder: z 1.520 1.540 4.000 4.000 1.040 sand_geopark
#cylinder: z 1.500 1.520 4.000 4.000 1.020 sand_geopark
#cylinder: z 1.480 1.500 4.000 4.000 1.000 sand_geopark
#cylinder: z 1.460 1.480 4.000 4.000 0.980 sand_geopark
#cylinder: z 1.440 1.460 4.000 4.000 0.960 sand_geopark
#cylinder: z 1.420 1.440 4.000 4.000 0.940 sand_geopark
#cylinder: z 1.400 1.420 4.000 4.000 0.920 sand_geopark
#cylinder: z 1.380 1.400 4.000 4.000 0.900 sand_geopark
#cylinder: z 1.360 1.380 4.000 4.000 0.880 sand_geopark
#cylinder: z 1.340 1.360 4.000 4.000 0.860 sand_geopark
#cylinder: z 1.320 1.340 4.000 4.000 0.840 sand_geopark
#cylinder: z 1.300 1.320 4.000 4.000 0.820 sand_geopark
#cylinder: z 1.280 1.300 4.000 4.000 0.800 sand_geopark
#cylinder: z 1.260 1.280 4.000 4.000 0.780 sand_geopark
#cylinder: z 1.240 1.260 4.000 4.000 0.760 sand_geopark
#cylinder: z 1.220 1.240 4.000 4.000 0.740 sand_geopark
#cylinder: z 1.200 1.220 4.000 4.000 0.720 sand_geopark
#cylinder: z 1.180 1.200 4.000 4.000 0.700 sand_geopark
#cylinder: z 1.160 1.180 4.000 4.000 0.680 sand_geopark
#cylinder: z 1.140 1.160 4.000 4.000 0.660 sand_geopark
#cylinder: z 1.120 1.140 4.000 4.000 0.640 sand_geopark
#cylinder: z 1.100 1.120 4.000 4.000 0.620 sand_geopark
#cylinder: z 1.080 1.100 4.000 4.000 0.600 sand_geopark
#cylinder: z 1.060 1.080 4.000 4.000 0.580 sand_geopark
#cylinder: z 1.040 1.060 4.000 4.000 0.560 sand_geopark
#cylinder: z 1.020 1.040 4.000 4.000 0.540 sand_geopark
#cylinder: z 1.000 1.020 4.000 4.000 0.520 sand_geopark
#cylinder: z 0.980 1.000 4.000 4.000 0.500 sand_geopark
#cylinder: z 0.960 0.980 4.000 4.000 0.480 sand_geopark
#cylinder: z 0.940 0.960 4.000 4.000 0.460 sand_geopark
#cylinder: z 0.920 0.940 4.000 4.000 0.440 sand_geopark
#cylinder: z 0.900 0.920 4.000 4.000 0.420 sand_geopark
#cylinder: z 0.880 0.900 4.000 4.000 0.400 sand_geopark
#cylinder: z 0.860 0.880 4.000 4.000 0.380 sand_geopark
```

164

Appendix A (Continued)

```
#cylinder: z 0.840 0.860 4.000 4.000 0.360 sand_geopark
#cylinder: z 0.820 0.840 4.000 4.000 0.340 sand_geopark
#cylinder: z 0.800 0.820 4.000 4.000 0.320 sand_geopark
#cylinder: z 0.780 0.800 4.000 4.000 0.300 sand_geopark
#cylinder: z 0.760 0.780 4.000 4.000 0.280 sand_geopark
#cylinder: z 0.740 0.760 4.000 4.000 0.260 sand_geopark
#cylinder: z 0.720 0.740 4.000 4.000 0.240 sand_geopark
#cylinder: z 0.700 0.720 4.000 4.000 0.220 sand_geopark
#cylinder: z 0.680 0.700 4.000 4.000 0.200 sand_geopark
#cylinder: z 0.660 0.680 4.000 4.000 0.180 sand_geopark
#cylinder: z 0.640 0.660 4.000 4.000 0.160 sand_geopark
#cylinder: z 0.620 0.640 4.000 4.000 0.140 sand_geopark
#cylinder: z 0.600 0.620 4.000 4.000 0.120 sand_geopark
#cylinder: z 0.580 0.600 4.000 4.000 0.100 sand_geopark
#cylinder: z 0.560 0.580 4.000 4.000 0.080 sand_geopark
#cylinder: z 0.540 0.560 4.000 4.000 0.060 sand_geopark
#cylinder: z 0.520 0.540 4.000 4.000 0.040 sand_geopark
#cylinder: z 0.500 0.520 4.000 4.000 0.020 sand_geopark
-----------------------------------------------------------------------
#hertzian_dipole: 1.0 250e6 ricker MyDipole
#analysis: 145 geopark1.out a
#tx: x 4.0 0.0 3.5 MyDipole 0.0 100e-9
#rx: 4.0 0.3 3.5
#tx_steps: 0.0 0.05 0.0
#rx_steps: 0.0 0.05 0.0
#end_analysis:
-----------------------------------------------------------------------
#messages: y
#title: geopark 1
#geometry_file: geopark1.geo
```

Geopark 3D Model B GPRMAX input file

```
#medium: 9.0 0.0 0.0 0.005 1.0 0.0 sand_geopark
#medium: 25.0 0.0 0.0 0.05 1.0 0.0 clay_geopark
-----------------------------------------------------------------------
#domain: 8.0 8.0 4.5
#dx_dy_dz: 0.02 0.02 0.02
#time_window: 120e-9
```

165

Appendix A (Continued)

```
------------------------------------------------------------------------
#box: 0.0 0.0 0.0 8.0 8.0 3.0 clay_geopark
#box: 0.0 0.0 3.0 8.0 8.0 4.0 sand_geopark
#box: 0.0 0.0 4.0 8.0 8.0 4.5 free_space
------------------------------------------------------------------------
#cylinder: z 2.980 3.000 4.000 4.000 2.000 sand_geopark
#cylinder: z 2.960 2.980 4.000 4.000 1.980 sand_geopark
#cylinder: z 2.940 2.960 4.000 4.000 1.960 sand_geopark
#cylinder: z 2.920 2.940 4.000 4.000 1.940 sand_geopark
#cylinder: z 2.900 2.920 4.000 4.000 1.920 sand_geopark
#cylinder: z 2.880 2.900 4.000 4.000 1.900 sand_geopark
#cylinder: z 2.860 2.880 4.000 4.000 1.880 sand_geopark
#cylinder: z 2.840 2.860 4.000 4.000 1.860 sand_geopark
#cylinder: z 2.820 2.840 4.000 4.000 1.840 sand_geopark
#cylinder: z 2.800 2.820 4.000 4.000 1.820 sand_geopark
#cylinder: z 2.780 2.800 4.000 4.000 1.800 sand_geopark
#cylinder: z 2.760 2.780 4.000 4.000 1.780 sand_geopark
#cylinder: z 2.740 2.760 4.000 4.000 1.760 sand_geopark
#cylinder: z 2.720 2.740 4.000 4.000 1.740 sand_geopark
#cylinder: z 2.700 2.720 4.000 4.000 1.720 sand_geopark
#cylinder: z 2.680 2.700 4.000 4.000 1.700 sand_geopark
#cylinder: z 2.660 2.680 4.000 4.000 1.680 sand_geopark
#cylinder: z 2.640 2.660 4.000 4.000 1.660 sand_geopark
#cylinder: z 2.620 2.640 4.000 4.000 1.640 sand_geopark
#cylinder: z 2.600 2.620 4.000 4.000 1.620 sand_geopark
#cylinder: z 2.580 2.600 4.000 4.000 1.600 sand_geopark
#cylinder: z 2.560 2.580 4.000 4.000 1.580 sand_geopark
#cylinder: z 2.540 2.560 4.000 4.000 1.560 sand_geopark
#cylinder: z 2.520 2.540 4.000 4.000 1.540 sand_geopark
#cylinder: z 2.500 2.520 4.000 4.000 1.520 sand_geopark
#cylinder: z 2.480 2.500 4.000 4.000 1.500 sand_geopark
#cylinder: z 2.460 2.480 4.000 4.000 1.480 sand_geopark
#cylinder: z 2.440 2.460 4.000 4.000 1.460 sand_geopark
#cylinder: z 2.420 2.440 4.000 4.000 1.440 sand_geopark
#cylinder: z 2.400 2.420 4.000 4.000 1.420 sand_geopark
#cylinder: z 2.380 2.400 4.000 4.000 1.400 sand_geopark
#cylinder: z 2.360 2.380 4.000 4.000 1.380 sand_geopark
#cylinder: z 2.340 2.360 4.000 4.000 1.360 sand_geopark
#cylinder: z 2.320 2.340 4.000 4.000 1.340 sand_geopark
#cylinder: z 2.300 2.320 4.000 4.000 1.320 sand_geopark
```

```
#cylinder: z 2.280 2.300 4.000 4.000 1.300 sand_geopark
#cylinder: z 2.260 2.280 4.000 4.000 1.280 sand_geopark
#cylinder: z 2.240 2.260 4.000 4.000 1.260 sand_geopark
#cylinder: z 2.220 2.240 4.000 4.000 1.240 sand_geopark
#cylinder: z 2.200 2.220 4.000 4.000 1.220 sand_geopark
#cylinder: z 2.180 2.200 4.000 4.000 1.200 sand_geopark
#cylinder: z 2.160 2.180 4.000 4.000 1.180 sand_geopark
#cylinder: z 2.140 2.160 4.000 4.000 1.160 sand_geopark
#cylinder: z 2.120 2.140 4.000 4.000 1.140 sand_geopark
#cylinder: z 2.100 2.120 4.000 4.000 1.120 sand_geopark
#cylinder: z 2.080 2.100 4.000 4.000 1.100 sand_geopark
#cylinder: z 2.060 2.080 4.000 4.000 1.080 sand_geopark
#cylinder: z 2.040 2.060 4.000 4.000 1.060 sand_geopark
#cylinder: z 2.020 2.040 4.000 4.000 1.040 sand_geopark
#cylinder: z 2.000 2.020 4.000 4.000 1.020 sand_geopark
#cylinder: z 1.980 2.000 4.000 4.000 1.000 sand_geopark
#cylinder: z 1.960 1.980 4.000 4.000 0.980 sand_geopark
#cylinder: z 1.940 1.960 4.000 4.000 0.960 sand_geopark
#cylinder: z 1.920 1.940 4.000 4.000 0.940 sand_geopark
#cylinder: z 1.900 1.920 4.000 4.000 0.920 sand_geopark
#cylinder: z 1.880 1.900 4.000 4.000 0.900 sand_geopark
#cylinder: z 1.860 1.880 4.000 4.000 0.880 sand_geopark
#cylinder: z 1.840 1.860 4.000 4.000 0.860 sand_geopark
#cylinder: z 1.820 1.840 4.000 4.000 0.840 sand_geopark
#cylinder: z 1.800 1.820 4.000 4.000 0.820 sand_geopark
#cylinder: z 1.780 1.800 4.000 4.000 0.800 sand_geopark
#cylinder: z 1.760 1.780 4.000 4.000 0.780 sand_geopark
#cylinder: z 1.740 1.760 4.000 4.000 0.760 sand_geopark
#cylinder: z 1.720 1.740 4.000 4.000 0.740 sand_geopark
#cylinder: z 1.700 1.720 4.000 4.000 0.720 sand_geopark
#cylinder: z 1.680 1.700 4.000 4.000 0.700 sand_geopark
#cylinder: z 1.660 1.680 4.000 4.000 0.680 sand_geopark
#cylinder: z 1.640 1.660 4.000 4.000 0.660 sand_geopark
#cylinder: z 1.620 1.640 4.000 4.000 0.640 sand_geopark
#cylinder: z 1.600 1.620 4.000 4.000 0.620 sand_geopark
#cylinder: z 1.580 1.600 4.000 4.000 0.600 sand_geopark
#cylinder: z 1.560 1.580 4.000 4.000 0.580 sand_geopark
#cylinder: z 1.540 1.560 4.000 4.000 0.560 sand_geopark
#cylinder: z 1.520 1.540 4.000 4.000 0.540 sand_geopark
#cylinder: z 1.500 1.520 4.000 4.000 0.520 sand_geopark
```

```
#cylinder: z 1.480 1.500 4.000 4.000 0.500 sand_geopark
#cylinder: z 1.460 1.480 4.000 4.000 0.480 sand_geopark
#cylinder: z 1.440 1.460 4.000 4.000 0.460 sand_geopark
#cylinder: z 1.420 1.440 4.000 4.000 0.440 sand_geopark
#cylinder: z 1.400 1.420 4.000 4.000 0.420 sand_geopark
#cylinder: z 1.380 1.400 4.000 4.000 0.400 sand_geopark
#cylinder: z 1.360 1.380 4.000 4.000 0.380 sand_geopark
#cylinder: z 1.340 1.360 4.000 4.000 0.360 sand_geopark
#cylinder: z 1.320 1.340 4.000 4.000 0.340 sand_geopark
#cylinder: z 1.300 1.320 4.000 4.000 0.320 sand_geopark
#cylinder: z 1.280 1.300 4.000 4.000 0.300 sand_geopark
#cylinder: z 1.260 1.280 4.000 4.000 0.280 sand_geopark
#cylinder: z 1.240 1.260 4.000 4.000 0.260 sand_geopark
#cylinder: z 1.220 1.240 4.000 4.000 0.240 sand_geopark
#cylinder: z 1.200 1.220 4.000 4.000 0.220 sand_geopark
#cylinder: z 1.180 1.200 4.000 4.000 0.200 sand_geopark
#cylinder: z 1.160 1.180 4.000 4.000 0.180 sand_geopark
#cylinder: z 1.140 1.160 4.000 4.000 0.160 sand_geopark
#cylinder: z 1.120 1.140 4.000 4.000 0.140 sand_geopark
#cylinder: z 1.100 1.120 4.000 4.000 0.120 sand_geopark
#cylinder: z 1.080 1.100 4.000 4.000 0.100 sand_geopark
#cylinder: z 1.060 1.080 4.000 4.000 0.080 sand_geopark
#cylinder: z 1.040 1.060 4.000 4.000 0.060 sand_geopark
#cylinder: z 1.020 1.040 4.000 4.000 0.040 sand_geopark
#cylinder: z 1.000 1.020 4.000 4.000 0.020 sand_geopark
------------------------------------------------------------------------
#cylinder: z 1.480 1.500 4.000 4.000 0.500 sand_geopark
#cylinder: z 1.460 1.480 4.000 4.000 0.490 sand_geopark
#cylinder: z 1.440 1.460 4.000 4.000 0.480 sand_geopark
#cylinder: z 1.420 1.440 4.000 4.000 0.470 sand_geopark
#cylinder: z 1.400 1.420 4.000 4.000 0.460 sand_geopark
#cylinder: z 1.380 1.400 4.000 4.000 0.450 sand_geopark
#cylinder: z 1.360 1.380 4.000 4.000 0.440 sand_geopark
#cylinder: z 1.340 1.360 4.000 4.000 0.430 sand_geopark
#cylinder: z 1.320 1.340 4.000 4.000 0.420 sand_geopark
#cylinder: z 1.300 1.320 4.000 4.000 0.410 sand_geopark
#cylinder: z 1.280 1.300 4.000 4.000 0.400 sand_geopark
#cylinder: z 1.260 1.280 4.000 4.000 0.390 sand_geopark
#cylinder: z 1.240 1.260 4.000 4.000 0.380 sand_geopark
#cylinder: z 1.220 1.240 4.000 4.000 0.370 sand_geopark
```

168

Appendix A (Continued)

```
#cylinder: z 1.200 1.220 4.000 4.000 0.360 sand_geopark
#cylinder: z 1.180 1.200 4.000 4.000 0.350 sand_geopark
#cylinder: z 1.160 1.180 4.000 4.000 0.340 sand_geopark
#cylinder: z 1.140 1.160 4.000 4.000 0.330 sand_geopark
#cylinder: z 1.120 1.140 4.000 4.000 0.320 sand_geopark
#cylinder: z 1.100 1.120 4.000 4.000 0.310 sand_geopark
#cylinder: z 1.080 1.100 4.000 4.000 0.300 sand_geopark
#cylinder: z 1.060 1.080 4.000 4.000 0.290 sand_geopark
#cylinder: z 1.040 1.060 4.000 4.000 0.280 sand_geopark
#cylinder: z 1.020 1.040 4.000 4.000 0.270 sand_geopark
#cylinder: z 1.000 1.020 4.000 4.000 0.260 sand_geopark
#cylinder: z 0.980 1.000 4.000 4.000 0.250 sand_geopark
#cylinder: z 0.960 0.980 4.000 4.000 0.240 sand_geopark
#cylinder: z 0.940 0.960 4.000 4.000 0.230 sand_geopark
#cylinder: z 0.920 0.940 4.000 4.000 0.220 sand_geopark
#cylinder: z 0.900 0.920 4.000 4.000 0.210 sand_geopark
#cylinder: z 0.880 0.900 4.000 4.000 0.200 sand_geopark
#cylinder: z 0.860 0.880 4.000 4.000 0.190 sand_geopark
#cylinder: z 0.840 0.860 4.000 4.000 0.180 sand_geopark
#cylinder: z 0.820 0.840 4.000 4.000 0.170 sand_geopark
#cylinder: z 0.800 0.820 4.000 4.000 0.160 sand_geopark
#cylinder: z 0.780 0.800 4.000 4.000 0.150 sand_geopark
#cylinder: z 0.760 0.780 4.000 4.000 0.140 sand_geopark
#cylinder: z 0.740 0.760 4.000 4.000 0.130 sand_geopark
#cylinder: z 0.720 0.740 4.000 4.000 0.120 sand_geopark
#cylinder: z 0.700 0.720 4.000 4.000 0.110 sand_geopark
#cylinder: z 0.680 0.700 4.000 4.000 0.100 sand_geopark
#cylinder: z 0.660 0.680 4.000 4.000 0.090 sand_geopark
#cylinder: z 0.640 0.660 4.000 4.000 0.080 sand_geopark
#cylinder: z 0.620 0.640 4.000 4.000 0.070 sand_geopark
#cylinder: z 0.600 0.620 4.000 4.000 0.060 sand_geopark
#cylinder: z 0.580 0.600 4.000 4.000 0.050 sand_geopark
#cylinder: z 0.560 0.580 4.000 4.000 0.040 sand_geopark
#cylinder: z 0.540 0.560 4.000 4.000 0.030 sand_geopark
#cylinder: z 0.520 0.540 4.000 4.000 0.020 sand_geopark
#cylinder: z 0.500 0.520 4.000 4.000 0.010 sand_geopark
------------------------------------------------------------------------
#hertzian_dipole: 1.0 250e6 ricker MyDipole
#analysis: 154 geopark3a.out b
#tx: x 4.0 0.0 4.0 MyDipole 0.0 120e-9
```

169

Appendix A (Continued)

```
#rx: 4.0 0.3 4.0
#rx: 4.0 0.4 4.0
#rx: 4.0 0.5 4.0
#rx: 4.0 0.6 4.0
#rx: 4.0 0.7 4.0
#rx: 4.0 0.8 4.0
#rx: 4.0 0.9 4.0
#rx: 4.0 1.0 4.0
#rx: 4.0 1.1 4.0
#rx: 4.0 1.2 4.0
#rx: 4.0 1.3 4.0
#rx: 4.0 1.4 4.0
#rx: 4.0 1.5 4.0
#rx: 4.0 1.6 4.0
#rx: 4.0 1.7 4.0
#rx: 4.0 1.8 4.0
#tx_steps: 0.0 0.05 0.0
#rx_steps: 0.0 0.05 0.0
#end_analysis:
-----------------------------------------------------------------------
#messages: y
#title: geopark 3a
#geometry_file: geopark3a.geo
-----------------------------------------------------------------------


-----------------------------------------------------------------------
Geopark 3D Model A rx_box GPRMAX input file

#medium: 9.0 0.0 0.0 0.005 1.0 0.0 sand_geopark
#medium: 25.0 0.0 0.0 0.05 1.0 0.0 clay_geopark
----------------------------------------------------------------------
#domain: 5.0 7.0 4.0
#dx_dy_dz: 0.02 0.02 0.02
#time_window: 100e-9
----------------------------------------------------------------------
#box: 0.0 0.0 0.0 5.0 7.0 2.5 clay_geopark
#box: 0.0 0.0 2.5 5.0 7.0 3.5 sand_geopark
#box: 0.0 0.0 3.5 5.0 7.0 4.0 free_space
----------------------------------------------------------------------
#cylinder: z 2.480 2.500 2.500 3.500 2.000 sand_geopark
```

170

Appendix A (Continued)

```
#cylinder: z 2.460 2.480 2.500 3.500 1.980 sand_geopark
#cylinder: z 2.440 2.460 2.500 3.500 1.960 sand_geopark
#cylinder: z 2.420 2.440 2.500 3.500 1.940 sand_geopark
#cylinder: z 2.400 2.420 2.500 3.500 1.920 sand_geopark
#cylinder: z 2.380 2.400 2.500 3.500 1.900 sand_geopark
#cylinder: z 2.360 2.380 2.500 3.500 1.880 sand_geopark
#cylinder: z 2.340 2.360 2.500 3.500 1.860 sand_geopark
#cylinder: z 2.320 2.340 2.500 3.500 1.840 sand_geopark
#cylinder: z 2.300 2.320 2.500 3.500 1.820 sand_geopark
#cylinder: z 2.280 2.300 2.500 3.500 1.800 sand_geopark
#cylinder: z 2.260 2.280 2.500 3.500 1.780 sand_geopark
#cylinder: z 2.240 2.260 2.500 3.500 1.760 sand_geopark
#cylinder: z 2.220 2.240 2.500 3.500 1.740 sand_geopark
#cylinder: z 2.200 2.220 2.500 3.500 1.720 sand_geopark
#cylinder: z 2.180 2.200 2.500 3.500 1.700 sand_geopark
#cylinder: z 2.160 2.180 2.500 3.500 1.680 sand_geopark
#cylinder: z 2.140 2.160 2.500 3.500 1.660 sand_geopark
#cylinder: z 2.120 2.140 2.500 3.500 1.640 sand_geopark
#cylinder: z 2.100 2.120 2.500 3.500 1.620 sand_geopark
#cylinder: z 2.080 2.100 2.500 3.500 1.600 sand_geopark
#cylinder: z 2.060 2.080 2.500 3.500 1.580 sand_geopark
#cylinder: z 2.040 2.060 2.500 3.500 1.560 sand_geopark
#cylinder: z 2.020 2.040 2.500 3.500 1.540 sand_geopark
#cylinder: z 2.000 2.020 2.500 3.500 1.520 sand_geopark
#cylinder: z 1.980 2.000 2.500 3.500 1.500 sand_geopark
#cylinder: z 1.960 1.980 2.500 3.500 1.480 sand_geopark
#cylinder: z 1.940 1.960 2.500 3.500 1.460 sand_geopark
#cylinder: z 1.920 1.940 2.500 3.500 1.440 sand_geopark
#cylinder: z 1.900 1.920 2.500 3.500 1.420 sand_geopark
#cylinder: z 1.880 1.900 2.500 3.500 1.400 sand_geopark
#cylinder: z 1.860 1.880 2.500 3.500 1.380 sand_geopark
#cylinder: z 1.840 1.860 2.500 3.500 1.360 sand_geopark
#cylinder: z 1.820 1.840 2.500 3.500 1.340 sand_geopark
#cylinder: z 1.800 1.820 2.500 3.500 1.320 sand_geopark
#cylinder: z 1.780 1.800 2.500 3.500 1.300 sand_geopark
#cylinder: z 1.760 1.780 2.500 3.500 1.280 sand_geopark
#cylinder: z 1.740 1.760 2.500 3.500 1.260 sand_geopark
#cylinder: z 1.720 1.740 2.500 3.500 1.240 sand_geopark
#cylinder: z 1.700 1.720 2.500 3.500 1.220 sand_geopark
#cylinder: z 1.680 1.700 2.500 3.500 1.200 sand_geopark
```

Appendix A (Continued)

```
#cylinder: z 1.660 1.680 2.500 3.500 1.180 sand_geopark
#cylinder: z 1.640 1.660 2.500 3.500 1.160 sand_geopark
#cylinder: z 1.620 1.640 2.500 3.500 1.140 sand_geopark
#cylinder: z 1.600 1.620 2.500 3.500 1.120 sand_geopark
#cylinder: z 1.580 1.600 2.500 3.500 1.100 sand_geopark
#cylinder: z 1.560 1.580 2.500 3.500 1.080 sand_geopark
#cylinder: z 1.540 1.560 2.500 3.500 1.060 sand_geopark
#cylinder: z 1.520 1.540 2.500 3.500 1.040 sand_geopark
#cylinder: z 1.500 1.520 2.500 3.500 1.020 sand_geopark
#cylinder: z 1.480 1.500 2.500 3.500 1.000 sand_geopark
#cylinder: z 1.460 1.480 2.500 3.500 0.980 sand_geopark
#cylinder: z 1.440 1.460 2.500 3.500 0.960 sand_geopark
#cylinder: z 1.420 1.440 2.500 3.500 0.940 sand_geopark
#cylinder: z 1.400 1.420 2.500 3.500 0.920 sand_geopark
#cylinder: z 1.380 1.400 2.500 3.500 0.900 sand_geopark
#cylinder: z 1.360 1.380 2.500 3.500 0.880 sand_geopark
#cylinder: z 1.340 1.360 2.500 3.500 0.860 sand_geopark
#cylinder: z 1.320 1.340 2.500 3.500 0.840 sand_geopark
#cylinder: z 1.300 1.320 2.500 3.500 0.820 sand_geopark
#cylinder: z 1.280 1.300 2.500 3.500 0.800 sand_geopark
#cylinder: z 1.260 1.280 2.500 3.500 0.780 sand_geopark
#cylinder: z 1.240 1.260 2.500 3.500 0.760 sand_geopark
#cylinder: z 1.220 1.240 2.500 3.500 0.740 sand_geopark
#cylinder: z 1.200 1.220 2.500 3.500 0.720 sand_geopark
#cylinder: z 1.180 1.200 2.500 3.500 0.700 sand_geopark
#cylinder: z 1.160 1.180 2.500 3.500 0.680 sand_geopark
#cylinder: z 1.140 1.160 2.500 3.500 0.660 sand_geopark
#cylinder: z 1.120 1.140 2.500 3.500 0.640 sand_geopark
#cylinder: z 1.100 1.120 2.500 3.500 0.620 sand_geopark
#cylinder: z 1.080 1.100 2.500 3.500 0.600 sand_geopark
#cylinder: z 1.060 1.080 2.500 3.500 0.580 sand_geopark
#cylinder: z 1.040 1.060 2.500 3.500 0.560 sand_geopark
#cylinder: z 1.020 1.040 2.500 3.500 0.540 sand_geopark
#cylinder: z 1.000 1.020 2.500 3.500 0.520 sand_geopark
#cylinder: z 0.980 1.000 2.500 3.500 0.500 sand_geopark
#cylinder: z 0.960 0.980 2.500 3.500 0.480 sand_geopark
#cylinder: z 0.940 0.960 2.500 3.500 0.460 sand_geopark
#cylinder: z 0.920 0.940 2.500 3.500 0.440 sand_geopark
#cylinder: z 0.900 0.920 2.500 3.500 0.420 sand_geopark
#cylinder: z 0.880 0.900 2.500 3.500 0.400 sand_geopark
```

#cylinder: z 0.860 0.880 2.500 3.500 0.380 sand_geopark
#cylinder: z 0.840 0.860 2.500 3.500 0.360 sand_geopark
#cylinder: z 0.820 0.840 2.500 3.500 0.340 sand_geopark
#cylinder: z 0.800 0.820 2.500 3.500 0.320 sand_geopark
#cylinder: z 0.780 0.800 2.500 3.500 0.300 sand_geopark
#cylinder: z 0.760 0.780 2.500 3.500 0.280 sand_geopark
#cylinder: z 0.740 0.760 2.500 3.500 0.260 sand_geopark
#cylinder: z 0.720 0.740 2.500 3.500 0.240 sand_geopark
#cylinder: z 0.700 0.720 2.500 3.500 0.220 sand_geopark
#cylinder: z 0.680 0.700 2.500 3.500 0.200 sand_geopark
#cylinder: z 0.660 0.680 2.500 3.500 0.180 sand_geopark
#cylinder: z 0.640 0.660 2.500 3.500 0.160 sand_geopark
#cylinder: z 0.620 0.640 2.500 3.500 0.140 sand_geopark
#cylinder: z 0.600 0.620 2.500 3.500 0.120 sand_geopark
#cylinder: z 0.580 0.600 2.500 3.500 0.100 sand_geopark
#cylinder: z 0.560 0.580 2.500 3.500 0.080 sand_geopark
#cylinder: z 0.540 0.560 2.500 3.500 0.060 sand_geopark
#cylinder: z 0.520 0.540 2.500 3.500 0.040 sand_geopark
#cylinder: z 0.500 0.520 2.500 3.500 0.020 sand_geopark

#hertzian_dipole: 1.0 250e6 ricker MyDipole
#analysis: 145 geopark1_rxbox.out b
#tx: x 2.5 1.1 3.5 MyDipole 0.0 100e-9
#rx_box: 0.1 1.1 3.5 4.9 6.9 3.5 0.1 0.1 0.1
#tx_steps: 0.0 0.05 0.0

#end_analysis:

#messages: y
#title: geopark 1 rxbox
#geometry_file: geopark1_rxbox.geo

Geopark 3D Model B rx_box GPRMAX input file

#medium: 9.0 0.0 0.0 0.005 1.0 0.0 sand_geopark
#medium: 25.0 0.0 0.0 0.05 1.0 0.0 clay_geopark

#domain: 5.0 7.0 4.5
#dx_dy_dz: 0.02 0.02 0.02

Appendix A (Continued)

#time_window: 120e-9

#box: 0.0 0.0 0.0 5.0 7.0 3.0 clay_geopark
#box: 0.0 0.0 3.0 5.0 7.0 4.0 sand_geopark
#box: 0.0 0.0 4.0 5.0 7.0 4.5 free_space

#cylinder:	z	2.980	3.000	2.500	3.500	2.000	sand_geopark
#cylinder:	z	2.960	2.980	2.500	3.500	1.980	sand_geopark
#cylinder:	z	2.940	2.960	2.500	3.500	1.960	sand_geopark
#cylinder:	z	2.920	2.940	2.500	3.500	1.940	sand_geopark
#cylinder:	z	2.900	2.920	2.500	3.500	1.920	sand_geopark
#cylinder:	z	2.880	2.900	2.500	3.500	1.900	sand_geopark
#cylinder:	z	2.860	2.880	2.500	3.500	1.880	sand_geopark
#cylinder:	z	2.840	2.860	2.500	3.500	1.860	sand_geopark
#cylinder:	z	2.820	2.840	2.500	3.500	1.840	sand_geopark
#cylinder:	z	2.800	2.820	2.500	3.500	1.820	sand_geopark
#cylinder:	z	2.780	2.800	2.500	3.500	1.800	sand_geopark
#cylinder:	z	2.760	2.780	2.500	3.500	1.780	sand_geopark
#cylinder:	z	2.740	2.760	2.500	3.500	1.760	sand_geopark
#cylinder:	z	2.720	2.740	2.500	3.500	1.740	sand_geopark
#cylinder:	z	2.700	2.720	2.500	3.500	1.720	sand_geopark
#cylinder:	z	2.680	2.700	2.500	3.500	1.700	sand_geopark
#cylinder:	z	2.660	2.680	2.500	3.500	1.680	sand_geopark
#cylinder:	z	2.640	2.660	2.500	3.500	1.660	sand_geopark
#cylinder:	z	2.620	2.640	2.500	3.500	1.640	sand_geopark
#cylinder:	z	2.600	2.620	2.500	3.500	1.620	sand_geopark
#cylinder:	z	2.580	2.600	2.500	3.500	1.600	sand_geopark
#cylinder:	z	2.560	2.580	2.500	3.500	1.580	sand_geopark
#cylinder:	z	2.540	2.560	2.500	3.500	1.560	sand_geopark
#cylinder:	z	2.520	2.540	2.500	3.500	1.540	sand_geopark
#cylinder:	z	2.500	2.520	2.500	3.500	1.520	sand_geopark
#cylinder:	z	2.480	2.500	2.500	3.500	1.500	sand_geopark
#cylinder:	z	2.460	2.480	2.500	3.500	1.480	sand_geopark
#cylinder:	z	2.440	2.460	2.500	3.500	1.460	sand_geopark
#cylinder:	z	2.420	2.440	2.500	3.500	1.440	sand_geopark
#cylinder:	z	2.400	2.420	2.500	3.500	1.420	sand_geopark
#cylinder:	z	2.380	2.400	2.500	3.500	1.400	sand_geopark
#cylinder:	z	2.360	2.380	2.500	3.500	1.380	sand_geopark
#cylinder:	z	2.340	2.360	2.500	3.500	1.360	sand_geopark
#cylinder:	z	2.320	2.340	2.500	3.500	1.340	sand_geopark

174

Appendix A (Continued)

#cylinder:	z	2.300	2.320	2.500	3.500	1.320	sand_geopark
#cylinder:	z	2.280	2.300	2.500	3.500	1.300	sand_geopark
#cylinder:	z	2.260	2.280	2.500	3.500	1.280	sand_geopark
#cylinder:	z	2.240	2.260	2.500	3.500	1.260	sand_geopark
#cylinder:	z	2.220	2.240	2.500	3.500	1.240	sand_geopark
#cylinder:	z	2.200	2.220	2.500	3.500	1.220	sand_geopark
#cylinder:	z	2.180	2.200	2.500	3.500	1.200	sand_geopark
#cylinder:	z	2.160	2.180	2.500	3.500	1.180	sand_geopark
#cylinder:	z	2.140	2.160	2.500	3.500	1.160	sand_geopark
#cylinder:	z	2.120	2.140	2.500	3.500	1.140	sand_geopark
#cylinder:	z	2.100	2.120	2.500	3.500	1.120	sand_geopark
#cylinder:	z	2.080	2.100	2.500	3.500	1.100	sand_geopark
#cylinder:	z	2.060	2.080	2.500	3.500	1.080	sand_geopark
#cylinder:	z	2.040	2.060	2.500	3.500	1.060	sand_geopark
#cylinder:	z	2.020	2.040	2.500	3.500	1.040	sand_geopark
#cylinder:	z	2.000	2.020	2.500	3.500	1.020	sand_geopark
#cylinder:	z	1.980	2.000	2.500	3.500	1.000	sand_geopark
#cylinder:	z	1.960	1.980	2.500	3.500	0.980	sand_geopark
#cylinder:	z	1.940	1.960	2.500	3.500	0.960	sand_geopark
#cylinder:	z	1.920	1.940	2.500	3.500	0.940	sand_geopark
#cylinder:	z	1.900	1.920	2.500	3.500	0.920	sand_geopark
#cylinder:	z	1.880	1.900	2.500	3.500	0.900	sand_geopark
#cylinder:	z	1.860	1.880	2.500	3.500	0.880	sand_geopark
#cylinder:	z	1.840	1.860	2.500	3.500	0.860	sand_geopark
#cylinder:	z	1.820	1.840	2.500	3.500	0.840	sand_geopark
#cylinder:	z	1.800	1.820	2.500	3.500	0.820	sand_geopark
#cylinder:	z	1.780	1.800	2.500	3.500	0.800	sand_geopark
#cylinder:	z	1.760	1.780	2.500	3.500	0.780	sand_geopark
#cylinder:	z	1.740	1.760	2.500	3.500	0.760	sand_geopark
#cylinder:	z	1.720	1.740	2.500	3.500	0.740	sand_geopark
#cylinder:	z	1.700	1.720	2.500	3.500	0.720	sand_geopark
#cylinder:	z	1.680	1.700	2.500	3.500	0.700	sand_geopark
#cylinder:	z	1.660	1.680	2.500	3.500	0.680	sand_geopark
#cylinder:	z	1.640	1.660	2.500	3.500	0.660	sand_geopark
#cylinder:	z	1.620	1.640	2.500	3.500	0.640	sand_geopark
#cylinder:	z	1.600	1.620	2.500	3.500	0.620	sand_geopark
#cylinder:	z	1.580	1.600	2.500	3.500	0.600	sand_geopark
#cylinder:	z	1.560	1.580	2.500	3.500	0.580	sand_geopark
#cylinder:	z	1.540	1.560	2.500	3.500	0.560	sand_geopark
#cylinder:	z	1.520	1.540	2.500	3.500	0.540	sand_geopark

Appendix A (Continued)

#cylinder:	z	1.500	1.520	2.500	3.500	0.520	sand_geopark
#cylinder:	z	1.480	1.500	2.500	3.500	0.500	sand_geopark
#cylinder:	z	1.460	1.480	2.500	3.500	0.480	sand_geopark
#cylinder:	z	1.440	1.460	2.500	3.500	0.460	sand_geopark
#cylinder:	z	1.420	1.440	2.500	3.500	0.440	sand_geopark
#cylinder:	z	1.400	1.420	2.500	3.500	0.420	sand_geopark
#cylinder:	z	1.380	1.400	2.500	3.500	0.400	sand_geopark
#cylinder:	z	1.360	1.380	2.500	3.500	0.380	sand_geopark
#cylinder:	z	1.340	1.360	2.500	3.500	0.360	sand_geopark
#cylinder:	z	1.320	1.340	2.500	3.500	0.340	sand_geopark
#cylinder:	z	1.300	1.320	2.500	3.500	0.320	sand_geopark
#cylinder:	z	1.280	1.300	2.500	3.500	0.300	sand_geopark
#cylinder:	z	1.260	1.280	2.500	3.500	0.280	sand_geopark
#cylinder:	z	1.240	1.260	2.500	3.500	0.260	sand_geopark
#cylinder:	z	1.220	1.240	2.500	3.500	0.240	sand_geopark
#cylinder:	z	1.200	1.220	2.500	3.500	0.220	sand_geopark
#cylinder:	z	1.180	1.200	2.500	3.500	0.200	sand_geopark
#cylinder:	z	1.160	1.180	2.500	3.500	0.180	sand_geopark
#cylinder:	z	1.140	1.160	2.500	3.500	0.160	sand_geopark
#cylinder:	z	1.120	1.140	2.500	3.500	0.140	sand_geopark
#cylinder:	z	1.100	1.120	2.500	3.500	0.120	sand_geopark
#cylinder:	z	1.080	1.100	2.500	3.500	0.100	sand_geopark
#cylinder:	z	1.060	1.080	2.500	3.500	0.080	sand_geopark
#cylinder:	z	1.040	1.060	2.500	3.500	0.060	sand_geopark
#cylinder:	z	1.020	1.040	2.500	3.500	0.040	sand_geopark
#cylinder:	z	1.000	1.020	2.500	3.500	0.020	sand_geopark

#cylinder:	z	1.480	1.500	2.500	3.500	0.500	sand_geopark
#cylinder:	z	1.460	1.480	2.500	3.500	0.490	sand_geopark
#cylinder:	z	1.440	1.460	2.500	3.500	0.480	sand_geopark
#cylinder:	z	1.420	1.440	2.500	3.500	0.470	sand_geopark
#cylinder:	z	1.400	1.420	2.500	3.500	0.460	sand_geopark
#cylinder:	z	1.380	1.400	2.500	3.500	0.450	sand_geopark
#cylinder:	z	1.360	1.380	2.500	3.500	0.440	sand_geopark
#cylinder:	z	1.340	1.360	2.500	3.500	0.430	sand_geopark
#cylinder:	z	1.320	1.340	2.500	3.500	0.420	sand_geopark
#cylinder:	z	1.300	1.320	2.500	3.500	0.410	sand_geopark
#cylinder:	z	1.280	1.300	2.500	3.500	0.400	sand_geopark
#cylinder:	z	1.260	1.280	2.500	3.500	0.390	sand_geopark
#cylinder:	z	1.240	1.260	2.500	3.500	0.380	sand_geopark

176

```
#cylinder:    z    1.220  1.240  2.500  3.500  0.370  sand_geopark
#cylinder:    z    1.200  1.220  2.500  3.500  0.360  sand_geopark
#cylinder:    z    1.180  1.200  2.500  3.500  0.350  sand_geopark
#cylinder:    z    1.160  1.180  2.500  3.500  0.340  sand_geopark
#cylinder:    z    1.140  1.160  2.500  3.500  0.330  sand_geopark
#cylinder:    z    1.120  1.140  2.500  3.500  0.320  sand_geopark
#cylinder:    z    1.100  1.120  2.500  3.500  0.310  sand_geopark
#cylinder:    z    1.080  1.100  2.500  3.500  0.300  sand_geopark
#cylinder:    z    1.060  1.080  2.500  3.500  0.290  sand_geopark
#cylinder:    z    1.040  1.060  2.500  3.500  0.280  sand_geopark
#cylinder:    z    1.020  1.040  2.500  3.500  0.270  sand_geopark
#cylinder:    z    1.000  1.020  2.500  3.500  0.260  sand_geopark
#cylinder:    z    0.980  1.000  2.500  3.500  0.250  sand_geopark
#cylinder:    z    0.960  0.980  2.500  3.500  0.240  sand_geopark
#cylinder:    z    0.940  0.960  2.500  3.500  0.230  sand_geopark
#cylinder:    z    0.920  0.940  2.500  3.500  0.220  sand_geopark
#cylinder:    z    0.900  0.920  2.500  3.500  0.210  sand_geopark
#cylinder:    z    0.880  0.900  2.500  3.500  0.200  sand_geopark
#cylinder:    z    0.860  0.880  2.500  3.500  0.190  sand_geopark
#cylinder:    z    0.840  0.860  2.500  3.500  0.180  sand_geopark
#cylinder:    z    0.820  0.840  2.500  3.500  0.170  sand_geopark
#cylinder:    z    0.800  0.820  2.500  3.500  0.160  sand_geopark
#cylinder:    z    0.780  0.800  2.500  3.500  0.150  sand_geopark
#cylinder:    z    0.760  0.780  2.500  3.500  0.140  sand_geopark
#cylinder:    z    0.740  0.760  2.500  3.500  0.130  sand_geopark
#cylinder:    z    0.720  0.740  2.500  3.500  0.120  sand_geopark
#cylinder:    z    0.700  0.720  2.500  3.500  0.110  sand_geopark
#cylinder:    z    0.680  0.700  2.500  3.500  0.100  sand_geopark
#cylinder:    z    0.660  0.680  2.500  3.500  0.090  sand_geopark
#cylinder:    z    0.640  0.660  2.500  3.500  0.080  sand_geopark
#cylinder:    z    0.620  0.640  2.500  3.500  0.070  sand_geopark
#cylinder:    z    0.600  0.620  2.500  3.500  0.060  sand_geopark
#cylinder:    z    0.580  0.600  2.500  3.500  0.050  sand_geopark
#cylinder:    z    0.560  0.580  2.500  3.500  0.040  sand_geopark
#cylinder:    z    0.540  0.560  2.500  3.500  0.030  sand_geopark
#cylinder:    z    0.520  0.540  2.500  3.500  0.020  sand_geopark
#cylinder:    z    0.500  0.520  2.500  3.500  0.010  sand_geopark
------------------------------------------------------------------------
#hertzian_dipole: 1.0 250e6 ricker MyDipole
#analysis: 145 geopark3_rxbox.out b
```

177

Appendix A (Continued)

```
#tx: x 2.5 1.1 4.0 MyDipole 0.0 120e-9
#rx_box: 0.1 1.1 4.0 4.9 6.9 4.0 0.1 0.1 0.1
#tx_steps: 0.0 0.05 0.0
#end_analysis:
-----------------------------------------------------------------------
#messages: y
#title: geopark 3 rxbox
#geometry_file: geopark3_rxbox.geo
-----------------------------------------------------------------------
```

Geopark 3D Model B rx_box off-axis GPRMAX input file

```
#medium: 9.0 0.0 0.0 0.005 1.0 0.0 sand_geopark
#medium: 25.0 0.0 0.0 0.05 1.0 0.0 clay_geopark
-----------------------------------------------------------------------
#domain: 5.0 7.0 4.5
#dx_dy_dz: 0.02 0.02 0.02
#time_window: 120e-9
-----------------------------------------------------------------------
#box: 0.0 0.0 0.0 5.0 7.0 3.0 clay_geopark
#box: 0.0 0.0 3.0 5.0 7.0 4.0 sand_geopark
#box: 0.0 0.0 4.0 5.0 7.0 4.5 free_space
-----------------------------------------------------------------------
#cylinder:    z    2.980  3.000  2.500  3.500  2.000  sand_geopark
#cylinder:    z    2.960  2.980  2.500  3.500  1.980  sand_geopark
#cylinder:    z    2.940  2.960  2.500  3.500  1.960  sand_geopark
#cylinder:    z    2.920  2.940  2.500  3.500  1.940  sand_geopark
#cylinder:    z    2.900  2.920  2.500  3.500  1.920  sand_geopark
#cylinder:    z    2.880  2.900  2.500  3.500  1.900  sand_geopark
#cylinder:    z    2.860  2.880  2.500  3.500  1.880  sand_geopark
#cylinder:    z    2.840  2.860  2.500  3.500  1.860  sand_geopark
#cylinder:    z    2.820  2.840  2.500  3.500  1.840  sand_geopark
#cylinder:    z    2.800  2.820  2.500  3.500  1.820  sand_geopark
#cylinder:    z    2.780  2.800  2.500  3.500  1.800  sand_geopark
#cylinder:    z    2.760  2.780  2.500  3.500  1.780  sand_geopark
#cylinder:    z    2.740  2.760  2.500  3.500  1.760  sand_geopark
#cylinder:    z    2.720  2.740  2.500  3.500  1.740  sand_geopark
#cylinder:    z    2.700  2.720  2.500  3.500  1.720  sand_geopark
#cylinder:    z    2.680  2.700  2.500  3.500  1.700  sand_geopark
#cylinder:    z    2.660  2.680  2.500  3.500  1.680  sand_geopark
```

178

Appendix A (Continued)

#cylinder:	z	2.640	2.660	2.500	3.500	1.660	sand_geopark
#cylinder:	z	2.620	2.640	2.500	3.500	1.640	sand_geopark
#cylinder:	z	2.600	2.620	2.500	3.500	1.620	sand_geopark
#cylinder:	z	2.580	2.600	2.500	3.500	1.600	sand_geopark
#cylinder:	z	2.560	2.580	2.500	3.500	1.580	sand_geopark
#cylinder:	z	2.540	2.560	2.500	3.500	1.560	sand_geopark
#cylinder:	z	2.520	2.540	2.500	3.500	1.540	sand_geopark
#cylinder:	z	2.500	2.520	2.500	3.500	1.520	sand_geopark
#cylinder:	z	2.480	2.500	2.500	3.500	1.500	sand_geopark
#cylinder:	z	2.460	2.480	2.500	3.500	1.480	sand_geopark
#cylinder:	z	2.440	2.460	2.500	3.500	1.460	sand_geopark
#cylinder:	z	2.420	2.440	2.500	3.500	1.440	sand_geopark
#cylinder:	z	2.400	2.420	2.500	3.500	1.420	sand_geopark
#cylinder:	z	2.380	2.400	2.500	3.500	1.400	sand_geopark
#cylinder:	z	2.360	2.380	2.500	3.500	1.380	sand_geopark
#cylinder:	z	2.340	2.360	2.500	3.500	1.360	sand_geopark
#cylinder:	z	2.320	2.340	2.500	3.500	1.340	sand_geopark
#cylinder:	z	2.300	2.320	2.500	3.500	1.320	sand_geopark
#cylinder:	z	2.280	2.300	2.500	3.500	1.300	sand_geopark
#cylinder:	z	2.260	2.280	2.500	3.500	1.280	sand_geopark
#cylinder:	z	2.240	2.260	2.500	3.500	1.260	sand_geopark
#cylinder:	z	2.220	2.240	2.500	3.500	1.240	sand_geopark
#cylinder:	z	2.200	2.220	2.500	3.500	1.220	sand_geopark
#cylinder:	z	2.180	2.200	2.500	3.500	1.200	sand_geopark
#cylinder:	z	2.160	2.180	2.500	3.500	1.180	sand_geopark
#cylinder:	z	2.140	2.160	2.500	3.500	1.160	sand_geopark
#cylinder:	z	2.120	2.140	2.500	3.500	1.140	sand_geopark
#cylinder:	z	2.100	2.120	2.500	3.500	1.120	sand_geopark
#cylinder:	z	2.080	2.100	2.500	3.500	1.100	sand_geopark
#cylinder:	z	2.060	2.080	2.500	3.500	1.080	sand_geopark
#cylinder:	z	2.040	2.060	2.500	3.500	1.060	sand_geopark
#cylinder:	z	2.020	2.040	2.500	3.500	1.040	sand_geopark
#cylinder:	z	2.000	2.020	2.500	3.500	1.020	sand_geopark
#cylinder:	z	1.980	2.000	2.500	3.500	1.000	sand_geopark
#cylinder:	z	1.960	1.980	2.500	3.500	0.980	sand_geopark
#cylinder:	z	1.940	1.960	2.500	3.500	0.960	sand_geopark
#cylinder:	z	1.920	1.940	2.500	3.500	0.940	sand_geopark
#cylinder:	z	1.900	1.920	2.500	3.500	0.920	sand_geopark
#cylinder:	z	1.880	1.900	2.500	3.500	0.900	sand_geopark
#cylinder:	z	1.860	1.880	2.500	3.500	0.880	sand_geopark

Appendix A (Continued)

#cylinder:	z	1.840	1.860	2.500	3.500	0.860	sand_geopark
#cylinder:	z	1.820	1.840	2.500	3.500	0.840	sand_geopark
#cylinder:	z	1.800	1.820	2.500	3.500	0.820	sand_geopark
#cylinder:	z	1.780	1.800	2.500	3.500	0.800	sand_geopark
#cylinder:	z	1.760	1.780	2.500	3.500	0.780	sand_geopark
#cylinder:	z	1.740	1.760	2.500	3.500	0.760	sand_geopark
#cylinder:	z	1.720	1.740	2.500	3.500	0.740	sand_geopark
#cylinder:	z	1.700	1.720	2.500	3.500	0.720	sand_geopark
#cylinder:	z	1.680	1.700	2.500	3.500	0.700	sand_geopark
#cylinder:	z	1.660	1.680	2.500	3.500	0.680	sand_geopark
#cylinder:	z	1.640	1.660	2.500	3.500	0.660	sand_geopark
#cylinder:	z	1.620	1.640	2.500	3.500	0.640	sand_geopark
#cylinder:	z	1.600	1.620	2.500	3.500	0.620	sand_geopark
#cylinder:	z	1.580	1.600	2.500	3.500	0.600	sand_geopark
#cylinder:	z	1.560	1.580	2.500	3.500	0.580	sand_geopark
#cylinder:	z	1.540	1.560	2.500	3.500	0.560	sand_geopark
#cylinder:	z	1.520	1.540	2.500	3.500	0.540	sand_geopark
#cylinder:	z	1.500	1.520	2.500	3.500	0.520	sand_geopark
#cylinder:	z	1.480	1.500	2.500	3.500	0.500	sand_geopark
#cylinder:	z	1.460	1.480	2.500	3.500	0.480	sand_geopark
#cylinder:	z	1.440	1.460	2.500	3.500	0.460	sand_geopark
#cylinder:	z	1.420	1.440	2.500	3.500	0.440	sand_geopark
#cylinder:	z	1.400	1.420	2.500	3.500	0.420	sand_geopark
#cylinder:	z	1.380	1.400	2.500	3.500	0.400	sand_geopark
#cylinder:	z	1.360	1.380	2.500	3.500	0.380	sand_geopark
#cylinder:	z	1.340	1.360	2.500	3.500	0.360	sand_geopark
#cylinder:	z	1.320	1.340	2.500	3.500	0.340	sand_geopark
#cylinder:	z	1.300	1.320	2.500	3.500	0.320	sand_geopark
#cylinder:	z	1.280	1.300	2.500	3.500	0.300	sand_geopark
#cylinder:	z	1.260	1.280	2.500	3.500	0.280	sand_geopark
#cylinder:	z	1.240	1.260	2.500	3.500	0.260	sand_geopark
#cylinder:	z	1.220	1.240	2.500	3.500	0.240	sand_geopark
#cylinder:	z	1.200	1.220	2.500	3.500	0.220	sand_geopark
#cylinder:	z	1.180	1.200	2.500	3.500	0.200	sand_geopark
#cylinder:	z	1.160	1.180	2.500	3.500	0.180	sand_geopark
#cylinder:	z	1.140	1.160	2.500	3.500	0.160	sand_geopark
#cylinder:	z	1.120	1.140	2.500	3.500	0.140	sand_geopark
#cylinder:	z	1.100	1.120	2.500	3.500	0.120	sand_geopark
#cylinder:	z	1.080	1.100	2.500	3.500	0.100	sand_geopark
#cylinder:	z	1.060	1.080	2.500	3.500	0.080	sand_geopark

180

Appendix A (Continued)

#cylinder:	z	1.040	1.060	2.500	3.500	0.060	sand_geopark
#cylinder:	z	1.020	1.040	2.500	3.500	0.040	sand_geopark
#cylinder:	z	1.000	1.020	2.500	3.500	0.020	sand_geopark

#cylinder:	z	1.480	1.500	2.500	3.500	0.500	sand_geopark
#cylinder:	z	1.460	1.480	2.500	3.500	0.490	sand_geopark
#cylinder:	z	1.440	1.460	2.500	3.500	0.480	sand_geopark
#cylinder:	z	1.420	1.440	2.500	3.500	0.470	sand_geopark
#cylinder:	z	1.400	1.420	2.500	3.500	0.460	sand_geopark
#cylinder:	z	1.380	1.400	2.500	3.500	0.450	sand_geopark
#cylinder:	z	1.360	1.380	2.500	3.500	0.440	sand_geopark
#cylinder:	z	1.340	1.360	2.500	3.500	0.430	sand_geopark
#cylinder:	z	1.320	1.340	2.500	3.500	0.420	sand_geopark
#cylinder:	z	1.300	1.320	2.500	3.500	0.410	sand_geopark
#cylinder:	z	1.280	1.300	2.500	3.500	0.400	sand_geopark
#cylinder:	z	1.260	1.280	2.500	3.500	0.390	sand_geopark
#cylinder:	z	1.240	1.260	2.500	3.500	0.380	sand_geopark
#cylinder:	z	1.220	1.240	2.500	3.500	0.370	sand_geopark
#cylinder:	z	1.200	1.220	2.500	3.500	0.360	sand_geopark
#cylinder:	z	1.180	1.200	2.500	3.500	0.350	sand_geopark
#cylinder:	z	1.160	1.180	2.500	3.500	0.340	sand_geopark
#cylinder:	z	1.140	1.160	2.500	3.500	0.330	sand_geopark
#cylinder:	z	1.120	1.140	2.500	3.500	0.320	sand_geopark
#cylinder:	z	1.100	1.120	2.500	3.500	0.310	sand_geopark
#cylinder:	z	1.080	1.100	2.500	3.500	0.300	sand_geopark
#cylinder:	z	1.060	1.080	2.500	3.500	0.290	sand_geopark
#cylinder:	z	1.040	1.060	2.500	3.500	0.280	sand_geopark
#cylinder:	z	1.020	1.040	2.500	3.500	0.270	sand_geopark
#cylinder:	z	1.000	1.020	2.500	3.500	0.260	sand_geopark
#cylinder:	z	0.980	1.000	2.500	3.500	0.250	sand_geopark
#cylinder:	z	0.960	0.980	2.500	3.500	0.240	sand_geopark
#cylinder:	z	0.940	0.960	2.500	3.500	0.230	sand_geopark
#cylinder:	z	0.920	0.940	2.500	3.500	0.220	sand_geopark
#cylinder:	z	0.900	0.920	2.500	3.500	0.210	sand_geopark
#cylinder:	z	0.880	0.900	2.500	3.500	0.200	sand_geopark
#cylinder:	z	0.860	0.880	2.500	3.500	0.190	sand_geopark
#cylinder:	z	0.840	0.860	2.500	3.500	0.180	sand_geopark
#cylinder:	z	0.820	0.840	2.500	3.500	0.170	sand_geopark
#cylinder:	z	0.800	0.820	2.500	3.500	0.160	sand_geopark
#cylinder:	z	0.780	0.800	2.500	3.500	0.150	sand_geopark

181

```
#cylinder:      z     0.760  0.780  2.500  3.500  0.140  sand_geopark
#cylinder:      z     0.740  0.760  2.500  3.500  0.130  sand_geopark
#cylinder:      z     0.720  0.740  2.500  3.500  0.120  sand_geopark
#cylinder:      z     0.700  0.720  2.500  3.500  0.110  sand_geopark
#cylinder:      z     0.680  0.700  2.500  3.500  0.100  sand_geopark
#cylinder:      z     0.660  0.680  2.500  3.500  0.090  sand_geopark
#cylinder:      z     0.640  0.660  2.500  3.500  0.080  sand_geopark
#cylinder:      z     0.620  0.640  2.500  3.500  0.070  sand_geopark
#cylinder:      z     0.600  0.620  2.500  3.500  0.060  sand_geopark
#cylinder:      z     0.580  0.600  2.500  3.500  0.050  sand_geopark
#cylinder:      z     0.560  0.580  2.500  3.500  0.040  sand_geopark
#cylinder:      z     0.540  0.560  2.500  3.500  0.030  sand_geopark
#cylinder:      z     0.520  0.540  2.500  3.500  0.020  sand_geopark
#cylinder:      z     0.500  0.520  2.500  3.500  0.010  sand_geopark
-----------------------------------------------------------------------
#hertzian_dipole: 1.0 250e6 ricker MyDipole
#analysis: 145 geopark5_rxbox.out b
#tx: x 2.8 1.1 4.0 MyDipole 0.0 120e-9
#rx_box: 0.1 1.1 4.0 4.9 6.9 4.0 0.1 0.1 0.1
#tx_steps: 0.0 0.05 0.0
#end_analysis:
-----------------------------------------------------------------------
#messages: y
#title: geopark 5 rxbox
#geometry_file: geopark3_rxbox.geo
-----------------------------------------------------------------------
```

Geopark 3D Model B snapshot GPRMAX input file

```
#medium: 9.0 0.0 0.0 0.005 1.0 0.0 sand_geopark
#medium: 25.0 0.0 0.0 0.05 1.0 0.0 clay_geopark
-----------------------------------------------------------------------
#domain: 8.0 8.0 4.5
#dx_dy_dz: 0.02 0.02 0.02
#time_window: 120e-9
-----------------------------------------------------------------------
#box: 0.0 0.0 0.0 8.0 8.0 3.0 clay_geopark
#box: 0.0 0.0 3.0 8.0 8.0 4.0 sand_geopark
#box: 0.0 0.0 4.0 8.0 8.0 4.5 free_space
```

182

Appendix A (Continued)

```
--------------------------------------------------------------------------
#cylinder: z 2.980 3.000 4.000 4.000 2.000 sand_geopark
#cylinder: z 2.960 2.980 4.000 4.000 1.980 sand_geopark
#cylinder: z 2.940 2.960 4.000 4.000 1.960 sand_geopark
#cylinder: z 2.920 2.940 4.000 4.000 1.940 sand_geopark
#cylinder: z 2.900 2.920 4.000 4.000 1.920 sand_geopark
#cylinder: z 2.880 2.900 4.000 4.000 1.900 sand_geopark
#cylinder: z 2.860 2.880 4.000 4.000 1.880 sand_geopark
#cylinder: z 2.840 2.860 4.000 4.000 1.860 sand_geopark
#cylinder: z 2.820 2.840 4.000 4.000 1.840 sand_geopark
#cylinder: z 2.800 2.820 4.000 4.000 1.820 sand_geopark
#cylinder: z 2.780 2.800 4.000 4.000 1.800 sand_geopark
#cylinder: z 2.760 2.780 4.000 4.000 1.780 sand_geopark
#cylinder: z 2.740 2.760 4.000 4.000 1.760 sand_geopark
#cylinder: z 2.720 2.740 4.000 4.000 1.740 sand_geopark
#cylinder: z 2.700 2.720 4.000 4.000 1.720 sand_geopark
#cylinder: z 2.680 2.700 4.000 4.000 1.700 sand_geopark
#cylinder: z 2.660 2.680 4.000 4.000 1.680 sand_geopark
#cylinder: z 2.640 2.660 4.000 4.000 1.660 sand_geopark
#cylinder: z 2.620 2.640 4.000 4.000 1.640 sand_geopark
#cylinder: z 2.600 2.620 4.000 4.000 1.620 sand_geopark
#cylinder: z 2.580 2.600 4.000 4.000 1.600 sand_geopark
#cylinder: z 2.560 2.580 4.000 4.000 1.580 sand_geopark
#cylinder: z 2.540 2.560 4.000 4.000 1.560 sand_geopark
#cylinder: z 2.520 2.540 4.000 4.000 1.540 sand_geopark
#cylinder: z 2.500 2.520 4.000 4.000 1.520 sand_geopark
#cylinder: z 2.480 2.500 4.000 4.000 1.500 sand_geopark
#cylinder: z 2.460 2.480 4.000 4.000 1.480 sand_geopark
#cylinder: z 2.440 2.460 4.000 4.000 1.460 sand_geopark
#cylinder: z 2.420 2.440 4.000 4.000 1.440 sand_geopark
#cylinder: z 2.400 2.420 4.000 4.000 1.420 sand_geopark
#cylinder: z 2.380 2.400 4.000 4.000 1.400 sand_geopark
#cylinder: z 2.360 2.380 4.000 4.000 1.380 sand_geopark
#cylinder: z 2.340 2.360 4.000 4.000 1.360 sand_geopark
#cylinder: z 2.320 2.340 4.000 4.000 1.340 sand_geopark
#cylinder: z 2.300 2.320 4.000 4.000 1.320 sand_geopark
#cylinder: z 2.280 2.300 4.000 4.000 1.300 sand_geopark
#cylinder: z 2.260 2.280 4.000 4.000 1.280 sand_geopark
#cylinder: z 2.240 2.260 4.000 4.000 1.260 sand_geopark
#cylinder: z 2.220 2.240 4.000 4.000 1.240 sand_geopark
```

```
#cylinder: z 2.200 2.220 4.000 4.000 1.220 sand_geopark
#cylinder: z 2.180 2.200 4.000 4.000 1.200 sand_geopark
#cylinder: z 2.160 2.180 4.000 4.000 1.180 sand_geopark
#cylinder: z 2.140 2.160 4.000 4.000 1.160 sand_geopark
#cylinder: z 2.120 2.140 4.000 4.000 1.140 sand_geopark
#cylinder: z 2.100 2.120 4.000 4.000 1.120 sand_geopark
#cylinder: z 2.080 2.100 4.000 4.000 1.100 sand_geopark
#cylinder: z 2.060 2.080 4.000 4.000 1.080 sand_geopark
#cylinder: z 2.040 2.060 4.000 4.000 1.060 sand_geopark
#cylinder: z 2.020 2.040 4.000 4.000 1.040 sand_geopark
#cylinder: z 2.000 2.020 4.000 4.000 1.020 sand_geopark
#cylinder: z 1.980 2.000 4.000 4.000 1.000 sand_geopark
#cylinder: z 1.960 1.980 4.000 4.000 0.980 sand_geopark
#cylinder: z 1.940 1.960 4.000 4.000 0.960 sand_geopark
#cylinder: z 1.920 1.940 4.000 4.000 0.940 sand_geopark
#cylinder: z 1.900 1.920 4.000 4.000 0.920 sand_geopark
#cylinder: z 1.880 1.900 4.000 4.000 0.900 sand_geopark
#cylinder: z 1.860 1.880 4.000 4.000 0.880 sand_geopark
#cylinder: z 1.840 1.860 4.000 4.000 0.860 sand_geopark
#cylinder: z 1.820 1.840 4.000 4.000 0.840 sand_geopark
#cylinder: z 1.800 1.820 4.000 4.000 0.820 sand_geopark
#cylinder: z 1.780 1.800 4.000 4.000 0.800 sand_geopark
#cylinder: z 1.760 1.780 4.000 4.000 0.780 sand_geopark
#cylinder: z 1.740 1.760 4.000 4.000 0.760 sand_geopark
#cylinder: z 1.720 1.740 4.000 4.000 0.740 sand_geopark
#cylinder: z 1.700 1.720 4.000 4.000 0.720 sand_geopark
#cylinder: z 1.680 1.700 4.000 4.000 0.700 sand_geopark
#cylinder: z 1.660 1.680 4.000 4.000 0.680 sand_geopark
#cylinder: z 1.640 1.660 4.000 4.000 0.660 sand_geopark
#cylinder: z 1.620 1.640 4.000 4.000 0.640 sand_geopark
#cylinder: z 1.600 1.620 4.000 4.000 0.620 sand_geopark
#cylinder: z 1.580 1.600 4.000 4.000 0.600 sand_geopark
#cylinder: z 1.560 1.580 4.000 4.000 0.580 sand_geopark
#cylinder: z 1.540 1.560 4.000 4.000 0.560 sand_geopark
#cylinder: z 1.520 1.540 4.000 4.000 0.540 sand_geopark
#cylinder: z 1.500 1.520 4.000 4.000 0.520 sand_geopark
#cylinder: z 1.480 1.500 4.000 4.000 0.500 sand_geopark
#cylinder: z 1.460 1.480 4.000 4.000 0.480 sand_geopark
#cylinder: z 1.440 1.460 4.000 4.000 0.460 sand_geopark
#cylinder: z 1.420 1.440 4.000 4.000 0.440 sand_geopark
```

#cylinder: z 1.400 1.420 4.000 4.000 0.420 sand_geopark
#cylinder: z 1.380 1.400 4.000 4.000 0.400 sand_geopark
#cylinder: z 1.360 1.380 4.000 4.000 0.380 sand_geopark
#cylinder: z 1.340 1.360 4.000 4.000 0.360 sand_geopark
#cylinder: z 1.320 1.340 4.000 4.000 0.340 sand_geopark
#cylinder: z 1.300 1.320 4.000 4.000 0.320 sand_geopark
#cylinder: z 1.280 1.300 4.000 4.000 0.300 sand_geopark
#cylinder: z 1.260 1.280 4.000 4.000 0.280 sand_geopark
#cylinder: z 1.240 1.260 4.000 4.000 0.260 sand_geopark
#cylinder: z 1.220 1.240 4.000 4.000 0.240 sand_geopark
#cylinder: z 1.200 1.220 4.000 4.000 0.220 sand_geopark
#cylinder: z 1.180 1.200 4.000 4.000 0.200 sand_geopark
#cylinder: z 1.160 1.180 4.000 4.000 0.180 sand_geopark
#cylinder: z 1.140 1.160 4.000 4.000 0.160 sand_geopark
#cylinder: z 1.120 1.140 4.000 4.000 0.140 sand_geopark
#cylinder: z 1.100 1.120 4.000 4.000 0.120 sand_geopark
#cylinder: z 1.080 1.100 4.000 4.000 0.100 sand_geopark
#cylinder: z 1.060 1.080 4.000 4.000 0.080 sand_geopark
#cylinder: z 1.040 1.060 4.000 4.000 0.060 sand_geopark
#cylinder: z 1.020 1.040 4.000 4.000 0.040 sand_geopark
#cylinder: z 1.000 1.020 4.000 4.000 0.020 sand_geopark

#cylinder: z 1.480 1.500 4.000 4.000 0.500 sand_geopark
#cylinder: z 1.460 1.480 4.000 4.000 0.490 sand_geopark
#cylinder: z 1.440 1.460 4.000 4.000 0.480 sand_geopark
#cylinder: z 1.420 1.440 4.000 4.000 0.470 sand_geopark
#cylinder: z 1.400 1.420 4.000 4.000 0.460 sand_geopark
#cylinder: z 1.380 1.400 4.000 4.000 0.450 sand_geopark
#cylinder: z 1.360 1.380 4.000 4.000 0.440 sand_geopark
#cylinder: z 1.340 1.360 4.000 4.000 0.430 sand_geopark
#cylinder: z 1.320 1.340 4.000 4.000 0.420 sand_geopark
#cylinder: z 1.300 1.320 4.000 4.000 0.410 sand_geopark
#cylinder: z 1.280 1.300 4.000 4.000 0.400 sand_geopark
#cylinder: z 1.260 1.280 4.000 4.000 0.390 sand_geopark
#cylinder: z 1.240 1.260 4.000 4.000 0.380 sand_geopark
#cylinder: z 1.220 1.240 4.000 4.000 0.370 sand_geopark
#cylinder: z 1.200 1.220 4.000 4.000 0.360 sand_geopark
#cylinder: z 1.180 1.200 4.000 4.000 0.350 sand_geopark
#cylinder: z 1.160 1.180 4.000 4.000 0.340 sand_geopark
#cylinder: z 1.140 1.160 4.000 4.000 0.330 sand_geopark

185

#cylinder: z 1.120 1.140 4.000 4.000 0.320 sand_geopark
#cylinder: z 1.100 1.120 4.000 4.000 0.310 sand_geopark
#cylinder: z 1.080 1.100 4.000 4.000 0.300 sand_geopark
#cylinder: z 1.060 1.080 4.000 4.000 0.290 sand_geopark
#cylinder: z 1.040 1.060 4.000 4.000 0.280 sand_geopark
#cylinder: z 1.020 1.040 4.000 4.000 0.270 sand_geopark
#cylinder: z 1.000 1.020 4.000 4.000 0.260 sand_geopark
#cylinder: z 0.980 1.000 4.000 4.000 0.250 sand_geopark
#cylinder: z 0.960 0.980 4.000 4.000 0.240 sand_geopark
#cylinder: z 0.940 0.960 4.000 4.000 0.230 sand_geopark
#cylinder: z 0.920 0.940 4.000 4.000 0.220 sand_geopark
#cylinder: z 0.900 0.920 4.000 4.000 0.210 sand_geopark
#cylinder: z 0.880 0.900 4.000 4.000 0.200 sand_geopark
#cylinder: z 0.860 0.880 4.000 4.000 0.190 sand_geopark
#cylinder: z 0.840 0.860 4.000 4.000 0.180 sand_geopark
#cylinder: z 0.820 0.840 4.000 4.000 0.170 sand_geopark
#cylinder: z 0.800 0.820 4.000 4.000 0.160 sand_geopark
#cylinder: z 0.780 0.800 4.000 4.000 0.150 sand_geopark
#cylinder: z 0.760 0.780 4.000 4.000 0.140 sand_geopark
#cylinder: z 0.740 0.760 4.000 4.000 0.130 sand_geopark
#cylinder: z 0.720 0.740 4.000 4.000 0.120 sand_geopark
#cylinder: z 0.700 0.720 4.000 4.000 0.110 sand_geopark
#cylinder: z 0.680 0.700 4.000 4.000 0.100 sand_geopark
#cylinder: z 0.660 0.680 4.000 4.000 0.090 sand_geopark
#cylinder: z 0.640 0.660 4.000 4.000 0.080 sand_geopark
#cylinder: z 0.620 0.640 4.000 4.000 0.070 sand_geopark
#cylinder: z 0.600 0.620 4.000 4.000 0.060 sand_geopark
#cylinder: z 0.580 0.600 4.000 4.000 0.050 sand_geopark
#cylinder: z 0.560 0.580 4.000 4.000 0.040 sand_geopark
#cylinder: z 0.540 0.560 4.000 4.000 0.030 sand_geopark
#cylinder: z 0.520 0.540 4.000 4.000 0.020 sand_geopark
#cylinder: z 0.500 0.520 4.000 4.000 0.010 sand_geopark

#hertzian_dipole: 1.0 250e6 ricker MyDipole
#analysis: 1 geopark3a_snap.out b
#tx: x 4.5 4.0 4.0 MyDipole 0.0 120e-9
#rx: 3.5 4.0 4.0

#snapshot: 1 0.0 0.0 0.0 8.0 8.0 4.5 0.02 0.02 0.02 5.0e-9 snap_gp3a_5.out b

Appendix A (Continued)

```
#snapshot: 1 0.0 0.0 0.0 8.0 8.0 4.5 0.02 0.02 0.02 10.0e-9 snap_gp3a_10.out b
#snapshot: 1 0.0 0.0 0.0 8.0 8.0 4.5 0.02 0.02 0.02 15.0e-9 snap_gp3a_15.out b
#snapshot: 1 0.0 0.0 0.0 8.0 8.0 4.5 0.02 0.02 0.02 20.0e-9 snap_gp3a_20.out b
#snapshot: 1 0.0 0.0 0.0 8.0 8.0 4.5 0.02 0.02 0.02 25.0e-9 snap_gp3a_25.out b
#snapshot: 1 0.0 0.0 0.0 8.0 8.0 4.5 0.02 0.02 0.02 30.0e-9 snap_gp3a_30.out b
#snapshot: 1 0.0 0.0 0.0 8.0 8.0 4.5 0.02 0.02 0.02 35.0e-9 snap_gp3a_35.out b
#snapshot: 1 0.0 0.0 0.0 8.0 8.0 4.5 0.02 0.02 0.02 40.0e-9 snap_gp3a_40.out b
#snapshot: 1 0.0 0.0 0.0 8.0 8.0 4.5 0.02 0.02 0.02 45.0e-9 snap_gp3a_45.out b
#snapshot: 1 0.0 0.0 0.0 8.0 8.0 4.5 0.02 0.02 0.02 50.0e-9 snap_gp3a_50.out b
#snapshot: 1 0.0 0.0 0.0 8.0 8.0 4.5 0.02 0.02 0.02 55.0e-9 snap_gp3a_55.out b
#snapshot: 1 0.0 0.0 0.0 8.0 8.0 4.5 0.02 0.02 0.02 60.0e-9 snap_gp3a_60.out b
#snapshot: 1 0.0 0.0 0.0 8.0 8.0 4.5 0.02 0.02 0.02 65.0e-9 snap_gp3a_65.out b
#snapshot: 1 0.0 0.0 0.0 8.0 8.0 4.5 0.02 0.02 0.02 70.0e-9 snap_gp3a_70.out b
#snapshot: 1 0.0 0.0 0.0 8.0 8.0 4.5 0.02 0.02 0.02 75.0e-9 snap_gp3a_75.out b
#snapshot: 1 0.0 0.0 0.0 8.0 8.0 4.5 0.02 0.02 0.02 80.0e-9 snap_gp3a_80.out b
#snapshot: 1 0.0 0.0 0.0 8.0 8.0 4.5 0.02 0.02 0.02 85.0e-9 snap_gp3a_85.out b
#snapshot: 1 0.0 0.0 0.0 8.0 8.0 4.5 0.02 0.02 0.02 90.0e-9 snap_gp3a_90.out b
#snapshot: 1 0.0 0.0 0.0 8.0 8.0 4.5 0.02 0.02 0.02 95.0e-9 snap_gp3a_95.out b
#snapshot: 1 0.0 0.0 0.0 8.0 8.0 4.5 0.02 0.02 0.02 100.0e-9 snap_gp3a_100.out b
#snapshot: 1 0.0 0.0 0.0 8.0 8.0 4.5 0.02 0.02 0.02 105.0e-9 snap_gp3a_105.out b
#snapshot: 1 0.0 0.0 0.0 8.0 8.0 4.5 0.02 0.02 0.02 110.0e-9 snap_gp3a_110.out b
#snapshot: 1 0.0 0.0 0.0 8.0 8.0 4.5 0.02 0.02 0.02 115.0e-9 snap_gp3a_115.out b
#snapshot: 1 0.0 0.0 0.0 8.0 8.0 4.5 0.02 0.02 0.02 120.0e-9 snap_gp3a_120.out b


------------------------------------------------------------------------------
#end_analysis:
-----------------------------------------------------------------------
#messages: y
#title: geopark 3a snapshot
#geometry_file: geopark3a.geo
-----------------------------------------------------------------------
```

Appendix B: MATLAB codes

```matlab
% plots the grid from the geopark3D model geometry file
% modified bgooch 3/2009

clear all; close all;
% note comments, restrictions below
%----------input parameters here-------------------------------------
--
 dyplot = 0.1; %spacing between x-z slices to plot
% dzplot = 0.1; %spacing between x-y slices to plot
%----------end input parameters--------------------------------------
--

[Mesh,ID,Header,Media]=gprmax3g('geopark3_rxbox.geo');
Header
size(Mesh)
%z is vertical
%Mesh = (x,y,z) in dimension

dx = Header(1).dx;
dy = Header(1).dy;
dz = Header(1).dz;
nx = Header(1).nx;
ny = Header(1).ny;
nz = Header(1).nz;



x=0:dx:(nx-1)*dx;
y=0:dy:(ny-1)*dy;
z=0:dz:(nz-1)*dz;

colormap(prism);
%!!! this assumes you won't have more than 5 different types of
material
colormin=1;
colormax=5;
clims = [colormin colormax];

%plot x-z (vertical) slices

yplot = 0:dyplot:max(y);
nyplot = length(yplot);
for jplot = 1:nyplot
    [temp jgrid]=min(abs(y-yplot(jplot)))
    i=1:nx; k=1:nz
```

188

Appendix B (Continued)

```matlab
    xzplane(i,k)=Mesh(i,jgrid,k);
    %need to flip so that z axis runs up image, increases with
increasing row
    xzplane = xzplane';
    figure;
    imagesc(x,z,xzplane,clims);
    %set imagesc so that vertical axis increases upwards
    axis xy;
    xlabel('x distance (m)'); ylabel('z distance (m)');
    title(['y = ' num2str(y(jgrid)) ' m']);
    daspect([1 1 1]);
    clear xzplane;
end


%plot x-y (horizontal) slices

zplot = 0:dzplot:max(z);
nzplot = length(zplot);
for kplot = 1:nzplot
    [temp kgrid]=min(abs(z-zplot(kplot)));
    i=1:nx; j=1:ny;
    xyplane(i,j)=Mesh(i,j,kgrid);
    %need to flip so that y axis runs up image, increases with
increasing row
    xyplane = xyplane';
    figure;
    imagesc(x,y,xyplane,clims);
    %set imagesc so that vertical axis increases upwards
    axis xy;
    xlabel('x distance (m)'); ylabel('y distance (m)');
    title(['z = ' num2str(z(kgrid)) ' m']);
    daspect([1 1 1]);
    clear xyplane;
end
```

```matlab
% plots the grid from the geopark2D model geometry file
% modified bgooch 3/2009

%------------enter input parameters here
filein = 'geopark3_2D.geo';
yground = 0.5;
%------------end input parameters


[Mesh,Header,Media]=gprmax2g(filein);
```

189

Appendix B (Continued)

```matlab
Header;
size(Mesh)
Mesh(:,200)
Media;


dx = Header(1).dx;
dy = Header(1).dy;



x=0:dx:(Header(1).nx-1)*dx;
y=-(Header(1).ny-1)*dy+yground:dy:yground;
colormap(jet);
imagesc(x,y,Mesh); axis xy
xlabel('distance(m)'); ylabel('depth (m)');
daspect([1 1 1]);
```

```matlab
% plot sum from every Rx of single TX for Rxbox models of GprMax
% bgooch 8/2009

% FIRST TIME THROUGH
clear all; close all;

%%%%%%%%%% INPUT first file name and select transmitter number here
%%%%%%%%%%%%%%
infile = 'geopark5_rxbox.out' ;
trans_num = 1 ;

%[Header,Fields]=gprmax_Exonly(infile);
[Header,Fields]=gprmax_Exonly_1tx_fast(infile,trans_num);

% print Header
Header

% convert time to ns
t=Fields(1).t*1.0e9;

% position for only 1 Tx converted from cell units to metrics
Tx_xposition = ( Header(1).tx * Header(1).dx ) + ( ( trans_num - 1 ) *
( Header(1).TxStepX * Header(1).dx ) ) ;

Tx_yposition = ( Header(1).ty * Header(1).dy ) + ( ( trans_num - 1 ) *
( Header(1).TxStepY * Header(1).dx ) ) ;
Tx_position = [ Tx_xposition , Tx_yposition ] ;
```

190

```matlab
% convert all Rx x and y positions from cell units to metrics
Rx_xpositions = Header(1).rx * Header(1).dx ;
Rx_ypositions = Header(1).ry * Header(1).dy ;

% % plot the Rx and Tx locations
% plot (Tx_xposition, Tx_yposition, 'x', Rx_xpositions, Rx_ypositions,
'o')
% axis equal tight

% extract Ex values and store in array
EX = Fields(1).ex  ;

% first time through save as #1
save gp5_tx1
```

```matlab
% plot sum from every Rx of single TX for Rxbox models of GprMax
% bgooch 8/2009

% FIRST TIME THROUGH
clear all; close all;

%%%%%%%%%% INPUT first file name and select transmitter number here
%%%%%%%%%%%%%%
infile = 'geopark1_rxbox.out' ;
trans_num = 1 ;

%[Header,Fields]=gprmax_Exonly(infile);
[Header,Fields]=gprmax_Ey_only_1tx_fast(infile,trans_num);

% print Header
Header

% convert time to ns
t=Fields(1).t*1.0e9;

% position for only 1 Tx converted from cell units to metrics

Tx_xposition = ( Header(1).tx * Header(1).dx ) + ( ( trans_num - 1 ) *
( Header(1).TxStepX * Header(1).dx ) ) ;
```

191

Appendix B (Continued)

```matlab
Tx_yposition = ( Header(1).ty * Header(1).dy ) + ( ( trans_num - 1 ) *
( Header(1).TxStepY * Header(1).dx ) ) ;
Tx_position = [ Tx_xposition , Tx_yposition ] ;

% convert all Rx x and y positions from cell units to metrics
Rx_xpositions = Header(1).rx * Header(1).dx ;
Rx_ypositions = Header(1).ry * Header(1).dy ;

% % plot the Rx and Tx locations
% plot (Tx_xposition, Tx_yposition, 'x', Rx_xpositions, Rx_ypositions,
'o')
% axis equal tight

% extract Ex values and store in array
EY = Fields(1).ey  ;

% first time through save as #1
save ey_gp1_tx1
```

```matlab
% plot GPRMax output for constant offset gather
% bgooch skruse 3/2009

clear all; close all;

infile = 'geopark3a.out';

offset = 1.8; % offset to plot in meters
ncrop = 5; % crop this many bad traces at start of record
crange = 0.1; % uses maximum range of color scale over this fraction of
data

[Header,Fields]=gprmax_Exonly(infile);
Header

%plot trace positions as midpoint between transmitter and receiver

%find which receiver corresponds to specified offset
noffset = round(offset/Header(1).dy);
 [xshift nrxplot] = min(abs((Header(1).ry-Header(1).ty(1))-noffset));
nrxplot
```

192

```matlab
offset = (Header(1).ry(nrxplot)-Header(1).ty(1))*Header(1).dy


trace_pos1 = (Header(1).ty(1)+Header(1).ry(nrxplot))/2*Header(1).dy;
trace_step = Header(1).RxStepY*Header(1).dy;
trace_position = trace_pos1:trace_step:trace_pos1+(Header(1).NSteps-
1)*trace_step;
t=Fields(1).t*1.0e9;
[nt nrec nstep]=size(Fields(1).ex)
Ex = zeros(nt,nstep);

% put into an array Ex that contains only traces for the specified
offset
it=1:nt;
iy=1:nstep;
Ex(it,iy)= Fields(1).ex(it,nrxplot,iy);


% crop out bad positions at beginning
for n=1:ncrop
    Ex(:,1)=[];
    trace_position(1) = [];
end

% plot
cmin = crange*min(min(Ex)); cmax = crange*max(max(Ex));
imagesc(trace_position,t,Ex);
caxis([cmin cmax]);
xlabel('distance (m)');
ylabel('time (ns)');
title(['offset = ' num2str(offset) ' m']);



% %plot a single trace
% figure;
% plotx = 4.0;
% [junk ix] = min(abs(nx-plotx));
% plot(t,Ex(:,ix));

%write out x min and x max for user to input into Reflex
trace_position(1)
trace_position(length(trace_position))
```

Appendix B (Continued)

```matlab
D = Ex'; %take transpose of array so that traces are rows, to match
format expected
          % expected for ASCII_MATRIX by Reflex

save geopark3a_ascii_180.txt D -ASCII;
```

```matlab
% plot GPRMax snapshot output
% bgooch skruse 8/2009

clear all; close all;
%-------INPUT PARAMETERS HERE----------------------------
infile = 'snap_gp3a_5.out'
xplot = 3.5;
yplot = 3.9;
zplot = 3.5;  %user must make sure these are inside grid
%-------END INPUT PARAMETERS HERE--------------------------

[Header,Fields]=gprmax(infile);
Header
[nx ny nz] = size(Fields(1).ex);

%assumes one corner of grid is at 0
y=0:Header(1).dy:(ny-1)*Header(1).dy;
x=0:Header(1).dx:(nx-1)*Header(1).dx;
z=0:Header(1).dz:(nz-1)*Header(1).dz;


[temp ixplot] = min(abs(x-xplot));
[temp iyplot] = min(abs(y-yplot));
[temp izplot] = min(abs(z-zplot));

%looks like fields are saved through the whole grid at the snaptime
% z = up direction, will plot differently
%direction of dipole source is not clear to me.

%if we want all 3 plots with same color scale, need to extract all
values,
%set axis limits, then plot

%get plane at ix = ixplot
Exx = zeros(ny,nz);
Exx(:,:) = Fields(1).ex(ixplot,:,:);
Exx = Exx';
```

194

Appendix B (Continued)

```matlab
minx = min(min(Exx)); maxx = max(max(Exx));

%get plane at iy = iyplot
Exy = zeros(nx,nz);
Exy(:,:) = Fields(1).ex(:,iyplot,:);
Exy = Exy';
miny = min(min(Exy)); maxy = max(max(Exy));

%get plane at iy = iyplot
Exz = zeros(nx,ny);
Exz(:,:) = Fields(1).ex(:,:,izplot);
Exz = Exz';
minz = min(min(Exz)); maxz = max(max(Exz));

minplot = min([minx miny minz]);
maxplot = max([maxx maxy maxz]);

% x plane plot
figure;
subplot(1,3,1)
imagesc(y,z,Exx); axis xy;
title(['Ex at x=' num2str(xplot) 'm']); xlabel('y'); ylabel('z');
daspect([1 1 1]);
%caxis([minplot maxplot]);
% print -djpeg -f1 -r300 snap_x_15.jpg

% y plane plot
figure;
subplot(1,3,2)
imagesc(x,z,Exy); axis xy;
title(['Ex at y=' num2str(yplot) 'm']); xlabel('x'); ylabel('z');
daspect([1 1 1]);
%caxis([minplot maxplot]);
% print -djpeg -f2 -r300 snap_y_15.jpg

% z plane plot
% figure;
% subplot(1,3,3)
hold on
imagesc(y,x,Exz); axis xy;

    R = 2;
    R1 = 0.5;
    Center = [ 4.0 , 4.0];
    circle(Center,R,1000,'k-');
    circle(Center,R1,1000,'k-');
```

195

Appendix B (Continued)

```matlab
    hold on
    plot(Center(1),Center(2),'k.')
    title(['Ex at z=' num2str(zplot) 'm']); xlabel('x'); ylabel('y');
    axis equal tight
    hold off


% daspect([1 1 1]);
%caxis([minplot maxplot]);
% print -djpeg -f3 -r300 snap_z_15.jpg

print -djpeg -r300 snap_5.jpg
```

```matlab
% plot difference between two Ex from Rxbox GprMax
% bgooch 8/2009

clear all; close all;

    load gp3_tx1 ; % name of second file
    EX2 = EX ;
    save EX2 EX2

clear all; close all;

% import saved EX matrices

    load gp1_tx1 ; % name of first file
    EX1 = EX ;
    save EX1

    load EX2 % reload

% crop larger matrix

%     for i=1:(length(EX2(:,1))-2597)
%
%         EX2(length(EX2(:,1)),:) = [] ;
%
%     end

    EX2 = EX2(1:2597,:) ; % much faster way!

% take difference of the two arrays
```

196

```matlab
    Ex_diff = abs( EX1 - EX2 ) ;

    Ex_sum = sum(Ex_diff) ;

% plotting the new matrix

    xlin = linspace(min(Rx_xpositions),max(Rx_xpositions));
    ylin = linspace(min(Rx_ypositions),max(Rx_ypositions));
    [X,Y] = meshgrid(xlin,ylin);
    Z = griddata(Rx_xpositions,Rx_ypositions,Ex_sum,X,Y,'cubic');

    hold on
    contourf(X,Y,Z);
    colorbar

    % sinkcenterx = 2.5;
    % sinkcentery = 4;
    % sinkrad = 2;
    % condrad = 1;
    hold on
    plot(Tx_xposition,Tx_yposition,'xk')
    % for i=1:360
    %     alpha = i/360*2*pi;
    %     xcircle(i) = sinkcenterx+cos(alpha)*sinkrad;
    %     ycircle(i) = sinkcentery+sin(alpha)*sinkrad;
    % end
    % plot(xcircle,ycircle,'k');

    % adds a plot of a circle of radius 2 and 0.5 to graph
    R = 2;
    R1 = 0.5;
    Center = [ 2.5 , 3.5];
    circle(Center,R,1000,'k-');
    circle(Center,R1,1000,'k-');
  hold on
    plot(Center(1),Center(2),'k.')
    axis equal tight
    hold off
    %axis([min(Rx_xpositions) max(Rx_xpositions) min(Rx_ypositions)
max(Rx_ypositions) min(Ex_sum) 50 min(Ex_sum) 50])

    % save jpeg image of graph

    print -djpeg -r300 Ex_diff_tx1.jpg
```

Appendix B (Continued)

```matlab
% plot difference between two Ey fields from Rxbox GprMax
% bgooch 8/2009

clear all; close all;

    load ey_gp3_tx1 ; % name of second file
    EY2 = EY ;
    save EY2 EY2

clear all; close all;

% import saved EY matrices

    load ey_gp1_tx1 ; % name of first file
    EY1 = EY ;
    save EY1

    load EY2 % reload

% crop larger matrix

%     for i=1:(length(EY2(:,1))-2597)
%
%         EY2(length(EY2(:,1)),:) = [] ;
%
%     end

    EY2 = EY2(1:2597,:) ; % much faster way!

% take difference of the two arrays

    Ey_diff = abs( EY1 - EY2 ) ;

    Ey_sum = sum(Ey_diff) ;

% plotting the new matrix

    xlin = linspace(min(Rx_xpositions),max(Rx_xpositions));
    ylin = linspace(min(Rx_ypositions),max(Rx_ypositions));
    [X,Y] = meshgrid(xlin,ylin);
    Z = griddata(Rx_xpositions,Rx_ypositions,Ey_sum,X,Y,'cubic');

    hold on
```

198

```
contourf(X,Y,Z);
colorbar

% sinkcenterx = 2.5;
% sinkcentery = 4;
% sinkrad = 2;
% condrad = 1;
hold on
plot(Tx_xposition,Tx_yposition,'xk')
% for i=1:360
%     alpha = i/360*2*pi;
%     xcircle(i) = sinkcenterx+cos(alpha)*sinkrad;
%     ycircle(i) = sinkcentery+sin(alpha)*sinkrad;
% end
% plot(xcircle,ycircle,'k');

% adds a plot of a circle of radius 2 and 0.5 to graph
R = 2;
R1 = 0.5;
Center = [ 2.5 , 3.5];
circle(Center,R,1000,'k-');
circle(Center,R1,1000,'k-');
hold on
plot(Center(1),Center(2),'k.')
axis equal tight
hold off
%axis([min(Rx_xpositions) max(Rx_xpositions) min(Rx_ypositions)
max(Rx_ypositions) min(Ex_sum) 50 min(Ex_sum) 50])

% save jpeg image of graph

print -djpeg -r300 Ey_diff_tx1.jpg
```

```
% plots shot gather from user-specified line in receiver field
% bgooch 8/2009

clear all; close all;

% load in a saved matlab workspace with extracted Ex info

  load gp1_tx1.mat

% select which profile along x-axis of rxbox to plot of 1.1-4.9 m
```

199

Appendix B (Continued)

```matlab
    profile_num = median(Rx_xpositions) ;

% extract selected profile from larger EX data

    start_col = round(59 * 10 * profile_num + 1) ;
    end_col   = start_col + 58 ;
    Ex = EX(:,start_col:end_col) ;

% plot the selected common shot gather

    y = Rx_ypositions(:,1:59) ;
    crange = 0.001 ; % uses maximum range of color scale over this
fraction of data
    cmin = crange * min( min(Ex) ) ;
    cmax = crange * max( max(Ex) ) ;
    imagesc( y, t, Ex ) ;
    caxis( [cmin cmax] ) ;
    xlabel('distance (m)');
    ylabel('time (ns)');
    title(['x = ' num2str(profile_num) ' m']);
    colorbar


    % save jpeg image of graph

    print -djpeg -r300 shot_gather_gp1_tx1.jpg
```

```matlab
% plots shot gather from user-specified line in receiver field
% bgooch 8/2009

clear all; close all;

% load in a saved matlab workspace with extracted Ex info

  load ey_gp1_tx1.mat

% select which profile along x-axis of rxbox to plot of 1.1-4.9 m

    profile_num = median(Rx_xpositions) ;

% extract selected profile from larger EX data
```

200

```matlab
    start_col = round(59 * 10 * profile_num + 1) ;
    end_col   = start_col + 58 ;
    Ey = EY(:,start_col:end_col) ;

% plot the selected common shot gather

    y = Rx_ypositions(:,1:59) ;
    crange = 0.001 ; % uses maximum range of color scale over this
fraction of data
    cmin = crange * min( min(Ey) ) ;
    cmax = crange * max( max(Ey) ) ;
    imagesc( y, t, Ey ) ;
    caxis( [cmin cmax] ) ;
    xlabel('distance (m)');
    ylabel('time (ns)');
    title(['x = ' num2str(profile_num) ' m']);
    colorbar


    % save jpeg image of graph

    print -djpeg -r300 EY_shot_gather_gp1_tx1.jpg
```

```matlab
% plot the difference between two Ex shot gathers
% bgooch 8/2009

clear all; close all;
%-----------------------load data-----------------------------------
--
    load gp3_tx1 ; % name of second file
    EX2 = EX ;
    save EX2 EX2

clear all; close all;

% import saved EX matrices

    load gp1_tx1 ; % name of first file
    EX1 = EX ;
    save EX1
```

201

Appendix B (Continued)

```
    load EX2 % reload

%----------------crop larger matrix-----------------------------------
--
    EX2 = EX2(1:2597,:) ; % much faster way!

% select which profile along x-axis of rxbox to plot of 1.1-4.9 m

    profile_num = median(Rx_xpositions) ;

% extract selected profile from larger EX data

    start_col = round(59 * 10 * profile_num + 1) ;
    end_col   = start_col + 58 ;
    Ex1 = EX1(:,start_col:end_col) ;
    Ex2 = EX2(:,start_col:end_col) ;



%------------------------take difference-------------------------------
----

    Ex_diff = ( Ex1 - Ex2 ) ;

%------------------ plot the selected common shot gather-------------
----

    y = Rx_ypositions(:,1:59) ;
    crange = 0.001 ; % uses maximum range of color scale over this
fraction of data
    cmin = crange * min( min(Ex_diff) ) ;
    cmax = crange * max( max(Ex_diff) ) ;
    imagesc( y, t, Ex_diff ) ;
    caxis( [cmin cmax] ) ;
    xlabel('distance (m)');
    ylabel('time (ns)');
    title(['x = ' num2str(profile_num) ' m']);
    colorbar


    % save jpeg image of graph

    print -djpeg -r300 diff_shot_gather_tx1.jpg
```

202

Appendix B (Continued)

```matlab
% plot the difference between two Ey shot gathers
% bgooch 8/2009

clear all; close all;
%-----------------------load data------------------------------------
--
    load ey_gp3_tx1 ; % name of second file
    EY2 = EY ;
    save EY2 EY2

clear all; close all;

% import saved EY matrices

    load ey_gp1_tx1 ; % name of first file
    EY1 = EY ;
    save EY1

    load EY2 % reload


%----------------crop larger matrix----------------------------------
--
    EY2 = EY2(1:2597,:) ; % much faster way!

% select which profile along x-axis of rxbox to plot of 1.1-4.9 m

    profile_num = median(Rx_xpositions) ;

% extract selected profile from larger EX data

    start_col = round(59 * 10 * profile_num + 1) ;
    end_col  = start_col + 58 ;
    Ey1 = EY1(:,start_col:end_col) ;
    Ey2 = EY2(:,start_col:end_col) ;


%------------------------take difference------------------------------
----

    Ey_diff = ( Ey1 - Ey2 ) ;

%-------------------- plot the selected common shot gather------------
----
```

203

Appendix B (Continued)

```matlab
    y = Rx_ypositions(:,1:59) ;
    crange = 0.001 ; % uses maximum range of color scale over this
fraction of data
    cmin = crange * min( min(Ey_diff) ) ;
    cmax = crange * max( max(Ey_diff) ) ;
    imagesc( y, t, Ey_diff ) ;
    caxis( [cmin cmax] ) ;
    xlabel('distance (m)');
    ylabel('time (ns)');
    title(['x = ' num2str(profile_num) ' m']);
    colorbar


    % save jpeg image of graph

    print -djpeg -r300 EY_diff_shot_gather_tx1.jpg
```

```matlab
function [Header,Fields]=gprmax_Exonly_1tx_fast(name,trans_num)


% GPRMAX3D   Read binary data generated by 'GprMax3D' and 'GprMax2D'
%            simulators for ground probing radar.
%
%            [Header, Fields] = gprmax( 'filename' )
%            filename is the name of a binary format file generated
either
%            from 'GprMax3D' or 'GprMax2D'
%
%            Header is a structure containing details of the model
%
%            Fields is a structure containing the electromagnetic fields
at
%                   the requested output points for a number of
requested
%                   steps
%
%
%            (NOTE: The field matrices of snapshots cary 3D data
%            Copyright: Antonis Giannopoulos, 1997, 2002, 2005
%            This file is not part of the 'GprMax3D' programme for
ground probing
%            radar simulation and can be freely distributed.
```

204

Appendix B (Continued)

```matlab
%  MODIFIED March 2009 Sarah Kruse to only store Ex to save memory
space
%  modification only valid for 3D step mode




FT_3D=30200;
FT_2D=20200;
SMALL=0;
BIG=0;
if(nargin==0)
error('GprMax3D requires at least one argument');
end;

if(nargin==1)
type='native';
end;

if(isstr(name)~=1)
error('First argument is not a filename');
end;

fid=fopen(name,'rb');
if(fid==-1)
error(['Can not open =',name]);
end;



ECHECK1=fread(fid,1,'char');
if(strcmp(setstr(dec2hex(ECHECK1)),'2B')==1 )
 SMALL=0;
 BIG=1;
end;
if(strcmp(setstr(dec2hex(ECHECK1)),'67')==1 )
 SMALL=1;
 BIG=0;
end;
ECHECK2=fread(fid,1,'char');
if(BIG==1)
 if(strcmp(setstr(dec2hex(ECHECK2)),'67') == 0)
 error(['This is not a GprMax2D/3D file.']);
 end;
end;
if(SMALL==1)
 if(strcmp(setstr(dec2hex(ECHECK2)),'2B') == 0)
```

205

```matlab
 error(['This is not a GprMax2D/3D file.']);
 end;
end;
% If you are here you have a valid file. Unless someone is playing a
but joke !!
% Close and open again to make sure you will read it properly.
fclose(fid);
if(SMALL==1)
fid=fopen(name,'rb','ieee-le');
end;
if(BIG==1)
fid=fopen(name,'rb','ieee-be');
end;
% Read Endian again but no check !
temp=fread(fid,1,'short');
% Read type of file
FileType=fread(fid,1,'short');
SWORD=fread(fid,1,'short');
SREAL=fread(fid,1,'short');
TITLELENGTH=fread(fid,1,'short');
SOURCELENGTH=fread(fid,1,'short');
MEDIALENGTH=fread(fid,1,'short');
RESERVED=fread(fid,2,'char');
if(SWORD==2)
 word='short';
end;
if(SWORD==4)
 word='long';
end;
if(SREAL==4)
 real='float';
end;
if(SREAL==8)
 real='double';
end;

% Set Defaults for all
Model=struct([]);
Rx=struct([]);

% Set title to none
%Model(1).title='No title';




switch FileType
```

206

www.manaraa.com

```matlab
case FT_2D+4 % 2D snapshot
    disp(['Reading GprMax2D #snapshot: file ...',name]);
    Model(1).title=fread(fid,TITLELENGTH,'char');
    Model(1).title=setstr(Model(1).title');
    Model(1).iterations=fread(fid,1,real);
    Model(1).dx=fread(fid,1,real);
    Model(1).dy=fread(fid,1,real);
    Model(1).dt=fread(fid,1,real);
    Model(1).globalTx=fread(fid,1,word);
    Model(1).Snapx1=fread(fid,1,word);
    Model(1).Snapy1=fread(fid,1,word);
    Model(1).Snapx2=fread(fid,1,word);
    Model(1).Snapy2=fread(fid,1,word);
    Model(1).Snapxs=fread(fid,1,word);
 Model(1).Snapys=fread(fid,1,word);
    stime=fread(fid,1,real);
    Model(1).snaptime=stime*Model(1).dt/1e-9;
    Model(1).Snapxsam=fread(fid,1,word);
    Model(1).Snapysam=fread(fid,1,word);

    Rx(1).ez=zeros(Model(1).Snapxsam,Model(1).Snapysam);
    Rx(1).hx=zeros(Model(1).Snapxsam,Model(1).Snapysam);
    Rx(1).hy=zeros(Model(1).Snapxsam,Model(1).Snapysam);




    Rx(1).ez=fread(fid,[Model(1).Snapxsam Model(1).Snapysam],real);

    Rx(1).hx=fread(fid,[Model(1).Snapxsam Model(1).Snapysam],real);

    Rx(1).hy=fread(fid,[Model(1).Snapxsam Model(1).Snapysam],real);




case FT_3D+4 % 3D snapshot
    disp(['Reading GprMax3D #snapshot: file ...',name]);
    Model(1).title=fread(fid,TITLELENGTH,'char');
    Model(1).title=setstr(Model(1).title');
    Model(1).iterations=fread(fid,1,real);
    Model(1).dx=fread(fid,1,real);
    Model(1).dy=fread(fid,1,real);
    Model(1).dz=fread(fid,1,real);
    Model(1).dt=fread(fid,1,real);
    Model(1).globalTx=fread(fid,1,word);
```

207

```
         Model(1).Snapx1=fread(fid,1,word);
         Model(1).Snapy1=fread(fid,1,word);
         Model(1).Snapz1=fread(fid,1,word);
         Model(1).Snapx2=fread(fid,1,word);
         Model(1).Snapy2=fread(fid,1,word);
         Model(1).Snapz2=fread(fid,1,word);
         Model(1).Snapxs=fread(fid,1,word);
         Model(1).Snapys=fread(fid,1,word);
         Model(1).Snapzs=fread(fid,1,word);
         stime=fread(fid,1,real);
         Model(1).snaptime=stime*Model(1).dt/1e-9;
         Model(1).Snapxsam=fread(fid,1,word);
         Model(1).Snapysam=fread(fid,1,word);

       Model(1).Snapzsam=fread(fid,1,word);


Rx(1).ex=zeros(Model(1).Snapxsam,Model(1).Snapysam,Model(1).Snapzsam);

Rx(1).ey=zeros(Model(1).Snapxsam,Model(1).Snapysam,Model(1).Snapzsam);

Rx(1).ez=zeros(Model(1).Snapxsam,Model(1).Snapysam,Model(1).Snapzsam);

Rx(1).hx=zeros(Model(1).Snapxsam,Model(1).Snapysam,Model(1).Snapzsam);

Rx(1).hy=zeros(Model(1).Snapxsam,Model(1).Snapysam,Model(1).Snapzsam);

Rx(1).hz=zeros(Model(1).Snapxsam,Model(1).Snapysam,Model(1).Snapzsam);

Rx(1).ix=zeros(Model(1).Snapxsam,Model(1).Snapysam,Model(1).Snapzsam);

Rx(1).iy=zeros(Model(1).Snapxsam,Model(1).Snapysam,Model(1).Snapzsam);

Rx(1).iz=zeros(Model(1).Snapxsam,Model(1).Snapysam,Model(1).Snapzsam);

        for i=1:Model(1).Snapxsam
            temp=fread(fid,[Model(1).Snapzsam Model(1).Snapysam],real);
            Rx(1).ex(i,:,:)=temp';
        end

        for i=1:Model(1).Snapxsam
            temp=fread(fid,[Model(1).Snapzsam Model(1).Snapysam],real);
            Rx(1).ey(i,:,:)=temp';
        end
        for i=1:Model(1).Snapxsam
            temp=fread(fid,[Model(1).Snapzsam Model(1).Snapysam],real);
            Rx(1).ez(i,:,:)=temp';
```

```matlab
            end

    for i=1:Model(1).Snapxsam
        temp=fread(fid,[Model(1).Snapzsam Model(1).Snapysam],real);
        Rx(1).hx(i,:,:)=temp';
    end

    for i=1:Model(1).Snapxsam
        temp=fread(fid,[Model(1).Snapzsam Model(1).Snapysam],real);
        Rx(1).hy(i,:,:)=temp';
    end
    for i=1:Model(1).Snapxsam

  temp=fread(fid,[Model(1).Snapzsam Model(1).Snapysam],real);
        Rx(1).hz(i,:,:)=temp';
    end
    for i=1:Model(1).Snapxsam
        temp=fread(fid,[Model(1).Snapzsam Model(1).Snapysam],real);
        Rx(1).ix(i,:,:)=temp';
    end
    for i=1:Model(1).Snapxsam
        temp=fread(fid,[Model(1).Snapzsam Model(1).Snapysam],real);
        Rx(1).iy(i,:,:)=temp';
    end
    for i=1:Model(1).Snapxsam
        temp=fread(fid,[Model(1).Snapzsam Model(1).Snapysam],real);
        Rx(1).iz(i,:,:)=temp';
    end



case FT_2D % 2D step
    disp(['Reading GprMax2D #analysis: file ...',name]);
    Model(1).title=fread(fid,TITLELENGTH,'char');
    Model(1).title=setstr(Model(1).title');
    Model(1).iterations=fread(fid,1,real);
    Model(1).dx=fread(fid,1,real);
    Model(1).dy=fread(fid,1,real);
    Model(1).dt=fread(fid,1,real);
    Model(1).NSteps=fread(fid,1,word);
    Model(1).TxStepX=fread(fid,1,word);
    Model(1).TxStepY=fread(fid,1,word);
    Model(1).RxStepX=fread(fid,1,word);
    Model(1).RxStepY=fread(fid,1,word);
    Model(1).ntx=fread(fid,1,word);
    Model(1).nrx=fread(fid,1,word);
    Model(1).nrx_box=fread(fid,1,word);
```

209

Appendix B (Continued)

```matlab
        for i=1:Model(1).ntx
            Model(1).tx(i)=fread(fid,1,word);
            Model(1).ty(i)=fread(fid,1,word);

Model(1).source(i,1:SOURCELENGTH)=fread(fid,SOURCELENGTH,'char')';
            Model(1).delay(i)=fread(fid,1,real);
            Model(1).removed(i)=fread(fid,1,real);
        end
        Model(1).source=char(Model(1).source);
        for i=1:Model(1).nrx


  Model(1).rx(i)=fread(fid,1,word);
            Model(1).ry(i)=fread(fid,1,word);

        end
        TotalOuts=Model(1).nrx;
        kk=Model(1).nrx;
        for i=1:Model(1).nrx_box
            Model(1).rx_box(i).nouts=fread(fid,1,word);
            TotalOuts=TotalOuts+Model(1).rx_box(i).nouts;
            for k=kk+1:kk+Model(1).rx_box(i).nouts
                Model(1).rx(k)=fread(fid,1,word);
                Model(1).ry(k)=fread(fid,1,word);
            end
            kk=kk+Model(1).rx_box(i).nouts;

        end

        Rx(1).t=(0:Model(1).iterations-1)'*Model(1).dt;

        %Read the data in single vector for speed

        F=fread(fid,inf,real);

        % Short out data in (Outputs,Iterations,Steps)



ez=reshape(F(1:3:end),TotalOuts,Model(1).iterations,Model(1).NSteps);

hx=reshape(F(2:3:end),TotalOuts,Model(1).iterations,Model(1).NSteps);

hy=reshape(F(3:3:end),TotalOuts,Model(1).iterations,Model(1).NSteps);
```

210

```matlab
        % Save the data in (Iterations,Outputs,Steps) format
        if Model(1).NSteps == 1
            Rx(1).ez=ez';
            Rx(1).hx=hx';
            Rx(1).hy=hy';

        else
            for i=1:TotalOuts
                Rx(1).ez(:,i,:)=ez(i,:,:);
                Rx(1).hx(:,i,:)=hx(i,:,:);
                Rx(1).hy(:,i,:)=hy(i,:,:);
            end
        end



    case FT_3D % 3D step
        disp(['Reading GprMax3D #analysis: file ...',name]);
        Model(1).title=fread(fid,TITLELENGTH,'char');
        Model(1).title=setstr(Model(1).title');
        Model(1).iterations=fread(fid,1,real);
        Model(1).dx=fread(fid,1,real);
        Model(1).dy=fread(fid,1,real);
        Model(1).dz=fread(fid,1,real);
        Model(1).dt=fread(fid,1,real);
        Model(1).NSteps=fread(fid,1,word);
        Model(1).TxStepX=fread(fid,1,word);
        Model(1).TxStepY=fread(fid,1,word);
        Model(1).TxStepZ=fread(fid,1,word);
        Model(1).RxStepX=fread(fid,1,word);
        Model(1).RxStepY=fread(fid,1,word);
        Model(1).RxStepZ=fread(fid,1,word);
        Model(1).ntx=fread(fid,1,word);
        Model(1).nrx=fread(fid,1,word);
        Model(1).nrx_box=fread(fid,1,word);
        for i=1:Model(1).ntx
            Model(1).polarization(i,:)=fread(fid,1,'char');

Model(1).polarization(i,:)=char(setstr(Model(1).polarization(i,:)'));
            Model(1).tx(i)=fread(fid,1,word);
            Model(1).ty(i)=fread(fid,1,word);
            Model(1).tz(i)=fread(fid,1,word);
```

211

```matlab
Model(1).source(i,1:SOURCELENGTH)=fread(fid,SOURCELENGTH,'char');
            Model(1).delay(i)=fread(fid,1,real);
            Model(1).removed(i)=fread(fid,1,real);
        end
        Model(1).source=char(Model(1).source);
        for i=1:Model(1).nrx
            Model(1).rx(i)=fread(fid,1,word);
            Model(1).ry(i)=fread(fid,1,word);
            Model(1).rz(i)=fread(fid,1,word);
        End

        TotalOuts=Model(1).nrx;
        kk=Model(1).nrx;
        for i=1:Model(1).nrx_box
            Model(1).rx_box(i).nouts=fread(fid,1,word);
            TotalOuts=TotalOuts+Model(1).rx_box(i).nouts;
            for k=kk+1:kk+Model(1).rx_box(i).nouts
                Model(1).rx(k)=fread(fid,1,word);
                Model(1).ry(k)=fread(fid,1,word);
                Model(1).rz(k)=fread(fid,1,word);
            end
            kk=kk+Model(1).rx_box(i).nouts;

        end



        Rx(1).t=(0:Model(1).iterations-1)'*Model(1).dt;

        %Read the data in single vector for speed
        % Impractical for large files with memory limitations in
Windows



%         F=fread(fid,inf,real);
%
%
%         % Short out data in (Outputs,Iterations,Steps)
%
%
ex=reshape(F(1:9:end),TotalOuts,Model(1).iterations,Model(1).NSteps);
%
ey=reshape(F(2:9:end),TotalOuts,Model(1).iterations,Model(1).NSteps);
%
ez=reshape(F(3:9:end),TotalOuts,Model(1).iterations,Model(1).NSteps);
```

212

Appendix B (Continued)

```
%
hx=reshape(F(4:9:end),TotalOuts,Model(1).iterations,Model(1).NSteps);
%
hy=reshape(F(5:9:end),TotalOuts,Model(1).iterations,Model(1).NSteps);
%
hz=reshape(F(6:9:end),TotalOuts,Model(1).iterations,Model(1).NSteps);
%
ix=reshape(F(7:9:end),TotalOuts,Model(1).iterations,Model(1).NSteps);
%
iy=reshape(F(8:9:end),TotalOuts,Model(1).iterations,Model(1).NSteps);
%
iz=reshape(F(9:9:end),TotalOuts,Model(1).iterations,Model(1).NSteps);
%
%          % Save the data in (Iterations,Outputs,Steps) format
%        if Model(1).NSteps == 1
%             Rx(1).ex=ex';
%             Rx(1).ey=ey';
%             Rx(1).ez=ez';
%             Rx(1).hx=hx';
%             Rx(1).hy=hy';
%             Rx(1).hz=hz';
%             Rx(1).ix=ix';
%             Rx(1).iy=iy';
%             Rx(1).iz=iz';
%        else
%             for i=1:TotalOuts
%                 Rx(1).ex(:,i,:)=ex(i,:,:);
%                 Rx(1).ey(:,i,:)=ey(i,:,:);
%                 Rx(1).ez(:,i,:)=ez(i,:,:);
%                 Rx(1).hx(:,i,:)=hx(i,:,:);
%                 Rx(1).hy(:,i,:)=hy(i,:,:);
%                 Rx(1).hz(:,i,:)=hz(i,:,:);
%                 Rx(1).ix(:,i,:)=ix(i,:,:);
%                 Rx(1).iy(:,i,:)=iy(i,:,:);
%                 Rx(1).iz(:,i,:)=iz(i,:,:);
%             end
%        end


% That is a rather slower way to read data !!!

tic
    %---skipping over results from all transmitters before ntrans------
---------
    for i = 1:trans_num-1  % number of transmitter for which we are
writing out receiver results
```

213

```matlab
        for j=1:Model(1).iterations
            disp(['Reading Iteration # ',num2str(j),' of
',num2str(Model(1).iterations), ' Iterations, on Transmitter #: ',
num2str(i), ' of ', num2str(trans_num)]);
            for k=1:Model(1).nrx
                temp=fread(fid,9,real); % skipping over receivers
listed in nrx
            end;
            kk=Model(1).nrx;
            for p=1:Model(1).nrx_box % skipping over receiver listed in
nrx_boxes
%                 disp(['Reading rx_box # ',num2str(p),' of
',num2str(Model(1).nrx_box),' rx_box']);
                for k=kk+1:kk+Model(1).rx_box(p).nouts
                    temp=fread(fid,9,real);
                end
                kk=kk+Model(1).rx_box(p).nouts;
            end
        end
    end
toc
    %-------------------------end skip-----------------------------
------
tic
    %---------store data for transmitter ntrans--------------------
----
    for j=1:Model(1).iterations
        disp(['Reading Iteration # ',num2str(j),' of
',num2str(Model(1).iterations), ' Iterations, for Transmitter #: ',
num2str(trans_num)]);
        for k=1:Model(1).nrx
            Rx(1).ex(j,k,1)=fread(fid,1,real);
            temp=fread(fid,8,real); % skip over non Ex information
        end;
        kk=Model(1).nrx;
        for p=1:Model(1).nrx_box
%                 disp(['Reading rx_box # ',num2str(p),' of
',num2str(Model(1).nrx_box),' rx_box']);
            for k=kk+1:kk+Model(1).rx_box(p).nouts
                Rx(1).ex(j,k,1)=fread(fid,1,real);
                temp=fread(fid,8,real); % skip over non Ex information
            end
            kk=kk+Model(1).rx_box(p).nouts;
        end
    end
toc
```

214

```matlab
    case FT_3D+5
        disp(['This is not a data file. It is a geometry file']);
        disp(['Use GPRMAX3G.']);

    case FT_2D+5
        disp(['This is not a data file. It is a geometry file']);

        disp(['Use GPRMAX2G.']);

    otherwise
        disp(['This is not a valid GprMax2D/3D Ver 2.0 data file.']);
        disp(['It may be an older version data file']);
end

Header=Model;
Fields=Rx;

%close file
fclose(fid);
```

```matlab
function [Header,Fields]=gprmax_Ey_only_1tx_fast(name,trans_num)

% GPRMAX3D  Read binary data generated by 'GprMax3D' and 'GprMax2D'
%           simulators for ground probing radar.
%
%           [Header, Fields] = gprmax( 'filename' )
%           filename is the name of a binary format file generated
either
%           from 'GprMax3D' or 'GprMax2D'
%
%           Header is a structure containing details of the model
%
%           Fields is a structure containing the electromagnetic fields
at
%                   the requested output points for a number of
requested
%                   steps
%
%
%           (NOTE: The field matrices of snapshots cary 3D data
%           Copyright: Antonis Giannopoulos, 1997, 2002, 2005
%           This file is not part of the 'GprMax3D' programme for
ground probing
```

215

```
%          radar simulation and can be freely distributed.

%  MODIFIED August 2009 Brad Gooch to only store Ey to save memory
space
%  modification only valid for 3D step mode



FT_3D=30200;
FT_2D=20200;
SMALL=0;
BIG=0;
if(nargin==0)
error('GprMax3D requires at least one argument');
end;

if(nargin==1)
type='native';
end;

if(isstr(name)~=1)
error('First argument is not a filename');
end;

fid=fopen(name,'rb');
if(fid==-1)
error(['Can not open =',name]);
end;


ECHECK1=fread(fid,1,'char');
if(strcmp(setstr(dec2hex(ECHECK1)),'2B')==1 )
 SMALL=0;
 BIG=1;
end;
if(strcmp(setstr(dec2hex(ECHECK1)),'67')==1 )
 SMALL=1;
 BIG=0;
end;
ECHECK2=fread(fid,1,'char');
if(BIG==1)
 if(strcmp(setstr(dec2hex(ECHECK2)),'67') == 0)
 error(['This is not a GprMax2D/3D file.']);
 end;
end;
if(SMALL==1)
```

216

```matlab
 if(strcmp(setstr(dec2hex(ECHECK2)),'2B') == 0)
 error(['This is not a GprMax2D/3D file.']);
 end;
end;
% If you are here you have a valid file. Unless someone is playing a
but joke !!
% Close and open again to make sure you will read it properly.
fclose(fid);
if(SMALL==1)
fid=fopen(name,'rb','ieee-le');
end;
if(BIG==1)
fid=fopen(name,'rb','ieee-be');
end;
% Read Endian again but no check !
temp=fread(fid,1,'short');
% Read type of file
FileType=fread(fid,1,'short');
SWORD=fread(fid,1,'short');
SREAL=fread(fid,1,'short');
TITLELENGTH=fread(fid,1,'short');
SOURCELENGTH=fread(fid,1,'short');
MEDIALENGTH=fread(fid,1,'short');
RESERVED=fread(fid,2,'char');
if(SWORD==2)
 word='short';
end;
if(SWORD==4)
 word='long';
end;
if(SREAL==4)
 real='float';
end;
if(SREAL==8)
 real='double';
end;

% Set Defaults for all
Model=struct([]);
Rx=struct([]);

% Set title to none
%Model(1).title='No title';
```

217

```matlab
switch FileType

    case FT_2D+4 % 2D snapshot
        disp(['Reading GprMax2D #snapshot: file ...',name]);
        Model(1).title=fread(fid,TITLELENGTH,'char');
        Model(1).title=setstr(Model(1).title');
      Model(1).iterations=fread(fid,1,real);
        Model(1).dx=fread(fid,1,real);
        Model(1).dy=fread(fid,1,real);
        Model(1).dt=fread(fid,1,real);
        Model(1).globalTx=fread(fid,1,word);
        Model(1).Snapx1=fread(fid,1,word);
        Model(1).Snapy1=fread(fid,1,word);
        Model(1).Snapx2=fread(fid,1,word);
        Model(1).Snapy2=fread(fid,1,word);
        Model(1).Snapxs=fread(fid,1,word);
        Model(1).Snapys=fread(fid,1,word);
        stime=fread(fid,1,real);
        Model(1).snaptime=stime*Model(1).dt/1e-9;
        Model(1).Snapxsam=fread(fid,1,word);
        Model(1).Snapysam=fread(fid,1,word);

        Rx(1).ez=zeros(Model(1).Snapxsam,Model(1).Snapysam);
        Rx(1).hx=zeros(Model(1).Snapxsam,Model(1).Snapysam);
        Rx(1).hy=zeros(Model(1).Snapxsam,Model(1).Snapysam);



        Rx(1).ez=fread(fid,[Model(1).Snapxsam Model(1).Snapysam],real);

        Rx(1).hx=fread(fid,[Model(1).Snapxsam Model(1).Snapysam],real);

        Rx(1).hy=fread(fid,[Model(1).Snapxsam Model(1).Snapysam],real);




    case FT_3D+4 % 3D snapshot
        disp(['Reading GprMax3D #snapshot: file ...',name]);
        Model(1).title=fread(fid,TITLELENGTH,'char');
        Model(1).title=setstr(Model(1).title');
        Model(1).iterations=fread(fid,1,real);
        Model(1).dx=fread(fid,1,real);
        Model(1).dy=fread(fid,1,real);
        Model(1).dz=fread(fid,1,real);
        Model(1).dt=fread(fid,1,real);
```

Appendix B (Continued)

```matlab
        Model(1).globalTx=fread(fid,1,word);
        Model(1).Snapx1=fread(fid,1,word);
        Model(1).Snapy1=fread(fid,1,word);
        Model(1).Snapz1=fread(fid,1,word);
        Model(1).Snapx2=fread(fid,1,word);
        Model(1).Snapy2=fread(fid,1,word);
        Model(1).Snapz2=fread(fid,1,word);
        Model(1).Snapxs=fread(fid,1,word);
        Model(1).Snapys=fread(fid,1,word);
        Model(1).Snapzs=fread(fid,1,word);
        stime=fread(fid,1,real);
        Model(1).snaptime=stime*Model(1).dt/1e-9;
        Model(1).Snapxsam=fread(fid,1,word);
        Model(1).Snapysam=fread(fid,1,word);
        Model(1).Snapzsam=fread(fid,1,word);


Rx(1).ex=zeros(Model(1).Snapxsam,Model(1).Snapysam,Model(1).Snapzsam);

Rx(1).ey=zeros(Model(1).Snapxsam,Model(1).Snapysam,Model(1).Snapzsam);

Rx(1).ez=zeros(Model(1).Snapxsam,Model(1).Snapysam,Model(1).Snapzsam);

Rx(1).hx=zeros(Model(1).Snapxsam,Model(1).Snapysam,Model(1).Snapzsam);

Rx(1).hy=zeros(Model(1).Snapxsam,Model(1).Snapysam,Model(1).Snapzsam);

Rx(1).hz=zeros(Model(1).Snapxsam,Model(1).Snapysam,Model(1).Snapzsam);

Rx(1).ix=zeros(Model(1).Snapxsam,Model(1).Snapysam,Model(1).Snapzsam);

Rx(1).iy=zeros(Model(1).Snapxsam,Model(1).Snapysam,Model(1).Snapzsam);

Rx(1).iz=zeros(Model(1).Snapxsam,Model(1).Snapysam,Model(1).Snapzsam);

        for i=1:Model(1).Snapxsam
            temp=fread(fid,[Model(1).Snapzsam Model(1).Snapysam],real);
            Rx(1).ex(i,:,:)=temp';
        end

        for i=1:Model(1).Snapxsam
            temp=fread(fid,[Model(1).Snapzsam Model(1).Snapysam],real);
            Rx(1).ey(i,:,:)=temp';
        end
        for i=1:Model(1).Snapxsam
            temp=fread(fid,[Model(1).Snapzsam Model(1).Snapysam],real);
            Rx(1).ez(i,:,:)=temp';
```

219

```matlab
        end

        for i=1:Model(1).Snapxsam
            temp=fread(fid,[Model(1).Snapzsam Model(1).Snapysam],real);
          Rx(1).hx(i,:,:)=temp';
        end

        for i=1:Model(1).Snapxsam
            temp=fread(fid,[Model(1).Snapzsam Model(1).Snapysam],real);
            Rx(1).hy(i,:,:)=temp';
        end
        for i=1:Model(1).Snapxsam
            temp=fread(fid,[Model(1).Snapzsam Model(1).Snapysam],real);
            Rx(1).hz(i,:,:)=temp';
        end
        for i=1:Model(1).Snapxsam
            temp=fread(fid,[Model(1).Snapzsam Model(1).Snapysam],real);
            Rx(1).ix(i,:,:)=temp';
        end
        for i=1:Model(1).Snapxsam
            temp=fread(fid,[Model(1).Snapzsam Model(1).Snapysam],real);
            Rx(1).iy(i,:,:)=temp';
        end
        for i=1:Model(1).Snapxsam
            temp=fread(fid,[Model(1).Snapzsam Model(1).Snapysam],real);
            Rx(1).iz(i,:,:)=temp';
        end



    case FT_2D % 2D step
        disp(['Reading GprMax2D #analysis: file ...',name]);
        Model(1).title=fread(fid,TITLELENGTH,'char');
        Model(1).title=setstr(Model(1).title');
        Model(1).iterations=fread(fid,1,real);
        Model(1).dx=fread(fid,1,real);
        Model(1).dy=fread(fid,1,real);
        Model(1).dt=fread(fid,1,real);
        Model(1).NSteps=fread(fid,1,word);
        Model(1).TxStepX=fread(fid,1,word);
        Model(1).TxStepY=fread(fid,1,word);
        Model(1).RxStepX=fread(fid,1,word);
        Model(1).RxStepY=fread(fid,1,word);
        Model(1).ntx=fread(fid,1,word);
        Model(1).nrx=fread(fid,1,word);
        Model(1).nrx_box=fread(fid,1,word);
        for i=1:Model(1).ntx
```

220

```matlab
        Model(1).tx(i)=fread(fid,1,word);
        Model(1).ty(i)=fread(fid,1,word);

Model(1).source(i,1:SOURCELENGTH)=fread(fid,SOURCELENGTH,'char')';
        Model(1).delay(i)=fread(fid,1,real);
        Model(1).removed(i)=fread(fid,1,real);
    end
    Model(1).source=char(Model(1).source);
    for i=1:Model(1).nrx

        Model(1).rx(i)=fread(fid,1,word);
        Model(1).ry(i)=fread(fid,1,word);

    end
    TotalOuts=Model(1).nrx;
    kk=Model(1).nrx;
    for i=1:Model(1).nrx_box
        Model(1).rx_box(i).nouts=fread(fid,1,word);
        TotalOuts=TotalOuts+Model(1).rx_box(i).nouts;
        for k=kk+1:kk+Model(1).rx_box(i).nouts
            Model(1).rx(k)=fread(fid,1,word);
            Model(1).ry(k)=fread(fid,1,word);
        end
        kk=kk+Model(1).rx_box(i).nouts;

    end

    Rx(1).t=(0:Model(1).iterations-1)'*Model(1).dt;

    %Read the data in single vector for speed

    F=fread(fid,inf,real);

    % Short out data in (Outputs,Iterations,Steps)


ez=reshape(F(1:3:end),TotalOuts,Model(1).iterations,Model(1).NSteps);

hx=reshape(F(2:3:end),TotalOuts,Model(1).iterations,Model(1).NSteps);

hy=reshape(F(3:3:end),TotalOuts,Model(1).iterations,Model(1).NSteps);
```

221

```matlab
        % Save the data in (Iterations,Outputs,Steps) format
     if Model(1).NSteps == 1
            Rx(1).ez=ez';
            Rx(1).hx=hx';
            Rx(1).hy=hy';

        else
            for i=1:TotalOuts
                Rx(1).ez(:,i,:)=ez(i,:,:);
                Rx(1).hx(:,i,:)=hx(i,:,:);
                Rx(1).hy(:,i,:)=hy(i,:,:);
            end
        end



    case FT_3D % 3D step
        disp(['Reading GprMax3D #analysis: file ...',name]);
        Model(1).title=fread(fid,TITLELENGTH,'char');
        Model(1).title=setstr(Model(1).title');
        Model(1).iterations=fread(fid,1,real);
        Model(1).dx=fread(fid,1,real);
        Model(1).dy=fread(fid,1,real);
        Model(1).dz=fread(fid,1,real);
        Model(1).dt=fread(fid,1,real);
        Model(1).NSteps=fread(fid,1,word);
        Model(1).TxStepX=fread(fid,1,word);
        Model(1).TxStepY=fread(fid,1,word);
        Model(1).TxStepZ=fread(fid,1,word);
        Model(1).RxStepX=fread(fid,1,word);
        Model(1).RxStepY=fread(fid,1,word);
        Model(1).RxStepZ=fread(fid,1,word);
        Model(1).ntx=fread(fid,1,word);
        Model(1).nrx=fread(fid,1,word);
        Model(1).nrx_box=fread(fid,1,word);
        for i=1:Model(1).ntx
            Model(1).polarization(i,:)=fread(fid,1,'char');

Model(1).polarization(i,:)=char(setstr(Model(1).polarization(i,:)'));
            Model(1).tx(i)=fread(fid,1,word);
            Model(1).ty(i)=fread(fid,1,word);
            Model(1).tz(i)=fread(fid,1,word);

Model(1).source(i,1:SOURCELENGTH)=fread(fid,SOURCELENGTH,'char');
            Model(1).delay(i)=fread(fid,1,real);
```

222

```matlab
                Model(1).removed(i)=fread(fid,1,real);
            end
        Model(1).source=char(Model(1).source);
        for i=1:Model(1).nrx
            Model(1).rx(i)=fread(fid,1,word);
            Model(1).ry(i)=fread(fid,1,word);
            Model(1).rz(i)=fread(fid,1,word);
        end
        TotalOuts=Model(1).nrx;
        kk=Model(1).nrx;
        for i=1:Model(1).nrx_box
            Model(1).rx_box(i).nouts=fread(fid,1,word);
            TotalOuts=TotalOuts+Model(1).rx_box(i).nouts;
            for k=kk+1:kk+Model(1).rx_box(i).nouts
                Model(1).rx(k)=fread(fid,1,word);
                Model(1).ry(k)=fread(fid,1,word);
                Model(1).rz(k)=fread(fid,1,word);
            end
            kk=kk+Model(1).rx_box(i).nouts;

        end




        Rx(1).t=(0:Model(1).iterations-1)'*Model(1).dt;

        %Read the data in single vector for speed
        % Impractical for large files with memory limitations in
Windows



%          F=fread(fid,inf,real);
%
%
%          % Short out data in (Outputs,Iterations,Steps)
%
%
ex=reshape(F(1:9:end),TotalOuts,Model(1).iterations,Model(1).NSteps);
%
ey=reshape(F(2:9:end),TotalOuts,Model(1).iterations,Model(1).NSteps);
%
ez=reshape(F(3:9:end),TotalOuts,Model(1).iterations,Model(1).NSteps);
%
hx=reshape(F(4:9:end),TotalOuts,Model(1).iterations,Model(1).NSteps);
%
hy=reshape(F(5:9:end),TotalOuts,Model(1).iterations,Model(1).NSteps);
```

223

Appendix B (Continued)

```
%
hz=reshape(F(6:9:end),TotalOuts,Model(1).iterations,Model(1).NSteps);
%
ix=reshape(F(7:9:end),TotalOuts,Model(1).iterations,Model(1).NSteps);
%
iy=reshape(F(8:9:end),TotalOuts,Model(1).iterations,Model(1).NSteps);
%
iz=reshape(F(9:9:end),TotalOuts,Model(1).iterations,Model(1).NSteps);
%
%            % Save the data in (Iterations,Outputs,Steps) format
%          if Model(1).NSteps == 1
%               Rx(1).ex=ex';
%               Rx(1).ey=ey';
%               Rx(1).ez=ez';
%               Rx(1).hx=hx';
%               Rx(1).hy=hy';
%               Rx(1).hz=hz';
%               Rx(1).ix=ix';
%               Rx(1).iy=iy';
%               Rx(1).iz=iz';
%          else
%              for i=1:TotalOuts
%                  Rx(1).ex(:,i,:)=ex(i,:,:);
%                  Rx(1).ey(:,i,:)=ey(i,:,:);
%                  Rx(1).ez(:,i,:)=ez(i,:,:);
%                  Rx(1).hx(:,i,:)=hx(i,:,:);
%                  Rx(1).hy(:,i,:)=hy(i,:,:);
%                  Rx(1).hz(:,i,:)=hz(i,:,:);
%                  Rx(1).ix(:,i,:)=ix(i,:,:);
%                  Rx(1).iy(:,i,:)=iy(i,:,:);
%                  Rx(1).iz(:,i,:)=iz(i,:,:);
%              end
%          end



% That is a rather slower way to read data !!!

tic
    %---skipping over results from all transmitters before ntrans------
---------
    for i = 1:trans_num-1  % number of transmitter for which we are
writing out receiver results
        for j=1:Model(1).iterations
```

224

```matlab
            disp(['Reading Iteration # ',num2str(j),' of
',num2str(Model(1).iterations), ' Iterations, on Transmitter #: ',
num2str(i), ' of ', num2str(trans_num)]);
            for k=1:Model(1).nrx
                temp=fread(fid,9,real); % skipping over receivers
listed in nrx
            end;
            kk=Model(1).nrx;
            for p=1:Model(1).nrx_box % skipping over receiver listed in
nrx_boxes
%                  disp(['Reading rx_box # ',num2str(p),' of
',num2str(Model(1).nrx_box),' rx_box']);
                for k=kk+1:kk+Model(1).rx_box(p).nouts
                    temp=fread(fid,9,real);
                end
                kk=kk+Model(1).rx_box(p).nouts;
            end
        end
    end
toc
    %---------------------------end skip-----------------------------
------
tic
    %----------store data for transmitter ntrans--------------------
----
    for j=1:Model(1).iterations
        disp(['Reading Iteration # ',num2str(j),' of
',num2str(Model(1).iterations), ' Iterations, for Transmitter #: ',
num2str(trans_num)]);
        for k=1:Model(1).nrx
            temp=fread(fid,1,real); % skip over non Ey information
            Rx(1).ey(j,k,1)=fread(fid,1,real);
            temp=fread(fid,7,real); % skip over non Ey information
        end;
        kk=Model(1).nrx;
        for p=1:Model(1).nrx_box
%                  disp(['Reading rx_box # ',num2str(p),' of
',num2str(Model(1).nrx_box),' rx_box']);
            for k=kk+1:kk+Model(1).rx_box(p).nouts
                temp=fread(fid,1,real); % skip over non Ey information
                Rx(1).ey(j,k,1)=fread(fid,1,real);
                temp=fread(fid,7,real); % skip over non Ey information
            end
            kk=kk+Model(1).rx_box(p).nouts;
        end
    end
toc
```

225

```matlab
    case FT_3D+5
        disp(['This is not a data file. It is a geometry file']);
        disp(['Use GPRMAX3G.']);

    case FT_2D+5
        disp(['This is not a data file. It is a geometry file']);
        disp(['Use GPRMAX2G.']);

    otherwise
        disp(['This is not a valid GprMax2D/3D Ver 2.0 data file.']);
        disp(['It may be an older version data file']);
end

Header=Model;
Fields=Rx;

%close file
fclose(fid);
```

226

Appendix C. Common Shot Gather Analysis

Since the rx_box command allows each receiver to record information for each individual transmitter location, it can be used to construct what is known as a common-shot gather or wide-angle reflection and refraction (WARR) survey (Reynolds, 1997; Burger et al, 2006). In this survey, a single transmitting source at a fixed location broadcasts an energy pulse while another receiver records at a set distance away. The receiver is then moved farther out at a fixed distance along the profile line for each transmission. If many receivers can be used at the same time, it is possible to lay them all out in a line and record with fewer moving transmission pulses (this known as a normal move-out survey). The information contained in the rx_box model results can be used to configure this survey type. The survey can also be viewed with receiving antennae positions the same as the transmitter (Ex) or perpendicular to it (Ey). These surveys were constructed for both Model A and B across the center line of the model (same as in previous section). Sample common-shot gather records for both Ex and Ey information of the two models may be viewed in Figures C.1-14.

These results do not suggest any other detailed structure than the common-shot gather survey results did in Chapter 2. A basic depression in the subsurface is visible but not the actual conduit structure itself. The differences between the common-shot gather results of the two models appear very similar, which makes comparison analysis more difficult. A routine (similar to that used in the previous rx_box analysis) to subtract the first 100 ns of both Model A and B's records made it easier to observe the subtle differences. These difference plots may be seen in Figures C.15-21. The difference plots

227

Appendix C (Continued)

add very little to the analysis, if any at all. In fact, the time records for both models are

identical until about 50-70 ns where a wave that is different begins to arrive and after that

there is a great deal of noise. Unfortunately, the difference shown is not enough to justify

locating conduit structure from modeling efforts.

228

Figure C.1a

x = 2.5 m

Figure C.1b

x = 2.5 m

229

www.manaraa.com
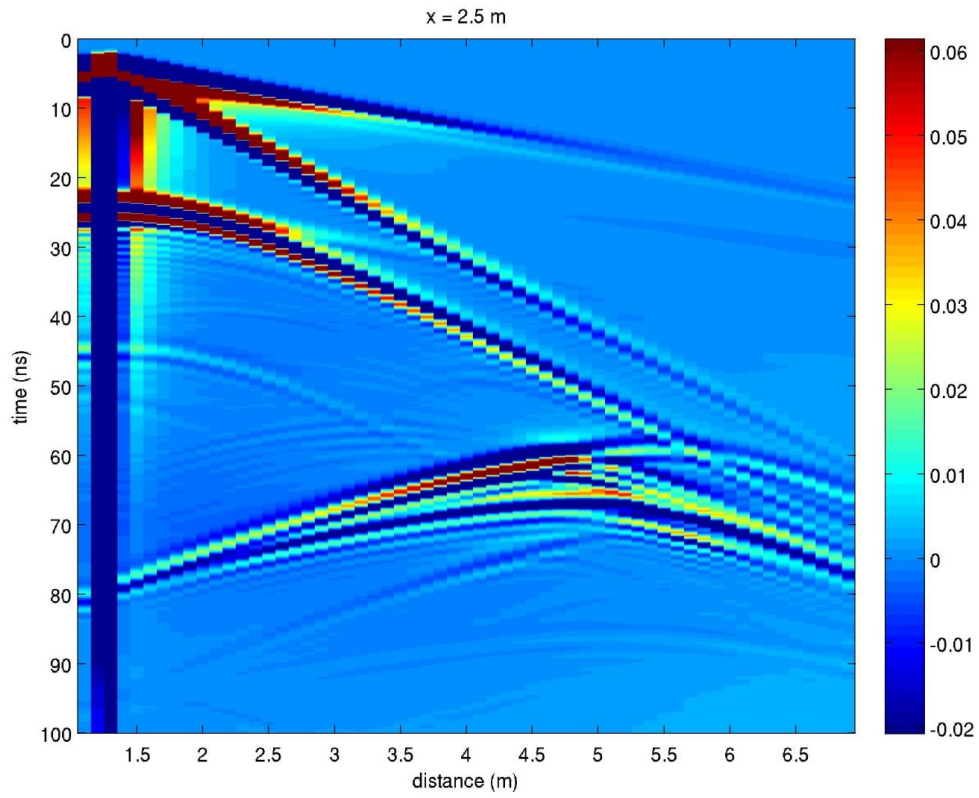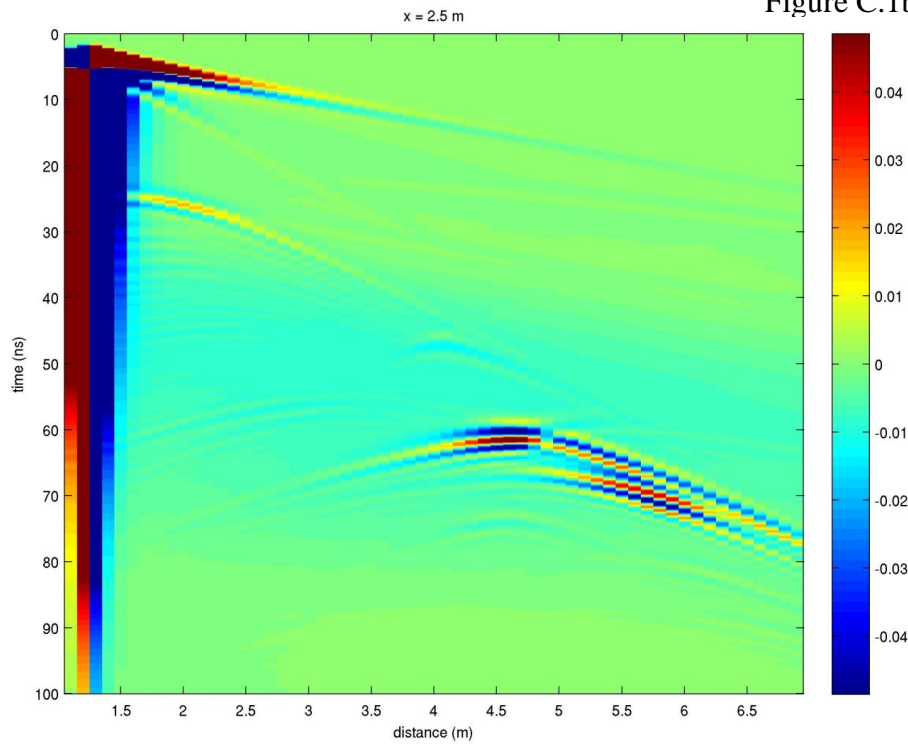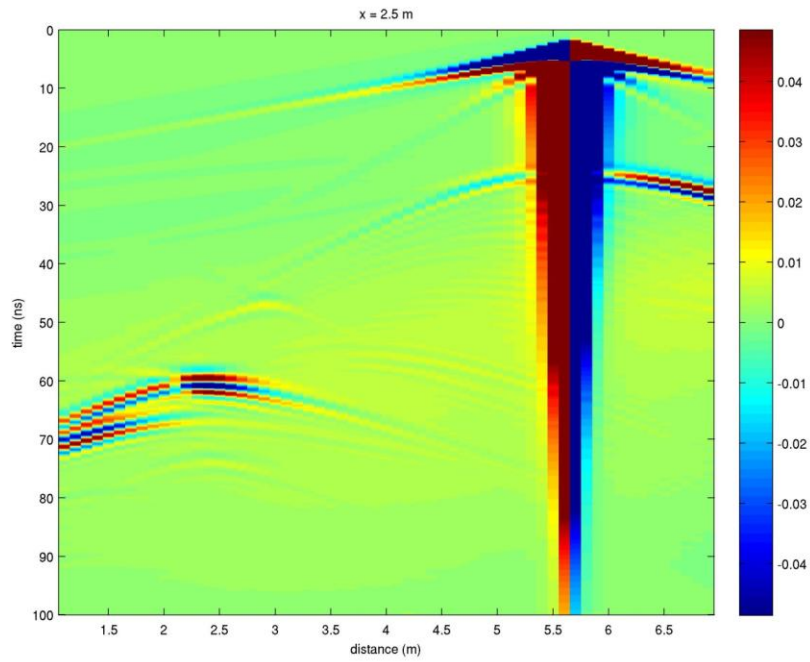
Figure C.1a. Top, previous page. Ex common-shot gather record for transmitter location #5 (same identification numbers as those in previous sections) for Model A. The x-axis represents the distance in the y-direction (for x = 2.5 m). The y-axis represents the time axis (in ns). Transmitter locations may be directly found by following air and ground waves to their source location at time zero.

Figure C.1b. Bottom, previous page. Ey common-shot gather record for transmitter location #5 for Model A. All values are the same as previous graph. Notice Ey signal strength is weaker than Ex record.
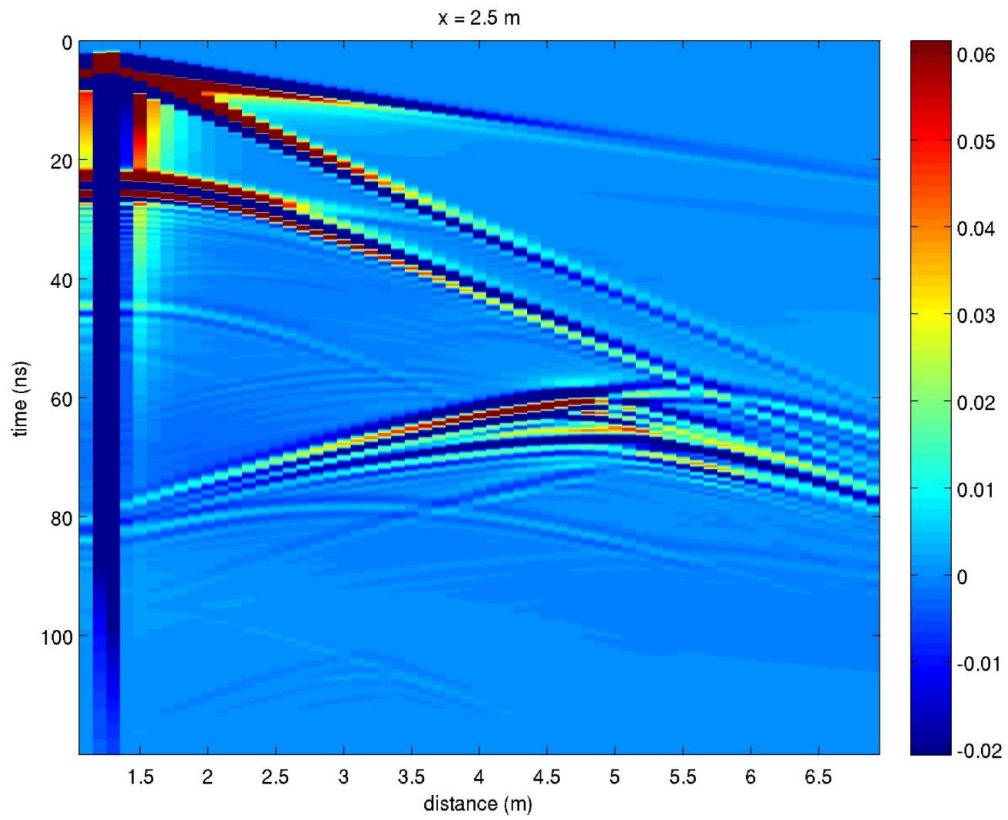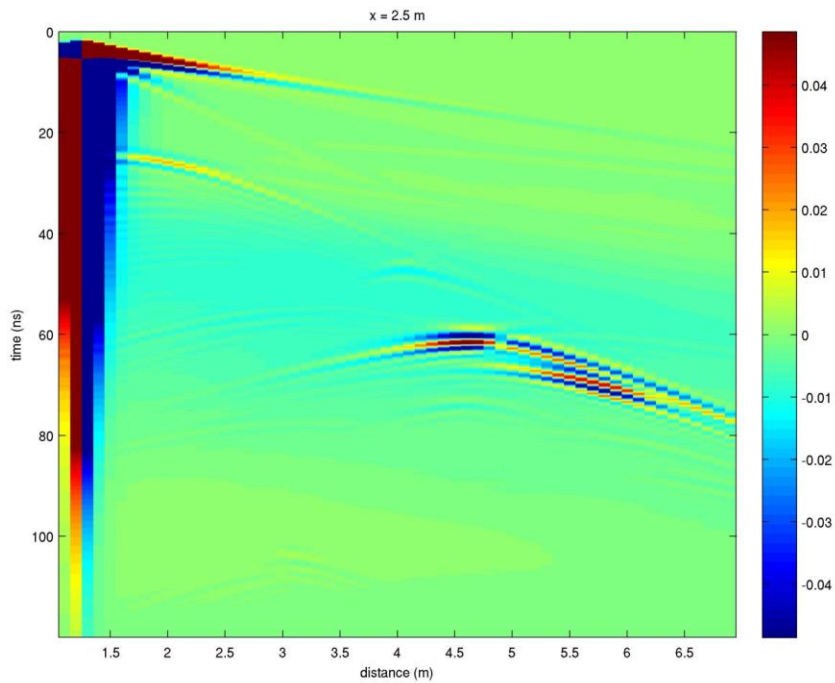
Appendix C (Continued)

Figure C.2a

Figure C.2b

231
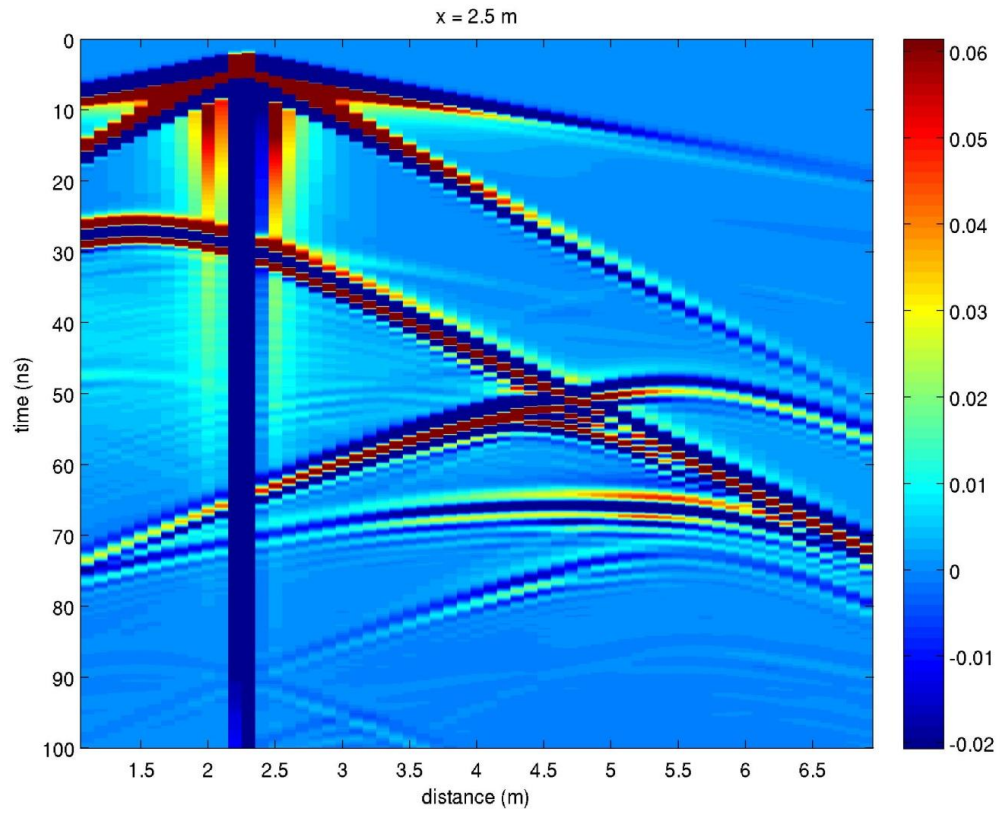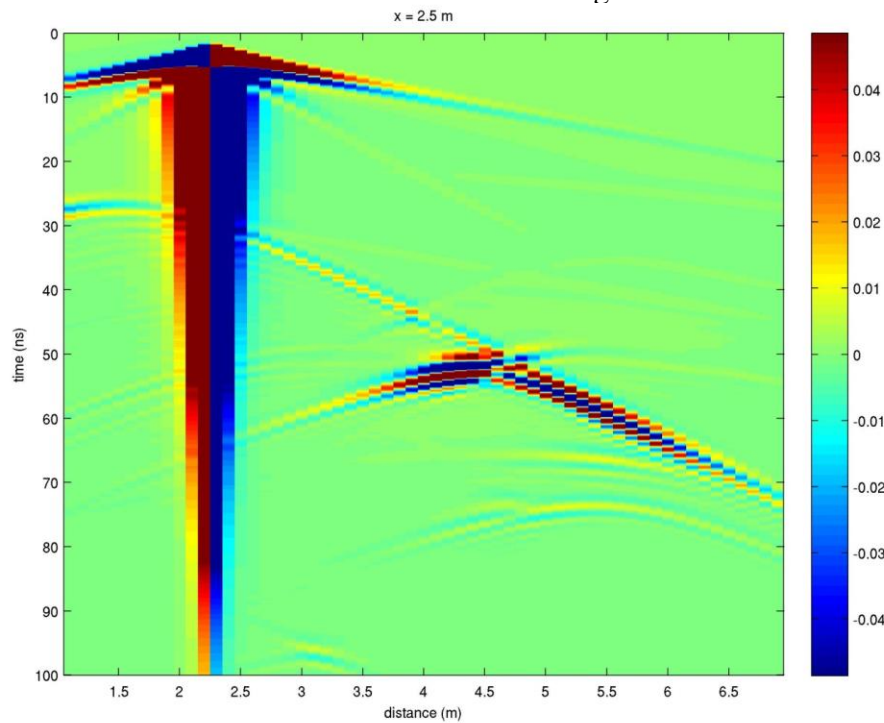
Figure C.2a. Top, previous page. Ex common-shot gather record for transmitter

location #30 (same identification numbers as those in previous sections) for

Model A. The x-axis represents the distance in the y-direction (for x = 2.5 m). The

y-axis represents the time axis (in ns). Transmitter locations may be directly

found by following air and ground waves to their source location at time zero.

Figure C.2b. Bottom, previous page. Ey common-shot gather record for

transmitter location #30 for Model A. All values are the same as previous graph.
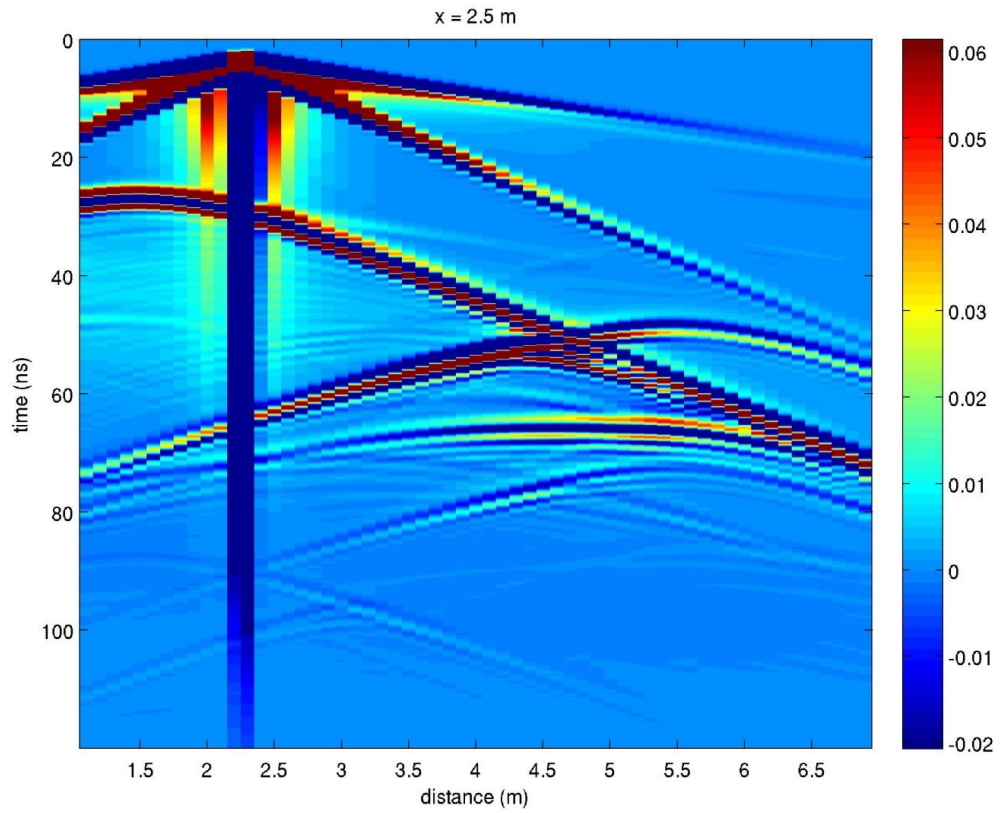
Notice Ey signal strength is weaker   than Ex record.

Appendix C (Continued)

Figure C.3a

Figure C.3b

233
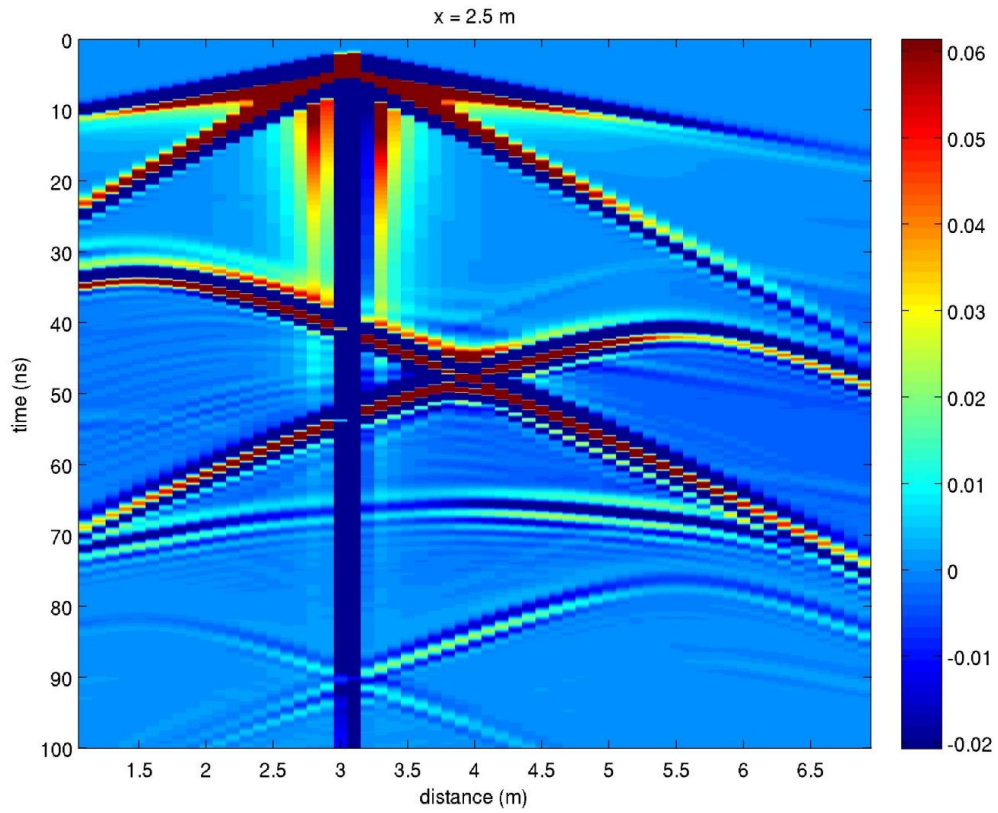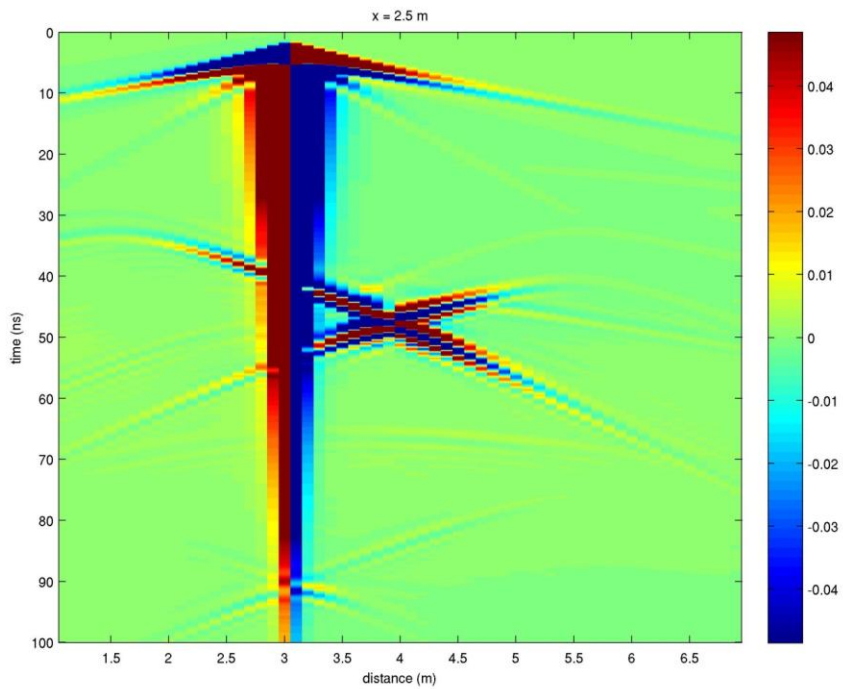
Figure C.3a. Top, previous page. Ex common-shot gather record for transmitter location #50 (same identification numbers as those in previous sections) for Model A. The x-axis represents the distance in the y-direction (for x = 2.5 m). The y-axis represents the time axis (in ns). Transmitter locations may be directly found by following air and ground waves to their source location at time zero. Figure C.3b. Bottom, previous page. Ey common-shot gather record for transmitter location #50 for Model A. All values are the same as previous graph. Notice Ey signal strength is weaker   than Ex record.
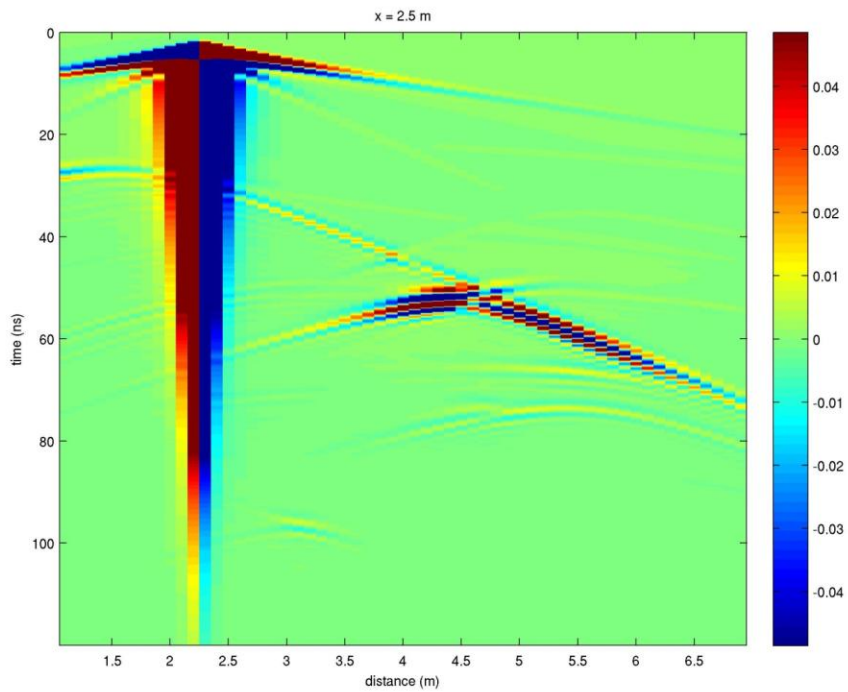
Appendix C (Continued)

Figure C.4a

Figure C.4b

235
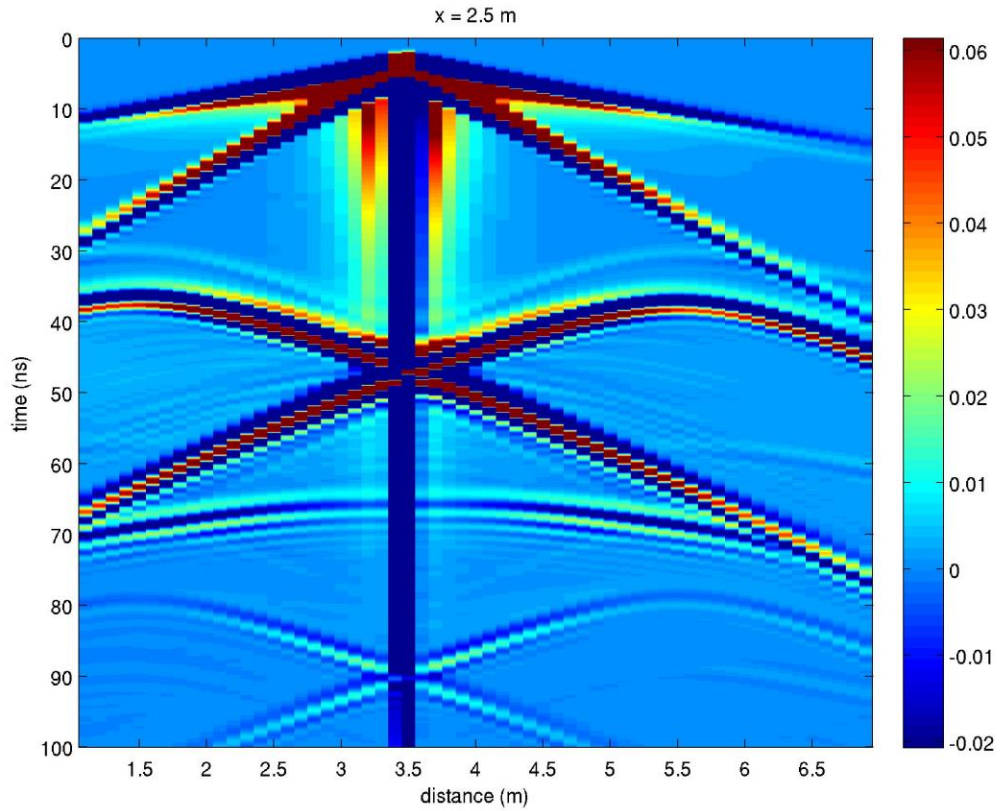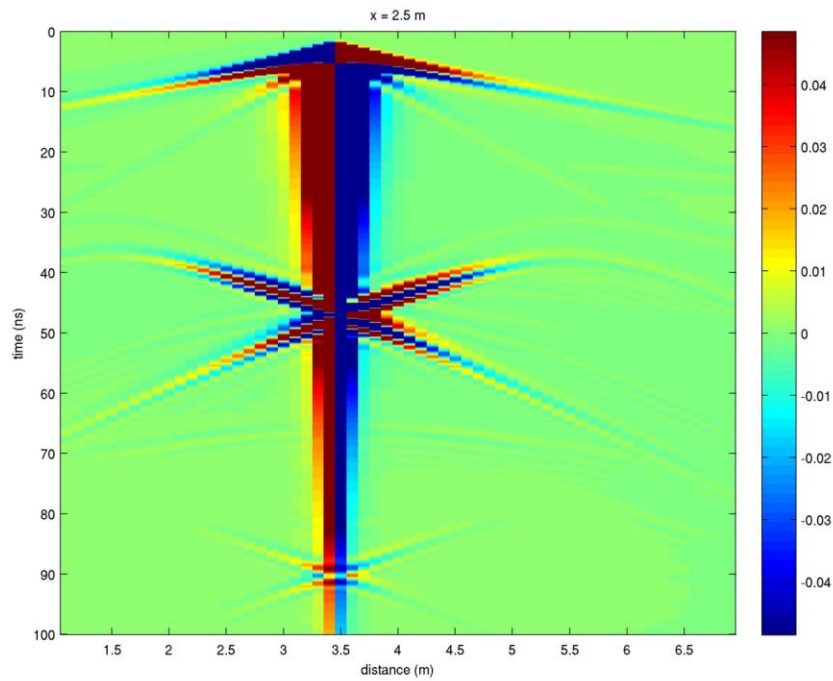
Figure C.4a. Top, previous page. Ex common-shot gather record for transmitter

location #60 (same identification numbers as those in previous sections) for

Model A. The x-axis represents the distance in the y-direction (for $x = 2.5$ m). The

y-axis represents the time axis (in ns). Transmitter locations may be directly

found by following air and ground waves to their source location at time zero.

Figure C.4b. Bottom, previous page. Ey common-shot gather record for

transmitter location #60 for Model A. All values are the same as previous graph.

Notice Ey signal strength is weaker   than Ex record.

Note: this is at the center of the conduit ($x = 2.5$ m, $y = 3.5$ m).

Appendix C (Continued)

Figure C.5a

Figure C.5b

237
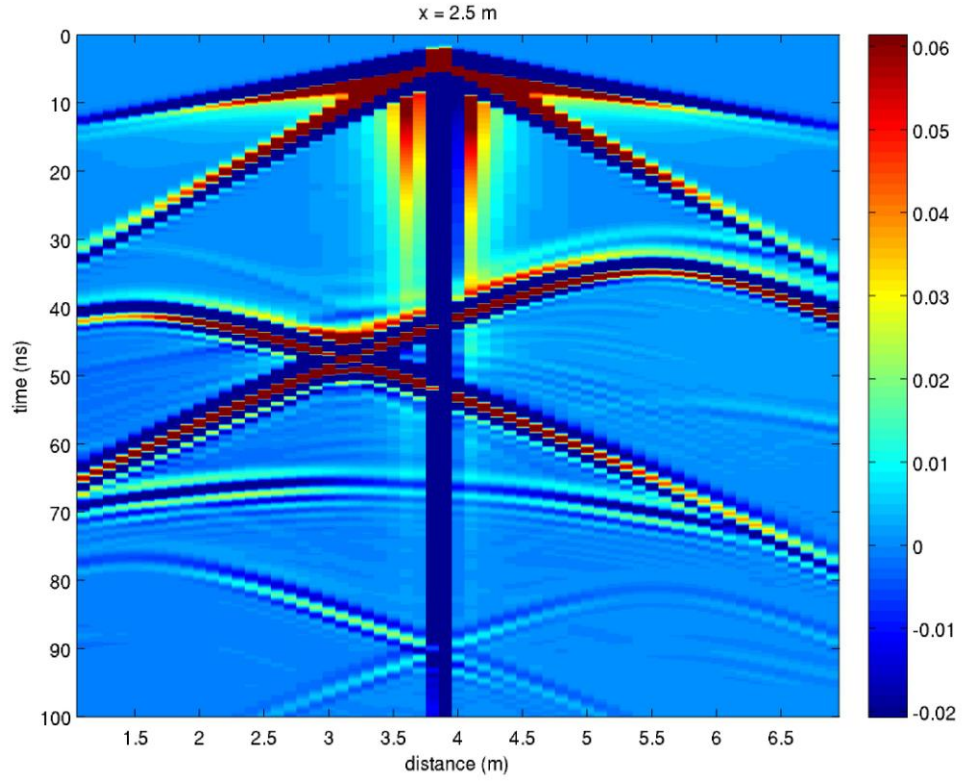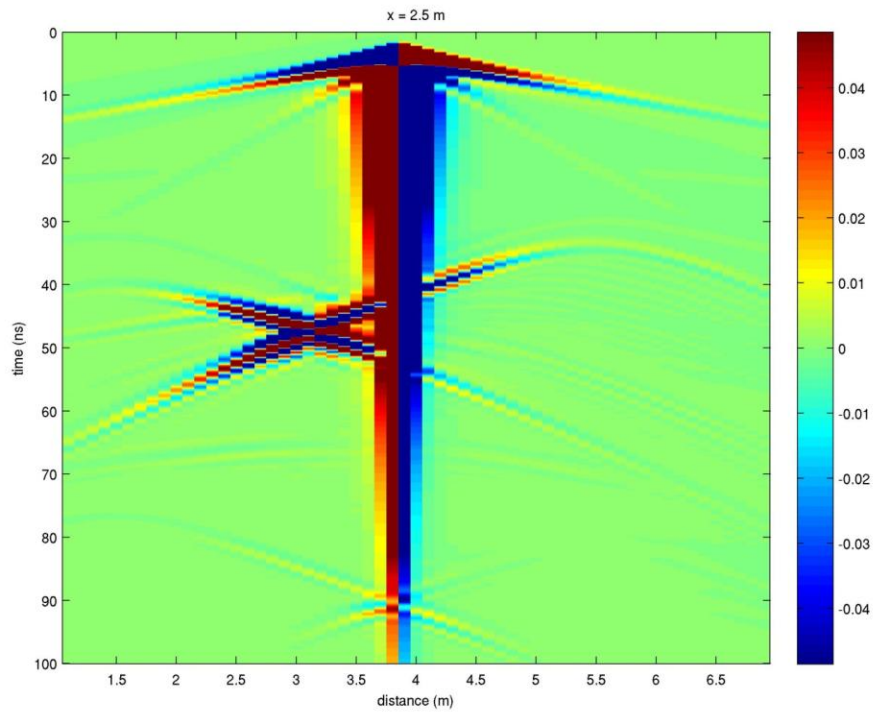
Figure C.5a. Top, previous page. Ex common-shot gather record for transmitter location #70 (same identification numbers as those in previous sections) for Model A. The x-axis represents the distance in the y-direction (for x = 2.5 m). The y-axis represents the time axis (in ns). Transmitter locations may be directly found by following air and ground waves to their source location at time zero. Figure C.5b. Bottom, previous page. Ey common-shot gather record for transmitter location #70 for Model A. All values are the same as previous graph. Notice Ey signal strength is weaker   than Ex record.
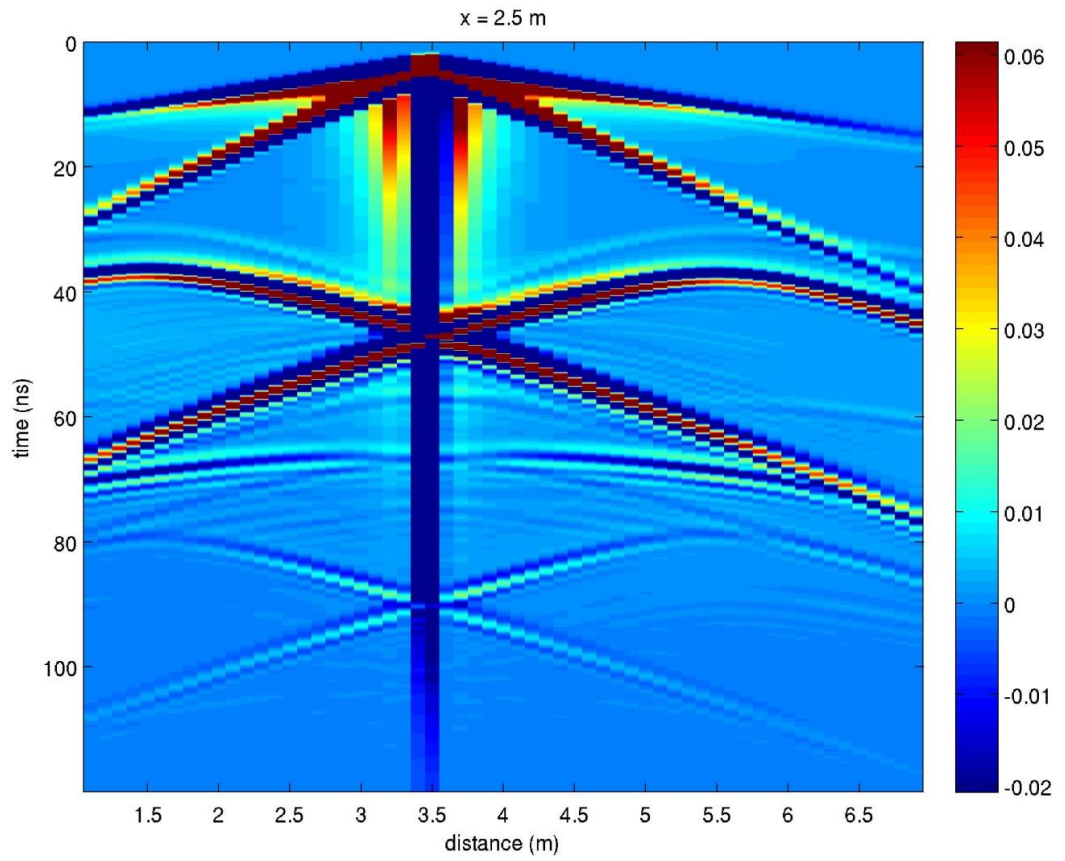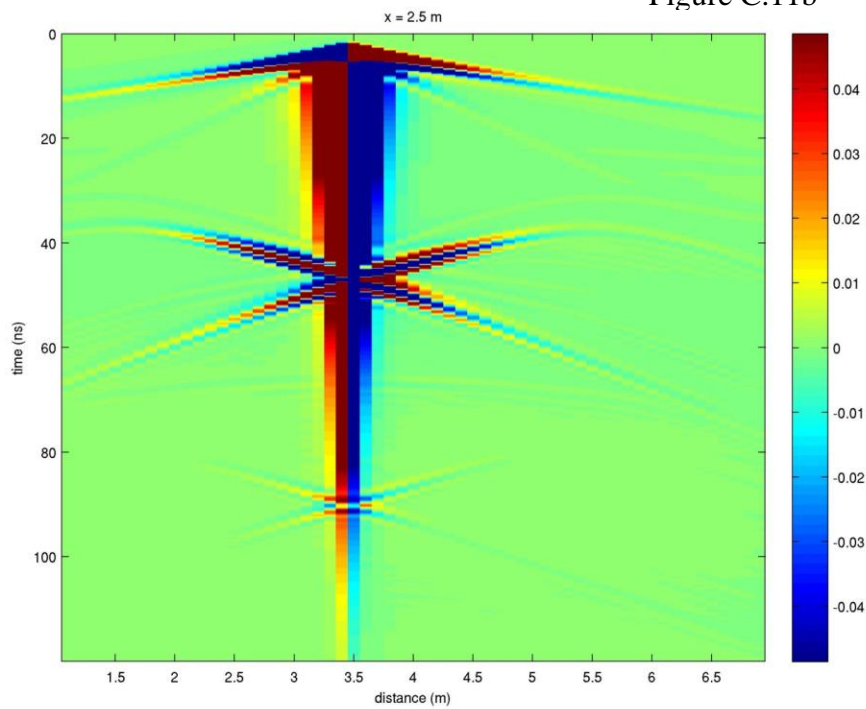
238

Figure C.6a

x = 2.5 m

Figure C.6b

x = 2.5 m

239
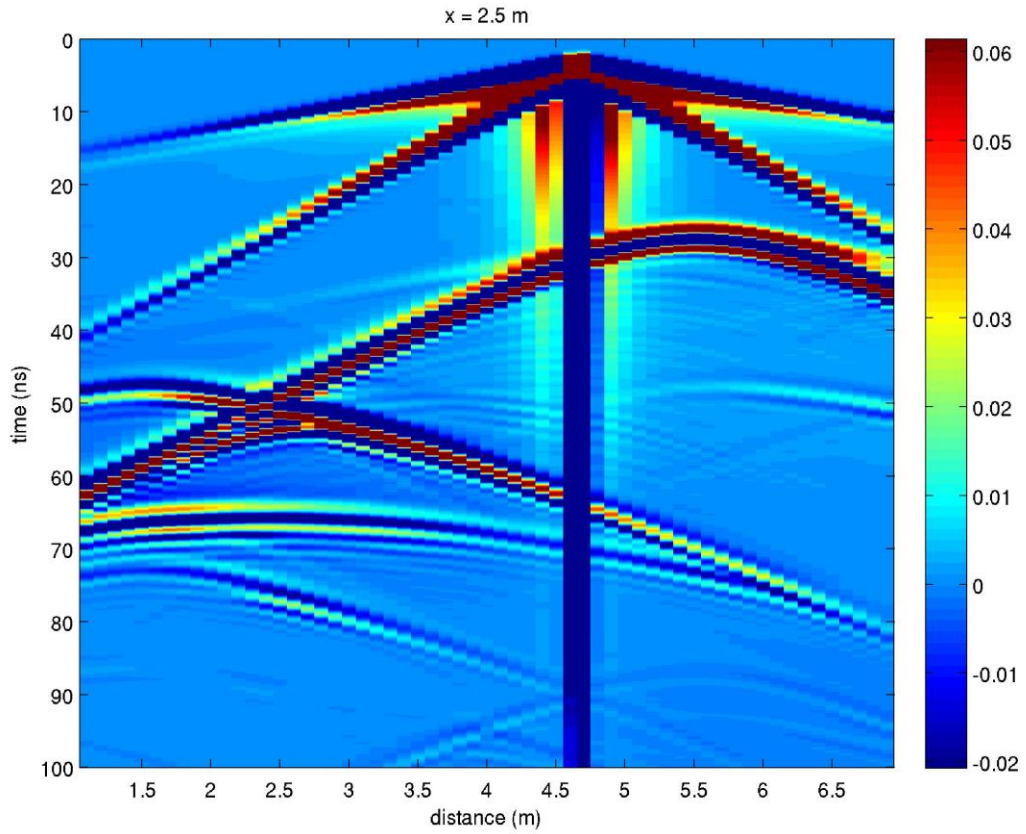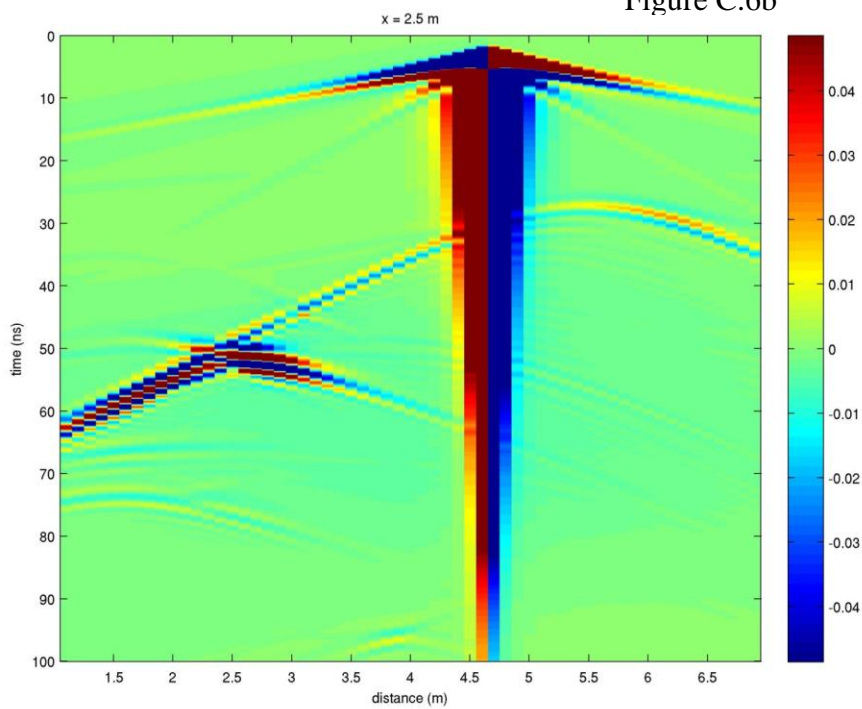
Figure C.6a. Top, previous page. Ex common-shot gather record for transmitter

location #90 (same identification numbers as those in previous sections) for

Model A. The x-axis represents the distance in the y-direction (for x = 2.5 m). The

y-axis represents the time axis (in ns). Transmitter locations may be directly

found by following air and ground waves to their source location at time zero.

Figure C.6b. Bottom, previous page. Ey common-shot gather record for

transmitter location #90 for Model A. All values are the same as previous graph.

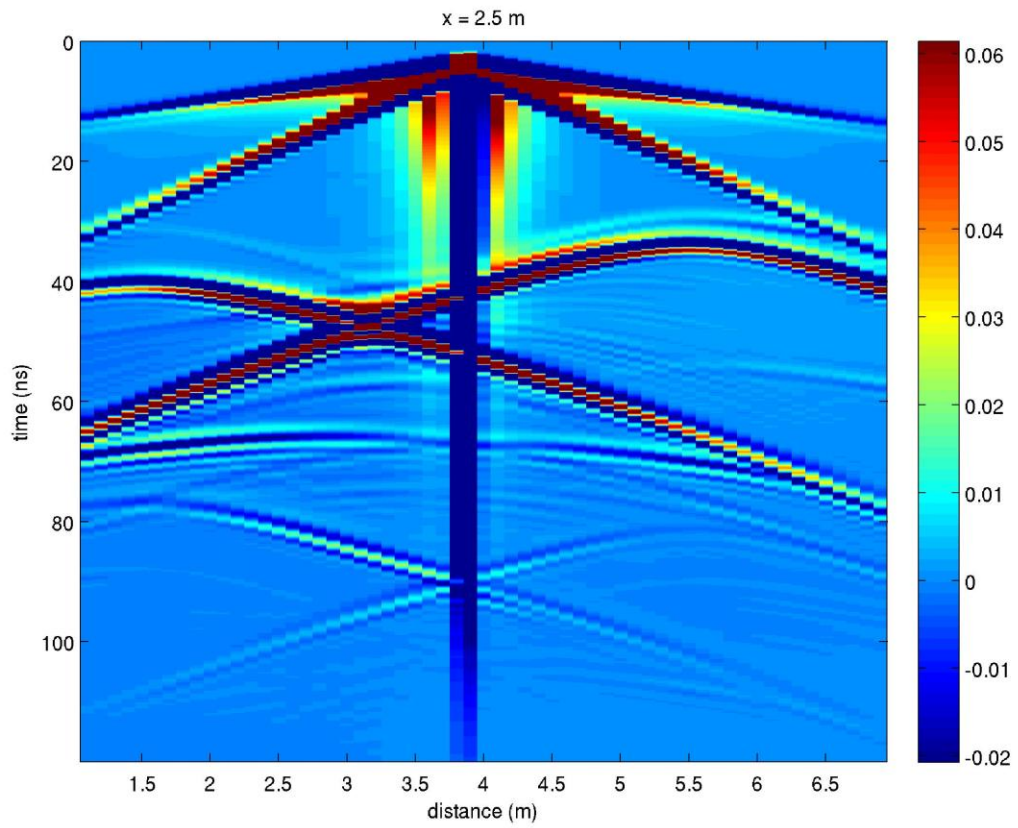Notice Ey signal strength is weaker than Ex record.

Figure C.7a

x = 2.5 m
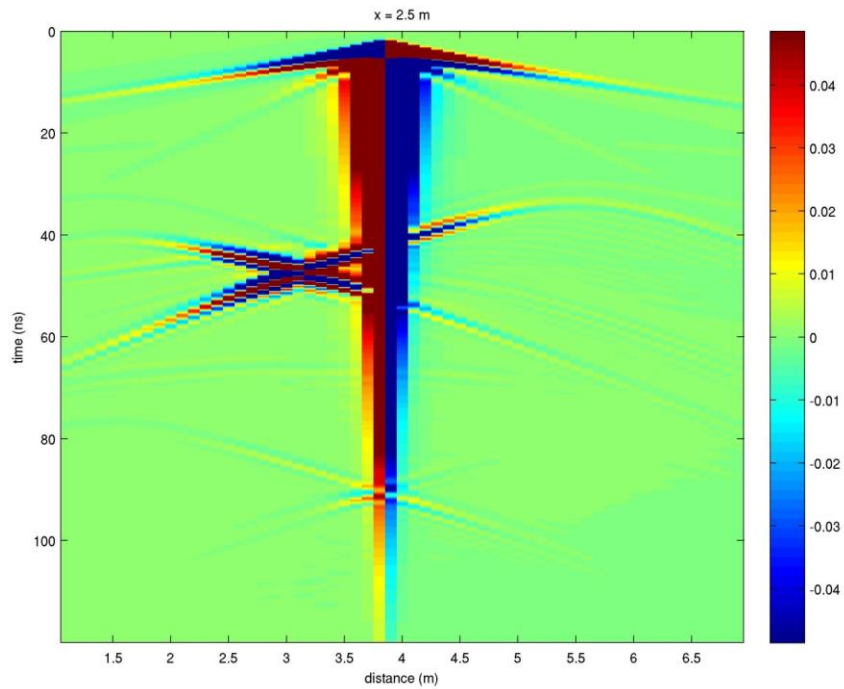
Figure C.7b

x = 2.5 m

241
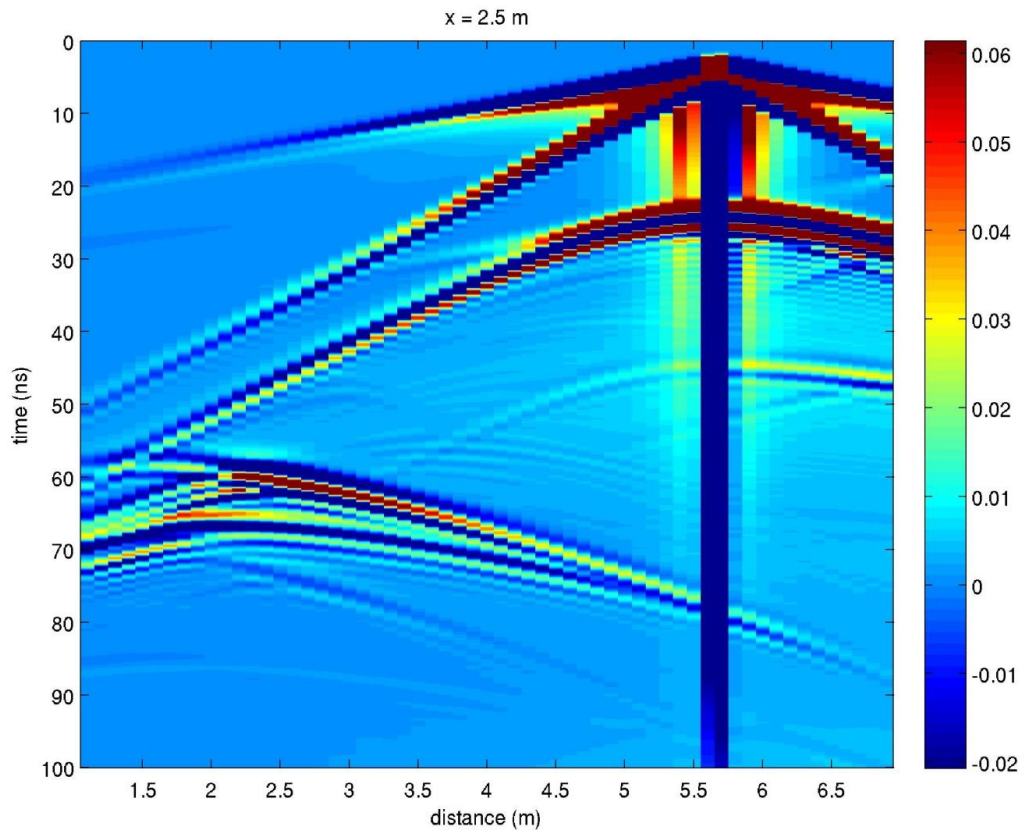
Figure C.7a. Top, previous page. Ex common-shot gather record for transmitter

location #115 (same identification numbers as those in previous sections) for

Model A. The x-axis represents the distance in the y-direction (for x = 2.5 m). The

y-axis represents the time axis (in ns). Transmitter locations may be directly

found by following air and ground waves to their source location at time zero.

Figure C.7b. Bottom, previous page. Ey common-shot gather record for

transmitter location #115 for Model A. All values are the same as previous graph.

Notice Ey signal strength is weaker than Ex record.

242

Figure C.8a

x = 2.5 m

Figure C.8b

x = 2.5 m

243

Figure C.8a. Top, previous page. Ex common-shot gather record for transmitter location #5 (same identification numbers as those in previous sections) for Model B. The x-axis represents the distance in the y-direction (for x = 2.5 m). The y-axis represents the time axis (in ns). Transmitter locations may be directly found by following air and ground waves to their source location at time zero.

Figure C.8b. Bottom, previous page. Ey common-shot gather record for transmitter location #5 for Model B. All values are the same as previous graph. Notice Ey signal strength is weaker than Ex record.
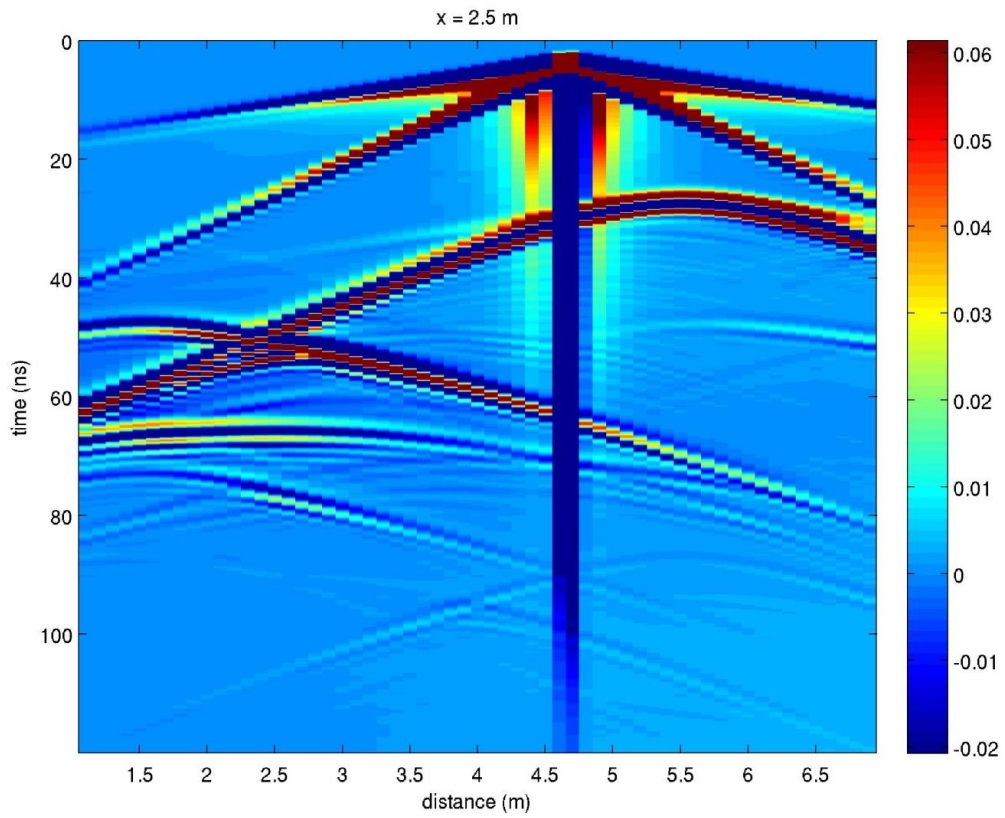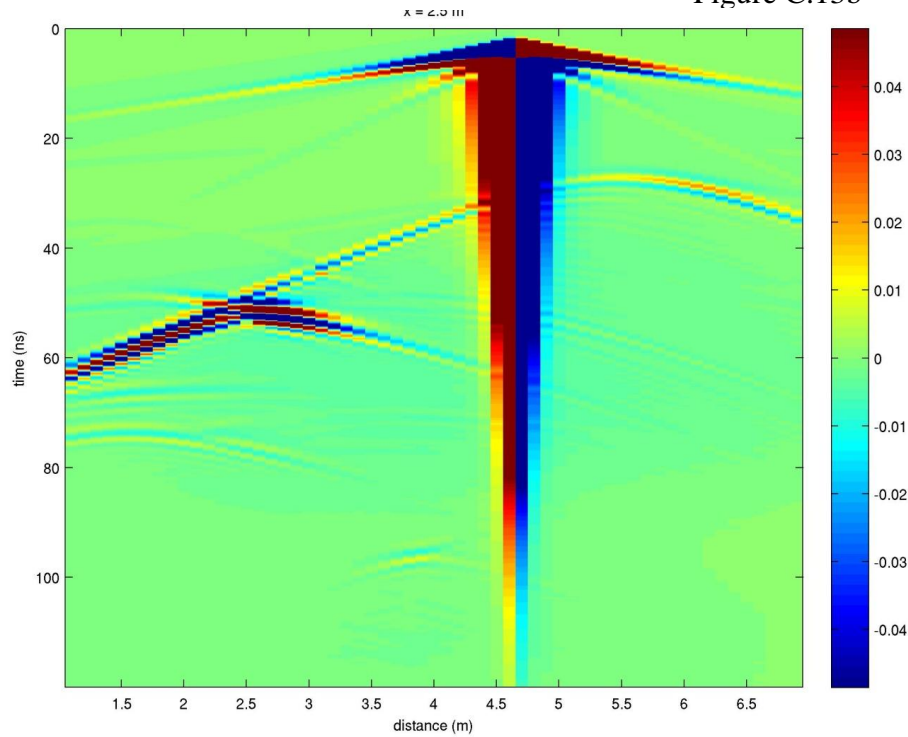
244

Figure C.9a

x = 2.5 m

Figure C.9b

x = 2.5 m

245

Figure C.9a. Top, previous page. Ex common-shot gather record for transmitter

location #30 (same identification numbers as those in previous sections) for

Model B. The x-axis represents the distance in the y-direction (for x = 2.5 m). The

y-axis represents the time axis (in ns). Transmitter locations may be directly

found by following air and ground waves to their source location at time zero.

Figure C.9b. Bottom, previous page. Ey common-shot gather record for

transmitter location #30 for Model B. All values are the same as previous graph.

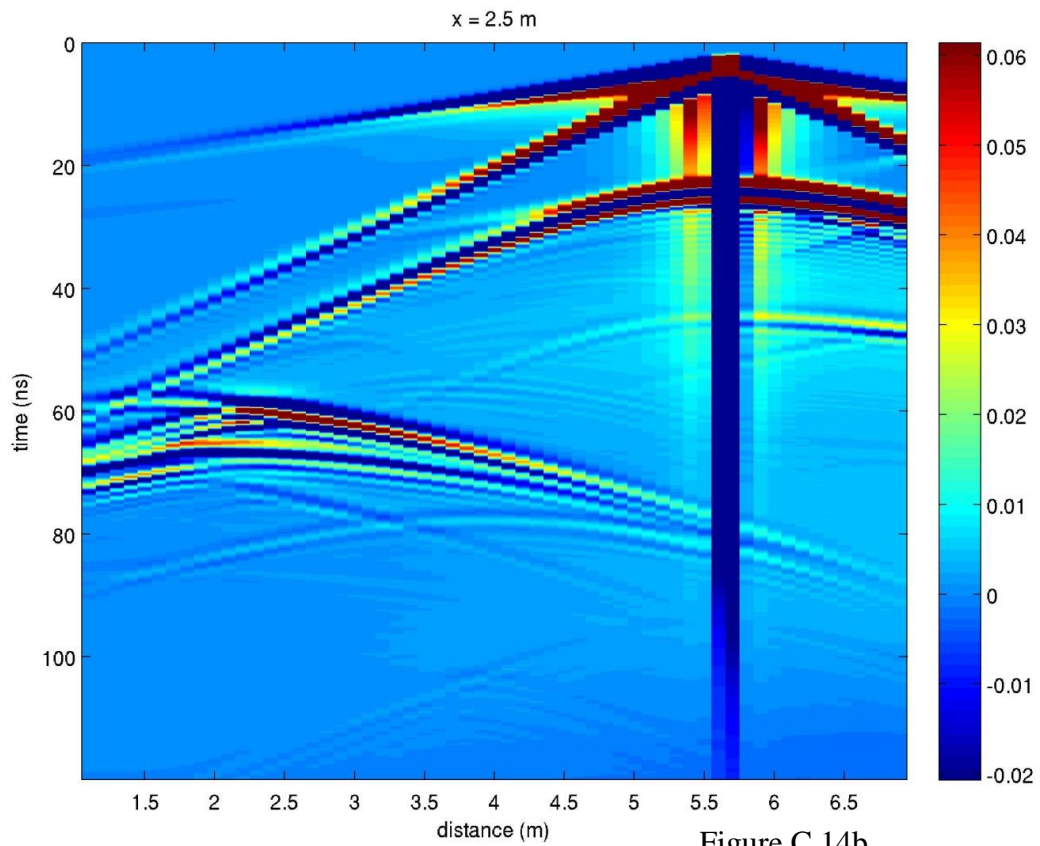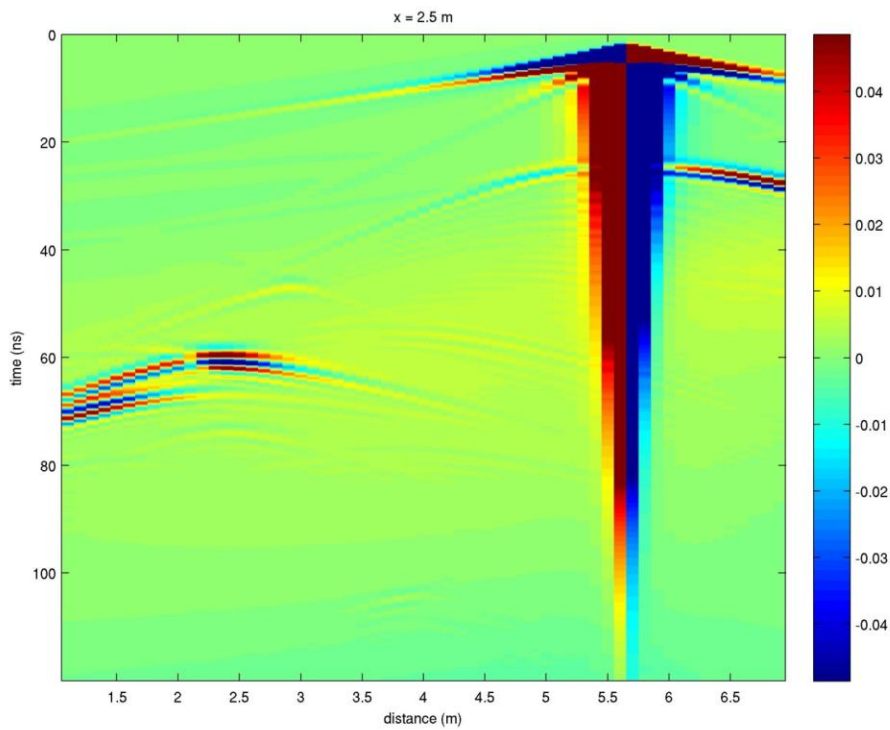Notice Ey signal strength is weaker than Ex record.

Figure C.10a

x = 2.5 m

Figure C.10b

x = 2.5 m

247
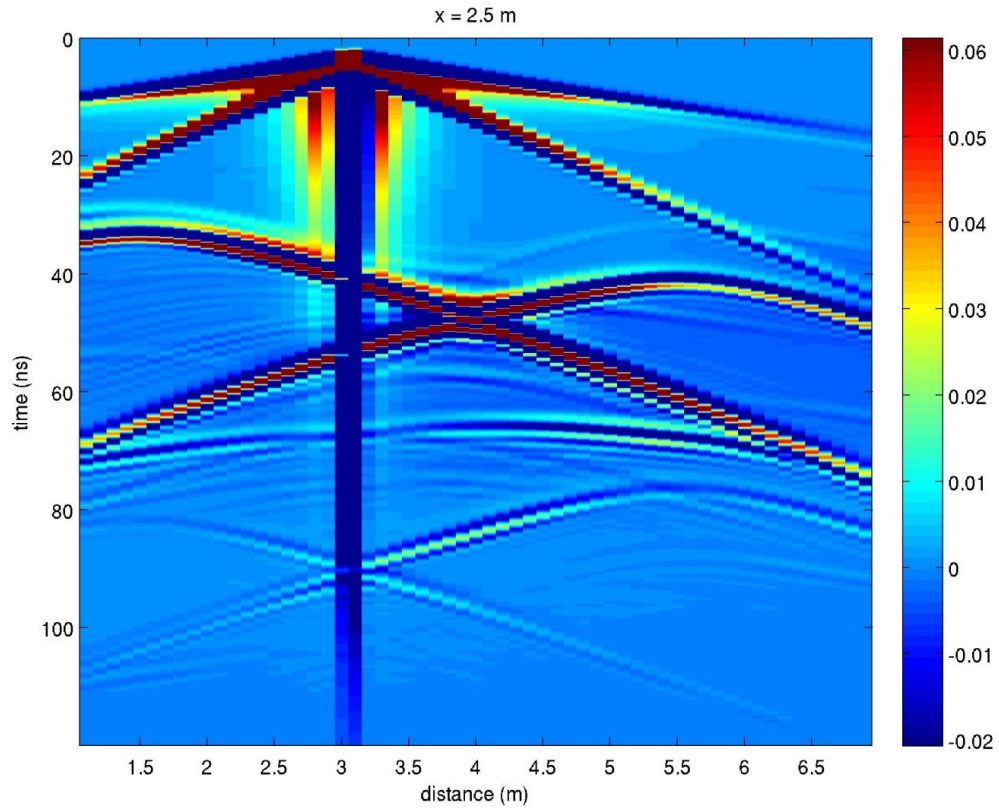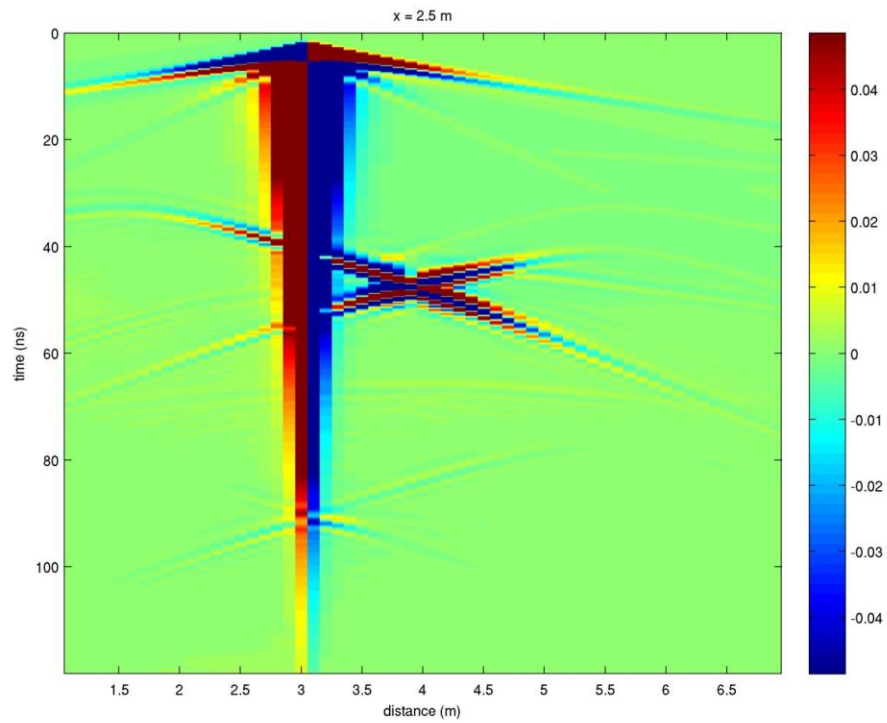
Appendix C (Continued)

Figure C.10a. Top, previous page. Ex common-shot gather record for transmitter location #50 (same identification numbers as those in previous sections) for Model B. The x-axis represents the distance in the y-direction (for x = 2.5 m). The y-axis represents the time axis (in ns). Transmitter locations may be directly found by following air and ground waves to their source location at time zero. Figure C.10b. Bottom, previous page. Ey common-shot gather record for transmitter location #50 for Model B. All values are the same as previous graph. Notice Ey signal strength is weaker   than Ex record.
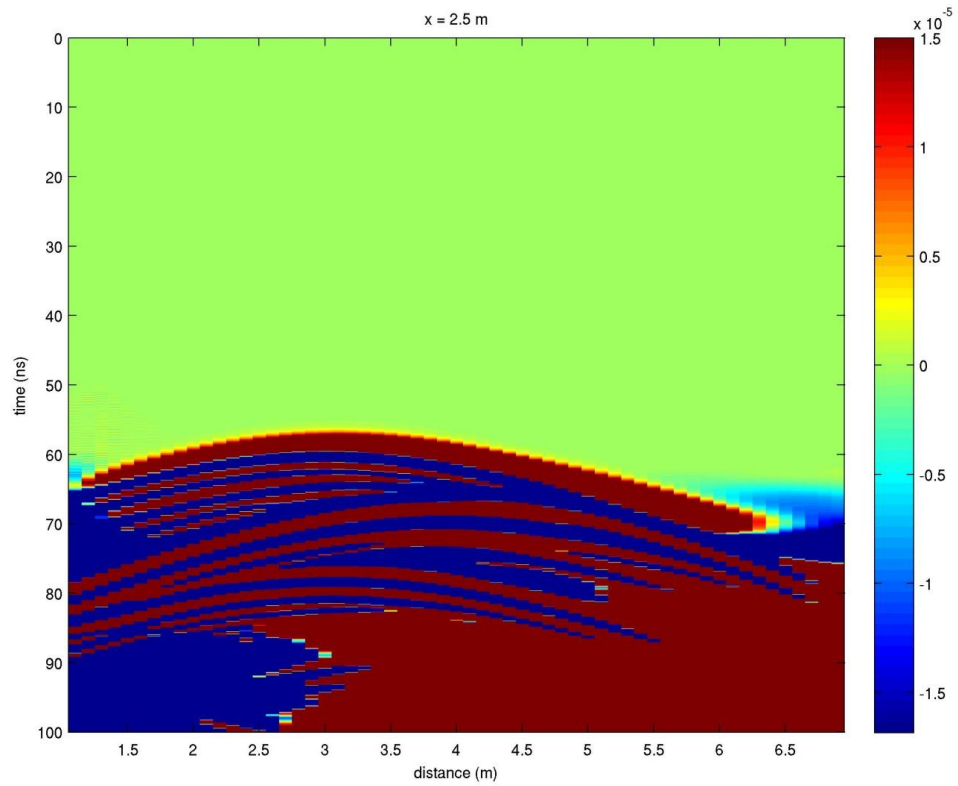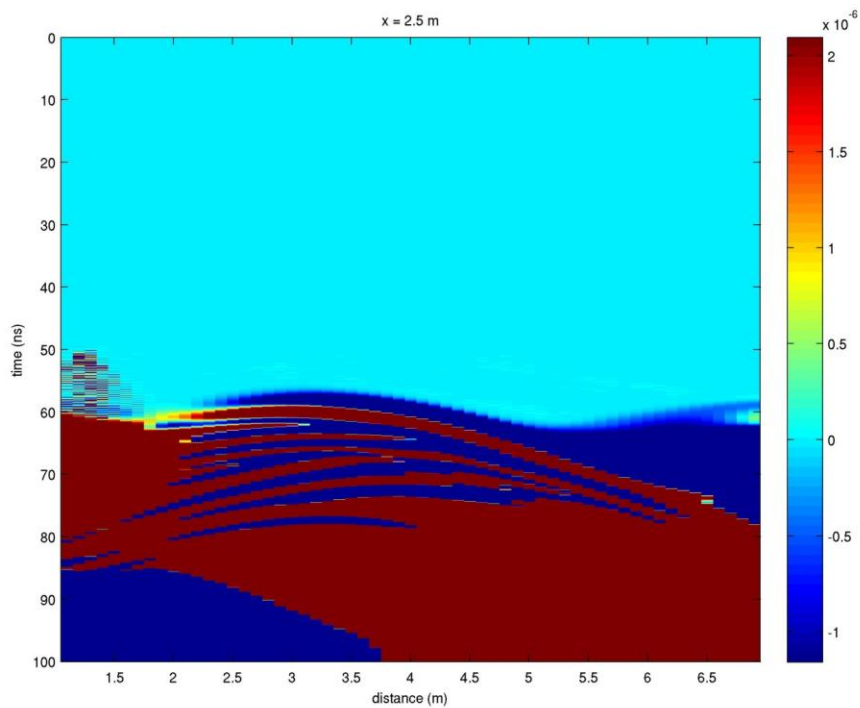
Figure C.11a

x = 2.5 m

Figure C.11b

x = 2.5 m

249

Figure C.11a. Top, previous page. Ex common-shot gather record for transmitter location #60 (same identification numbers as those in previous sections) for Model B. The x-axis represents the distance in the y-direction (for x = 2.5 m). The y-axis represents the time axis (in ns). Transmitter locations may be directly found by following air and ground waves to their source location at time zero.

Figure C.11b. Bottom, previous page. Ey common-shot gather record for transmitter location #60 for Model B. All values are the same as previous graph. Notice Ey signal strength is weaker than Ex record.

Note: this is at the center of the conduit (x = 2.5 m, y = 3.5 m).

Appendix C (Continued)

Figure C.12a

x = 2.5 m

Figure C.12b

x = 2.5 m

Appendix C (Continued)

Figure C.12a. Top, previous page. Ex common-shot gather record for transmitter

location #70 (same identification numbers as those in previous sections) for

Model B. The x-axis represents the distance in the y-direction (for x = 2.5 m). The

y-axis represents the time axis (in ns). Transmitter locations may be directly

found by following air and ground waves to their source location at time zero.

Figure C.12b. Bottom, previous page. Ey common-shot gather record for

transmitter location #70 for Model B. All values are the same as previous graph.

Notice Ey signal strength is weaker than Ex record.

Appendix C (Continued)

Figure C.13a

x = 2.5 m

Figure C.13b

x = 2.5 m

Figure C.13a. Top, previous page. Ex common-shot gather record for transmitter

location #90 (same identification numbers as those in previous sections) for

Model B. The x-axis represents the distance in the y-direction (for x = 2.5 m). The

y-axis represents the time axis (in ns). Transmitter locations may be directly

found by following air and ground waves to their source location at time zero.

Figure C.13b. Bottom, previous page. Ey common-shot gather record for

transmitter location #90 for Model B. All values are the same as previous graph.

Notice Ey signal strength is weaker   than Ex record.

254

Appendix C (Continued)

Figure C.14a

x = 2.5 m

Figure C.14b

x = 2.5 m

255

www.manaraa.com

Figure C.14a. Top, previous page. Ex common-shot gather record for transmitter

location #115 (same identification numbers as those in previous sections) for

Model B. The x-axis represents the distance in the y-direction (for x = 2.5 m). The

y-axis represents the time axis (in ns). Transmitter locations may be directly

found by following air and ground waves to their source location at time zero.

Figure C.14b. Bottom, previous page. Ey common-shot gather record for

transmitter location #115 for Model B. All values are the same as previous graph.

Notice Ey signal strength is weaker than Ex record.

Figure C.15a
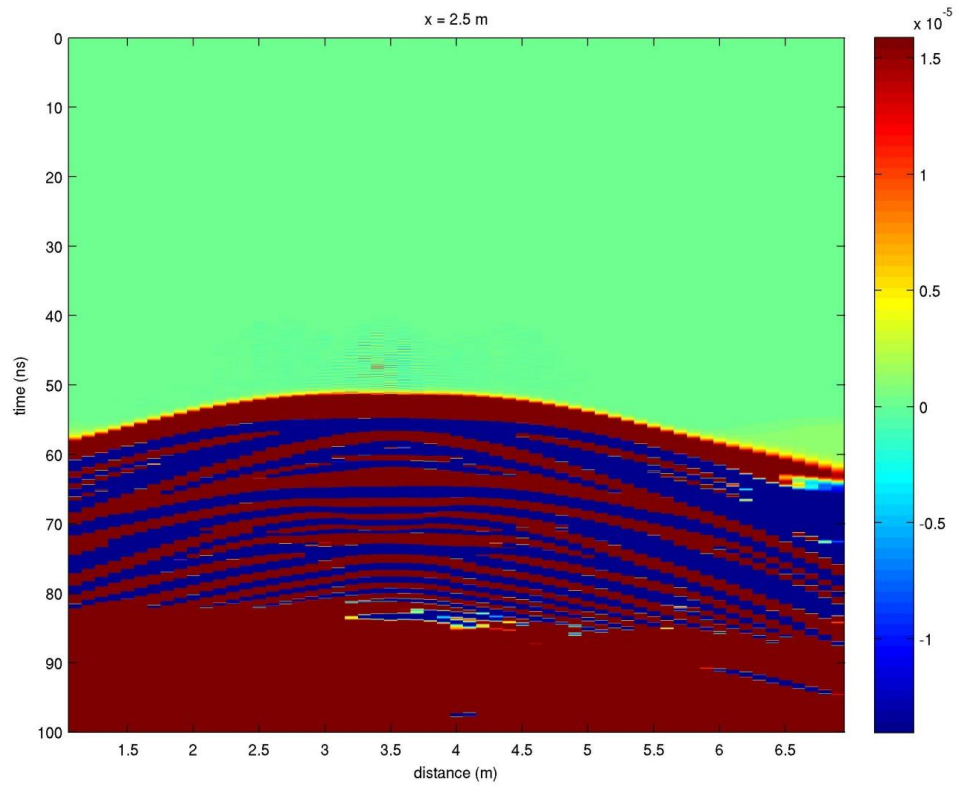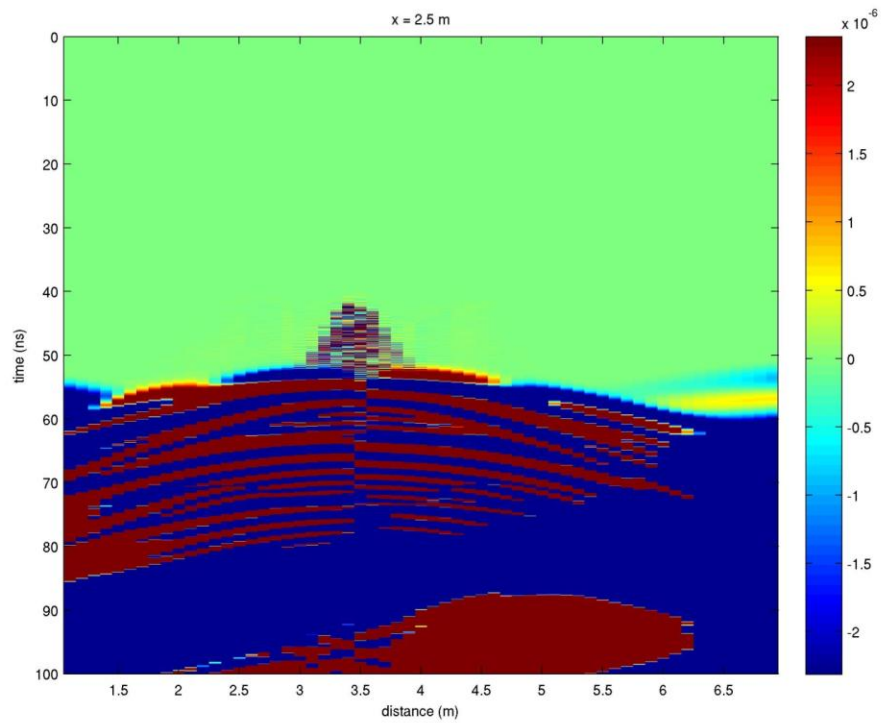

Figure C.15b

257

Figure C.15a. Top, previous page. Ex difference plot between Model A and B for transmitter location #5 (same identification numbers as those in previous sections). The x-axis represents the distance in the y-direction (for $x = 2.5$ m). The y-axis represents the time axis (in ns). Transmitter locations may be are the same as those in previous figures.

Figure C.15b. Bottom, previous page. Ey difference plot between Model A and B for transmitter location #5. All values are the same as previous graph. Notice miniscule order of magnitude of relative difference in each graph.
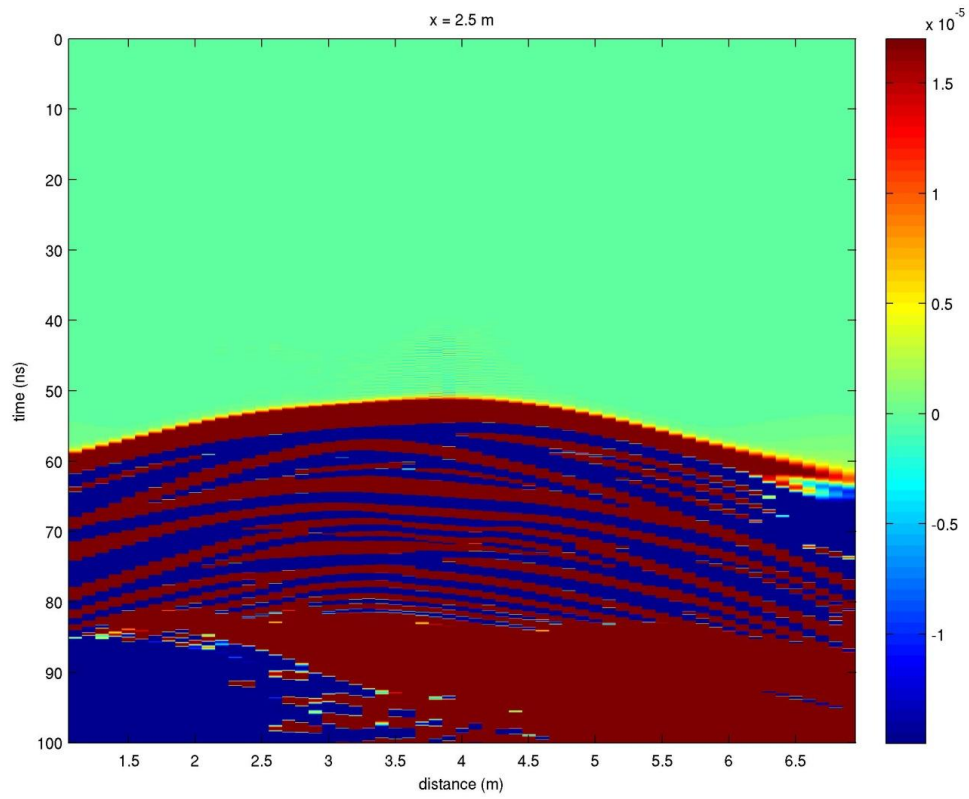
Appendix C (Continued)

Figure C.16a

Figure C.16b

259
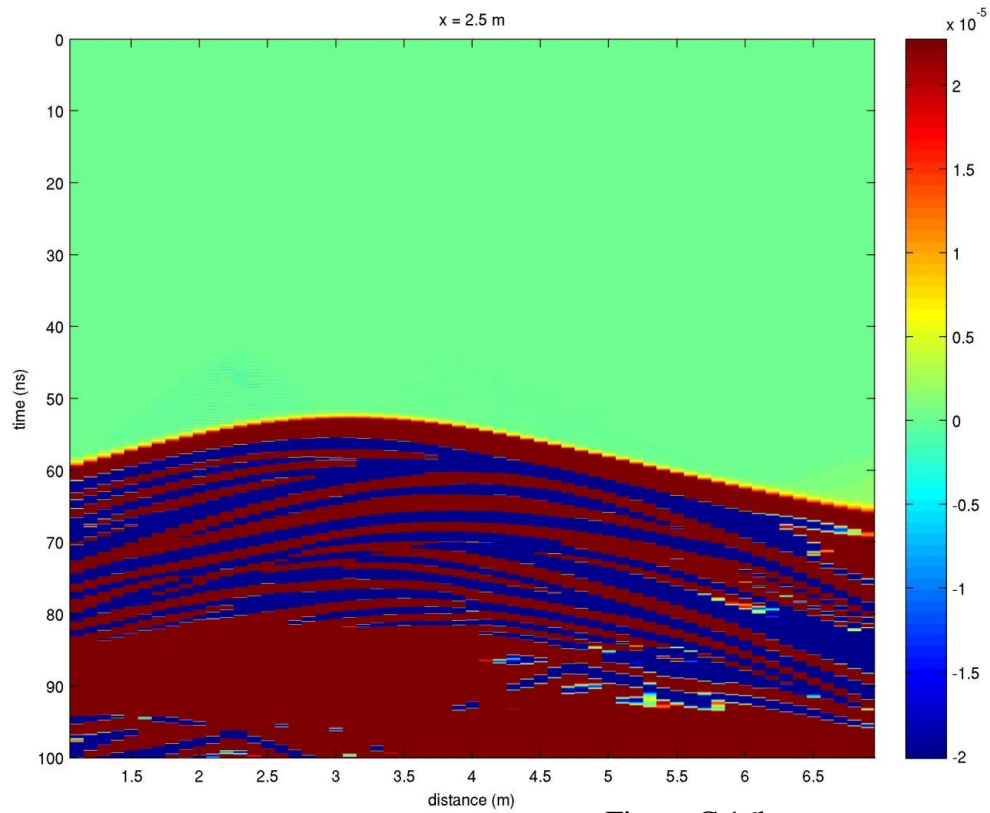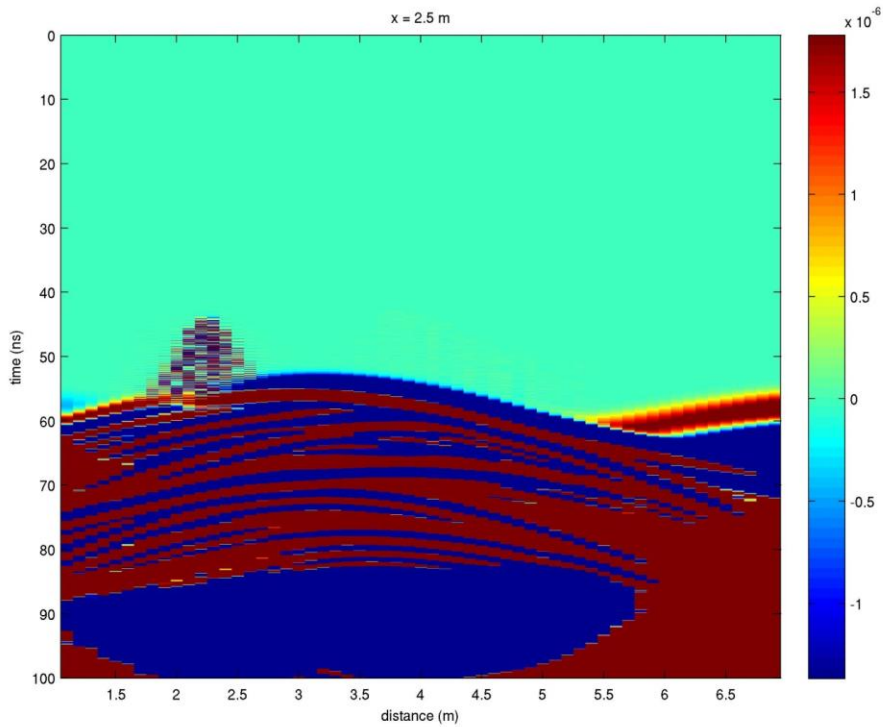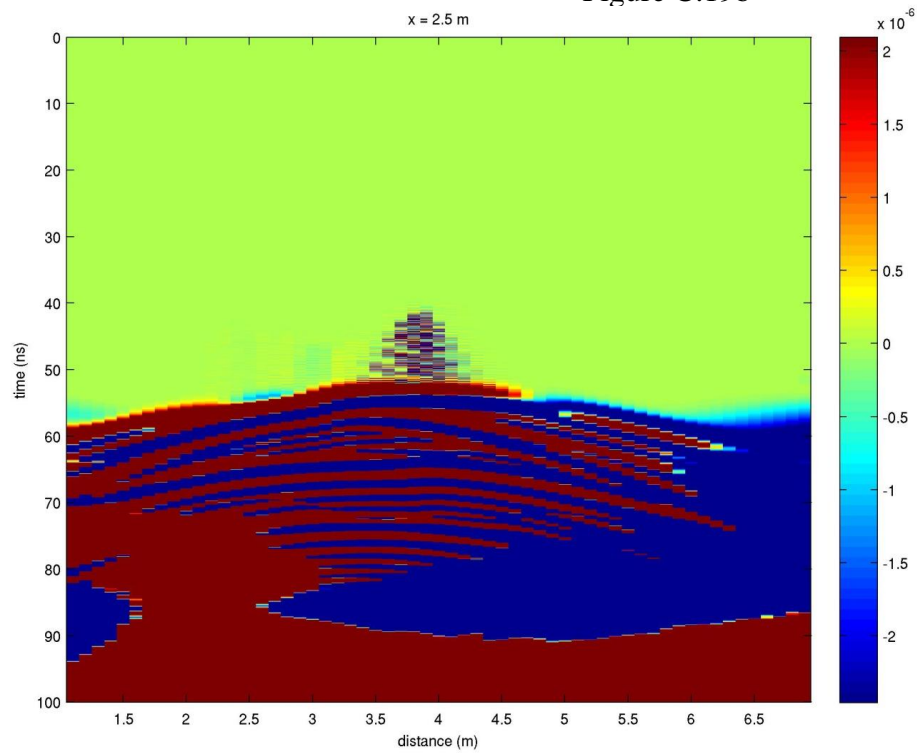
Appendix C (Continued)

Figure C.16a. Top, previous page. Ex difference plot between Model A and B for transmitter location #30 (same identification numbers as those in previous sections). The x-axis represents the distance in the y-direction (for $x = 2.5$ m). The y-axis represents the time axis (in ns). Transmitter locations may be are the same as those in previous figures.

Figure C.16b. Bottom, previous page. Ey difference plot between Model A and B for transmitter location #30. All values are the same as previous graph. Notice miniscule order of magnitude of relative difference in each graph.

Figure C.17a

Figure C.17b

261
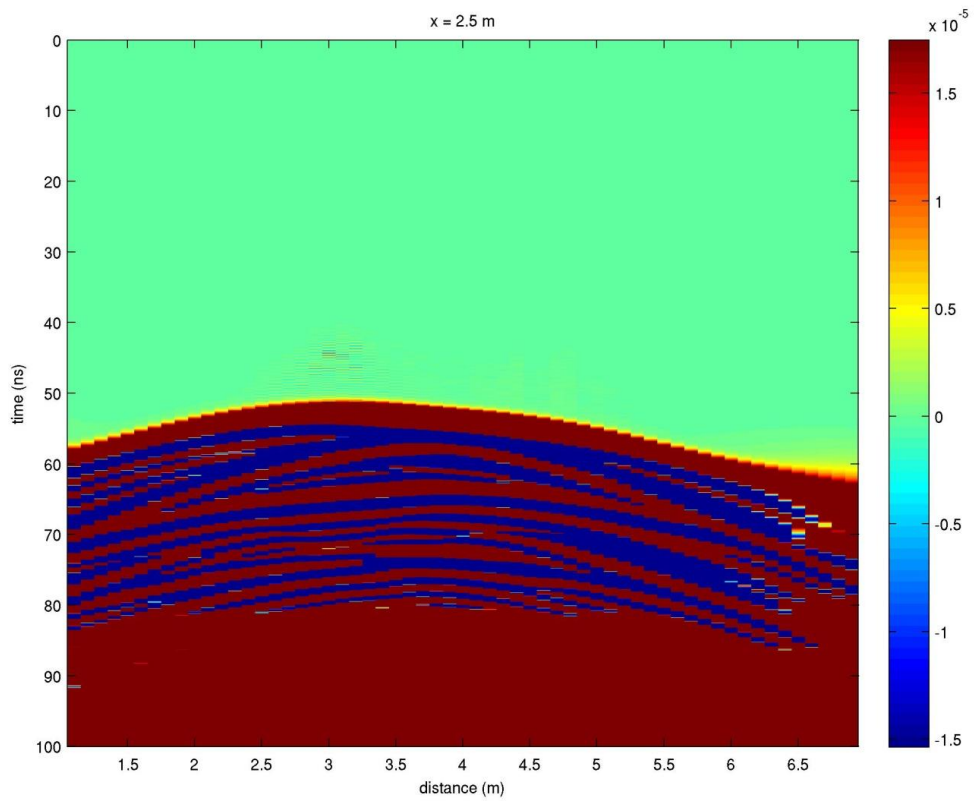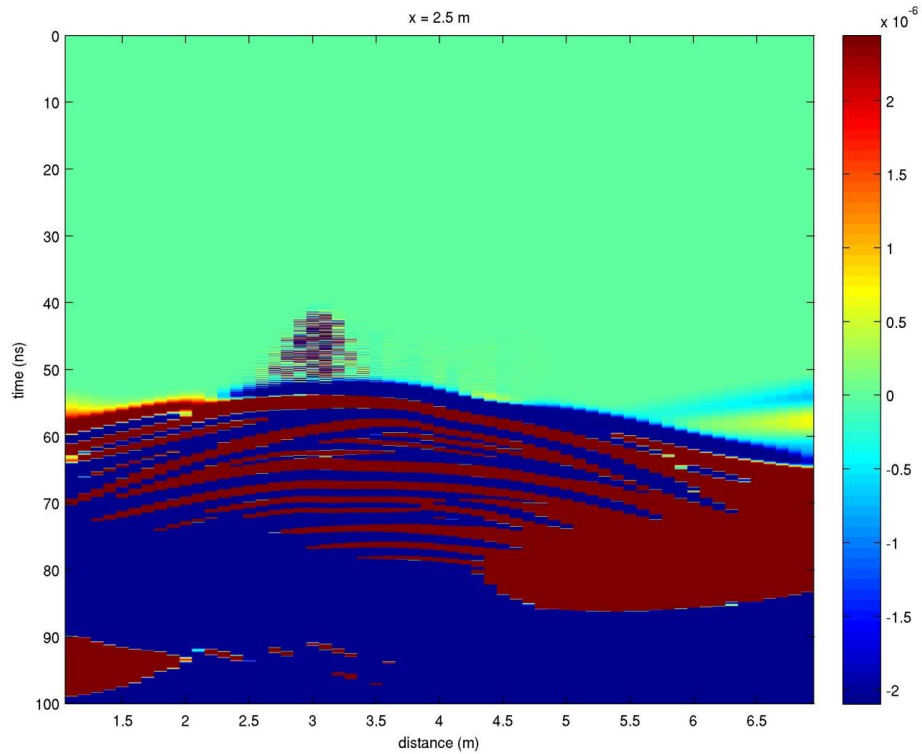
Figure C.17a. Top, previous page. Ex difference plot between Model A and B for transmitter location #50 (same identification numbers as those in previous sections). The x-axis represents the distance in the y-direction (for x = 2.5 m). The y-axis represents the time axis (in ns). Transmitter locations may be are the same as those in previous figures.

Figure C.17b. Bottom, previous page. Ey difference plot between Model A and B for transmitter location #50. All values are the same as previous graph. Notice miniscule order of magnitude of relative difference in each graph.
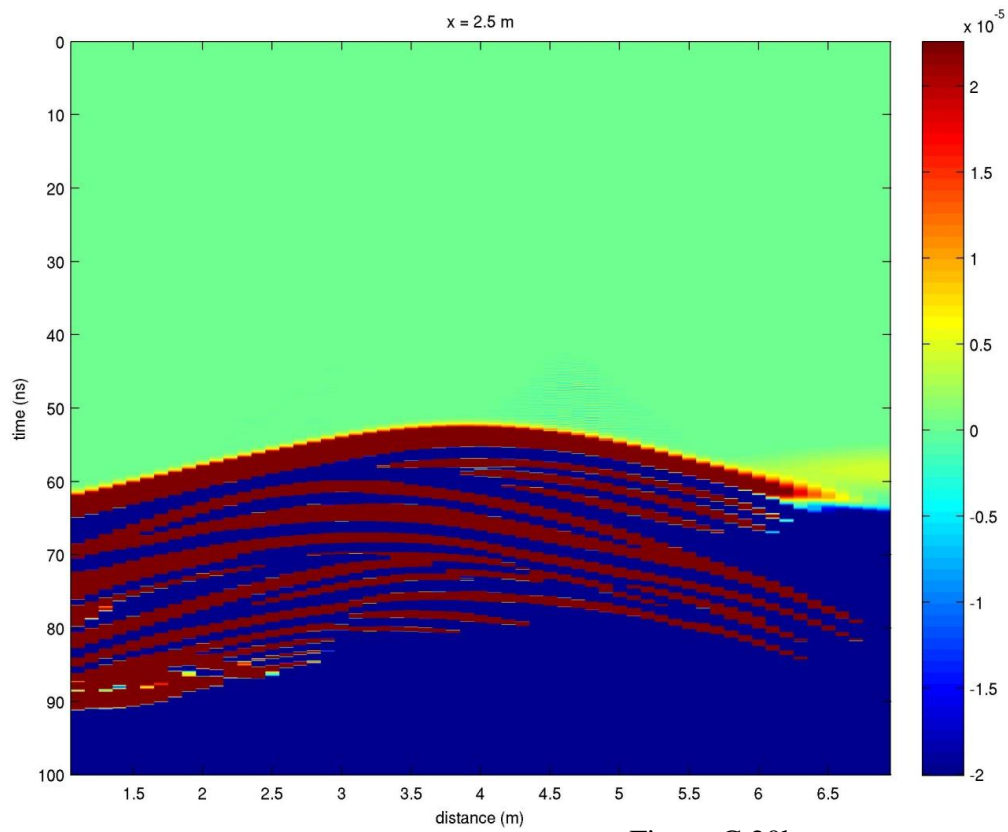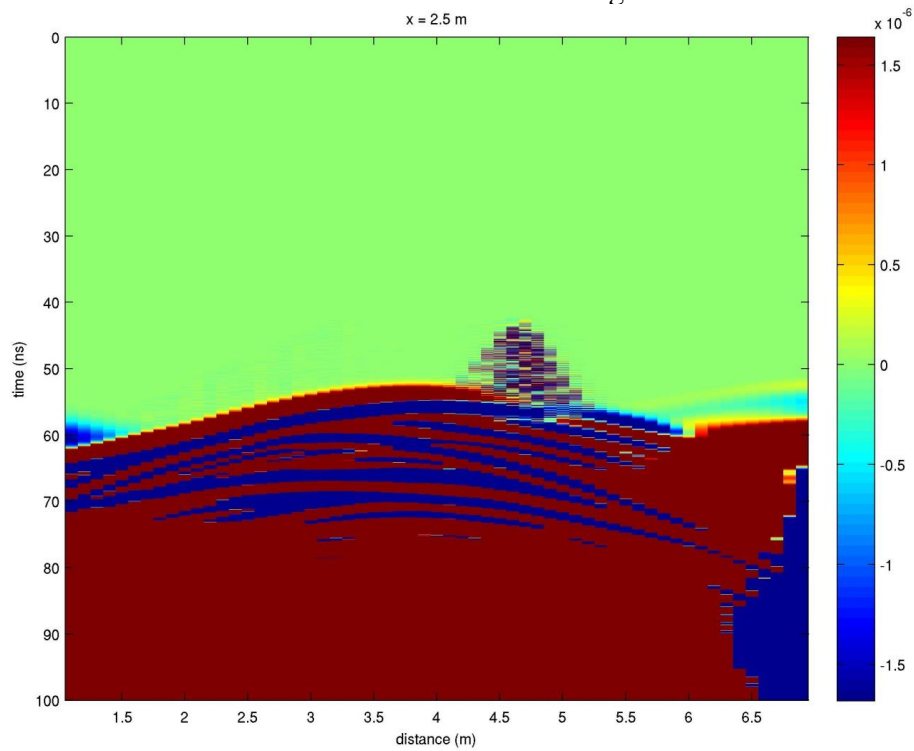
Figure C.18a

Figure C.18b

263

Figure C.18a. Top, previous page. Ex difference plot between Model A and B for transmitter location #60 (same identification numbers as those in previous sections). The x-axis represents the distance in the y-direction (for x = 2.5 m). The y-axis represents the time axis (in ns). Transmitter locations may be are the same as those in previous figures.

Figure C.18b. Bottom, previous page. Ey difference plot between Model A and B for transmitter location #60. All values are the same as previous graph. Notice miniscule order of magnitude of relative difference in each graph.

Note: this is at the center of the conduit (x = 2.5 m, y = 3.5 m).

Appendix C (Continued)

Figure C.19a

Figure C.19b

265

Appendix C (Continued)

Figure C.19a. Top, previous page. Ex difference plot between Model A and B for transmitter location #70 (same identification numbers as those in previous sections). The x-axis represents the distance in the y-direction (for x = 2.5 m). The y-axis represents the time axis (in ns). Transmitter locations may be are the same as those in previous figures.

Figure C.19b. Bottom, previous page. Ey difference plot between Model A and B for transmitter location #70. All values are the same as previous graph. Notice miniscule order of magnitude of relative difference in each graph.

266

Appendix C (Continued)

Figure C.20a

x = 2.5 m

Figure C.20b

x = 2.5 m

267

www.manaraa.com

Figure C.20a. Top, previous page. Ex difference plot between Model A and B for transmitter location #90 (same identification numbers as those in previous sections). The x-axis represents the distance in the y-direction (for x = 2.5 m). The y-axis represents the time axis (in ns). Transmitter locations may be are the same as those in previous figures.

Figure C.20b. Bottom, previous page. Ey difference plot between Model A and B for transmitter location #90. All values are the same as previous graph. Notice miniscule order of magnitude of relative difference in each graph.

Figure C.21a

Figure C.21b

269
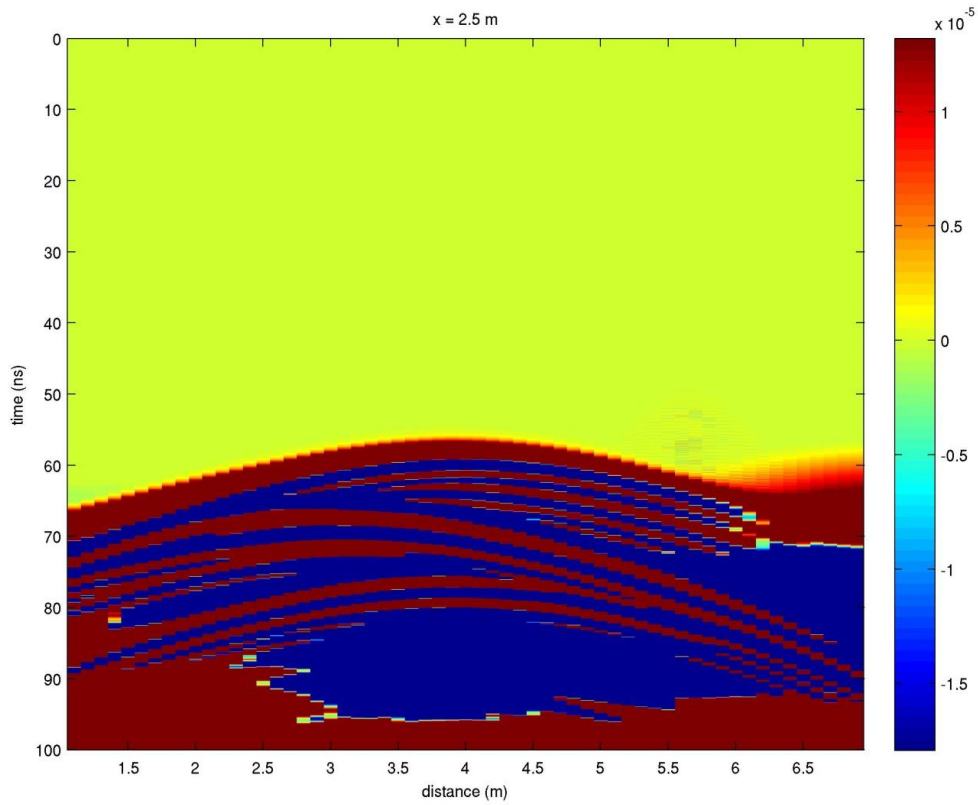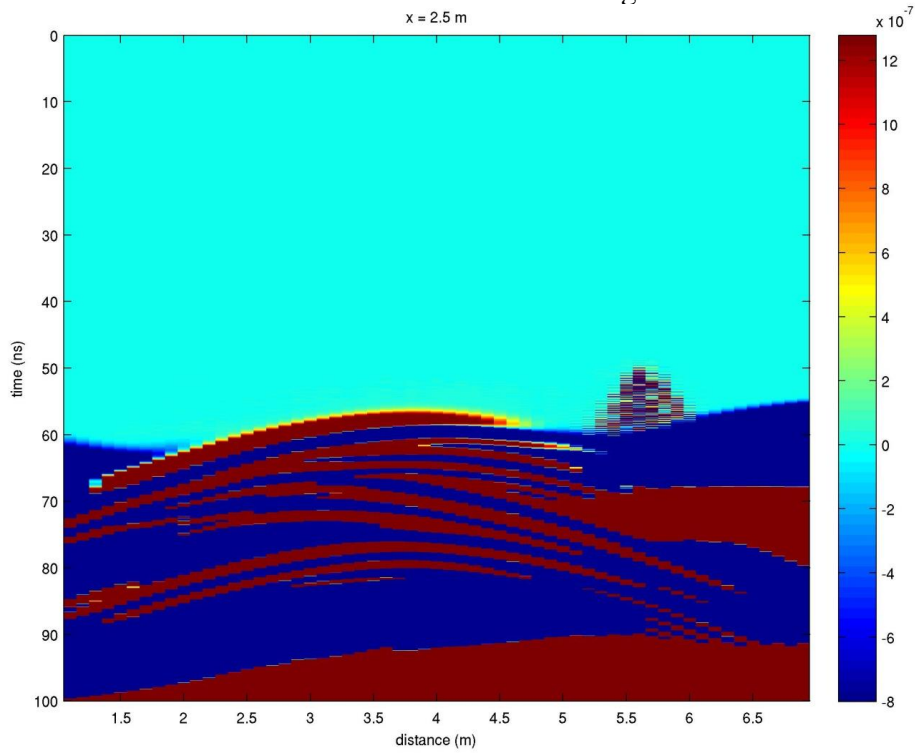
Figure C.21a. Top, previous page. Ex difference plot between Model A and B for
transmitter location #115 (same identification numbers as those in previous
sections). The x-axis represents the distance in the y-direction (for x = 2.5 m). The
y-axis represents the time axis (in ns). Transmitter locations may be are the same
as those in previous figures.

Figure C.21b. Bottom, previous page. Ey difference plot between Model A and B
for transmitter location #115. All values are the same as previous graph. Notice
the miniscule order of magnitude of relative difference in each graph.

All previous simulated surveys were run with the transmitting and receiving pair
of antenna in a line through the center of the conduit. One final analysis was made to
observe the results of doing an off-axis common-shot gather where the transmitting line
was off by 0.3 m to one side (specifically, x = 2.8 m) of the center line of the model. The
rx_box and model geometry was still the same as used in the Model B. By placing the
new line only 0.3 m to one side, the survey line was still over the conduit but not exactly
in the middle of it. It was hypothesized that there might be a better return of energy by
doing this experiment. The results of this experiment can be seen in Figure C.22-28. The
experiment, unfortunately, did not reveal anything worth further investigation.
Essentially, the side of the larger conical depression was discernible but nothing else of
value could be gleamed from it.

All the previous results of the performed common-shot gathers were negative in
extracting information about the presence of the modeled conduit structure. This result is,
however, an important one in that it explains how similar conduit structure might actually

270

Appendix C (Continued)

exist in subsurface geology but is frequently not recognized. More rigorous modeling

research may eventually prove useful in extracting similar conduit structure, but for now

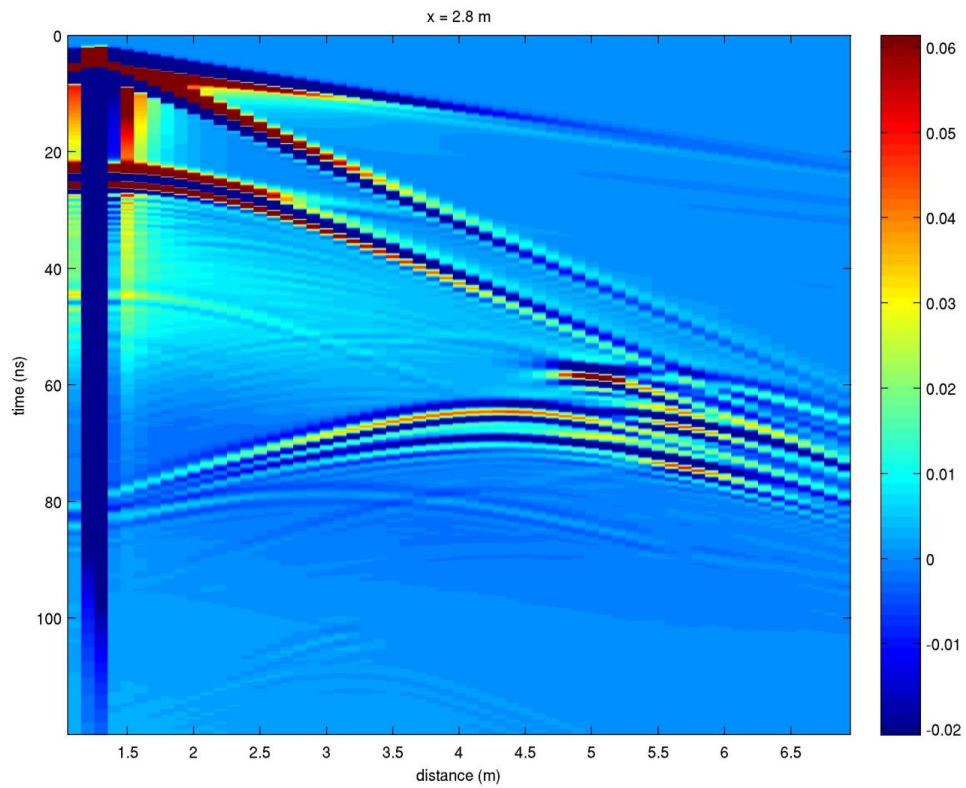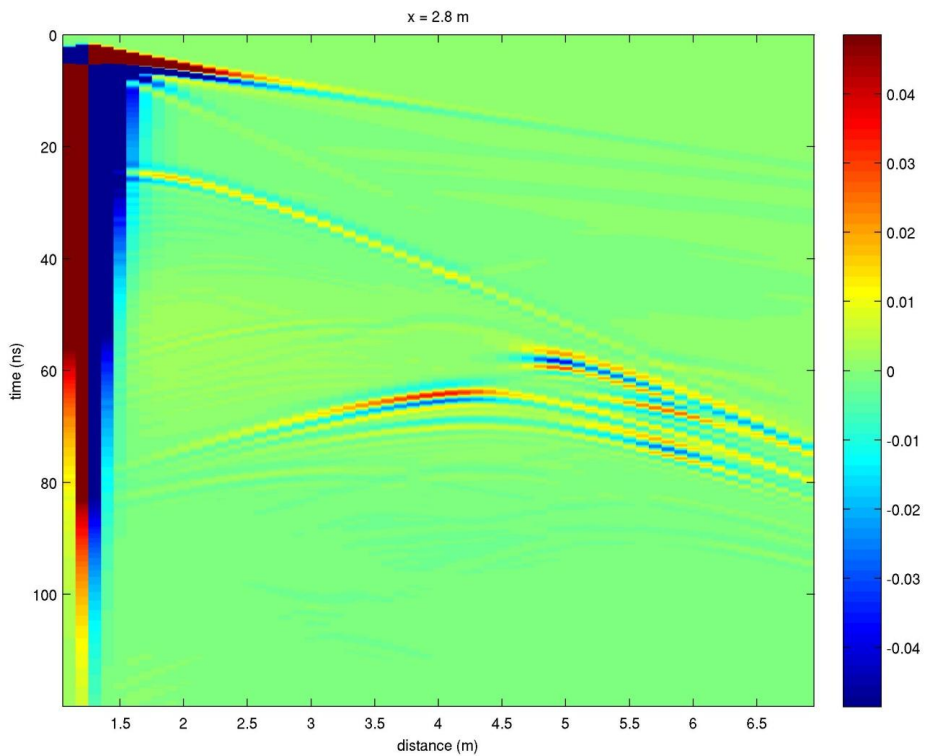the results are inconclusive.
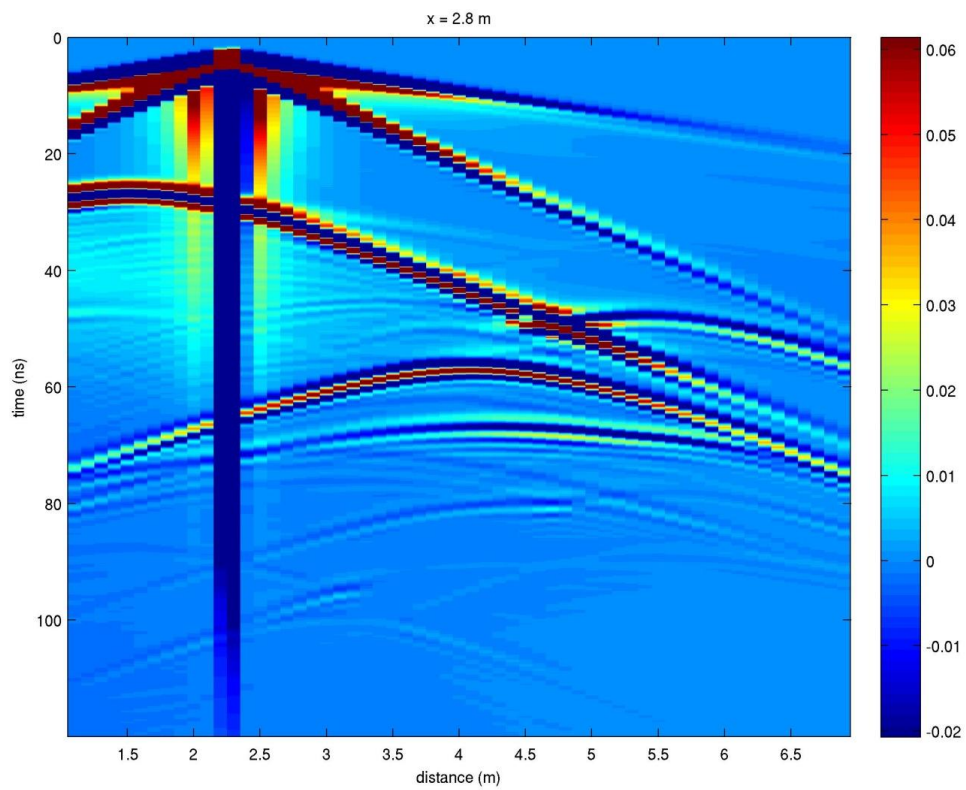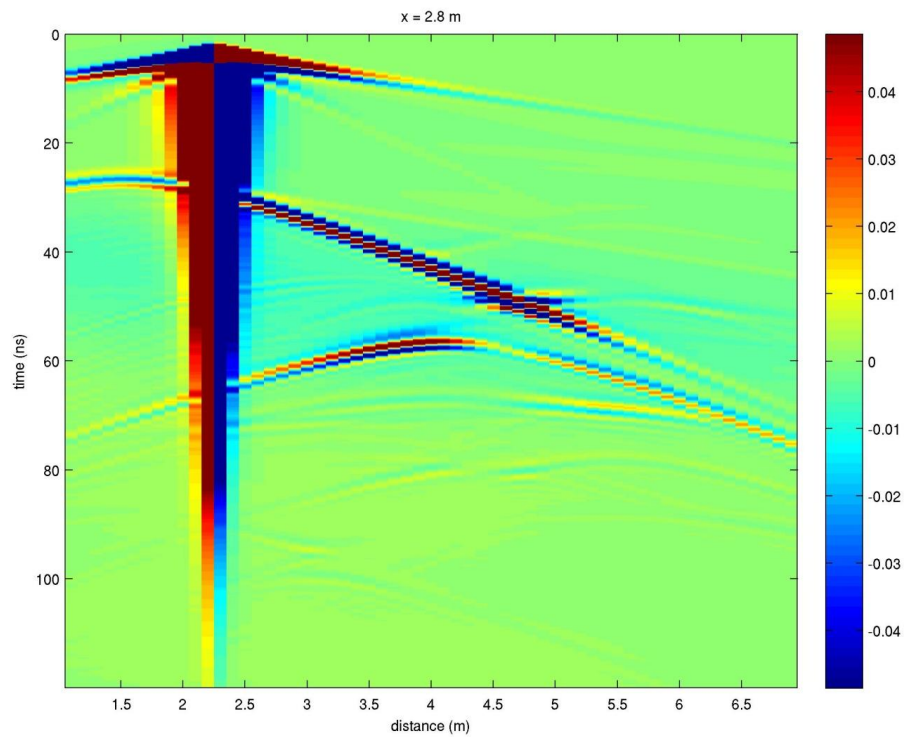
271

Figure C.22a

x = 2.8 m

Figure C.22b

x = 2.8 m

272

Appendix C (Continued)

Figure C.22a. Top, previous page. Ex common-shot gather record for transmitter

location #5 (same identification numbers as those in previous sections) for off-

axis Model B. The x-axis represents the distance in the y-direction (for x = 2.8 m).

The y-axis represents the time axis (in ns). Transmitter locations may be directly

found by following air and ground waves to their source location at time zero.

Figure C.22b. Bottom, previous page. Ey common-shot gather record for

transmitter location #5 for off-axis Model B. All values are the same as previous
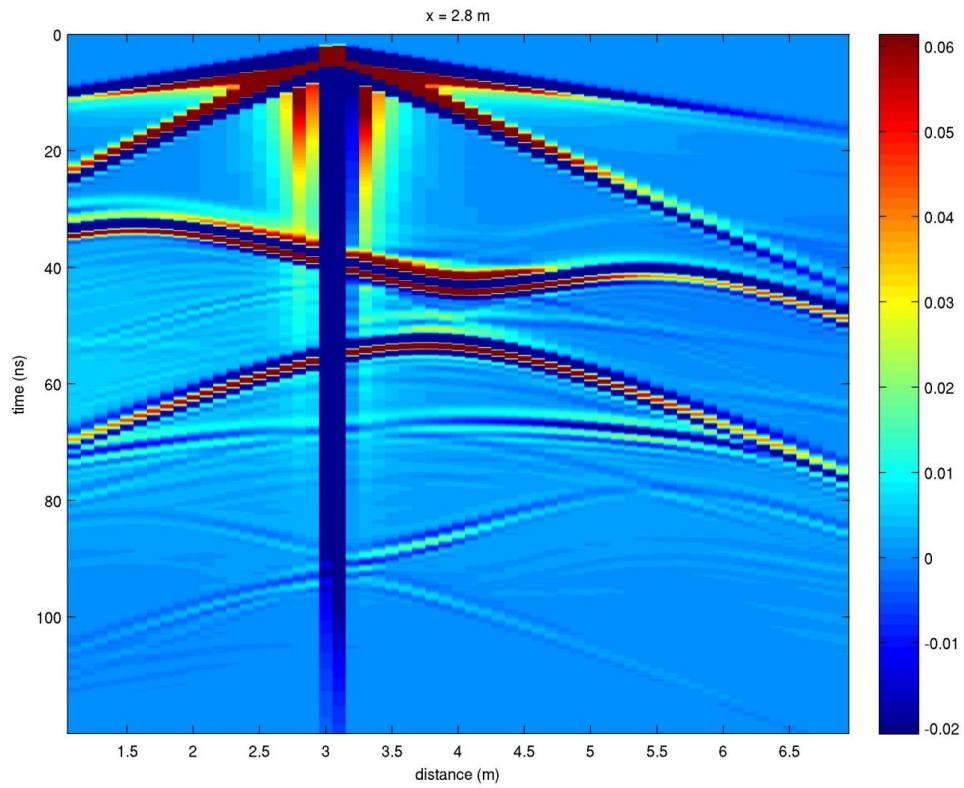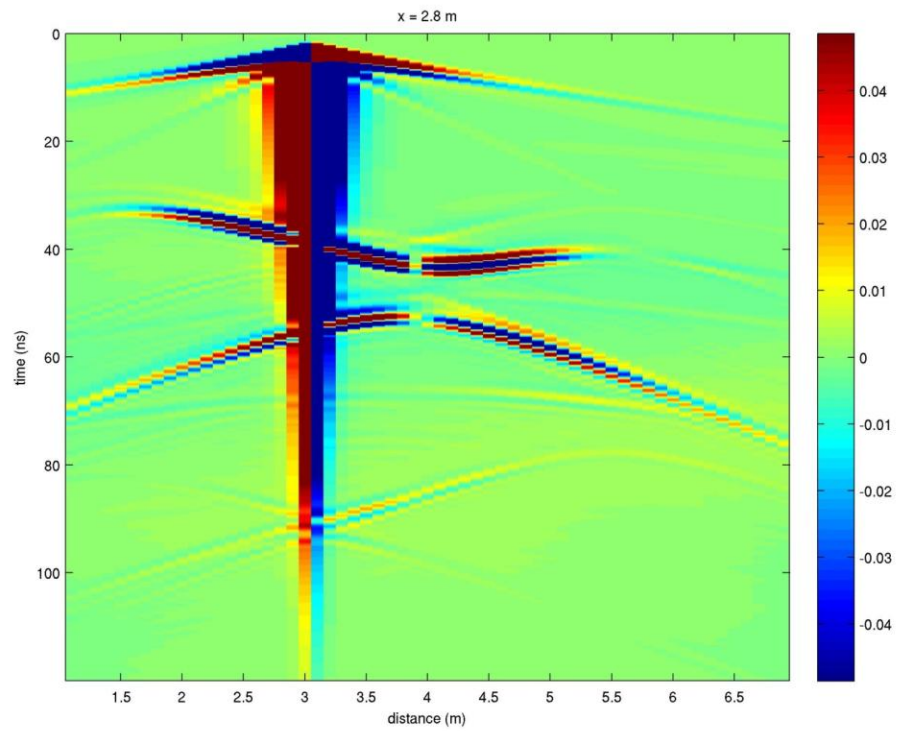
graph. Notice Ey signal strength is weaker than Ex record.

273

Figure C.23a

x = 2.8 m

Figure C.23b

x = 2.8 m

274

www.manaraa.com

Figure C.23a. Top, previous page. Ex common-shot gather record for transmitter location #30 (same identification numbers as those in previous sections) for off-axis Model B. The x-axis represents the distance in the y-direction (for x = 2.8 m). The y-axis represents the time axis (in ns). Transmitter locations may be directly found by following air and ground waves to their source location at time zero.

Figure C.23b. Bottom, previous page. Ey common-shot gather record for transmitter location #30 for off-axis Model B. All values are the same as previous graph. Notice Ey signal strength is weaker than Ex record.
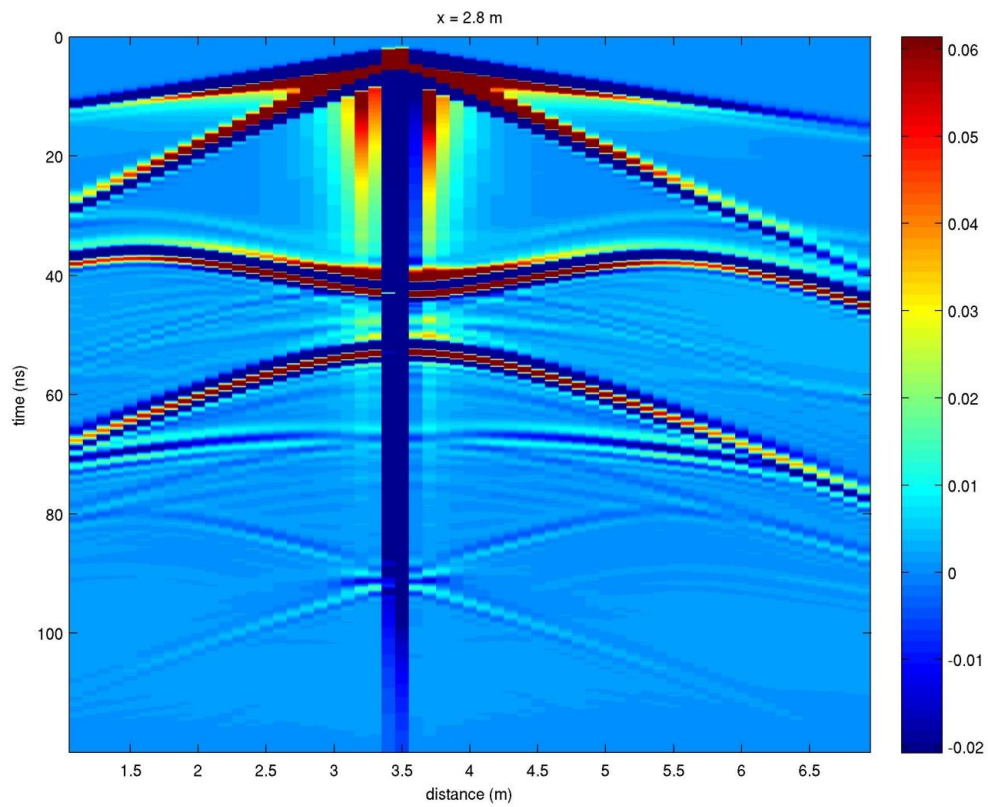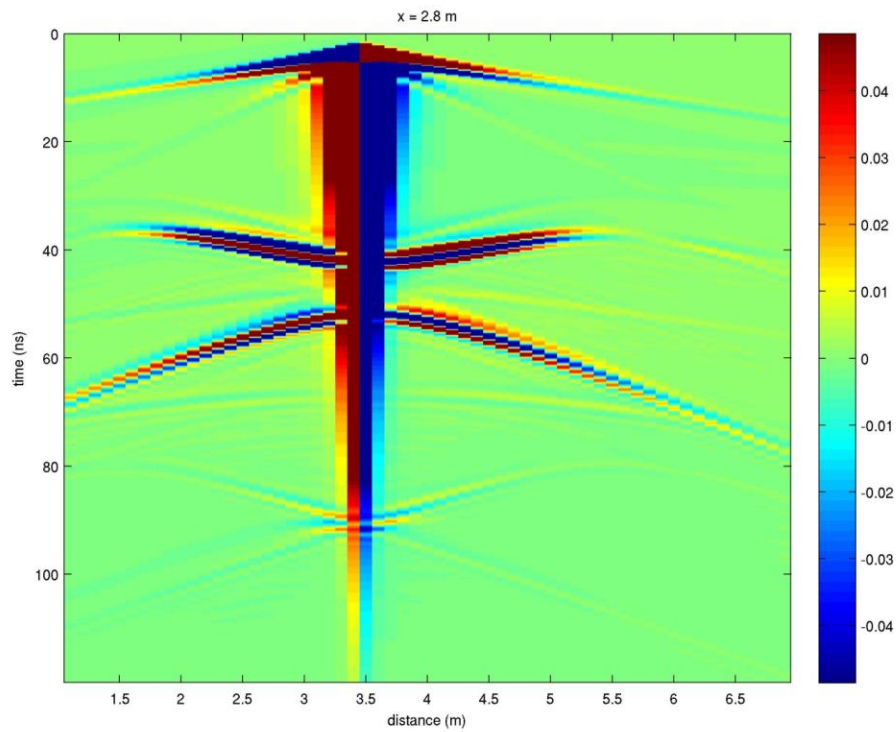
Figure C.24a

x = 2.8 m

Figure C.24b

x = 2.8 m

276

Figure C.24a. Top, previous page. Ex common-shot gather record for transmitter location #50 (same identification numbers as those in previous sections) for off-axis Model B. The x-axis represents the distance in the y-direction (for x = 2.8 m). The y-axis represents the time axis (in ns). Transmitter locations may be directly found by following air and ground waves to their source location at time zero. Figure C.24b. Bottom, previous page. Ey common-shot gather record for transmitter location #50 for off-axis Model B. All values are the same as previous graph. Notice Ey signal strength is weaker than Ex record.

Figure C.25a

Figure C.25b

278

Figure C.25a. Top, previous page. Ex common-shot gather record for transmitter location #60 (same identification numbers as those in previous sections) for off-axis Model B. The x-axis represents the distance in the y-direction (for x = 2.8 m). The y-axis represents the time axis (in ns). Transmitter locations may be directly found by following air and ground waves to their source location at time zero. Figure C.25b. Bottom, previous page. Ey common-shot gather record for transmitter location #60 for off-axis Model B. All values are the same as previous graph. Notice Ey signal strength is weaker than Ex record.

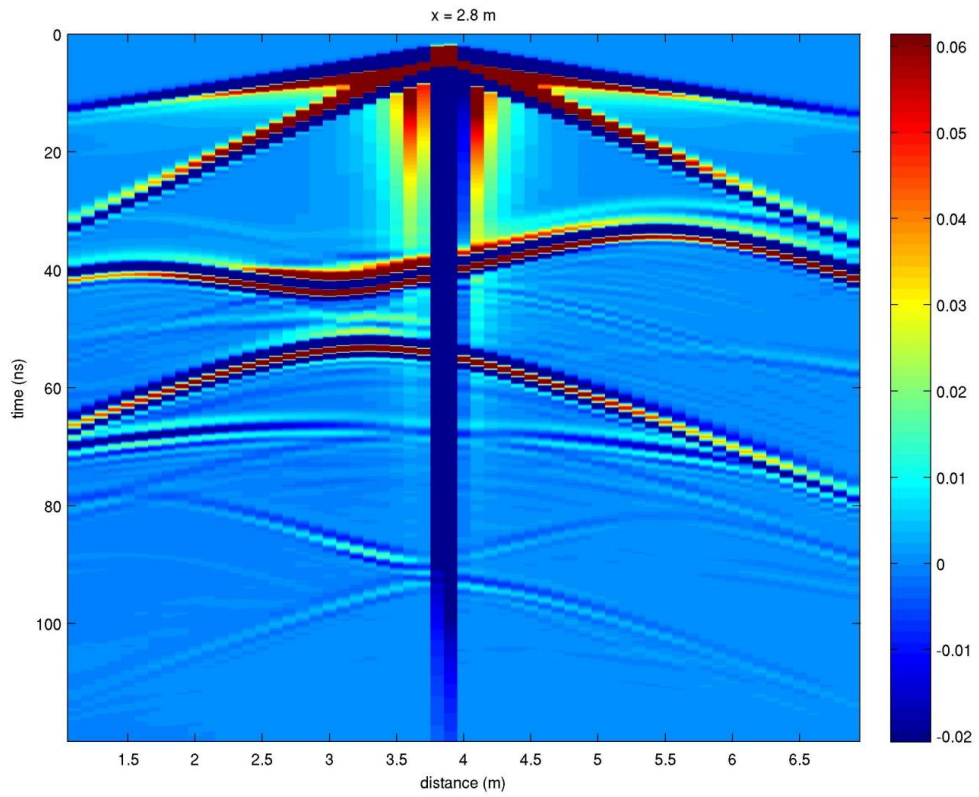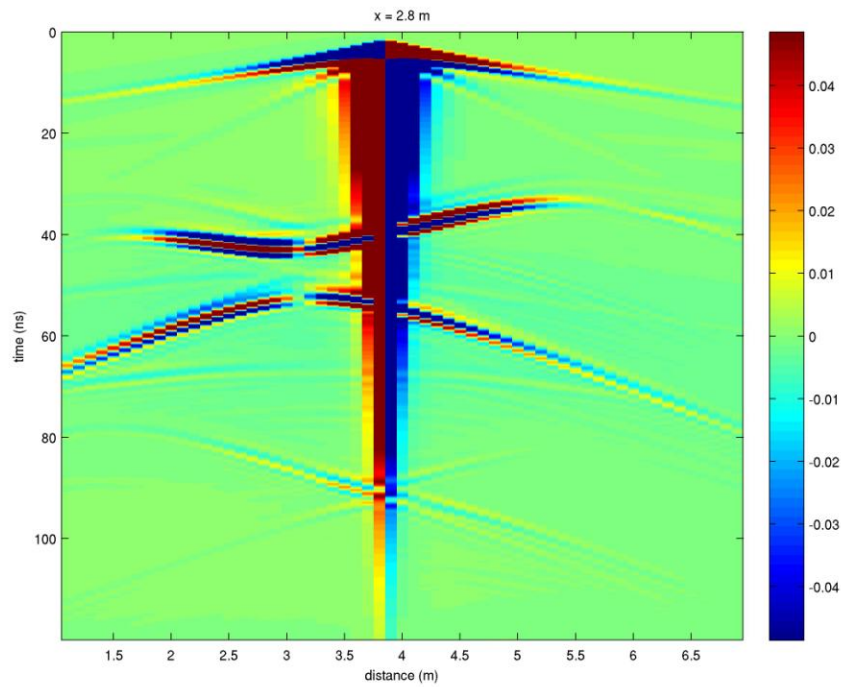Note: this is at the center of the conduit (x = 2.5 m, y = 3.5 m).

Figure C.26a

x = 2.8 m

Figure C.26b

x = 2.8 m

280

www.manaraa.com

Figure C.26a. Top, previous page. Ex common-shot gather record for transmitter location #70 (same identification numbers as those in previous sections) for off-axis Model B. The x-axis represents the distance in the y-direction (for x = 2.8 m). The y-axis represents the time axis (in ns). Transmitter locations may be directly found by following air and ground waves to their source location at time zero. Figure C.26b. Bottom, previous page. Ey common-shot gather record for transmitter location #70 for off-axis Model B. All values are the same as previous graph. Notice Ey signal strength is weaker than Ex record.
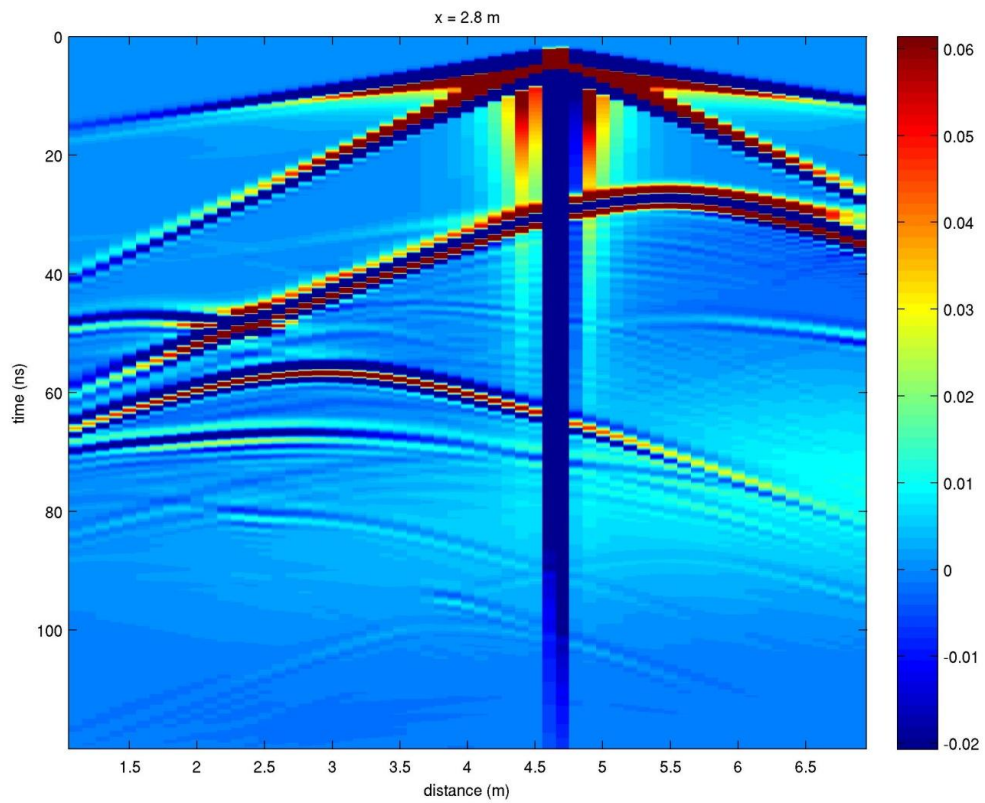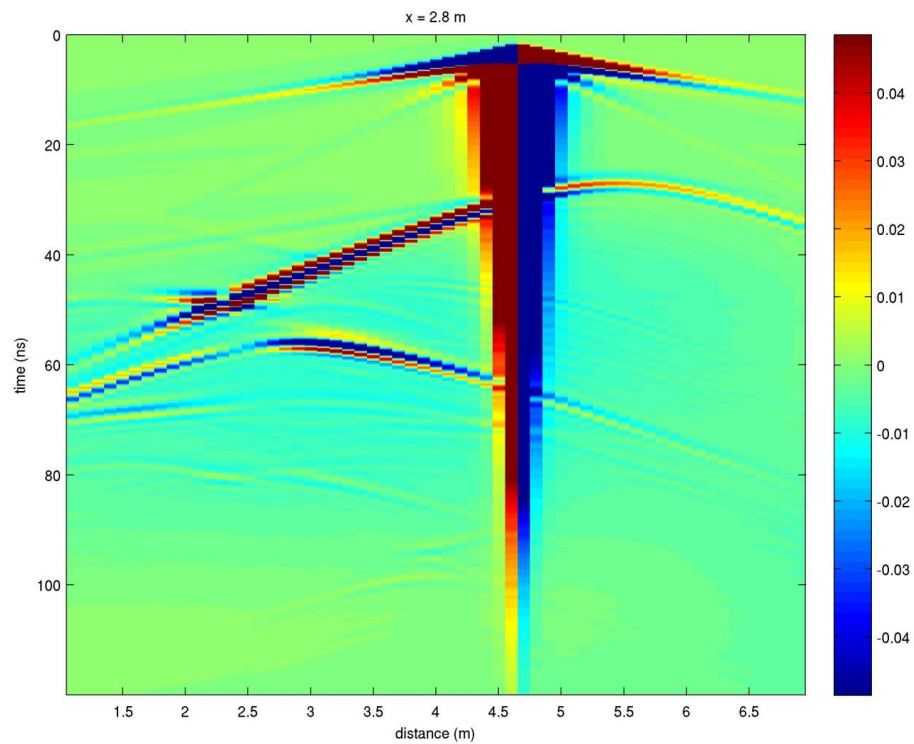
Appendix C (Continued)

Figure C.27a

x = 2.8 m

Figure C.27b

x = 2.8 m

Figure C.27a. Top, previous page. Ex common-shot gather record for transmitter

location #90   (same identification numbers as those in previous sections) for off-

axis Model B. The x-axis represents the distance in the y-direction (for x = 2.8 m).

The y-axis represents the time axis (in ns). Transmitter locations may be directly

found by following air and ground waves to their source location at time zero.

Figure C.27b. Bottom, previous page. Ey common-shot gather record for

transmitter location #90 for off-axis Model B. All values are the same as previous

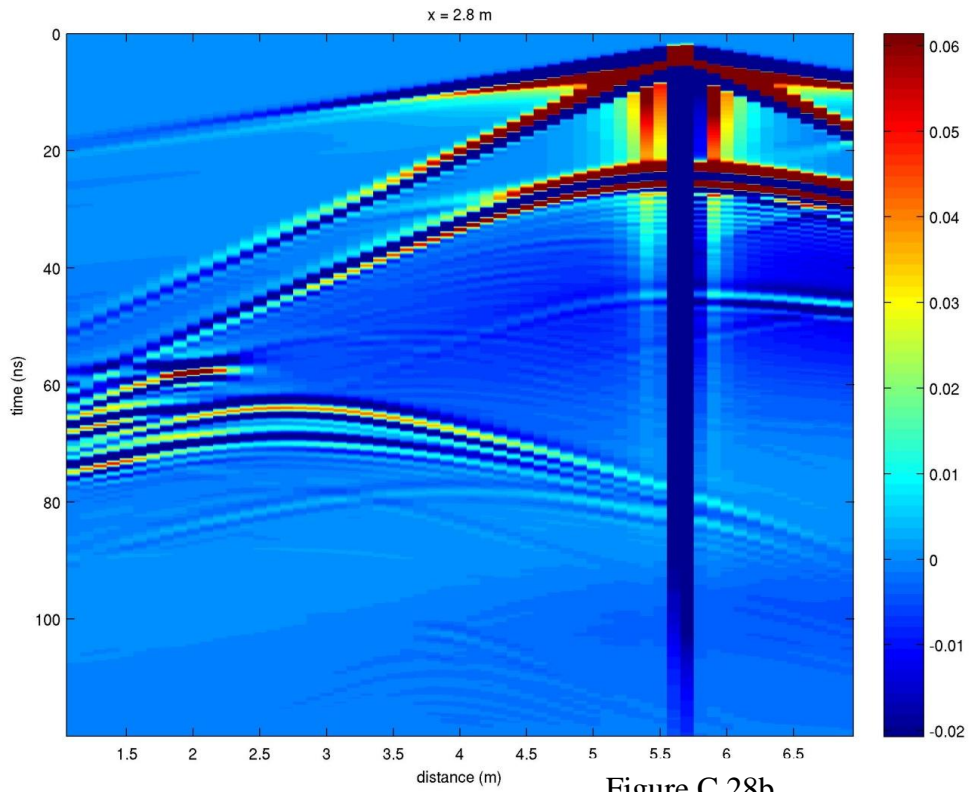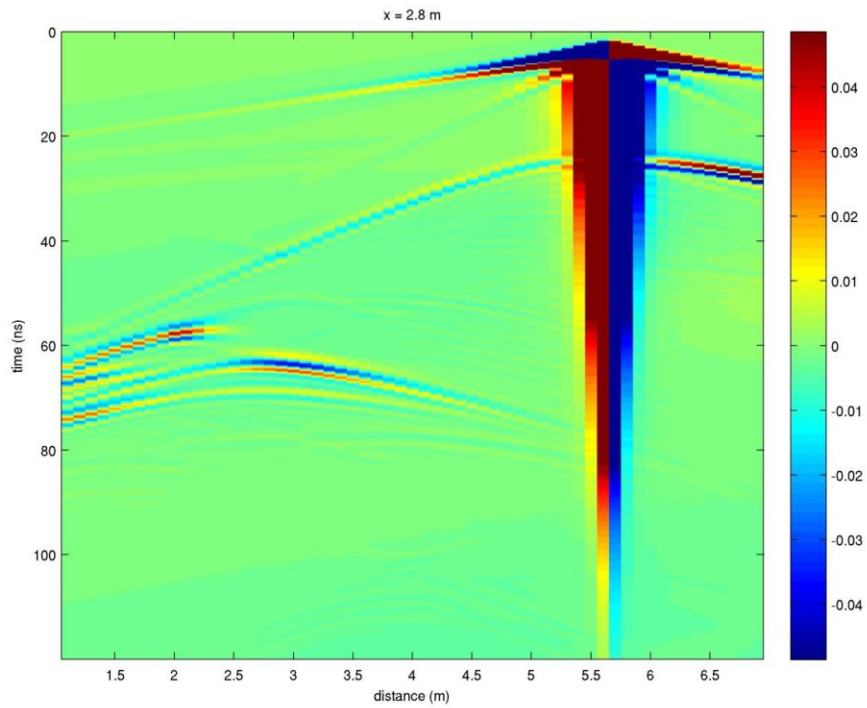graph. Notice Ey signal strength is weaker than Ex record.

Figure C.28a

Figure C.28b

284

Figure C.28a. Top, previous page. Ex common-shot gather record for transmitter location #115 (same identification numbers as those in previous sections) for off-axis Model B. The x-axis represents the distance in the y-direction (for x = 2.8 m). The y-axis represents the time axis (in ns). Transmitter locations may be directly found by following air and ground waves to their source location at time zero. Figure C.28b. Bottom, previous page. Ey common-shot gather record for transmitter location #115 for off-axis Model B. All values are the same as previous graph. Notice Ey signal strength is weaker than Ex record.

285